ASPECTS OF FLOW INJECTION ATOMIC ABSORPTION SPECTROMETRY.

by

Stephen George OFFLEY, BSc (Hons), GRSC.

A Doctoral Thesis Submitted in partial fulfilment of the requirements for the award of Doctor of Philosophy of the University of Technology, Loughborough, UK.

February 1992

Supervisors: J. F. Tyson, BSc, DIC, PhD, CChem FRSC
N. J. Seare, BSc, PhD, GRSC.

I dedicate this work to my wife Beckie for her love, care and support and for simply having faith in my ability.

Acknowledgements

I thank Prof. J.F. Tyson for the opportunity to undertake this research under his experienced supervision and for his encouragement and friendship throughout it.

I thank Dr. N. Seare for all the invaluable help she has given both on an academic and administrative level and her encouragement and ever open ear.

I thank jointly the SERC and Unicam Ltd for financial support and provision of equipment that made the work possible. My thanks go also to all those at Unicam Ltd that have played an active supervisory role in the work, in particular Dr H. Kibble and more recently Mr C. Fellows. The cooperation and help of all the technical staff in the Analytical Chemistry Section at Loughborough University of Technology is gratefully acknowledged.

I thank ~~me~~ my research colleagues at both Loughborough University of Technology and the University of Massachusettes for their help, encouragement and friendship.

I thank Mr and Mrs Hindocha for their time and effort in producing this final presented thesis.

Last but not least I thank my family for the love, support and patience without which this work would not have been possible.

TABLE OF CONTENTS

Abstract.

The literature relevant to the generation of volatile hydrides for analytical atomic spectroscopy has been reviewed, with particular reference to atomic absorption spectrometry (AAS). This reveals some conflicting information concerning the nature of various interference effects and strategies to overcome them. The use of flow injection (FI) procedures has been demonstrated by several research groups, to be beneficial. A review of the literature concerning the application of FI techniques to AAS shows that there is a sustained interest in the use of such a combination for analytical purposes. In particular, an interest in the on-line coupling of chemical pretreatment of samples is evident.

Atomic absorption spectrometry has a limited working range and requires frequent calibration, consequently, there is a need for a rapid, precise on-line dilution procedure. The potential of FI systems with wide bore manifold tubing for on-line dilution was assessed and found to be limited by variations in dispersion coefficient arising from differences in specific gravities between the sample and carrier fluids. This could be overcome only by the use of unrealistically high flow rates.

The use of FI procedures for the generation of volatile hydrides of selenium and arsenic was investigated. Optimization studies of system parameters, including the atomization step, were undertaken which demonstrated the benefits in applying FI in hydride generation atomic absorption spectrometry (HGAAS). Analytical methods were devised and evaluated for the determination of Se in copper metal and As in nickel alloy. These procedures involved the use of an on-line matrix removal step in which potentially interfering matrix elements were retained on a strong cation exchange resin (Dowex 50W). The manifold was designed so that the FI value acted as the interface between the matrix isolation stage and the vapour generation stage, a strategy which allowed independent optimization of each stage. Location of the ion exchange resin in the sample loop of a six-port rotary valve allowed the resin to be regenerated easily and rapidly, with a throughput capability of the order of 50 h^{-1} and permit the proposed full automation of the whole analytical procedure. In the determination of As in nickel alloy a novel stopped-flow pre-reduction step was developed to permit As^{III} quantitation, therefore, achieve optimum sensitivity. The two systems permitted limits of detection for Se and As of 2.1 and 3.9 ng ml^{-1} respectively. Direct comparisons were made with existing matrix isolation systems to emphasise the benefits of system design.

Keywords: Atomic absorption spectrometry; flow injection; hydride generation; interference removal; on-line matrix isolation; on-line dilution.

PUBLICATIONS.

"Determination of Selenium in Copper Metal using flow injection hydride generation Atomic Absorption Spectrometry with Continuous Flow Matrix Isolation,"

Offley, S.G., Seare, N.J., Tyson, J.F. and Kibble, H.A.B., *Anal. Proc.*, 1991, 28, 18.

"Elimination of Copper Interference by Continuous Flow Matrix Isolation in the Determination of Selenium by Flow Injection Hydride Generation Atomic Absorption Spectrometry,"

Offley, S.G., Seare, N.J., Tyson, J.F., and Kibble, H.A.B., *J. Anal. At. Spectrom.*, 1991, 6, 133.

"Determination of Arsenic in a Nickel Based Alloy by Flow Injection Hydride Generation Atomic Absorption Spectrometry Incorporating Continuous Flow Matrix Isolation and Stopped-Flow Pre-reduction Procedures."

Tyson, J.F., Offley, S.G., Seare, N.J., Kibble, H.A.B. and Fellows, C., *J. Anal. At. Spectrom.*, Accepted for publication.

CONFERENCE PRESENTATIONS.

"An Automated Multi-range Flow Injection Analyser for Flame Atomic Absorption Spectrometry," **Tyson, J.F., Bysouth, S.R., and Offley, S.G.,**
Poster Presentation, RSC, SAC 89 Conference, Cambridge, U.K., July 1989.

"Extending the Calibration Range of Conventional Flame AAS by Continuous Flow Techniques," **Tyson, J.F.,** Bysouth, S.R., Debrah, E., and Offley, S.G., lecture/slide presentation, Pittsburgh Conference on Analytical Chemistry and Spectroscopy, New York, U.S.A., March 1990.

"Determination of Selenium in Copper Alloys using Flow Hydride Generation Atomic Absorption Spectrometry with On-line Matrix Isolation," **Offley, S.G.,** Seare, N.J., and Tyson, J.F., Poster presentation, RSC meeting, Research and Development Topics in Analytical Chemistry, ICI C&P Ltd. Runcorn, Cheshire, U.K., July 1990.

"Use of Wide Bore Tubing in a Flow Injection Manifold to Obtain Controlled On-line Dilution for Flame Atomic Absorption Spectrometry," **Offley, S.G.,** Seare, N.J., and Tyson, J.F., Poster presentation, 5th Biennial National Atomic Spectroscopy Symposium (BNAAS), Loughborough, U.K., July 1990.

"Determination of Selenium in Copper Alloys using Flow Injection Hydride Generation Atomic Spectrometry with On-line Matrix Isolation," **Offley, S.G.,** Seare, ad Tyson, J.F., lecture/slide presentation, 5th Biennial National Atomic Spectroscopy Symposium (BNAAS), Loughborough, U.K., July 1990.

"Determination of Hydride-Forming Elements in Metals by Flow Injection Spectrometry with On-line Matrix Isolation," **Offley, S.G.,** Seare, N.J., Tyson, J.F., and Kibble, H.A.B., lecture/slide presentation, Pittsburgh Conference on Analytical Chemistry and Spectroscopy, Chicago, U.S.A., March 1991.

"Determination of Hydride-Forming Elements in Metals by Flow Injection Atomic Absorption Spectrometry with On-line Matrix Isolation," **Tyson, J.F.,** Kibble, H.A.B., Offley, S.G., and Seare, N.J., Lecture/slide presentation, CSI Meeting, Bergen, Norway, June 1991.

"Determination of Hydride-Forming Elements in Metals by Flow Injection Atomic Absorption Spectrometry with On-line Matrix Isolation," **Tyson, J.F.,** Offley, S.G., Seare, N.J., and Kibble, H.A.B., Poster presentation, Flow Analysis V Conference, Kumamoto, Japan, August 1991.

CHAPTER ONE

HYDRIDE GENERATION ATOMIC ABSORPTION SPECTROMETRY.

1.1 INTRODUCTION.

The concept of atomic absorption spectrometry (AAS) was first introduced by Walsh [1] at CSIRO in Australia in 1955. Since its birth some 35 years ago the technique of AAS has now become widely accepted and used for the analysis of 67 mainly "metallic" elements at the trace and ultra-trace level. The technique of AAS is now sufficiently well known that numerous text books exist covering its use including those of Ebdon [2] and Cantle[3]. At present over 1000 publications covering the whole spectrum of AAS appear in a variety of journals each year [4]. Reviews appear in Analytical Chemistry [5] every two years and yearly in the Journal of Analytical Atomic Spectrometry [6].

Sample introduction and subsequent atomization in AAS is achieved by three main methods, flame atomic absorption spectrometry (FAAS), electrothermal atomic absorption spectrometry (ETAAS) and hydride generation atomic absorption spectrometry (HGAAS). Each method has its respective advantages and disadvantages.

Flame atomization is currently perhaps the most used and understood method of atomization. The combustion flame proposed by Walsh [1] provides a remarkably simple means of converting inorganic analytes in solution into free atoms. The major advantage of the technique is the rapid rate of analysis obtained making routine analysis quick and cheap. Disadvantages of the technique include limited sensitivity and chemical interference effects. The sensitivity of FAAS is restricted due to the inefficient performance of the nebulizer and spray chamber system which delivers only about 10% of the sample solution to the flame, and the low atom number density attained in the flame due to the dilution effects of flame support gases.

The electrothermal atomization procedure was first proposed by L'vov [7] in 1961. A relatively small volume of solution was applied to the tip of a resistively heated carbon electrode which was introduced into a cylindrical electrically heated furnace. Electrothermal atomization offers vastly superior sensitivity over FAAS with detection limits normally in the low ng ml^{-1} range. The inherent atomization efficiency of ETAAS is though to some extent obtained at a cost to analysis time. A typical cycle time of 2 minutes is significantly longer than in FAAS which takes in the order of 15 seconds. Operation and optimization of ETAAS is far more complicated than FAAS and even with automatic sampling, precision is inferior to that of FAAS.

Hydride generation was developed in response to a need for the determination of "environmentally" important elements, such as As, Ge, Sb, Se and Te. Such elements had proved difficult to measure accurately using both FAAS and ETAAS. The main difficulty faced in determining these elements is that their optimum analytical lines are in the low ultraviolet (between 190 and 230 nm). The background absorption in a flame atomizer at such wavelengths is high. Kahn and Schallis [8] reported a 62% background absorption by the air-acetylene flame at the arsenic 193.7 nm line. Alternative flames such as the argon-entrained air-hydrogen flame can reduce the background absorption. However, use of this very low temperature flame (~300°C) can result in greater interferences caused by incomplete salt dissociation and molecular absorption. In ETAAS the use of short wavelengths causes other specific problems. Light scattering by particulate matter is severe and molecular absorption is a serious problem. For relatively volatile elements such as Se, matrix modification procedures are necessary to reduce analyte loss during the charing ~~and~~ or ashing steps.

Hydride generation overcomes the problems faced in the determination of such elements (As, Bi, Ge, Pb, Sb, Se, Sn and Te) by FAAS and ETAAS through the formation of volatile hydride species which are separated from the sample matrix prior to determination by AAS. The hydride generation process, used for years in the classical Marsh reaction and Gutzeit method [9], for the determination of As, was first applied to AAS by Holak [10] in 1969. The hydride generation system described can be divided into three steps: (i) the generation and volatilization of the hydride; (ii) transfer of the hydride including collection and (iii) the atomization of the hydride in the light beam of the spectrometer. Holak [10] reported that the major advantage of his gas sampling technique was its suitability to trace analysis. In comparison with liquid sample introduction, the methodology allowed preconcentration of the sample from a relatively large volume of solution into a relatively small volume of vapour and sample transport was accomplished with an efficiency approaching 100%, compared with 1-10% typical of FAAS. Applying the method of hydride generation a detection limit of 0.04 μg of As was achieved, (preconcentration of hydride over 30 minutes). Holak [10] also reported that since the element was isolated from the matrix, interference associated with the nebulization of solutions of high dissolved solids (such as light scattering) as well as chemical interferences were eliminated. No data was presented though as evidence for the rather optimistic postulation that chemical interferences were eliminated. Clearly the major disadvantage of the hydride generation process is its limited application to only eight elements making it a very specific technique in comparison with FAAS and ETAAS. In its early days the technique was very labour intensive, tedious and with a low throughput capability [10,11]. This drawback has been overcome to an extent through the application of both continuous flow [12] and flow injection [13] methodology. Although reported by Holak [10] to be virtually interference free, later work has shown that the

technique is susceptible to numerous effects both in the aqueous and gas phases [14,15]. A possible drawback of the technique, if care is not taken is that its performance is affected by the chemical nature of the analyte [11,16]. However, the ability of the technique to permit chemical speciation in samples is very beneficial because toxicity, bioavailability, bioaccumulation and transport of a particular element depends critically on the chemical form [17,18]. Such information is less available using FAAS or ETAAS without extensive sample pretreatment.

1.2 BACKGROUND AND DEVELOPMENT.

To date a number of reviews have been made of hydride generation atomic absorption spectrometry [17-22]. Of these three are of particular note. Godden and Thomerson [19] provided an excellent coverage of the development and growth of HGAAS in its early years. Nakahara [21] reviewed the application of hydride generation, not only to atomic absorption but atomic fluorescence and plasma atomic emission spectroscopy. Excellent detail was given of its application to real sample analysis. Dedina [22] reviewed hydride generation and atomization in AAS. Great detail was paid to the theoretical aspects of both the generation and atomization processes.

1.2.1 Chemistry.

In the first reported application of hydride generation to atomic absorption by Holak [10] the covalent hydride (arsine) was formed using the zinc-hydrochloric acid reduction system. The reaction proceeds according to the following equation 1.2.1,

$$Zn + 2HCl \longrightarrow ZnCl_2 + 2H \xrightarrow{E^{m+}} EH_n + H_2 \text{ (excess)} \qquad (1.2.1)$$

(m may or may not equal n), where E is the element of interest.

The zinc-hydrochloride acid system was restricted though to the formation of AsH_3, SbH_3 and H_2Se. In later work [11] a zinc column was used in the formation of hydrides

Indentation (0,25 in)

cmsj

Loughborough University Computing Services

Request id: cca4m1-6319 Printer: cca4m1

Processed job on: Fri Jan 21 16:54:16 GMT 1994

Account balance on Fri Jan 21 16:54:16 GMT 1994: 980p

WordTemp-3

left 1.7

Right 0.8

Top 1,2

bottom 0.98

Chapter (1) → Word Temp-3

Chapter (1) (2)
- left 1.7
  right 0.8
  top 1.2
  bottom 0.98

Driver revision cca4m1/9.0

Chapter (2)

Indentation 1.25 left line at least
right 0 in 18 pts
first -1.25 in

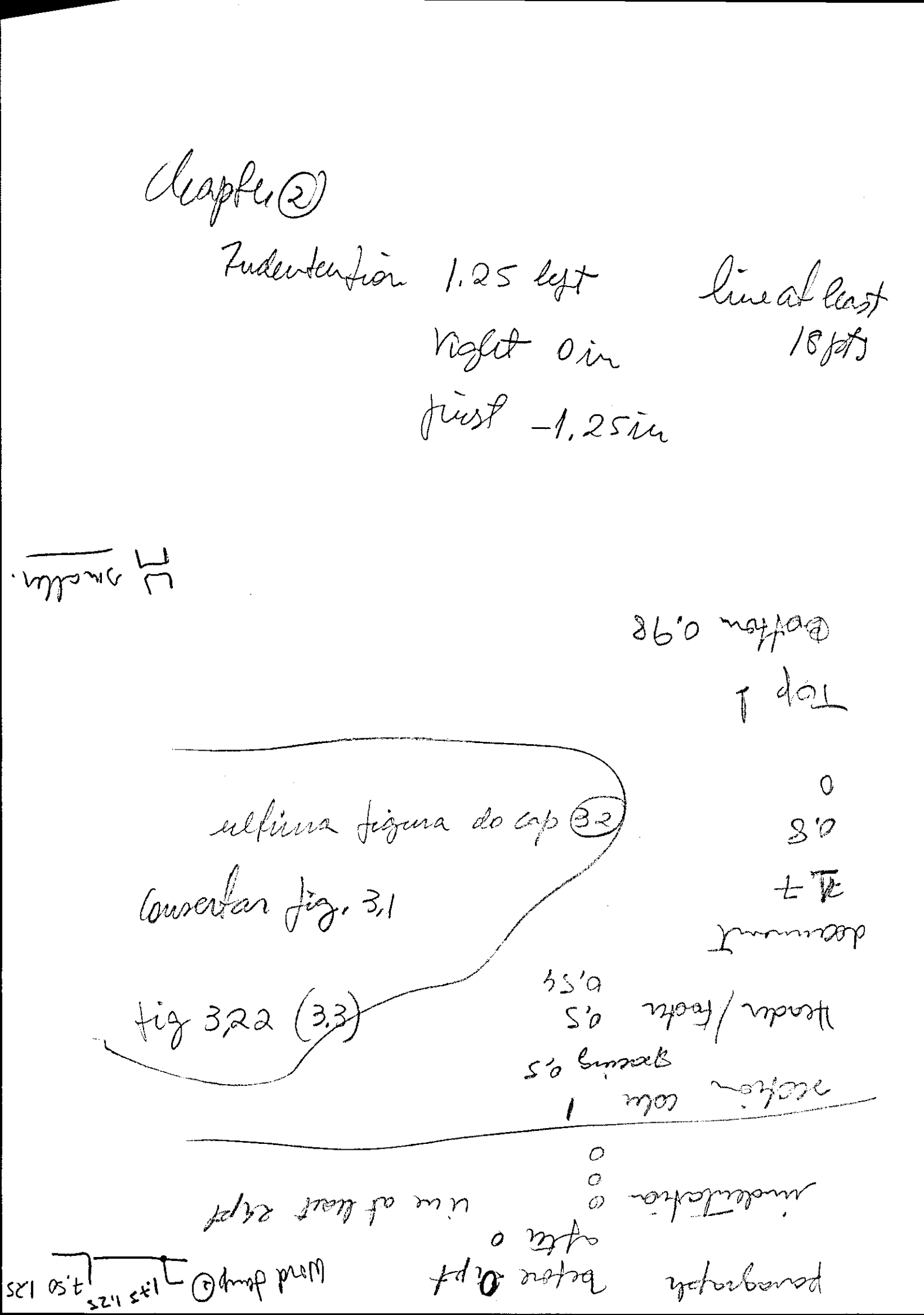

as shown in *Fig. 1.1(a)*. The acidified sample was injected through the septum cap at the top of the column and the resulting hydride was carried in the nitrogen stream out at the bottom of the column to the atomization cell.

Other metal-acid reactions have been investigated for the formation of covalent hydrides including Al powder and HCl [23] and a mixture of Mg metal and titanium(III)chloride reacted with HCl [24]. The major drawbacks of the metal-acid reaction were that it could only be used for As, Sb and Se and the long time required for the completion of the reaction, in some cases approaching 10 minutes. This kinetic feature prevented automation of the procedure.

The first reported use of the presently accepted HGAAS reduction system was published in 1974 by Thompson and Thomerson [11]. Methods for the determination of eight elements (As, Bi, Ge, Pb, Sb, Se, Sn, Te) were described. The hydrides were generated by adding the acidified sample to a dilute sodium tetrahydroborate (1% m/v) solution.

Hydride generation proceeds according to the following equation 1.2.2,

$$NaBH_4 + 3H_2O + HCl \longrightarrow H_3BO_3 + NaCl + 8H \xrightarrow{E^{m+}} EH_n + H_2 \qquad (1.2.2)$$

(m may or may not equal n) where E is the element of interest.

The $NaBH_4$ system was reported to give improved sensitivity over the previous zinc reduction system. The design of a typical batch hydride generation cell used for the sodium tetrahydroborate procedure is shown in *Fig. 1.1(b)*.

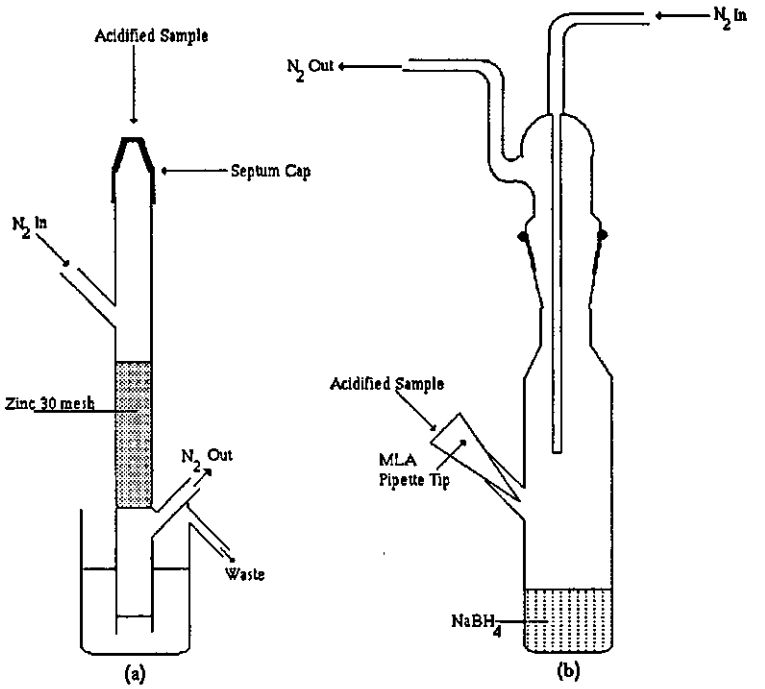

Fig. 1.1. Methods of Hydride Generation[11].

(a) Zinc column reduction unit.
(b) $NaBH_4$ reduction hydride generator cell.

The generation efficiencies and relative rates of formation for the sodium tetrahydroborate system have been studied by a number of groups [15, 22, 25, 26, 27], but have been restricted solely to the formation of hydrogen selenide. Hydride generation efficiencies have been determined through the use of a ^{75}Se radio tracer [15,25]. The rate of formation of the hydride has been investigated in most cases indirectly through measuring the rate of decomposition of sodium tetrahydroborate [26, 27]. The amount of undecomposed tetrahydroborate was measured by iodometric titration at intervals after the mixing of reagent with acidified sample. Sodium hydroxide was added to the reaction mixture, to stop the decomposition reaction, and permit the measurement of sodium tetrahydroborate concentration under static conditions. Direct comparison of the results from these investigations though is very difficult due to the variety of different hydride generation devices, varied reagent concentrations and system variables used. One of the most comprehensive studies of the hydride generation process to date was that made by Narsito *et al.* [27] in 1990. Reaction rates of the formation of hydrides and the

decomposition rate of the reducing agent sodium tetrahydroborate in alkaline and acidic media were studied in a continuous flow system. The hydride formation was assumed to be a simple second-order reaction of the type,

$$A^{n+} + BH_4^- \rightarrow AH_n \qquad (1.2.3)$$

where A^{n+} was the analyte used and AH_n the analyte hydride formed.

The formation rate constant k_f was therefore given by equation 1.2.4.

$$-\frac{d}{dt}[A^{n+}] = k_f\,[A^{n+}]\,[BH_4^-] \qquad (1.2.4)$$

Following the manipulation of equation 1.2.4 the formation constant k_f was simplified to equation 1.2.5,

$$k_f = -\,k_d \left(\frac{[H_3O^+]}{[B]}\right) \ln f \qquad (1.2.5)$$

where [B] was the initial molar concentration of $NaBH_4$, f the fraction of analyte left in the waste after reduction and k_d the decomposition rate constant for $NaBH_4$. A summary of the results obtained in the study are shown in Table 1.1. The concentration of $NaBH_4$ required for the conversion of analyte increased in the order $Sb^{III}<Se^{IV}<As^{III}<As^{V}$. The order of reaction rate was $Sb^{III}>Se^{IV}>As^{III}>As^{V}$. Evidence for the rapid rate of hydride formation was given by the observed rapid decomposition rate of $NaBH_4$. Agterdenbos and Bax [26] previously reported that $NaBH_4$ was completely decomposed within 10 ms of mixing with acidified sample, therefore, the hydride formation reaction time was assumed to be below 10 ms.

Table 1.1. Fraction of Sb, As and Se left in the liquid waste after hydride generation from Sb^{III}, As^{III}, As^{V} and Se^{IV} as a function of $NaBH_4$ concentration and the calculated formation rate constant k_f of the hydrides [27].

$NaBH_4$ % m/v	Fraction of Analyte in Waste (%)				log [k_f (mol dm^{-3} min^{-1})]			
	Sb^{III}	As^{III}	As^{V}	Se^{IV}	Sb^{III}	As^{III}	As^{V}	Se^{IV}
0	100	100	100	100	-			
0.001	12	-	-	96	12.4			10.7
0.01	3	-	-	59	11.6			10.8
0.02	2	-	-	37	11.3			10.7
0.05	1	47	94	14	11.0	10.2	9.1	10.6
0.10	0	30	82	2		10.1	9.3	10.6
0.20	0	17	53	0		10.0	9.5	
0.50	0	3	10	0		9.9	9.7	
1.0	0	0	0	0				

1.2.2 Methods of Hydride Generation.

There are two basic modes of hydride generation *(See Fig. 1.2)*. In the direct mode, hydride released from the sample solution is directly transported to the atomizer cell. In the collection mode, the hydride is collected until the evolution is completed and then released and transported to the atomizer.

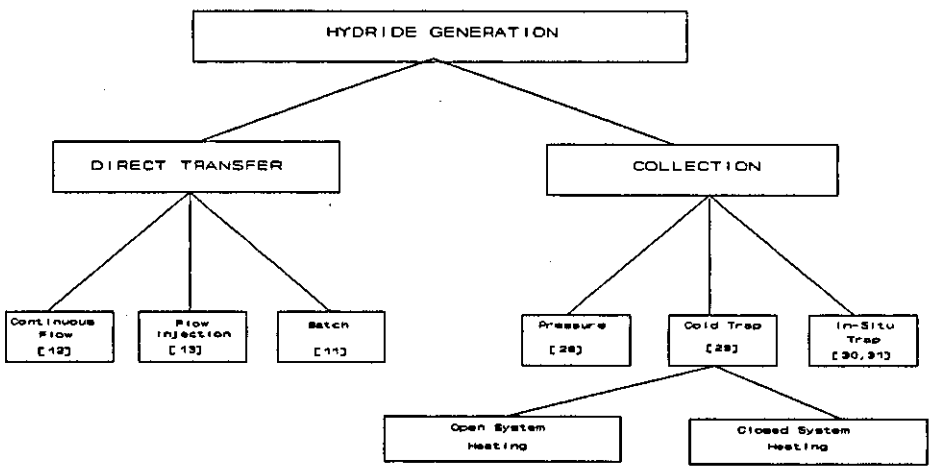

Fig. 1.2. Methods of Hydride Generation.

The direct transfer mode of hydride generation has been reported employing batch [11], continuous flow [12] and flow injection [13] methodologies.

In the collection mode pressure collection [28] or cold trap [29] procedures have been developed. In the pressure collection [28] approach the hydride released from the sample solution is collected under pressure together with hydrogen resulting from sodium tetrahydroborate decomposition. Cold trap collection [29] is carried out using a U-tube immersed in liquid nitrogen. Hydrogen passes through and is not collected. The trapped hydride is most often purged into an atomizer in an open system following evaporation in a heating bath (cold trap collection and open system heating) but it can also be evaporated in a closed volume of the collection device and purged into the atomizer after evaporation has been completed, (cold trap collection with closed system heating). The advantages of cold trap collection are that the hydride can be collected from a virtually unlimited volume of sample and the procedure is not limited by the kinetics of the formation and separation processes.

A third and most recent method of hydride collection is in-situ trapping in a graphite furnace [30,31].

1.2.3 Methods of Hydride Atomization.

In the first reported application of hydride generation to AAS by Holak [10] a conventional air-acetylene flame was used for the atomization of arsine. Since that first reported method a number of different flames have been used as atomization sources, including dinitrogen oxide-acetylene [32], argon-hydrogen [33] and nitrogen-hydrogen [34] flames.

The "flame-in-tube" atomizer was first reported by Siemer and Hagemann [35] in 1975. Excess hydrogen generated in the hydride generation process was used to carry the hydride to the T-shaped quartz tube. A small amount of oxygen was added to support combustion and atomization of the hydride. The "flame-in-tube" atomizer has since been reported with the application of oxygen-hydrogen [36] and air-hydrogen [37] flames. A diagram of the flame-in-tube atomizer used by Dedina and Rubeska [36] in 1980 is shown in *Fig. 1.3(a)*.

The externally heated quartz tube atomizer is probably now the most popular atomization procedure. Schmidt and Royer [38] first reported the use of a quartz furnace tube externally heated by an argon-hydrogen flame. Thompson and Thomerson [11] later applied the same procedure with a stoichiometric air-acetylene flame. A diagram of the

silica atomization tube is shown in *Fig. 1.3(b)*.

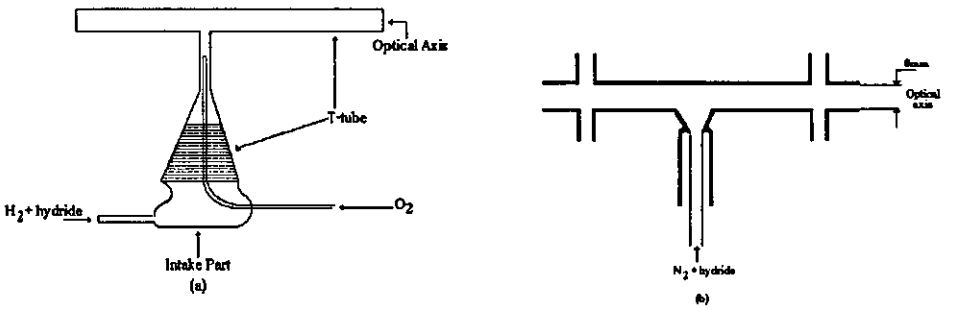

Fig. 1.3. Hydride atomization cells.

(a) The flame in tube atomizer [36]
(b) Externally heated silica atomizer tube [11].

The first reported application of electrical heating of the silica atomization tube was made by Chu *et al.* [39] and applied to the decomposition of arsine in an argon atmosphere. The advantages reported for the externally heated quartz atomizer over the argon-hydrogen flame were improved sensitivity due to a longer residence time of the atom cloud in the optical path and its lower dilution and much reduced noise levels.

More recently the use of graphite furnace atmoizers has been documented [30,31,40,41]. Use of this atomization procedure is increasingly becoming more and more popular, not only to achieve sample preconcentration [30,31] but as a means of overcoming mutual interferences among hydride forming elements that have hindered previous atomization methods [40,41].

1.3 INTERFERENCE EFFECTS.

1.3.1 Mechanistic Studies.

In most of the early published work on hydride generation, the technique was assumed to be interference free, making it superior to both FAAS and ETAAS. The assumptions were made generally without experimental evidence however and so, until the work of

Smith [14] in 1975, little was known about the limitations of the technique for the analysis of real samples.

Smith [14] made an in-depth study of the interferences of 48 elements in HGAAS, with a system based on a batch sodium tetrahydroborate reduction and an argon-hydrogen flame. From the study it was shown that copper, silver, gold, platinum, rhodium, ruthenium, nickel and cobalt (except for silver with germanium) interfered with the determination of all the hydride forming elements. Another observation made was that all the volatile hydrides formed interfered with all the other volatile hydrides, (except for the hydrides of bismuth and tellurium with those of antimony and selenium). Many of the elements that interfered formed precipitates or coloured solutions after the addition of $NaBH_4$. Smith postulated, therefore, that the preferential reduction of the metal ion interferent in solution to a different valency state or to the free metal could cause precipitation of that valency species that could either co-precipitate the metal of interest, adsorb the volatile hydride formed, catalytically decompose it or slow down or completely stop its evolution from solution. Another possibility considered was that due to the preferential reduction of the interferent, insufficient $NaBH_4$ was available for the generation of the hydride.

Following the work of Smith [14], Pierce and Brown [42] investigated the interference of a range of cations and anions in the determination of both As and Se, using an automated hydride generation system. An interesting observation was made that the degree of interference was highly dependent on the order of reagent addition. Addition of hydrochloric acid prior to sodium tetrahydroborate was shown to significantly improve the interference tolerance when compared with the reverse order of addition. In several cases, as reported by Smith [14], dark precipitates were observed. It was proposed that the interfering cations were competing with As and Se for the reducing agent. The decrease in interference observed with hydrochloric acid addition prior to sodium tetrahydroborate was explained by the increased solubility of the interfering cations.

The effect of acid on the interference of hydride generation was further studied by Kirkbright and Taddia [43]. In an investigation of the nickel interference on As, an increase in acidity appeared to decrease the interference observed. The reasons given for this were the more violent reaction of sodium tetrahydroborate and subsequent more rapid evolution of hydride at higher acidities and the increased solubility of the reduced metal in concentrated acid. Interference in the determination of As by Ni, Pt and Pd, all

hydrogenation catalysts, therefore capable of hydrogen absorption, was suggested to be due to the capture and decomposition of the evolved arsine by finely dispersed metal, as proposed by Smith [14]. Interference due to such mechanisms was shown though to be not applicable to all precipitated metals, due to the observed negligible interference in the presence of copper. The addition of copper powder (700 mg) during the hydride generation process produced only a 20% suppression of the observed As signal response.

Meyer *et al.* [44] in contrast to all previous work, in the determination of Se made no mention of any interferent precipitation. They proposed that the hydrogen selenide, after its generation, forms insoluble selenides or stable complexes with the free ions or the interfering metals in a secondary reaction when it is transported through the sample solution by the carrier gas. Interference was observed to be independent of analyte to interferent ratio but dependent on the final interferent concentration in the analysed sample. These workers also found that the transition metal interferences observed for Se depended very strongly on the acid concentration of the sample solution.

Welz and Melcher [45] investigated the mechanism of interference on Se of cobalt, copper, iron and nickel. Hydrogen selenide was passed directly through solutions of these cations. Only at high concentrations (above 10-100 $\mu g\ ml^{-1}$) was any significant interference observed. The mechanism of interference proposed was the formation of insoluble selenides or complexes between the hydrogen selenide and interfering ions, as postulated by Meyer *et al.* [44]. The severe interferences reported in all earlier work were postulated to be due to the capture and decomposition of hydrogen selenide by finely dispersed metal precipitate, obtained after sodium tetrahydroborate reduction of the cationic species. Evidence for the mechanism was provided by the substantial increase in concentration of the interferent which could be tolerated in the determination of Se at high acid concentrations, because of the increased solubility of the reduced metal as suggested by Kirkbright and Taddia [43] in the determination of As. The suggestion that inference was caused by competition of the interferent with Se for sodium tetrahydroborate [14,42] was dismissed on the grounds that the sodium tetrahydroborate was present in a large excess.

Yamamoto *et al.* [28] provided further evidence for the mechanism of interference proposed by Welz and Melcher [45]. On decreasing the sodium tetrahydroborate concentration, an increase in the concentration range of interference free determination of As was observed which was attributed to the selective reduction of As^{III} to AsH_3, over the interferent species, by the dilute sodium tetrahydroborate solution. These

observations clearly dismissed the proposed interference through competition for the reducing agent [14, 42].

Taking this work a step further, Welz and Schubert-Jacobs [46] investigated the influence of hydrochloric acid and sodium tetrahydroborate concentrations on the interferences in As and Se determinations. The proposed mechanism given for the reduction in interference with higher acid and lower sodium tetrahydroborate concentrations was that the interferent was reduced to a lesser extent to the metal owing to:

i. better solubility of the metal in concentrated acid;
ii. the formation of chlorocomplexes, thus reducing the concentration of free ions, and
iii. a larger percentage of sodium tetrahydroborate being consumed by acid.

In the case of copper interference on Se a decrease in interference was observed with increased hydrochloric acid and sodium tetrahydroborate concentrations respectively, contradicting all other observations. The interference mechanism in this case was reported to be the formation of relatively insoluble copper selenide as proposed by Meyer *et al.* [44]. Improved interference tolerance at high hydrochloric acid concentrations was explained by increased solubility of the selenide and the formation of chlorocomplexes. The increased interference tolerance with increased sodium tetrahydroborate concentrations was explained by two observations. Increased sodium tetrahydroborate concentration was reported to increase the rate at which the gaseous hydride diffused through the reaction solution to the gas-liquid interface, therefore, limiting its residence time and so the degree of copper selenide formation. A change in colour of the reaction solution to reddish was observed on the addition of sodium tetrahydroborate. This was postulated to be due to the reduction of Cu^{II} to Cu^{I}, resulting in a depletion in the relative concentration of interfering ions, particulary at high sodium tetrahydroborate concentrations.

In contrast to early proposals Bye [47] suggested that interfering bivalent cations in the determination of Se, actually reacted with sodium tetrahydroborate to form metal borides [48], which being highly reactive in character decomposed the hydrogen selenide. This proposal in many respects was rather speculative though since rather limited practical evidence was given in its defence. Only in the case of nickel was boron positively identified within the precipitate formed and no attempt was made to identify the stoichiometry of the metal boride in question. The proposal to a degree solely relied on

the observations of others and particulary the reported use of sodium tetrahydroborate in the synthesis of metal borides [48].

In 1986 Agterdenbos and Bax [26] proposed a further possible interference mechanism. In a study of the effects of cobalt, copper and nickel on Se^{IV} determination, observations were made indicating that the interference arose partly from the decomposition of sodium tetrahydroborate. Corrections to the mechanism proposed by Welz and Melcher [45] were outlined. It was postulated that the reaction between metal ions and sodium tetrahydroborate in several cases resulted in the formation of metal borides (as proposed by Bye [47]) and not simply a metal precipitate, which were in part attributed to be the cause of interference. No attempt was made though to prove the formation and identify any metal boride species. As in the work of Bye [47] the proposed formation of borides was based solely on the observations of others.

In further work Bax *et al.* [49] proposed that the decomposition of the sodium tetrahydroborate reagent was catalysed by interferent metal ions or their reaction products (metal and metal boride). This decomposition was so rapid that there was insufficient time for the reagent to convert the analyte completely into its hydride. A combination of the catalytic decomposition of sodium tetrahydroborate and the elimination of hydride by reaction products [26] was given as an explanation for the interferences observed. The mechanisms proposed by Meyer *et al.* [44] for interference in the determination of Se were dismissed with the exception of that for copper for which the authors were in agreement with Welz and Schubert-Jacobs [46]. On the basis of the proposed catalytic decomposition reaction the reported increase of interference with increasing concentration of sodium tetrahydroborate [46] was explained by the promotion of the formation of the metal borides. Independent evidence for the proposed catalytic decomposition mechanism [26, 49] was later provided by Aggett and Boyes [50]. The rate of hydrolysis of sodium tetrahydroborate was shown to be significantly increased in the presence of cobalt and nickel, but affected only slightly by copper. The interference mechanism was postulated to be determined by the method used for the determination of As^{III}. In continuous flow methods, acceleration of the hydrolysis reaction by cobalt and nickel was shown to be significant. In the manual method, however, the major contribution to interference was identified as being the loss of hydride after its generation as reported by others [14,44,45, 47].

Narsito *et al.* [51] later investigated the interference mechanism for the determination of Sb in the presence of cobalt, copper, iron and nickel. It was reported that the interference was at least partly due to the capture of analyte hydride by precipitate formed by the reaction of reagent and interferent [45]. No evidence for the catalytic decomposition of sodium tetrahydroborate reagent was given . This observation was explained by the fact that the reagent concentration was about 1000 times more than required for the complete formation of stibine. This reagent excess was significantly higher than that used in previous work [26,49].

In 1987 Aggett and Hayashi [52] made a comprehensive study into the interference of copper, cobalt and nickel in the determination of As^{III} and As^{V}. The previously proposed interference mechanism of arsine adsorption on metals [45,46] was rejected in favour of a new mechanism involving the formation of soluble species. The new mechanism was proposed in an attempt to explain the observations that, in the copper(II)-arsenic system precipitation occurred without interference whereas in the nickel(II)-arsenic system interference occurred without precipitation. Similar observations had been made in numerous earlier works but without full explanation [14, 43]. Evidence for the rejection of the arsine adsorption on precipitated metal interference mechanism [45,46] was obtained from the analysis data for the nickel precipitate, formed in a minute quantity. The arsenic content of the insoluble nickel precipitate was found to be only 6% of the arsenic present in the initial hydride generation reaction. This low percentage did not account for the observed 78% loss in signal response. Evidence for the formation of soluble interferent species was obtained by the observed quantitative arsine generation from the spent reaction mixture containing nickel, (waste reaction mixture after initial hydride generation process) after the addition of thiourea and a second volume of sodium tetrahydroborate. In conclusion it was suggested that lower oxidation states of nickel could form compounds with arsine which could exist temporarily during the early stages of reaction with sodium tetrahydroborate.

The effect of oxidation state on the interference of hydride generation was reported by two independent groups. Welz and Melcher [53] observed during the investigation of copper, iron and nickel interference on As that As^{V} experienced a higher degree of interference than As^{III}. This phenomena was explained by the slower formation of arsine from As^{V} in comparison with that from As^{III}, and therefore the more complete precipitation of the interfering metals by the time the hydride was formed. Castillo *et al.* [54] made similar observations in an investigation of the interference of iron, nickel, cobalt and copper in the determination of Sb^{III} and Sb^{V}.

1.3.2 Interference Removal.

1.3.2.1 Masking and Releasing Agents.

The use of masking agents to remove interferences associated with hydride generation is well documented. Belcher *et al.* [55] as early as 1975 reported the benefits of EDTA as a masking agent in the determination of As and Sb by molecular emission cavity analysis (MECA). The masking agent prevented or at least slowed down the reduction of the interfering ions and thus prevented the elimination of the generated hydride. As the generation procedure was common to both MECA and atomic absorption spectrometry, the releasing effect of EDTA was postulated to be equally applicable to AAS.

A thorough investigation into the use of masking agents to eliminate the interference on As was made by Peacock and Singh [56]. A study of KCN, KCNS, KF, dipyridyl, 1,10-phenanthroline, diethylammonium dithiocarbamate and thiourea showed that thiourea was the most effective masking agent. Thiourea has since been reported for interference reduction by other authors for the determination of As, Sb and Se in the presence of such interferents as cobalt, copper, iron and nickel [51, 52, 57]. Bye *et al.* [57] postulated that the beneficial use of thiourea in the reduction of copper interference in the determination of Se^{IV} was not solely attributed to its ability to form copper complexes but also the reduction of Cu^{II} to Cu^{I} by this reagent. Although the quantitative determination of Se^{IV} with up to 75 $\mu g\ ml^{-1}$ Cu^{II} was achieved a standard additions procedure was required to compensate for the reduction in sensitivity observed at that copper concentration, even in the presence of thiourea.

To date the application of numerous individual and combinations of making agents have been reported for interference removal in HGAAS. These masking agents include thiosemicarbazide [43], KI [50, 58, 59], KI-NH_2OH [59], KI-ascorbic acid [60], 1,10-phenan throline [43, 51, 56, 61, 62], citric acid [63] and L-cystine [64].

Welz and Melcher [65] in 1984 reported the use of iron(III) as a releasing agent for the elimination of the nickel interference on As and Se. The releasing effect was explained by the preferential reduction of iron(III) to iron(II) which inhibited the precipitation of the interfering nickel as the metal. The use of iron(III) as a releasing agent has subsequently been reported by others [66-68].

Welz and Melcher [69] studied the effect of copper on the interference of selenium(IV) in the determination of As^{III} and As^{V}. It was observed that copper at low concentrations prevented evolution of hydrogen selenide but not that of arsine, thus removing the mutual gas phase interference between Se and As hydrides. An identical approach was later applied to a flow injection system by Wang and Fang [70] in 1988.

Marshall and van Staden [71] reported the in-line addition of tellurium to overcome interference from noble metals using a flow injection system. The application of tellurium as a releasing agent was shown to be beneficial in decreasing the extent of the palladium interference on Se^{IV}, As^{III} and Bi^{III} and the platinum interference on Se^{IV}.

The use of masking agents although reported to be successful in the reduction of interference in HGAAS have a number of inherent disadvantages. As yet a universal masking agent capable of eliminating a wide range of interferences in the determination of hydride forming elements has not been reported, although thiourea goes some way to meeting this criteria [51, 52, 57]. The required introduction of additional steps of sample manipulation and the use of standard additions [57, 64] reported to be necessary for quantitative analysis, extends the length of analysis, therefore expense, over and above the cost of the chemical reagents themselves.

1.3.2.2 Matrix Isolation.

To overcome the major interferences of HGAAS a number of matrix isolation techniques have been reported. Bedard and Kerbyson [72] applied a co-precipitation procedure employing a lanthanum hydroxide collector, to the determination of Bi in copper. To reduce the copper concentration though to a level at which interference was eliminated a double precipitation was necessary. In later work, Bedard and Kerbyson [73] extended the co-precipitation procedure to the determination As, Se, Sn, and Te in copper. The multi-step sample preparation procedure outlined was manually undertaken, therefore, clearly tedious and time consuming if applied on a routine basis. Welz and Melcher [74] reported a matrix isolation procedure for the determination of Se in nickel based materials. Instead of co-precipitating the determinand, the nickel interferent was precipitated with sodium hydroxide and removed by filtration. In very recent work the same precipitation procedure was

applied to the determination of Se in both nickel and copper standard reference materials by Wickstrom et al. [75]. The detection limit of the method was approximated to 1 $\mu g\ g^{-1}$, but as appears to be the case in most reported precipitation methods [72-74], the procedure was rather slow and drawn out. Without any consideration of sample digestion the time required for the precipitation step of the method was reported to be in excess of an hour.

A novel method for the removal of copper interference in the determination of Se was reported by Bye [76] in 1985. The copper interferent was removed electrolytically from the sample solution using a traditional electrogravimetric method for the determination of Cu. The method reported although required a total sample preparation time in excess of 4 hours was successfully applied to the analysis of an unalloyed copper standard reference material (NBS 498).

Ion exchange as a means of matrix isolation for HGAAS was demonstrated by Jones *et al.* [77]. Acid digested plant and animal tissue sample solutions were passed down a Chelex 100 resin column manually. Trace elements including cadmium, copper, molybdenum, nickel, vanadium and zinc were quantitatively retained. The subsequent determination of unretained As, Se and Sb was reported to be interference free.

Narasaki and Ikeda [78] used a cation exchange resin Dianion SK1B and the chelate resin Chelex 100 for the isolation of both As^{V} and Se^{IV} from copper and nickel matrices. Recovery of As^{V} and Se^{IV} following the use of the cation exchange resin though was reported as being non-quantitative. The reason for this was postulated as being the mutual interaction between anion (AsO_4^{3-} or SeO_3^{2-}) and cation (Cu^{2+} or Ni^{2+}).

Narasaki [79] later applied the same Chelex 100 resin to the determination of As and Se in copper and nickel powders. Recoveries of As and Se added to copper powders though were observed to be non-quantitative without the application of masking agents. This was postulated to be due to the partial elution of copper from the resin due to the interaction between anions and Cu^{2+} as proposed in earlier work [78].

A thorough investigation into the use of ion exchange resins to reduce the inter-element interferences in HGAAS was carried out by Hershey and Keliher [80]. Three resins were investigated Chelex 100, Dowex 50WX16 and AG 50WX16 (purified Dowex 50WX16) for the determination of As and Se in the presence of the most

severely interfering elements, (Sb, As, Bi, Co, Cu, Ge, Sb, Mo, Pd, Pt, Rh, Ag and Te) identified in an earlier study [81]. In the analysis of real samples, such as coal fly ash leachates, the AG 50WX16 resin was found more beneficial than the Chelex 100 resin. For the Chelex 100 resin it was reported that nearly 75% of the arsenic present was lost on the resin. This effect was attributed to the chelating ability of the resin and the retention on it of arsenic complexes formed with certain metals. Other resins used for the removal of nickel and copper/nickel interferences in the determinations of Se and As respectively have been Muramac A-1 [82] and SCX [83].

1.3.2.3 Optimization of System Design.

Developments in HGAAS instrumentation from the original manual batch system [84] through automated [78] and continuous flow [85] systems to the flow injection [13, 86] methods, currently under study, have been reported which include a significant improvement in interference tolerance, (Table 1.2).

Table 1.2 Comparison of permissible levels[a] of interfering ions in the determination of Se^{IV} by various hydride generation techniques.

Interfering Ion	Manual Batch Method [84]	Automated Method [78]	Continuous Flow Method [85]	Flow Injection Method [86]
Cu^{2+}	30	2.5	50	1000
Co^{2+}	60	500	50	1000
Ni^{2+}	30	50	50	1000
Pb^{2+}	330	15,000	100	1000
Hg^{2+}	-	-	10	1000
Sn^{2+}	30	5	5	500
Bi^{III}	-	100,000	5	100
As^{III}	-	-	10	100
Sb^{III}	-	50	10	10

a Permissible amounts (mass ratio) correspond to the concentrations that give 10% or less negative error. [78] 8 ng ml^{-1} Se^{IV} [84-86] 10 ng ml^{-1} Se^{IV}.

Continuous flow techniques enabled optimization studies to be made of system interference tolerance. Variables such as reagent concentrations [13,87], order of reagent addition [42,87], manifold dimensions and pumping rates [13] were all reported to effect significantly the interference tolerance.

An explanation for the superior interference tolerance observed with FI-HGAAS [13,58,86,88,89] was first given by Astrom [13] in 1982 and confirmed later by other independent workers [86, 88, 89] due to the short residence time of the reaction mixture in the flow injection system. In 1989 Fang [90] reviewed and discussed the mechanisms proposed. It was concluded that the major reason for higher interference tolerance was the short residence time of the reaction mixture in the flow injection system, favouring the faster formation of hydrides, over the slower interfering reactions. Irrespective of the interference mechanism involved, reduction of the residence time was considered beneficial in decreasing the probability of contact of hydrides with interfering species, present in the system. A second reason proposed was the significant reduction in sample volume and therefore absolute amount of interferent introduced in FI-HGAAS [44]. With a smaller absolute amount of interfering species being introduced into the system, it was proposed that there was less chance for their accumulation in the reactor and separator and hence less chance of their contact with the hydride. Although the proposed mechanism was very feasible, evidence in its defense was restricted to the observations of Meyer *et al.* [44] reported for a batch hydride generation procedure. No systematic study of the effect of sample injection volume on interference tolerance in FI-HGAAS as yet appears to have been undertaken.

1.4 HYDRIDE ATOMIZATION AND GAS PHASE INTERFERENCE EFFECTS.

In 1980 Dedina and Rubeska [36] made one of the first in depth investigations into the mechanism of hydride atomization. The decomposition of hydrogen selenide in a cool, highly fuel-rich, hydrogen-oxygen combustion flame burning in the inlet of a T-shaped quartz tube was investigated. It was concluded that atomization proceeded most probably by two consecutive reactions with prevailing H radicals.

$$SeH_2 + H \rightarrow SeH + H_2 \quad (1.4.1)$$

$$SeH + H \rightarrow Se + H_2 \quad (1.4.2)$$

The formation of H radicals was proposed to have occurred within the reaction zone of the diffusion flame according to the following reactions 1.4.3-1.4.5.

$$H + O_2 \rightleftharpoons OH + O \quad (1.4.3)$$

$$O + H_2 \rightleftharpoons OH + H \quad (1.4.4)$$

$$OH + H_2 \rightleftharpoons H_2O + H \quad (1.4.5)$$

It was observed that the hydride was atomized with close to 100% efficiency at the inlet part of the atomization T-tube. The decay of selenium atoms was reported to start after entering the optical tube, mainly due to reactions on the tube walls. These reactions were observed to be affected by the quality of the quartz surface.

Using the same atomization procedure Dedina [15] later investigated the interference of other hydride forming elements in the determination of Se^{IV}. An interference mechanism scheme was proposed as shown in *Fig. 1.4* to outline the various interference reactions that could be observed both in the liquid and gas phases.

Arsenic, bismuth, tin and tellurium interfered strongly. Two mechanisms were proposed; the gaseous interferent accelerated either the decay of hydrogen radicals responsible for atomization or the decay of free analyte atoms in the quartz tube, either by modification of the surface or by direct vapour-phase reaction. Decreased gas-phase interference was achieved through control of the atomization conditions. A small T-cell gave better suppression of analyte decay interferences, negligible memory interferences and decreased direct interference, but at the expense of sensitivity. Analyte decay interferences were decreased further by increasing the hydrogen and oxygen flow rates, thereby lowering the probability of free analyte atom contact with the T-cell surface. As the quartz T-cell played no beneficial role in the atomization process and was identified as being responsible for interference effects Dedina [15] proposed that quartz could be replaced by other materials. No suitable replacement for quartz though was suggested.

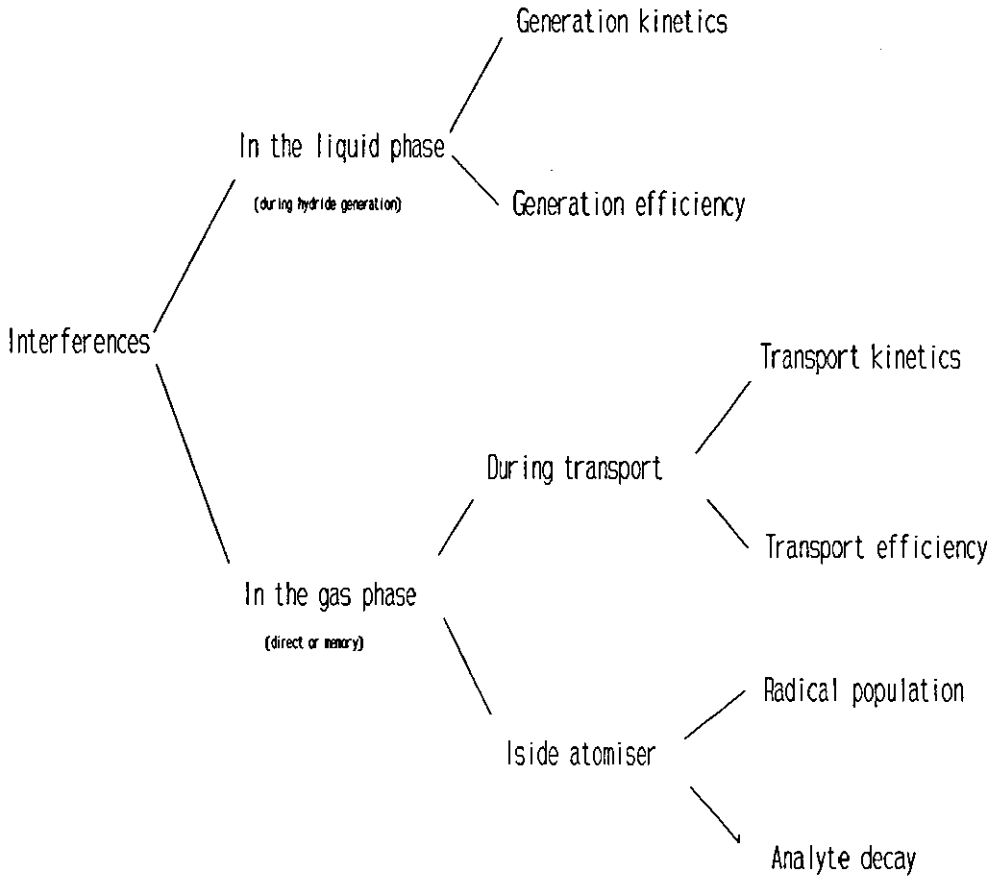

Fig. 1.4. Schematic diagram of possible liquid and gas phase interferences.

Welz and Melcher [91] later in 1983 postulated that the atomization mechanism proposed by Dedina and Rubeska [36] could be applied almost directly to the externally heated quartz atomizer. Atomization was proposed to be by interaction with hydrogen radicals, formed in a reaction with oxygen above 600°C (see equations 1.4.3-1.4.5) according to the following reactions.

$$MH_x + H \longrightarrow MH_{x-1} + H_2 \qquad (1.4.6)$$

$$\vdots$$

$$MH + H \longrightarrow M + H_2 \qquad (1.4.7)$$

Hydrogen radical formation was proposed through the decomposition of hydrogen molecules, bound at the quartz surface which had a strongly catalytic effect at temperatures around 1000° C. This active participation of the T-cell surface was used to explain the depressing effect on signal responses by surface contaminants, through decreased radical formation and increased radical recombination.

Although it was suggested that the externally heated quartz atomizer cell, in the presence of a small amount of air or oxygen, behaved in the same way as the flame-in-tube atomizer [36], the clear difference between the two was the different roles of the atomizer cell surface in the radical formation reactions. The lack of any involvement of the quartz cell in the formation of radical species in the flame-in-tube atomizer [36] may account for its more robust and efficient atomization performance in comparison with that reported for the externally heated atomizer cell [91].

In the absence of hydrogen AsH_3 was thermally decomposed in the heated quartz cell but not atomized. The species formed during the thermal decomposition was initially postulated to be As_2 and or As_4 but later formation of As_2O_3 was also proposed [92]. This decomposition product was re-volatilized and partly atomized on the introduction of hydrogen to the quartz cell.

Criticising the work of Welz and Melcher [91] evidence for the atomization mechanism proposed in many respects was rather limited. A lot of assumptions appear to have been made, based on the observations of Dedina and Rubeska [36] without quantitative support, as commented upon by Bax *et al.* [94]. Proof for the active participation of hydrogen radicals according to equations 1.4.6-1.4.7 for example was limited to the fact that radical scavengers had a severe depressing effect on signal response. No comment was made though to the fact that this observation could also have been explained by the assumption that radicals catalyse the atomization reaction, according to some other mechanism [96].

Agterdenbos *et al.* [93] studied the atomization mechanism of selenium in an electrically heated atomization T-cell. The formation of Se_2 and other polymeric species, predicted on the basis of thermodynamic calculations on the decomposition of SeH_2 into Se and H_2, was investigated. A test for the presence of Se_2 was the measurement of the light absorption at 334 nm, where Se_2 has an absorption band. The presence of Se_2 within the quartz atomization cell was shown by this method at high Se^{IV} concentrations (5 $\mu g\ ml^{-1}$ Se^{IV}) and increased residence times within the atomizer. In subsequent investigations similar dimer species were identified in the determination of As [96,97] and Sb [27].

Bax *et al.* [94] continuing the work of Agterdenbos *et al.* [93] dismissed the atomization mechanism proposed by Welz and Melcher [91] for selenium. The argument given against the mechanism was that the reaction required that the pressure of H radicals be at least twice as high as the pressure of SeH_2 molecules (approx. 10^{-7} atm). However, at T= 650 - 700°C atomization already occurred and at this temperature the equilibrium concentration for H, calculated from thermodynamic data for the $H_2 \rightleftharpoons 2H$ equilibrium, was about 100 to 100 times lower. The involvement of hydrogen radicals in the atomization mechanism was not rejected totally but were assumed to play more of a catalytic role in the decomposition of SeH_2. The presence of H_2 and O_2 was shown to be necessary for the decomposition of SeH_2, indicating a possible involvement of OH radicals [95]. A decrease in signal response though was observed at excessively high O_2 concentrations. This effect was explained by the possible inadequate concentration of essential radicals present under the experimental conditions or the formation of SeO_2, but no attempt was made to identify which.

For the decomposition of arsine, Bax *et al.* [96] rejected the mechanism proposed by Welz and Melcher [91] on the grounds of an insufficient concentration of hydrogen radical species as they had in the case of selenium [94]. Atom formation due to the thermodynamic decomposition of arsine according to reaction 1.4.8 was also rejected. Thermodynamic data predicted that atomization according to reaction 1.4.8 would not occur at temperatures below 800°C but experimental results showed appreciable atomization at 700°C.

$$2\ AsH_3 \rightarrow 2As + 3H_2 \qquad (1.4.8)$$

An atomization mechanism, catalysed by both H and OH radicals, was postulated (reaction 1.4.9).

$$4\ AsH_3 + 3\ O_2 \rightarrow 4\ As + 6\ H_2O \qquad (1.4.9)$$

Further evidence for this mechanism was later reported by Narsito and Agterdenbos [97]. In the presence of excess hydrogen addition of air, and therefore of oxygen, was reported to favour the formation of arsenic atoms in the cuvette. Parisis and Heyndrickx [98] independently reported the benefits of adding oxygen on sensitivity and precision in HGAAS, explained by the accelerated production of radicals.

In one of the most recent studies, Welz *et al.* [99] used mass spectrometry to identify active species in a heated quartz atomization tube, and therefore clarify possible atomization mechanisms. Products identified within the reacted quartz atomizer tube gave evidence for the equilibrium reaction (1.4.10) at 600° C and the back reaction (1.4.11) at 900° C.

$$AsH_3 + H \rightleftharpoons AsH_2 + H_2 \qquad (1.4.10)$$

$$2\ As + 3\ H_2 \rightarrow 2\ AsH_3 \qquad (1.4.11)$$

The formation of molecular arsenic species (As_2 and/or arsenic clusters) in agreement with the findings of Bax *et al.* [96] was detailed. These forms of arsenic were only retained in the heated quartz tube to a small extent and were reported to be transported over relatively long distances. Arsenic species containing oxygen were not detected in any of the experiments thereby eliminating the previously proposed formation of As_2O_3 [92].

The active role of the surface of the atomization cell in both atomization and analyte decay reactions has been reported widely [15,36,91,92,100]. Deteriorations in system performance through surface contamination by NaOH [44], Na_2SO_4 [101], interferent metal salts [46,49], hydrides [15,101,102] and other metals [91] have been reported. To overcome these contamination processes and optimize the atomization process a variety of different cleaning and conditioning procedures have been used. These procedures include acid washing [101], soaking in HF solutions [46,49,69,61,96,100,101,103], prolonged hydride introduction [49,93,100,103], prolonged heating at elevated temperatures [91,93], polishing with alumina [102] and scouring [101,102].

Agterdenbos and Bax [100] proposed that conditioning of the T-cell in many cases removes active sites on the silica surface and so prevents both the recombination of radical species and analyte dimerization.

Conditioning procedures have also been reported for the hydride generator [98,103,104]. In 1981 Reamer *et al.* [104] reported that, in the determination of Se^{IV}, performance was significantly affected by the choice of material used in the manufacture of the reaction vessel. Adsorption of selenium on glass and polypropylene was eliminated by conditioning the system with high concentrations of the hydride. It was proposed that available adsorption sites were filled deactivating the surface to further SeH_2 adsorption. The surface of the glass was also deactivated to SeH_2 adsorption by coating it with a silanizing agent (dimethyldichlorosilane).

The severe gaseous phase interference effects reported for both flame-in-tube and externally heated atomization cells [15,102] have not been observed for graphite furnace atomization [40,41]. Krivan and Petrick [41] reported an increase in the acceptable concentration range of interfering elements of up to three orders of magnitude using atomization temperatures of 1800 - 2300° C. At such temperatures atomization was achieved by thermal dissociation without any requirement for the presence of hydrogen radicals. Clearly for this reason the severe gas-phase interferences reported in both flame-in-tube [15] and externally heated atomizers [91], due in part to hydrogen radical decay were eliminated and the formation of diatomic molecules such as AsSe, AsSb etc. prevented [40]. Drawbacks of the use of graphite furnaces though, clearly evident from the work, were high background absorption, limited precision, relatively long process cycles (~ 2 minutes) and the rapid deterioration of the graphite tube furnace. The background absorption and deterioration of the graphite tube furnace were attributed to the reaction of water vapour and hydrogen, formed as byproducts of the hydride generation reaction, with the graphite tube furnace itself. Carbon monoxide and acetylene were postulated to be the reaction products for water vapour and hydrogen respectively. Akman *et al.* [105] reported that in the introduction of arsine into a graphite furnace the AsH_3 is decomposed on the graphite furnace wall before the atomization temperature is reached. The elemental arsenic is vapourized as As_4 which is then decomposed to As_2 and finally atomized by gas phase dissociation as shown in reaction scheme 1.4.12.

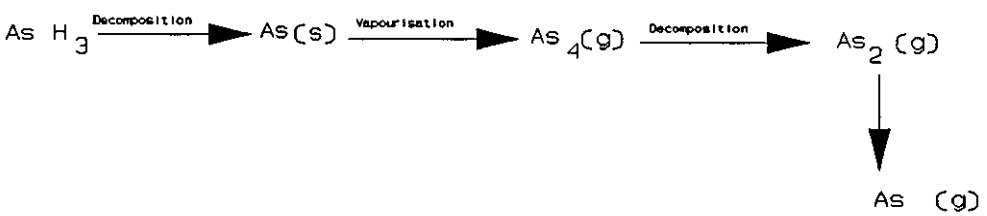

(1.4.12)

CHAPTER TWO
FLOW INJECTION ANALYSIS.

2.1 INTRODUCTION.

In the chemical laboratory any analytical measurement involving liquid materials comprises the following operations: solution handling, analyte detection, data collection and computation of results. Although today there is no shortage of computers and sophisticated detectors to aid the analytical chemist, solution handling in many cases is considerably outdated. Mixing, decanting, pipetting and other volumetric operations are still manual tasks and in many cases are carried out with tools designed more than 200 years ago. Irrespective of the quality of the detection system the accuracy, precision and speed of analysis is dependent on the dexterity of the analyst at carrying out the manual sample preparations. For many analyses, sample preparation is the rate determining step. Often skilled chemists are employed to carry out repetitive and tedious sample preparations thereby increasing analysis costs considerably. For the reasons discussed significant interest has been shown in the automation of analytical procedures particulary over the last three decades. Developments in the automation of such procedures have been reviewed in some depth [106, 107].

Attempts have been made to automate analysis through mechanisation of each manual sample preparation task, for which various approaches have been developed, including the use of robots. Robots, though, require extensive programming and, due to cost, are justified only if large numbers of repetitive operations are to be handled over prolonged periods.

A particulary successful approach for the automation of batch operations has been the use of flow operations which have been shown to be much easier to automate. Flow systems are easier to miniaturise and to control in space and time, since using closed tubing avoids evaporation of liquids, provides exactly repeatable paths through which measured solutions move, and provides a mechanism for the highly reproducible mixing of components and formation of reaction products.

A breakthrough in the automation of analytical methods was made by Skeggs [108] in 1957 with the introduction of 'segmented flow analysis' (SFA). Air-segmentation of the flow stream was used to overcome the sample carryover problems, previously reported in continuous flow analysis (CFA), whilst still retaining the benefits of flow operation.

The term "flow injection analysis" (FIA) was first introduced by Ruzicka and Hansen [109] in 1975. The technique has now gained widespread acceptance in academia and its use in the industrial community is increasing.

The subject of flow injection analysis has been covered in some depth since its birth in a number of reports and reviews, [110-118], five books [90,119-122] and the *Journal of Flow Injection Analysis* [123], published by the Japanese Association for Flow Injection Analysis since 1984 (Japanese). Along with published work a biennial conference concerned predominantly with flow injection development, "Flow Analysis", has been held regularly since 1979 [124].

2.2 PRINCIPLES AND INSTRUMENTATION.

2.2.1 Definition.

Flow injection, as defined by Ruzicka and Hansen [109], is based on the injection of a liquid sample into a moving, non-segmented continuous carrier stream of a suitable liquid. The injected sample forms a zone, which is then transported toward a detector that continuously records the absorbance, electrode potential, or other physical parameter as this continuously changes due to the passage of the sample material through the flow cell.

The essential features of FIA can be summarised as follows:

(i) The flow is not segmented by air bubbles, which is a fundamental difference from CFA methods.

(ii) The sample is injected or inserted directly into the flow stream instead of being aspirated into it.

(iii) The injected plug is transported within the system. A physicochemical process (chemical reaction, dialysis, liquid-liquid extraction, etc.,) may occur in addition to transport.

(iv) The partial dispersion or dilution of the analyte during transport operation can be manipulated by controlling the geometric and hydrodynamic characteristics of the system.

(v) A continuously sensing system yields a transient signal which is suitably recorded.

(vi) Chemical equilibrium need not have been attained when the signal is detected.

(vii) The operational timing must be highly reproducible because measurements are made under non-steady state conditions.

2.2.2 Instrumentation.

The basic FIA system (*Fig. 2.2.1*) consists of four major components. Although over the years the manifolds reported have become more complicated, in general they still contain these simple components.

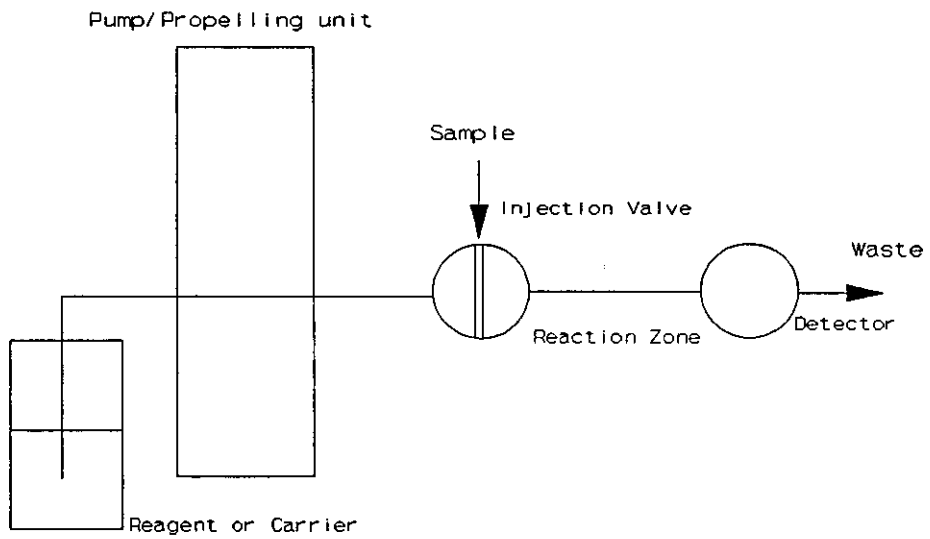

Fig. 2.2.1. Basic schematic diagram of a FIA system.

A propelling unit is used to produce a constant flow rate of either reagent or carrier solution. Peristaltic pumps are most commonly used for this purpose, but syringe [125] and gas-pressurised or constant head vessels have also been used [126,127]. An injection system is used to insert reproducibly an accurately measured sample volume into the carrier stream, without having to stop it. Methods of injection may be divided into two main categories: time and volume - based injection. In time-based injection, a sample is loaded for a precise time at a given flow rate [128]. Volume-based injection is the most common method of injection for which rotary valves [129], slider (or commutator) valves [130] and hydrodynamic injection [131] have been used. Timed injection benefits over fixed volume injection in that the volume of sample used can be controlled continuously through adjustment of either flow rate or sampling time, with ease and speed. Fixed volume injection as its name suggests generally is applied using a single predetermined injection volume. Control of sample volume is achieved in discrete steps through interchanging sample loops of different dimensions, but this is slow and tedious. A

benefit of fixed volume injection is its high precision since it is not affected by imprecision in sample pumping rate as is the case in timed-injection. Transport of the sample zone along an enclosed length of PTFE tubing (0.3-1.0mm i.d.) or channels in a polymethylmethacrylate (PMA) "chemifold" block enables chemical reaction, dispersion etc. to be performed reproducibly. A flow-cell, accommodated in a detector transduces some property of the analyte into a continuous signal which is fed into a recorder and/or microcomputer.

Increase in demand and interest in FIA has resulted, particulary over the last few years, in the production of a number of commercially available flow-injection analyzers. At present Tecator Control Equipment Corporation, Eppendorf (Fiatron), Hitachi Ltd and Lachat Instruments all produce FIA systems. A number of these include their own built-in UV/VIS and other detectors and specifically designed interchangeable manifold blocks, permitting a large number of different analyses to be undertaken.

More recently specifically designed flow injection systems for application to AAS have been introduced. Perkin-Elmer have introduced the FIAS-200, a fully automated computer-controlled system, designed for application to both FAAS and HGAAS. GBC Scientific have introduced a commercial unit for the analysis of samples containing high dissolved solids by FAAS applying flow injection.

2.2.3 FIA Signal Response.

The response of the detection unit of a FIA system is a transient signal peak (*Fig. 2.2.2*) of which height, H, width, W, and area, A, are related to the concentration of the analyte. The time span between sample injection, S, and the peak maximum is the residence time, T, during which dispersion and/or chemical reaction takes place.

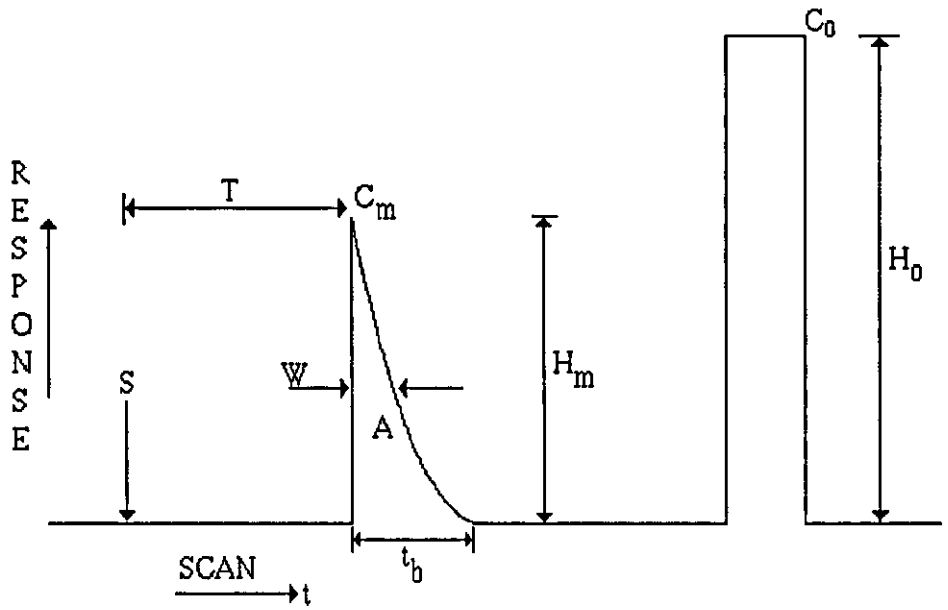

Fig. 2.2.2. Typical transient signal response peak for a FIA system (*Fig. 2.2.1*) compared with steady state instrument response.

H_o - height corresponding to steady state	C_o - original analyte concentration
H_m - peak height maximum	C_m - concentration at peak maximum
S - time of injection	T - residence time
A - peak area	t_b - peak width at base line

2.2.4 Sample Dispersion

When the sample zone is injected into a carrier stream it forms a dispersed zone whose shape depends on the geometry of the channel and flow velocity. In order to quantify the degree of dilution of the injected sample on its way toward the detector the term dispersion coefficient, D, has been defined [120] as the ratio of concentrations of sample material before and after the dispersion process.

$$D = C_o/C_m \qquad (2.2.1)$$

Where C_o is the original analyte concentration and C_m is the analyte concentration at peak maximum after dispersion, (*Fig. 2.2.2*).

If the instrument response is directly proportional to the analyte concentration,

$$D = A_o / A_m = H_o / H_m \quad (2.2.2.)$$

Where A_o, A_m, H_o and H_m are steady state absorbance, peak absorbance, steady state recorder height and recorder peak height respectively, (*Fig. 2.2.2*).

Through manipulation of flow velocity, sample injection volume and manifold dimensions the dispersion coefficient can be classified as follows [120].

1.	preconcentration	(D < 1)
2.	Limited sample dispersion	(D= 1-3)
3.	Medium sample dispersion	(D= 3-10)
4.	Large sample dispersion	(D > 10)

2.2.5 Benefits of FIA in comparison with CFA

Although FIA and SFA are both flow systems, there are significant differences between the two, accounting for the inherent advantages of FIA over SFA. A detailed comparison between the technical features of FIA and SFA is given in Table 2.2.1. The major difference between the two is the segmentation of flow by air bubbles in the SFA system. There is no need for air segmentation in FIA since the use of non-wettable narrow bore tubing eliminates sample carryover problems in FIA.

Table 2.2.1 Comparison of the technical features of SFA and FIA

Parameter	SFA	FIA
Sample introduction	aspiration	injection
Sample volume	0.2 - 2 ml	10 - 500 µl
Response time	2 - 30 min	3 - 60 s
Bore of tubing	2 mm	0.3 - 1.0 mm
Detection	at equilibrium (homogeneity)	with controlled dispersion
Sample throughput	≤ 80 h^{-1}	≤ 300 h^{-1}
Precision	1 - 2%	1 - 2%
Reagent consumption	high	low
Wash-out cycle	essential	not required
Continuous kinetic analysis	not feasible	stopped-flow
Data	peak-height	peak-height, area, width peak-to-peak distance.

Flow injection analysis is therefore more advantageous for the following reasons:

(i) More reproducible flow rates are achieved.
(ii) The apparatus required is uncomplicated, and hence inexpensive.
(iii) The system is readily miniaturised.
(iv) The sampling rate is high.
(v) The analytical potential and scope of application are very wide.

In SFA quantitative readings are made under steady state conditions (usually when at least 95% of the maximum signal has been attained) and the plug passing through the detector is homogeneous, resulting in a flat-topped signal response. In FIA on the other hand the plug is not homogeneous and equilibrium has not been reached by the time the measurement is made. Consequently less reaction time is required during transport to the detector in FIA and so a higher sample throughput is obtained with reduced reagent and sample consumption.

2.3 APPLICATIONS OF FIA TO ATOMIC ABSORPTION SPECTROMETRY

2.3.1 Introduction

The application of flow injection techniques to AAS, first reported in 1979 [132, 133], is generating widespread interest. The subject has now been reviewed in depth both in regular AAS reviews [5,6] and in more specific FI-AAS reviews [134-140]. A book directed solely to flow injection atomic spectroscopy was published in 1989 covering work reported prior to 1986 [90].

2.3.2 Discrete Nebulization and Flow Injection Performance.

The advantages of discrete nebulization over continuous nebulization was identified in the work of Cresser [141] as early as 1975. In addition to the obvious reduced sample volume requirement, the tendency of burners to clog during the analysis of sample containing high dissolved solids was eliminated, and the use of organic solvents was possible without the danger of the flame being extinguished or vast generation of toxic combustion products. Rocks *et al.* [142] later identified similar benefits for micro-volume sample introduction but reported FIA to be superior to discrete nebulization. Use of a continuously pumped aqueous carrier in the FI-FAAS system was shown to both remove erratic flame conditions and the effect of sample viscosity and aspiration rate on signal response, experienced with the discrete nebulization technique. The precision of the FIA technique was also shown to be superior to that of discrete nebulization. For discrete

nebulization the determination of Cu and Zn gave precisions of 4.4% and 8% respectively. In the case of FIA precisions were 2.1% for Cu and 1.7% for Zn. Superior precision achieved with the use of an aqueous carrier in FIA was subsequently confirmed by Attiyat and Christian [143] but at the expense of throughput.

In the literature opinions are divided as to the best operating conditions for the flow injection atomic adsorption spectrometry. Brown and Ruzicka [144] in a study of the sensitivity and precision of FIA showed that for optimum performance the rate of flow of the carrier stream pumped into the nebulizer should always be greater than the natural aspiration rate of the nebulizer. A further observation made was that sensitivity was a function of both the natural aspiration and FIA flow rate into the nebulizer. Precision obtained when a peristaltic pump was used to deliver the carrier was comparable with that of continuous aspiration.

Harnly and Beecher [145] following the work of Brown and Ruzicka [144] investigated the signal to noise ratio for FI-FAAS. The signal to noise ratio for FI-FAAS was compared with conventional nebulization for a number of sample volumes and flow rates. In conclusion to the work it was reported that by reducing the sample flow rate (with a constant nebulizer gas flow rate) an improvement in the nebulization efficiency of between 4 and 12 times could be obtained, in agreement with the earlier work of Wolf and Stewart [133]. Peak area signal to noise ratios were reported to be better than for peak height in every instance but increased with a reduction in flow and increase in injection volume. The signal to noise ratio for FI-FAAS peak height and peak area approached but never exceeded the ratio for conventional nebulization. FI-FAAS with peak area measurement achieved a detection limit for Cu only a factor at two worse than conventional nebulization but requiring just 13% of the sample volume.

In contrast to the work of Harnly and Beecher [145], Tyson *et al.* [138,146] reported that for best detection limits peak height measurements should be used and that the flow rate should be that at which the flow injection response is maximal and without air-compensation. Tyson *et al.* [138, 146] postulated that the confusion into the benefits of low flow rate, peak area measurement was possibly due to the individual nature of performance characteristics of atomic absorbtion nebulizers and spray chambers.

Confusion also appears to exist over the benefits of the application of air or solvent compensation to FI-FAAS. In one of the earliest reported studies Yoza *et al.* [147]

showed water and air-compensating methods to be effective in obtaining sensitive and reproducible measurements of Mg, but air-compensation gave higher peak responses. Garcia *et al.* [148] later showed that air-compensation improved sensitivity in FI-FAAS, particularly at low carrier flow rates, due to an increase in nebulization efficiency. The reproducibility obtained for peak height and peak area was comparable with that given by conventional FAAS. These results were not in agreement with the findings of Sweileh and Cantwell [149] who reported that use of air-compensation yielded a variable baseline and poor reproducibility of the AA Signal.

In addition to increased sensitivity Garcia *et al.* [148] reported with air-compensation a reduction in the phosphate interference on Ca as a result of greater nebulizer efficiency, therefore, higher rate of atomization. Similar observations were also made by Tyson *et al.* [146] and Adeeyinwo and Tyson [150] respectively. Fang and Welz [151] later though dismissed this proposed mechanism for the elimination of phosphate interference on Ca and attributed the observations to simply the dilution of interferent concentration, through sample dispersion, during transport to the nebulizer.

Fang and Welz [151] made a thorough investigation into the optimization of experimental parameters for FI-FAAS using the Perkin-Elmer 3030 atomic absorption spectrometer. Employing sufficiently large samples (~400 µl) it was shown that FI-FAAS systems could be optimized to operate at carrier flow rates much lower than the nebulizer uptake rate. In contradiction to Brown and Ruzicka [144], the use of pumping rates below the uptake rate of the nebulizer, without air-compensation, produced sensitivities, precisions and detections limits comparable with or slightly better than conventional nebulization. Air-compensation produced lower sensitivity but at low pumping rates it gave better precision than the non-compensating system. Although better precision was obtained at lower flow rates when air-compensation was used the detection limits were inferior compared with those obtained at higher carrier flows without air-compensation as reported by Tyson *et al.* [138, 146]. An interesting observation made by Fang and Welz [151] was the influence the presence of a flow spoiler had on results obtained. This gives further evidence to the critical role nebulizer and spray chamber design has on system performance characteristics for FI sample introduction, as proposed by Tyson *et al.* [138, 146].

In one of the most resent studies Fang *et al.* [152] extended the investigation into the optimization of experimental parameters for FI-FAAS [151] to the contribution of system components to dispersion. The use of short length ($\leq$ 150 mm) small bore conduits (0.35 mm i.d.) was reported to achieve signal responses relative to steady state analysis

of 90 and 98% for 45 and 65 µl sample volumes respectively. Precision and detection limits for Pb identical to those of conventional aspiration were also achieved using FI under optimum conditions. Peak area measurement was shown to give optimum detection limit at flow rates less than 2.5 ml min^{-1} only. Optimum detection limit overall was reported using peak height measurements at a carrier flow rate of 4 ml min^{-1} (35 µl, 0.09 µl ml^{-1} Pb, natural uptake rate 7.2 ml min^{-1}) in agreement with previous work [138, 146, 151]. The successful application of short, small bore conduits in the work of Fang *et al.* [152] it is suggested may though be limited in other systems simply due to physical dimension restrictions faced coupling the FI system to the spectrometer.

2.3.3 Dilution and Calibration

Since its conception the technique of flow injection has been shown to be very versatile particulary in the area of on-line sample dilution and novel calibration procedures. In 1988 Tyson [153] reviewed the subject of flow injection calibration techniques with particular reference to atomic spectroscopy.

Early concepts - One of the most beneficial features of FIA is its ability to produce reproducible sample dilution. Ruzicka and Hansen [120] have reported in depth on the control of sample dispersion through the manipulation of such parameters as injection volume and manifold dimensions. Tyson *et al.* [154] made similar observations for FI-FAAS. More recently McGowan and Pacey [155] extended investigation to large bore flow injection systems. Use of wide bore manifold tubing of diameters up to at least 1.3 mm permitted relatively high values of dispersion coefficient (D > 20, L = 300 mm, 1.3 mm i.d.). Rocks *et al.* [156], in one of the earliest applications of FI-FAAS to real sample analysis, used a dispersion coefficient of 12 for the determination of Li in serum. For the determination of Mg in serum, Rocks *et al.* [157] later reported a dispersion coefficient of 100 for a single line manifold (4 µl injection volume, 2 m 1.0 mm i.d. tubing, 3.5 ml min^{-1}).

Zagatto *et al.* [132] described a dilution system incorporating merging zones (*Fig. 2.3.1*). Merging the injected sample zone with an injected lanthanum reagent zone prior to a dispersion coil produced a 1:13 dilution. Splitting the flow before measurement directed only a fraction of the sample zone to the burner. A total dispersion coefficient of 40 was obtained for a sample throughput of 300 h^{-1}. Reis *et al.* [158] later reported a zone-sampling process capable of even high dispersion coefficients. The system described

(*Fig. 2.3.1*) involved sampling a small portion of a dispersed zone and injecting it into a second carrier, for which a dispersion coefficient of 130 and throughput of 120 h^{-1} was achieved. The proposed method was claimed to be more efficient in achieving a high degree of dispersion than the use of small injected volumes, long coils or even more complex systems. As for the system of Zagatto *et al.* [132] the performance of the system was clearly though critically reliant on exact timing, synchronisation of injections as well as smooth reproducible carrier flow, which is difficult without the use of expensive apparatus.

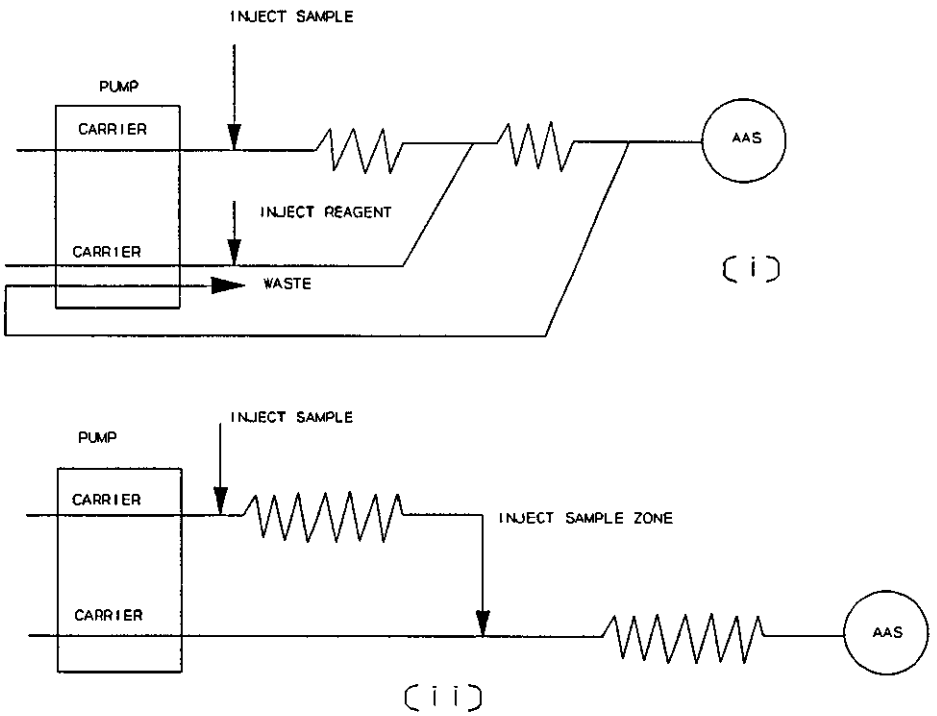

Fig. 2.3.1. Early FI systems used for on-line dilution.
(i) Merging Zone manifold [132]
(ii) Zone sampling manifold [158]

Network System - Tyson *et al.* [159] in 1986 described a novel network system capable of variable sample dilution and single standard calibration in FAAS. Dispersion coefficients ranging from 5.93 to 38.8 in six discrete stages were reported for replicate injections of 12.5 µl volumes into an aqueous carrier stream flowing down lines of different lengths (600 mm 0.7 mm i.d.- 2290 mm 1.1 mm i.d.). Single standard calibration was achieved simply by directing the injected stock standard down each of the lines in turn. Dispersion coefficient showed no dependency on the concentration and relative standard deviations ranged from 0.75 to 3.1%. Limitations of the procedure evident from

the work were though, the need for extensive calibration of dispersion coefficient for each manifold line and the requirement for accurate and precise control of carrier flow. A similar procedure was later applied by Tyson *et al.* [160] based on the system of Fernandez *et al.* [161]. The system worked on the division of the injected sample, with each sub-sample resulting from the division passing through reactors with different characteristics (dimensions) and the confluence of these channels before their arrival at the detector. A two-peak output (*Fig. 2.3.2*) was obtained as a consequence of the different residence times of each sub-sample, so different degrees of dispersion, producing three points of calibration. For the two maxima and the minimum between the partially overlapping peaks dispersion coefficient of 3.4, 20 and 77 were obtained. With the manifold a concentration range for magnesium of 0.2-100 $\mu g\ ml^{-1}$ was covered with a relative standard deviation of about 2%. A three branch network was also investigated but rejected due to observed fluctuations in flow rate which gave poor day to day reproducibility.

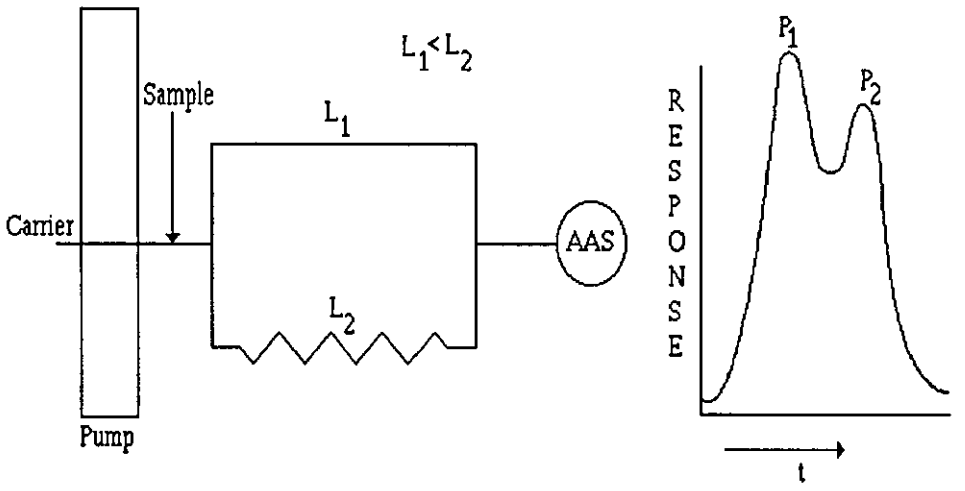

Fig. 2.3.2. Network manifold employed for splitting the sample zone [160].
P_1 peak from L_1, P_2 peak from L_2

Mixing chambers- One of the first reported applications of a mixing chamber in FAAS was made by Tyson *et al.* [162-164] following reported success in FIA with other detection systems [165]. A mixing chamber was used to obtain a concentration gradient

using a single concentrated standard solution. The basic system consisted of a water-filled ideally stirred tank, into which a stream of stock solution was switched to produce an effluent concentration, which was an exponential function of the time elapsed after switching.

The exponential concentration - time profile was described by the equation

$$C_x = C_m [1 - \exp (-ut^x / V)] \qquad (2.3.1)$$

where C_x is the effluent concentration at time t after the start of the concentration gradient, C_m is the concentration of stock calibrant solution, u is the flow rate and V is the volume of the mixing chamber. The absorbance - time profile was generated and then a sample was admitted directly to the nebulizer at the same flow rate as the calibrant and its absorbance was noted. By interpolation a corresponding value of t^x was obtained which was substituted into equation 2.3.1, giving the concentration of the sample. The continuous-dilution calibration procedure was reported to extend over the entire working concentration range of the analyte with an uncertainty of less than 1%. Subsequent use of similar mixing chambers have been reported with FI sample introduction [166, 167]. De la Guardia *et al.* [166] demonstrated the successful dilution of samples through the introduction of a discrete sample slug (100 µl) into a continuously stirred mixing chamber (827 and 2245 µl). A single standard calibration procedure was discussed using the trailing edge of a concentrated standard peak absorption profile and the exponential relationship between concentration and time (equation 2.3.1), as reported by Tyson *et al.* [162-164]. The system was successfully applied to the determination of Ca, Mg, Na and K in waters with a throughput of 180 h^{-1}. Beinrohr *et al.* [167] used a variable volume (0.1 - 10 ml) dilution chamber and varied sample injection volume to control dilution in the determination of Cu. The lack of any stirring mechanism within the dilution chamber though was reported to have no detrimental effect on system performance. Since peak area quantitation was used, it was reported that the significance of mixing efficiency was limited. An increase in the linear dynamic range of FAAS of 2-3 orders of magnitude was achieved with a reproducibility of 2-4%. No indication of throughput capability though was given.

On-line dilution systems - Following the successful early use of FI to obtain on-line dilution further more advanced systems have been developed. Bysouth and Tyson [168] demonstrated the use of a flow manifold for automated on-line dilution of standards for FAAS employing a null measurement method. The manifold (Fig. 2.3.3) was based on

a fixed-speed pump, together with a computer controlled stream switching valve and pump. Operating the fixed speed pump at 6 ml min^{-1} close to the natural aspiration rate of the nebulizer the diluent solution was pumped continuously into the nebulizer. The flow rate of standard delivered by the computer controlled pump, to be merged with the diluent flow prior to the nebulizer, was manipulated to give appropriate dilutions according to equation 2.3.2,

$$C^N = \frac{C^S \times F^s}{F^N} \qquad (2.3.2)$$

where C^N is the concentration of the standard solution produced, C^S is the concentration of the stock solution, F^S is the flow rate of the stock standard solution and F^N is the flow rate delivered to the nebulizer. The stock standard solution was automatically diluted by a known factor until its absorbance matched that of the sample. Limitations of the procedure were reported though due to problems with pulsations in flow caused by the peristaltic pump rollers and consequent difficulties in accurate flow rate measurements, an inherent draw back of the use of peristaltic pumps in on-line dilution procedures.

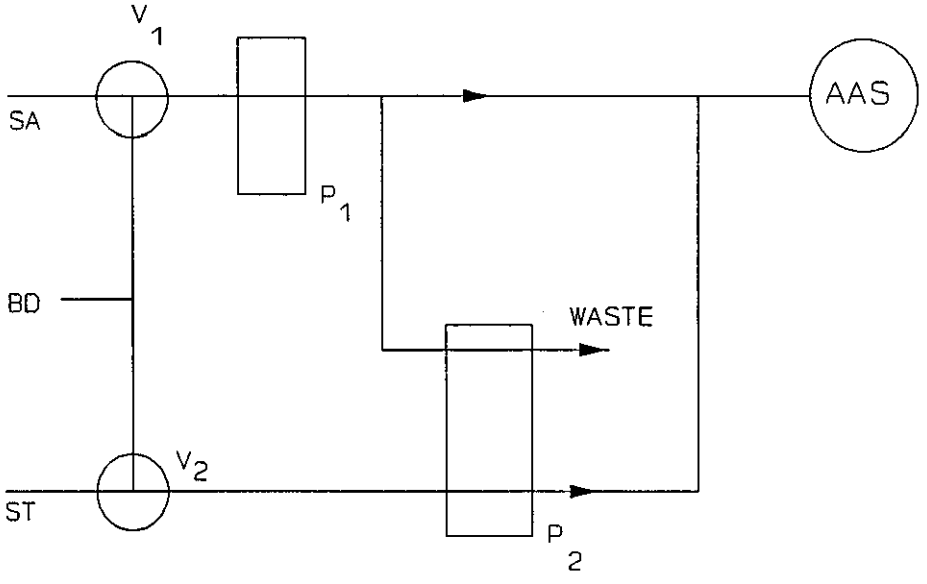

Fig. 2.3.3 Schematic diagram of manifold used in a null measurement method of on-line dilution [168].
P_1, Fixed speed pump; P_2, Computer controlled pump
V_1, V_2, Switching valves; SA, Sample
BD, Diluent; ST, Standard

Sherwood *et al.* [128] in 1985 developed a system called controlled-dispersion analysis (CDA) to capitalise on the inherent control of sample dispersion possible through varying sample volume and overcome the wasteful nature of sample injection in FIA. The new approach dispensed with the need for injection septa or valves. Sample was aspirated

into a probe or pump tube by the precise rotation of a peristaltic pump, driven by a stepper motor. The advantage of the CDA system was the almost infinite number of different injection volumes that could be used simply by altering the number of rotations of the peristaltic pump, during the sampling procedure. Injection volumes of between 2.5 and 200 µl produced dispersion coefficients of up to 80 for the manifold in question and permitted single standard calibration. The system was applied to the determination of Li, Mg, Zn, Cu and Ca with a precision of between 0.9 and 2.0% relative standard deviation and sample throughput of 120 h^{-1}. A similar time controlled variable volume injector was later reported by Burguera *et al.* [169], capable of injection volumes of between 4-62 µl with a precision of less than 0.9% (RSD). The system was applied to the determination of Mg by FAAS using a single standard calibration procedure.

Peak-width calibration - The first reported use of peak width measurement for quantification in atomic spectroscopy was by Stewart and Rosenfeld [165] who applied the method to AES in 1982. Tyson [170] later demonstrated the same procedure in AAS using the previously developed well stirred tank model [162-164]. The peak width of a FIA peak at any concentration was shown to be proportional to a logarithmic function of concentration according to equation 2.3.3,

$$t' = \frac{V}{u} \ln \left(\frac{C_m}{C'} - 1 \right) - \frac{V}{u} \ln (D - 1) \qquad (2.3.3)$$

where C_m is the concentration of the stock standard, V is the volume of a well stirred mixing chamber, u is flow rate and t^l the peak width at concentration, C^l. In subsequent work Bysouth and Tyson [171] demonstrated a microcomputer-based peak-width method to extend calibration for FI-FAAS based on the above expression [170]. All data collection and reduction was done on a microcomputer interfaced to the spectrometer. The method produced an estimate of concentration, without dilution, of off-range samples. To obtain a calibration, data was converted from time and absorbance to peak-width and concentration as in *Fig. 2.3.4.* Plotting the calibration data t^l vs $\ln[(C_m/C^l) - 1]$ made possible the determination of unknown off-range samples knowing both t^l and C^l. Calibrations covering the ranges 40-1000 µg ml^{-1}, 10-50 µg ml^{-1} and 20-1000 µg ml^{-1} were obtained for Cr, Mg and Ni respectively. Although the FI manifold was very simple the system was limited by the inadequate data acquisition rate of the microcomputer and poor reproducibility of the absorbance/time profile. Due to the logarithmic relationship between peak-width and concentration results showed a relatively poor precision of about 8% (RSD).

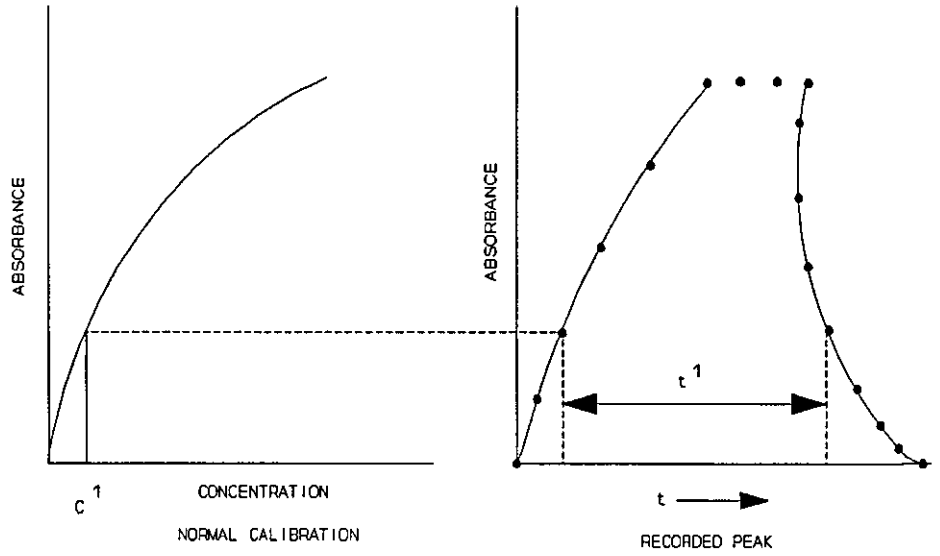

Fig. 2.3.4. Data conversion from time and absorbance to peak width and concentration in a peak width quantification method [171].

Electronic dilution and calibration- Sperling *et al.* [172] as recently as 1991 demonstrated a flow injection gradient ratio calibration procedure permitting calibration with a single standard in FAAS. The procedure was adapted from the previously reported concept of electronic dilution [173]. A computer run algorithm "CLAIR" (calibration graph linearisation and interfered signal reconstruction) was described, based on the calculation of the ratios of signal response for a reference solution and sample at delay times over the peak profile. Use of the CLAIR alogarithm was reported to significantly extend the linear working range of FAAS and correct for multiplicative matrix interference effects such as phosphate interference in the determination of Ca. The inherent advantage of the system was the necessity for only one standard reference signal to achieve calibration over the entire working range. Sophisticated computer data handing facilities though required for this process clearly were not cheap.

Standard addition methods - In 1981 Tyson [174] described a FI analogue of the standard addition method. The sample was used as the carrier stream into which standards of increasing concentration were injected. Standards of lower concentration than the sample were shown to give "negative" FI peaks and those of greater

concentration "positive" peaks (*Fig. 2.3.5*). A plot of ΔA vs the concentration of standard produced a plot which intercepted the concentration axis ($\Delta A = 0$) at the concentration of the unknown (*Fig. 2.3.5*). As the method was interpolative rather than extrapolative as in conventional calibration it was shown that the curve slope did not have to be linear. In later work the standard additions procedure was applied to the determination of Cr in steel [162, 163, 175] and Ca in iron ore [176]. Although simple and rapid a slight limitation of the procedure was the requirement, relative to other FI procedures of a high sample volume due to its role as the carrier. In the determination of Cr in steel [175] a sample volume in excess of 40 ml was used.

Modifications of the standards addition method of Tyson [174] have since been reported for use with flame photometry [177,178].

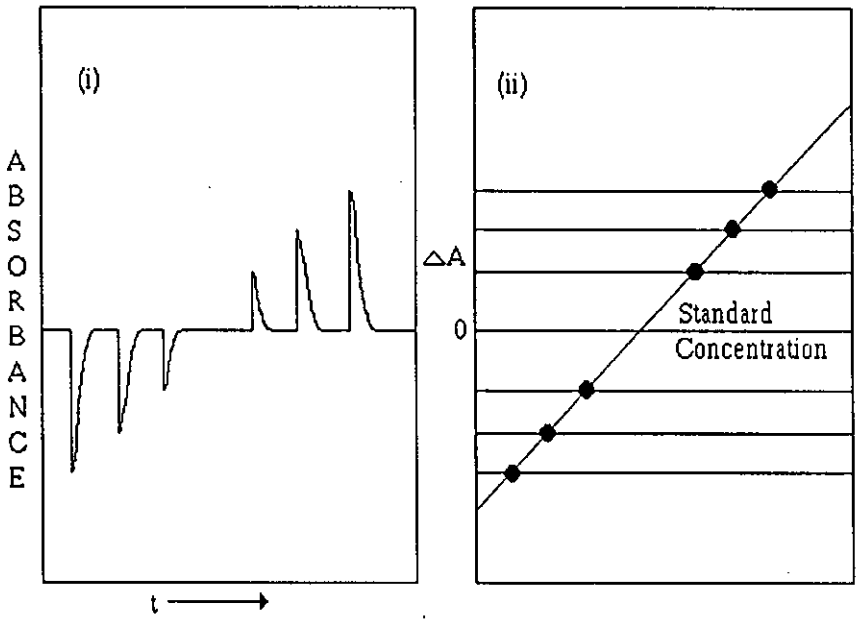

Fig. 2.3.5. Standard additions calibration method [175].
(i) Typical chart recording
(ii) Plot of ΔA against standard concentration.

2.3.4 Matrix Isolation and Preconcentration

A large number of publications, including review articles by Valcarcel and Luque de Castro [179] and Fang *et al.* [180] have appeared during the last decade describing the use of preconcentration in flow injection analysis.

Liquid-Liquid extraction- Liquid-liquid extraction has been reported in FI-FAAS for both preconcentration and matrix isolation and a number of studies have been made into its theoretical and practical development [181, 182].

In 1981 Nord and Karlberg [183] described a manifold which allowed continuous liquid-liquid extraction of aqueous solutions of metal ions. Sample was pumped continuously and mixed with ammonium pyrrolidinedithiocarbamate (APDC) solution. Segmentation of the stream by isobutyl methyl ketone (IBMK) with the aid of a segmentor was followed by extraction in an extraction coil. A substantial fraction of the organic phase was separated from the aqueous phase by a membrane separator and passed through the sample loop of an injector. For the determination of copper a preconcentration factor of 5.5 was obtained in comparison with direct aspiration of aqueous samples. The advantage of the procedure was that it allowed the extraction system to work independently of the nebulizer feed system which required a high flow rate (6.0 ml min^{-1}) to take full advantage of the FAAS sensitivity. The flow rate of the organic solvent in the extraction was less than 1 ml min^{-1}. Later Nord and Karlberg [184] applied the same system to the determination of Cu, Ni, Pb and Zn. Increases in sensitivity of between 15 and 20 time were achieved.

Extraction systems based on the design of Nord and Karlberg [183, 184] have subsequently been reported by other workers [180, 185] applying discrete nebulization. The organic sample was transported to the nebulizer either via the natural flow of air produced by the suction of the nebulizer [180] or by the use of an air carrier stream [185]. Improved sensitivity in comparison with the use of anaqueous carrier was reported in both cases, no comment was made though to the evident deterioration in precision expected from the observations of others [142, 143].

The use of liquid-liquid extraction FI-FAAS to eliminate interferences was first reported by Sweileh and Cantwell [149]. The determination of Zn in iron, which suffers from a spectral overlap of the Zinc line at 213.856 nm by a weakly absorbing iron line at 213.859 nm was achieved by selective extraction of Zn as $Zn(SCN)_2$ into IBMK.

The indirect determination of both perchlorate [186] and diethyldithiocarbamate [187], based on the use of previously developed extraction manifolds, have recently been reported. The two systems were based on the extraction and detection by FAAS of the copper(I)/6-methylpicolinealdehydeazine/perchlorate ion-pair and copper(II)/diethyldithiocarbamate complex respectively.

Solid phase extraction- The first reported on-line column preconcentration system was that of Olsen *et al.* [188] in 1983. A carrier solution of 0.06 mol dm^{-3} ammonium acetate into which a 1 ml sample was injected was pumped through a micro-column of Chelex 100 resin. Metals retained from the neutral media were released on the injection of 180 µl of 2 mol dm^{-3} HNO_3 solutions. The metals originally present in the 1 ml sample volume were therefore released into a much smaller volume of acid, facilitating preconcentration and transport to the nebulizer. Problems with resin swelling and column blocking experienced in a single-line manifold, were overcome by directing the preconcentration and elution steps in opposite directions through the column, in a two-line manifold. During the preconcentration step unretained sample matrix was pumped to waste rather than the nebulizer, so the necessity for any background correction was obviated. The work culminated in the development of a fully automated system for the preconcentration of Pb, Cd and Zn, capable of a sampling rate of between 30 and 60 h^{-1}. The use of Chelex 100 has subsequently been reported by other groups [189-191]. Lui and Ingle [189] demonstrated the use of complexing reagents such as cysteine and ethylenediaminetetraacetic acid (EDTA) as stripping agents to eliminate the resin swelling obtained with mineral acids. A stopped-flow technique was developed to allow complete elution of transition metals from the Chelex 100 resin that reacted more slowly with the stripping complexing ligands. Implementation of the stopped-flow elution step though must have contributed to the rather poor throughput capability reported. A typical analysis time of 2-3 mins was quoted to obtain enrichment factors in the range 6 to 8.

To improve the inherent low throughput capability, therefore, overall efficiency of early preconcentration systems, Fang *et al.* [190, 191, 192] developed dual column preconcentration systems. Two such systems were reported separately, employing simultaneous [190, 191] and sequential [192] sampling procedures for which the preconcentration efficiency was claimed to be twice that of a single column system. Further improvements in system efficiency were restricted though since the two columns were shown to produce different signal peak heights, due to variations in the tightness of packing materials. This observation indicated the need for the construction of separate calibration curves for each of the columns, therefore, an increase in total analysis times. Irrespective of these requirements in the determination of Co in water an enrichment factor of 48 was achieved at a sampling frequency of 60 h^{-1} [191]. Fang and Welz [193] in 1989 made further improvements in system efficiency with a, high efficiency, low sample consumption, on-line ion exchange preconcentration system. Conical ion exchange columns and short, small bore conduits were used to achieve a sampling frequency of

120 h^{-1} and low sample volume requirement of 1.6 ml per determination. Enrichment factors of 25-31 (CE = 50-61 EF min^{-1}) were reported for Cu, Cd and Pb with relative standard deviations of 1.2-1.8%.

Recently, Ruzicka and Arndal [194] demonstrated a system to facilitate the extraction of metals as their chelates from aqueous samples. The chelates were formed in the flow stream, sorbed on C-18 bonded silica and then eluted with methanol. The proposed method was shown to be useful for the preconcentration of Cu and Pb by means of chelation with diethyldithiocarbamate or 8-quinolinol. The importance of the findings made was not though the degree of preconcentration achieved but an indication that the method would permit the development of truly selective methods of analysis. Fang *et al.* [195] later applied the same methodology to the determination of Cd, Pb and Cu in samples using diethylammonium diethyldithiocarbamate chelating agent.

With the growth of interest in on-line preconcentration numerous other different resins and active groups attached to a variety of supports have been employed in AAS. These include N,N,N^{l}-tri(2-pyridylmethyl)ethylenediamine (Tripen) [196], 8-hydroxyquinoline derivatives [197-203], activated alumina [204, 205] and poly(hydroxamic acids) [206].

The use of solid phase extraction has been shown to be beneficial in speciation work. Pacey and Bubnis [207] in one of the first applications used Dowex 1 anion exchange resin for the speciation of Fe^{II} and Fe^{III}. Procedures for the speciation of free and EDTA complexed copper ions [208], Cr^{VI}/Cr^{III} [209] and V^{IV}/V^{V} [210] have subsequently followed.

Along with preconcentration, solid phase extraction procedures have been reported for interference reduction in AAS with some success. Kamson and Townshend [211] used an Amberlite IRA-400 ion exchange resin filled column for the removal of phosphate, sulphate and silicate interferences in the determination of Ca. Attempts to remove the interference of aluminium by its conversion to hexafluoroaluminate and removal on the same anion exchange column were though unsuccessful.

More recently a variety of resins have been applied to the elimination of interferences in FI-HGAAS including AG50W [71], Muromac A-1 [82] and SCX [83]. These are to be discussed in more detail in section 2.3.5.

A significant breakthrough made over the last couple of years, concerning on-line solid phase preconcentration and matrix isolation in AAS has been its successful reported application to ETAAS [212-215]. This combination has previously not been possible due to the absence of technology to permit the coupling of relatively high flow rates used in FIA (ml min^{-1}) to the batch operated ETAAS system.

Sperling *et al.* [215] in one of the most recently reported pieces of work described an on-line preconcentration system for the determination of ultratrace amounts of Cd, Cu, Ni and Pb in water samples by ETAAS. The sorbent extraction method used was based on that reported previously using a 15µl conically shaped micro-column of C-18 bonded silica [195]. Metal diethyldithiocarbamate chelates were formed on-line, loaded onto the column for 60 s (3 ml min^{-1}), washed with 0.02 % v/v HNO_3 and then eluted with ethanol using a 'time based' technique. The eluate pump was activated for a clearly defined time interval in order to transfer a 40 µl segment of the total sample eluate volume (200 µl) directly into the furnace. Precise timing ensured that only the centre of the eluate bolus was sampled. A complete cycle of preconcentration and eluate introduction into the furnace, consisting of seven stages took 145 s. Using this procedure for the preconcentration of a sample volume of 3 ml the sensitivity of the graphite furnace technique was enhanced 20 fold compared with a 40 µl injection volume. Detection limits achieved were 0,.8, 6.5, 17 and 36 pg ml^{-1} for Cd, Pb, Cu and Ni respectively. Results presented indicated the successful analysis of water samples, including sea water, without any matrix interference effects.

On-line precipitation - A preconcentration procedure for the determination of trace amounts of lead by continuous precipitation was demonstrated by Martinez-Jimenez *et al.* [216] in 1987. The procedure was based on previous methods for the indirect atomic absorption determination of chloride [217-219], iodide [218], hydroxide [219] and oxalate [219]. A 10-250 ml volume of sample containing 0.3-15 µg of Pb at pH 0.5-6.0 was continuously pumped and mixed thoroughly with the precipitating reagent (1.5 mol dm^{-3} ammonia). The precipitated basic salt formed was retained on a stainless-steel filter before being dissolved in a stream of 2 mol dm^{-3} nitric acid, producing a signal response proportional to sample concentration. Although the system was successfully applied to the determination of Pb in water samples the use of masking agents was found necessary to eliminate the interferences of both iron and sulphide. In comparison with solid phase extraction [195] the system performance characteristics were significantly inferior. To achieve a detection limit of 3 ng ml^{-1} of Pb a throughput of 4 h^{-1} (sample volume 50 ml) and precision of 2.8% (100 ng ml^{-1}, n= 11) were quoted. These findings compared with

a throughput of 120 h^{-1} (sample volume 1.4 ml) and precision of 1% (200 ng ml^{-1} Pb, n=11) for the solid phase extraction method [195].

Debrah *et al.* [220] later reported a similar procedure for the preconcentration of Cu through the precipitation of its hydroxide and subsequent collection on a cellulose acetate membrane filter. A detection limit of 0.01 μg ml^{-1} of Cu (sample volume 11 ml) was obtained compared with 0.1 μg ml^{-1} for normal aspiration.

Along with preconcentration on-line precipitation has been successfully applied to interference removal through matrix isolation. Adeeyinwo and Tyson [150, 221] demonstrated one such method for the removal of aluminium interference in the determination of Ca. A two line manifold was developed in which calcium was precipitated as its oxalate and retained on a membrane filter, prior to dissolution by hydrochloric acid. In later work, after manifold optimization an enrichment factor of over 650 was obtained and the interference free determination of Ca (10 μg ml^{-1}) in the presence of aluminium at concentrations up to 1000 μg ml^{-1} was achieved [220, 222].

In recent work the use of glass bead filled and knotted rector coils [223, 224] have been shown to be an efficient alternative to the use of membrane filters. Fang *et al.* [224] demonstrated a procedure for the co-precipitation of lead with the iron(II)-hexahydrozepinium hexahydroazepin-1-ylformate (hexamethyleneammonium hexamethylenedithiocarbamate) complex. The precipitate was collected in a knotted rector (150 cm x 0.5 mm i.d.) then dissolved in IBMK. A detection limit of 2 ng ml^{-1} of Pb was achieved with a sampling frequency of 90 h^{-1}. These figures were significantly superior to the earlier work of Martinez-Jimenez *et al.* [216]. The method was also reported to be able to tolerate up to 2500 μg ml^{-1} of iron in the sample solution indicating its further superiority. Efficiency of the system in comparison with on-line filter devices was postulated to be due to the minimisation of dispersion.

Novel preconcentration methods- Along with the procedures already reviewed two very novel methods of preconcentration have been demonstrated through the use of electrochemical potentiometric stripping [225] and Donnan dialysis [226]. Although both procedures achieved high enrichment factors their major limitation was very poor throughput capability. Electrochemical preconcentration permitted in the determination of Pb an enrichment factor of 30.4 but with a corresponding throughput of 12 h^{-1}. In the case of Donnan dialysis in the determination of Cu 100 fold enrichment factors were reported for dialysis times of the order of 5 minutes.

2.3.5 Flow Injection Hydride Generation Atomic Absorption Spectrometry.

Since 1982 the technique of flow injection hydride generation atomic absorption spectrometry (FI-HGAAS) has been researched in depth by many groups as a means of overcoming the limitations of HGAAS. Recently, a review of the subject was made in a book covering the subject of flow injection and its applications to atomic spectroscopy [90]. Particular interest into the technique has been shown by many Chinese groups. A percentage of the work published therefore is only available in Chinese, limiting the amount of information that can be attained and making a truly comprehensive review difficult.

Development- The technique of FI-HGAAS developed from previous continuous flow systems which had evolved to overcome the tedious, slow and operator intensive nature of manual batch methodology.

The first reported automated continuous flow system was demonstrated by Vijan and Wood [12] in 1974. A continuously pumped sample was merged with an air-segmented sodium tetrahydroborate reagent stream and Ar carrier gas, then passed through a reactor coil to the gas-liquid separator. A novel U-tube gas-liquid separator was used which allowed the aqueous reaction products to be drained to waste and the gaseous hydride to be transported by the Ar carrier gas to the electrically heated quartz atomization cell. The system was applied to the determination of As in atmospheric particulate matter, but results for the determination of Sb, Bi and Se were also given. Introduction of an air-line in the manifold was reported to increase sensitivity as well as smooth the peak shapes. A sensitivity of 1 ng ml^{-1} was achieved in the determination of As for a sample volume of 4 ml. The most attractive feature of the system was its automatic, unattended operation which permitted the analysis of twenty samples in an hour. The same system was later applied to the determination of Sn [227] and Pb [228] respectively. For the determination of Pb no air-segmentation was used in the manifold. On-line addition of masking agents (KCN, citric acid) was used to improve interference tolerance.

Other continuous flow analyzers have subsequently been reported by other groups, many based on the system of Vijan and Wood [12], for the determination of As [85, 87, 229] and Se [85] by HGAAS and Hg [230] by cold vapour atomic absorption spectrometry (CVAAS). Continuous flow hydride generation has been combined with a variety of hydride collection and preconcentration procedures including pressure

collection [78] and cryogenic trapping [231-233].

The first application of FIA to hydride generation was reported by Astrom [13] in 1982 for the determination of Bi. A 700 µl sample solution was injected into a continuous flowing stream of hydrochloric acid. After reaction with $NaBH_4$ solution in a mixing coil the reaction mixture was merged with a nitrogen stream and the evolved hydride swept from a miniaturised version of the gas-liquid separator, reported by Vijan and Wood [12], into an electrically heated quartz tube. The dimensions of the miniaturised gas-liquid separator were though not included in the paper. The FIA system was reported to permit the interference free determination of Bi with about 100 to 1000 times higher concentrations of interferents in comparison with previous systems [42]. The superior interference tolerance was attributed to the controlled short reaction time favouring the main hydride generation reaction (Section 1.3.2.3). Evidence for this postulation was given by an observed reduction in interference with both reduced rector coil length (cobalt, copper, nickel) and increased pumping speed (cobalt). A rather critical absence from the paper though was the actual carrier and reagent flow rates used in the manifold. At a sample throughput of 180 h^{-1} the relative standard deviation was 0.8% for a solution containing 30 ng ml^{-1} of Bi with a detection limit of 0.08 ng ml^{-1}, for the optimum conditions with respect to the suppression of interference effects. These figures were a significant improvement on those reported by Thompson and Thomerson [11] who used a manual batch HGAAS method. For the system in question a relative standard deviation of 3.9% (100 ng ml^{-1} Bi, n = 10) and detection limit of 0.2 ng ml^{-1} (sample volume 1 ml) were achieved.

Yamamoto *et al.* [88] in 1985 reported the so called use of FIA in hydride generation. When considering though the definition of FIA [109] their system does not comply truly since it employed a gas-segmented carrier stream. The gas segmentation process was reported to be effective in minimising broadening of the sample zone and increasing sensitivity in the determination of As, Bi, Sb, Se and Te. A rather uncharacteristic feature of the manifold was that the nitrogen carrier gas was actually added prior to $NaBH_4$. High interference tolerance was reported for the system and explained by the mechanisms proposed by Astrom [13]. No consideration was paid though to the fact that potassium iodide was added in the determination of As and Sb to permit the in-line pre-reduction of As^V and Sb^V to As^{III} and Sb^{III} respectively. As later proposed by Pacey *et al.* [58] the high interference tolerance reported for the system must be due, in part, to the presence of KI and its action as a masking agent [59].

The beneficial coupling of FIA to HGAAS was further documented in the work of Fang *et al.* [86]. In the determination of Se a detection limit of 0.06 ng ml^{-1} Se^{IV} was reported for a 400 µl sample volume, giving a far improved absolute detection limit (2×10^{-11} g Se) over that of the manual batch method used previously. The benefits of reduced reagent consumption and superior interference tolerance were also shown. Wang and Fang [67, 70, 234] in later work miniaturised the gas-liquid separator which was based on the initial design of Vijan and Wood [12]. The internal diameter of the separator bulb was decreased from 20 to 15 mm to increase sensitivity in the determination of As[70] and Se[67, 234].

Ikeda [235] in 1985 described a pseudo FI type system for the determination of As, which was entitled "miniaturised suction-flow hydride generation". A 300 µl sample solution was dropped into a PTFE sample suction cup and pumped into an alkaline sodium tetrahydroborate stream which was acidified in a reaction coil. To prevent air entrainment a stream of argon was passed over the inlet of the sample suction cup, producing gas segmentation of the carrier stream. For this reason the system cannot be truly defined as using flow injection, as in the case of the system of Yamamoto *et al.* [88]. Addition of sodium tetrahydroborate prior to hydrochloric acid and the use of an optimized reactor coil length of 1000 mm (3 mm i.d.) was shown to eliminate the difference in sensitivity between As^{V} and As^{III} without any pre-reduction by potassium iodide. These system variables may though account for the rather poor interference tolerance of the system relative to other FI systems [58,88] and, therefore, the requirement for the in-line addition of potassium iodide and hydroxylamine interference suppressants in the analysis of low alloy steel standard reference materials.

Membrane gas-liquid separators- A major development in FI-HGAAS was made by De Andrade *et al.* [236] in 1983 with the development of a PTFE membrane phase separator for use in CVAAS. The device was based on the permeability of PTFE tape to mercury vapour. Mercury vapour was formed in a carrier stream on one side of the PTFE membrane which then diffused directly into the absorption cell positioned in the light path of the spectrometer. A sampling rate of 110 h^{-1} was obtained and a detection limit of 1.4 ng ml^{-1} of Hg. Fang *et al.* [86] later modified the membrane phase separator through the inclusion of a nylon gauze to reinforce the PTFE membrane and optimization of separator dimensions, following which a detection limit of 0.06 ng ml^{-1} of Hg was attained. This value was observed though to be no better than that achieved with a miniaturised U-tube gas liquid separator[12]. Fang *et al.* [86]

reported that although the membrane phase-separator gained sensitivity by eliminating the large dead volume of the conventional gas-liquid separator, it lost sensitivity through the incomplete transport of mercury through the membrane. Other FI-CVAAS methods have subsequently been reported with the application of various gas-liquid separator designs [237,238].

One of the first reported applications of a membrane gas-liquid separator to FI-HGAAS was made by Pacey *et al.* [58] in 1986. In the dual phase gas diffusion system (GD-FIA) described a liquid phase donor stream containing sample was passed on the underside of the membrane with a stream of gas (H_2 (g)) on its reverse side (Diffusion area 70 mm^2). The gaseous analyte was therefore passed through the membrane into the gas stream and transported to the detector. In the determination of As, the system although capable of a sample throughput of 180 h^{-1} exhibited a relatively poor detection limit of 10 ng ml^{-1} As. This value compared with 0.08 and 0.2 ng ml^{-1} reported earlier by Ikeda [235] and Yamamoto *et al.* [88] respectively. Increase in the size of the gas-diffusion channel to permit the use of larger sample sizes and the use of stopped-flow, to increase diffusion efficiency, was postulated though to possibly reduce this figure. System interference tolerance was quoted to be superior to previously reported continuous flow methods. Some confusion appears to exist though since the performance data tabulated does not agree with the references given. In my opinion in Table I reference ten and eleven should read reference eleven and twelve.

A very similar membrane gas-liquid separator to that demonstrated by Pacey *et al.* [58] has recently been applied by Chan *et al.* [239] to the determination of Bi by FI-HGAAS. A stainless-steel screen was used to back the membrane and so improve its working life time.

Yamamoto *et al.* [89] reported the use of a novel membrane tube separator as a gas-liquid separator for FI-HGAAS. Microporous PTFE tubing was used as an inner tube and pyrex glass tubing as the outer tube of the separator . The mixture of AsH_3, H_2, Ar, air and the reacted solution were passed into the microporous PTFE tube and AsH_3, Ar and air separated from the solution to the outer side of the microporous PTFE tube, diffusing through its wall. A characteristic concentration of 0.058 ng ml^{-1} of As was obtained with a precision of 2.5% (3 ng ml^{-1} As, n=10) and throughput of 120 h^{-1}. The improvement in sensitivity achieved in comparison with the previously used U-tube gas-liquid separator [88] was shown in part to be due to a reduced dead

volume of the gas-liquid separator. The design of separator achieved a total diffusion area of the PTFE tubing of 25, 000 mm^2. This figure was significantly larger than the area of 70 mm^2 used in the system of Pacey *et al.* [58] and would therefore account for its superior performance characteristics.

In very recent work, Marshall and van Staden [240] described a perspex chamber gas-liquid separator incorporating a cotton gauze membrane. The role of the membrane was not though to allow the formed hydride to pass through it as in earlier systems [58, 89, 239] but to simply assist in stripping of the hydride from the effluent solution. Performance data was presented for the determination of As, Bi, Sb, Se and Te which was significantly poorer than that reported in earlier work [88]. Detection limits varied in the range of 2 to 10 ng ml^{-1} and precisions where quoted between 2.2 to 3.7%. A rather uncharacteristic feature of the system which may account for its poor performance characteristics was the low carrier flow rates employed. The carrier flow rates in each case were restricted to below 3.0 ml min^{-1} but without explanation. Irrespective of the poor performance characteristics of the system a novel standard additions method was implemented with success in the determination of Bi in the presence of palladium and the determination of As in samples of industrial effluent.

With the development of FI-HGAAS technology an increasing number of general application papers have been reported. These include the determination of Se in geological samples [61], bovine liver [241], blood plasma and serum [242], and the determination of As, Bi, Sb and Se in a variety of geological and environmental sample types [243, 244].

Preconcentration and matrix isolation- The application of column preconcentration procedures in FI-HGAAS to date has been limited. Fang *et al.* [180] in 1988 reported a dual column preconcentration system for the determination of Se and Hg. For Se determination a microporous anion exchanger (D-201) was capable of a concentration efficiency (CE) of 12, therefore, an improved limit of detection of 0.002 ng ml^{-1} of Se^{IV} with a sampling frequency of 50 h^{-1}. Zhang *et al.* [203] later demonstrated the same system for the preconcentration of Bi using a chelating ion exchanger (CPG-8Q). A concentration efficiency (CE) of 24 with a precision of 1.1% at 0.5 ng ml^{-1} of Bi was achieved permitting a limit of detection of 0.001 ng ml^{-1} of Bi.

The first reported use of continuous flow matrix isolation in HGAAS was documented by Ikeda [82] in 1985. The previously described suction flow hydride

generation system [235] was applied to the determination of Se in which a micro-column of chelating resin was employed for the in-line removal of interferences. A 500 µl sample was injected manually into a PTFE suction cup and carried to the top of the column with a continuous flow of water. The effluent of the column was subsequently introduced directly into the HGAAS manifold. A 500,000 fold excess of either copper or nickel could be tolerated in the determination of Se permitting the successful analysis of copper and nickel based alloys. A sample throughput of 30 h^{-1}, detection limit of 0.2 ng ml^{-1} of Se and precision of 3.8% (5 ng ml^{-1} Se^{IV}, n=10) was reported. The fact that the system relied on manual sample pipetting may explain the rather limited precision achieved. As implemented in the earlier system [235] sodium tetrahydroborate addition was carried out prior to acidification but without full explanation, and possible deterioration in the interference tolerance of the system [42, 87]. Although the column had a high capacity no column regeneration procedure was described. The column was simply replaced by a new one after every 25 measurements of a sample containing 2.5 mg of copper or nickel.

Riby *et al.* [83] later reported the use of a micro-column of strong cation exchange material (SCX) for in-line matrix isolation. The system was applied to the determination of As in nickel based alloy. A limit of detection of 1.3 ng ml^{-1} of As with a precision of 3.0% (10 ng ml^{-1} As, n=10) was reported but no indication of throughput capability. Although successfully applied to the analysis in question the in-line incorporation of the micro-column in the aqueous carrier required significant compromise to be made between the performance characteristics of the matrix isolation system and hydride generation manifold itself, as discussed in more detail in Chapters four and five respectively. A crude column regeneration procedure was described but intermittent replacement of the column was still necessary due to compaction of the exchange material resulting in excessive back pressures within the system. Without matrix isolation the interference tolerance of the system was limited to only 5 µg ml^{-1} of nickel. This was possibly due to a degree to the addition of sodium tetrahydroborate prior to hydrochloric acid as discussed for the system of Ikeda [82].

In very recent work Marshall and van Staden [71] applied the same in-line matrix isolation procedure [83] using a micro-column packed with AG50W X8 cation exchange resin. Dilute acid carrier streams (0.05 mol dm^{-3} H_2SO_4, 0.1 mol dm^{-3} HCl) were shown to be successful for the isolation of As and Se from a variety of separate synthetic interfering matrices (Fe, Co, Cr, Cu and Ni, 1000 µg ml^{-1}). The overall

performance characteristics of the system though were limited by the poor performance characteristics of the gas-liquid separator as documented previously [240]. Determinand concentrations used to validate the matrix isolation procedure were 1000 ng ml^{-1} of As and Se respectively. Inclusion of the micro-column in-line was shown to deteriorate sensitivity even further due to increased dispersion of the sample plug. Column regeneration was achieved by pumping a 2 mol dm^{-3} solution of eluent (10 ml) directly through the column. At an eluent flow rate of 2 ml min^{-1} this procedure though required a regeneration time of five minutes and since the column was not disconnected from the rest of the system the eluted interferents were passed directly into the gas-liquid separator. It is suggested that this action is detrimental to overall system performance and to be avoided if at all possible due to the increased possibility of interference memory effects.

2.3.6 Real Sample Analysis.

Difficult samples- The application of FIA to FAAS has been shown by numerous workers to be advantageous especially in the analysis of so-called difficult samples. Mindel and Karlberg [245] were first to report the ability of FI to handle samples with high dissolved solids. A solution containing 25% m/v magnesium chloride was analysed for cadmium. Direct aspiration resulted in rapid blocking of the burner but with the FIA-AAS system no burner blockage was observed and viscosity problems were eliminated. The same observations have been made subsequently by numerous other groups for a variety of different sample types [86, 142, 152, 154, 246]. Fang *et al.* [246] reported that the concentration limit of dissolved solids in a sample was in fact determined by the degree of matrix interference, such as solute-volatilization interferences, and not by difficulties in the process of sample introduction. Toleration of high concentrations of dissolved solids in samples was attributed to the extremely short contact times of undiluted sample with nebulizer and burner (1-2 s per sample) and the effective rinsing of the carrier stream between sample injections. Further evidence for the ability of FIA in the handling of difficult samples has recently been reported through its application to slurry nebulization/atomization procedures [247, 248] and the analysis of oil emulsions [249].

Sample pretreatment- Although to date a number of real analyses have been tackled by FI-FAAS using various designs of manifold, many of the sample pretreatment processes can be traced back to the early work of Zagatto *et al.* [132, 250] and Rocks *et al.* [142, 156, 157, 251]. A summary of the variety of analyses to which FI-FAAS has been successfully applied is given in Table 2.3.1.

Zagatto *et al.* [132] demonstrated the use of the merging zones method in the determination of Ca, Mg and K in plant material. Consumption of 0.5 mg of lanthanum per sample was reported which was a significant reduction from 50 mg per sample for conventional aspiration. Sample dilution was obtained through on-line dispersion, coupled with dilution at the merging point, (dispersion coefficient 40).

Rocks *et al.* [157] reported the use of a single line manifold for the determination of Ca and Mg in serum. No pre-dilution or addition of masking agents and releasing agents was required. For the determination of Ca a carrier stream of 0.01 mol dm^{-3} lanthanum in 0.05 mol dm^{-3} HCl was used into which a 4 µl of serum was injected directly. Dilution of the injected serum sample to within the working range of the detector was obtained through on-line dispersion during transport to the nebulizer, (dispersion coefficient 54).

One of the biggest breakthroughs in FI-FAAS in connection with sample pretreatment was made by Burguera *et al.* [252, 253] through the application of microwave assisted decomposition. Burguera *et al.* [252] described a method for the determination of Cu, Zn and Fe in whole blood. Untreated blood was injected (100 µl) directly into an aqueous carrier containing Triton X-100 and merged with HCl/HNO_3 reagent. The merged sample was then transported along a coiled pyrex decomposition tube located inside the microwave oven prior to the nebulizer of the atomic absorption spectrometer. The system required no prior sample pretreatment, had a sampling rate of 80 h^{-1} and relative standard deviation of better than 3%. In a later system [253] the microwave decomposition of biological tissue was carried out in a closed flow circuit interfaced to a FI-FAAS manifold. Digested samples were pumped around the closed flow circuit from which aliquots (20 µl for Zn and 100 µl for Cd) were injected into a continuously flowing water carrier stream. Recoveries of 97-103% for Zn and 96-98% for Cd with a precision of 2-6% were obtained. A similar design of system has recently been applied to the determination of Pb in sewage sludge [254]. The system described although successful to the analysis in question only attained partial digestion of the sample matrix and, therefore, relied on the ability of FI to handle slurry nebulization [247, 248].

A novel method for the automation of sample preparation was demonstrated by Yuan *et al.* [255] in 1991 with the on-line electrolytic dissolution of solid metal samples. An electrolysis cell was described and applied to the determination of Cu in aluminium alloys. The detection limit was a function of electrolysis time and current. Sample

analysis times of only a few minutes were required with a reproducibility of 4% for the same sampling point and 5% for different points on the alloy sample.

Table 2.3.1 Real Sample Analysis by FI-AAS.

Sample	Analyte	System feature	Reference
CLINICAL			
Serum	Cu, Zn		142,(1982)
	Ca, Mg		157,(1984)
	Se	HGAAS	242,(1990)
Blood Plasma	Se	HGAAS	242,(1990)
Blood	Cu, Fe, Zn	on-line microwave digestion	252,(1986)
	Pb	Slotted tube atom trap	256,(1988)
Biological tissues	Se	HGAAS	241,(1986)
	Cd, Zn	microwave digestion	253,(1988)
Parotid saliva	Cu, Fe, Zn		257,(1986)
Cerebrospinal fluid	Ca, Cu, Fe, Mg, K, Zn		259,(1986)
Urine	Pb	Off-line solvent extraction	259,(1986)
Hair	Pb		260,(1987)
FOOD			
Rice powder (NBS SRM 1568)	As	HGAAS	70,(1988)
	Se	HGAAS	88,(1985)
Wheat flour (NBS SRM 1567)	As, Se	HGAAS	88,(1985)
Spinach (NBS SRM 1570)	Cu, Zn		133,(1979)
Foodstuffs	Fe, Zn	slurry nebulization/atomization	247,(1990)
	Cd, Pb		261,(1987)
Powdered milk	Cu, Fe		262,(1987)
Milk	Ca		263,(1990)
ENVIROMENTAL			
Water			
Polluted sea water	Cd, Cu, Pb, Zn		188,(1983)
	Cd, Pb, Zn	On-line ion exchange preconcentration	188,(1983)
Sea water	Cd, Cu, Pb	On-line ion exchange preconcentration	193,(1989)
Tap, snow and mineral	Bi, Se	HGAAS/on-line ion exchange preconcentration	203,(1989)
Drinking and mineral	As	HGAAS	243,(1990)
Plant material	Ca, K, Mg		132,(1979)
	Fe		250,(1981)

cont/..

Sample	Analyte	System Feature	Reference
Orchard leaves (NBS SRM 1571)	As, Bi, Sb, Te	HGAAS	88,(1985)
	Cu, Zn		133,(1979)
Soil	Cd		86,(1986)
Sediments	As	HGAAS	243,(1990)
Coal fly ash (NBS SRM 1633a)	As, Sb, Se	HGAAS	88,(1985)
	As, Sb, Se	HGAAS	243,(1990)
Sewage sludge	Pb	On-line microwave digestion	254,(1990)
Geological materials	Se	HGAAS	61,(1985)
Silicate rocks	Co	On-line precipitation dissolution	264,(1989)
INDUSTRIAL			
Pigments	Cu, Cr, Mg, Zn	Slurry nebulization/atomization	248,(1991)
Lubricating oils	Ca		249,(1989)
Gasoline	Pb		265,(1986)
METALLURGY			
Steels	Cr	Standard additions	162,163,(1983)
	Cr		266,(1986)
	As, Bi, Sb, Se, Te	HGAAS	88,(1985)
	As, Bi, Sb, Se	HGAAS	243,(1990)
Leaded gun metal	Bi	HGAAS	239,(1990)
Electronic flow solder	Bi	HGAAS	239,(1990)
Nickel based alloys	As	HGAAS/ On-line ion exchange matrix isolation	83,(1989)
Aluminium alloy	Cu	On-line electrolytic dissolution	255,(1991)
Copper based alloys	Pb	Slotted tube atom trap	267,(1989)

CHAPTER THREE

ON-LINE DILUTION IN FAAS THROUGH THE APPLICATION OF FI AND WIDE BORE MANIFOLD TUBING.

3.1 INTRODUCTION.

The use of flow injection for on-line dilution and calibration strategies in FAAS has been reported extensively by numerous groups, as reviewed in section 2.3.3. To date though little attempt has been made by instrument manufacturers to develope commercial instrumentation based on these methods. To some extent this is due to a variety of limitations of the systems reported including their limited dilution ranges, lack of robust operation, complicated computer operation and use of expensive components.

Early methods based on the fundamental principles of flow injection and dilution through on-line dispersion, were capable of relatively high values of dispersion. Rocks *et al.* [157] for example achieved a dispersion coefficient of 100. These methods were though, in general, limited to a single predetermined dilution factor. Development of network manifolds [159] have successfully extended the working range of the procedure to achieve up to six independent dilution values for a single sample. Although simple and inexpensive the full potential of the method is restricted by the build up of back pressure when long lengths of narrow bore (0.5 mm i.d.) manifold tubing are used. Initial studies into the use of wide bore manifold tubing of up to 1.3 mm i.d., [155] has shown promise in overcoming such restrictions and at the same time producing large dispersions without the need for lengthy manifolds. For a manifold length of only 300 mm (1.3 mm i.d.) a dispersion coefficient of approximately 25 was achieved. To overcome the limited dilution ranges achieved by the simple on-line dispersion principle various modifications have been reported over the years. The use of merging zones [132] and zone sampling [158] procedures have been successfully applied. The requirement of exact timing and synchronisation of manifold operations in such systems though has made the process more complicated, requiring expensive components.

Recent developments have moved away from carrying out the physical dilution of samples but have achieved the same procedure through manipulating the analytical data available within the FI transient signal response itself [166, 171-173]. Although successfully applied to the determination of off-range samples through the application of mathematical models, they rely on computer programs and computer controlled instrumentation, required to achieve precise timing, data collection and data evaluation. As a result these systems are complicated and expensive.

This chapter describes an investigation into the use of wide bore manifold tubing (0.8 - 5.0mm i.d.) in a flow injection manifold to permit a simple, cheap and robust method for on-line dilution in FAAS. The system was evaluated for possible commercialisation based on the use of a network manifold [159] to obtain discrete values of dispersion. The target performance for the manifold was to achieve dilution factors of up to 100 with a precision of 1% relative standard deviation (RSD).

3.2 APPARATUS AND REAGENTS.

The atomic absorption spectrometer (Philips Scientific model SP9) was connected to either a Tekman TE200 chart recorder or the SP9 computer for absorbance measurements. Philips data coded hollow cathode lamps were used for all determinations. An air-acetylene flame was used throughout for which the nebulizing air support gas was supplied by an air-compressor.

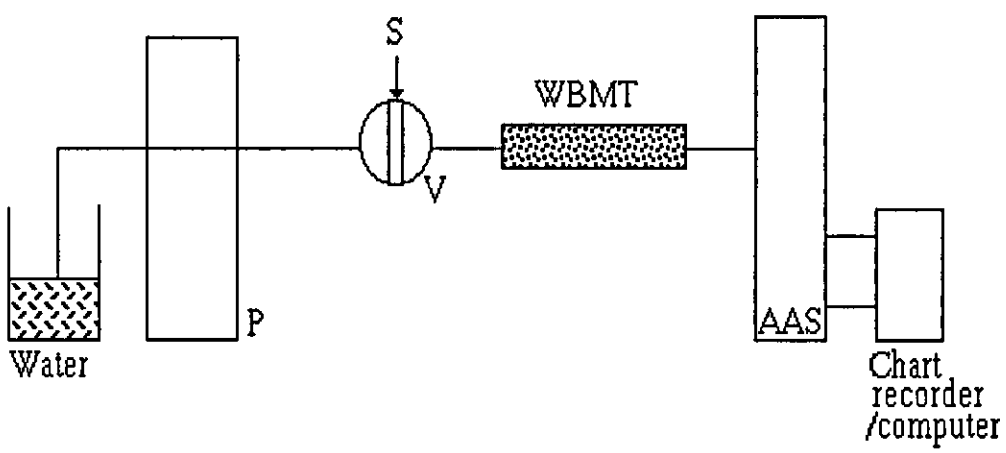

Fig. 3.1. Schematic diagram of a single line FI manifold for use with wide bore tubing: P, peristaltic pump; V, sample injection valve; S, sample; WBMT, wide bore manifold tubing.

Single line manifolds (see *Fig. 3.1*) were used for all FIA investigations. The manifolds were constructed from sections of wide bore tubing (0.8 - 5.0 mm i.d.). Short sections of small i.d. manifold tubing (0.8, 0.5 mm i.d.) were used to connect the sections of wide bore manifold tubing to the injection valve and nebulizer of the spectrometer respectively. Connecting tubing and wide bore manifold tubing (0.8 and 1.5 mm i.d.) were fitted together using conventional FI gripper fittings and connectors. For the larger 3.0 and 5.0 mm i.d. tubes short sleeves of tightly fitting pump tubing were used for the same purpose, as shown in *Fig. 3.2.*

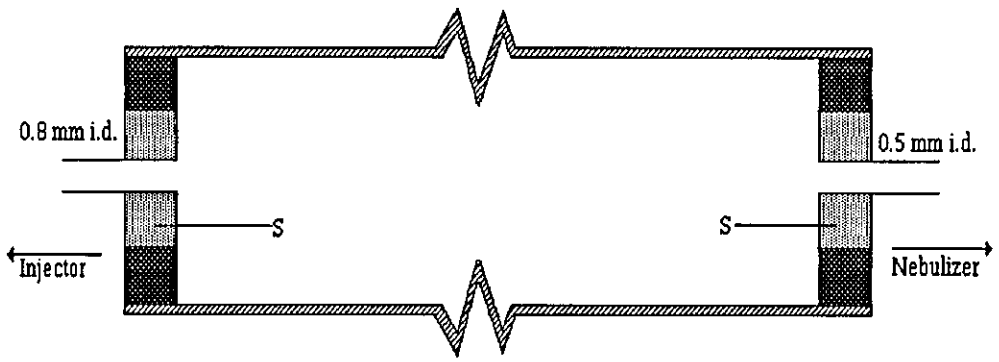

Fig. 3.2. Cross section of wide bore manifold tubing (WBMT): S, sleeves of pump tubing.

For visual mixing characterisation studies the PTFE wide bore tubing was replaced with transparent PVC tubing. A Gilson Manipuls 3 peristaltic pump was used with a variety of different internal diameter PVC pump tubings (Altec) to control carrier flow rates. A Rheodyne model 5020 fixed volume loop, manually operated, injector valve was used. To achieve a low sample injection volume (20-30 µl) short lengths of 0.8 mm i.d. PTFE manifold tubing were flanged directly to the back plate of the injector valve after removing the standard connecting arms.

Calcium, lead and zinc solutions were prepared by diluting stock 1000 µg ml^{-1} solutions (BDH SpectrosoL grade). Nitric acid (BDH, SpectrosoL grade) and analytical-reagent grade water produced by a liquipure RG system (reverse osmosis followed by ion exchange) were used for all sample and carrier solutions. To study mixing characteristics visually, coloured sample solutions were prepared from methylene blue (Boots, Quality control standard).

3.3 PROCEDURES AND RESULTS.

3.3.1 Optimization of Philips SP9 Spectrometer.

The manufacturer's quoted variables [268] were used as a starting point for the optimization of the spectrometer for the steady state determination of Ca. The principle spectral line 422.7 nm was chosen and a slit width at 0.5 nm, with no use of background correction or signal damping. Analytical-reagent grade water was aspirated to zero absorbance and a 10 µg ml^{-1} Ca solution was used to obtain absorbance readings as the instrument variables were altered. All signal quantification was carried out with the SP9 computer using precision program N° 91 (n = 9, integration time 2.0 s). A nebulizer uptake tube (185 mm, 0.5 mm i.d.) was used to introduce the calcium solution at a

natural uptake rate of 5.2 ml min^{-1} (Flow settings; air 27.5, acetylene 20.5 Arbitrary units). The effect of acetylene flow rate, burner height and lamp current on Ca absorbance are shown in *Figs. 3.3 and 3.4* respectively. The final optimized spectrometer settings are shown in Table 3.1.

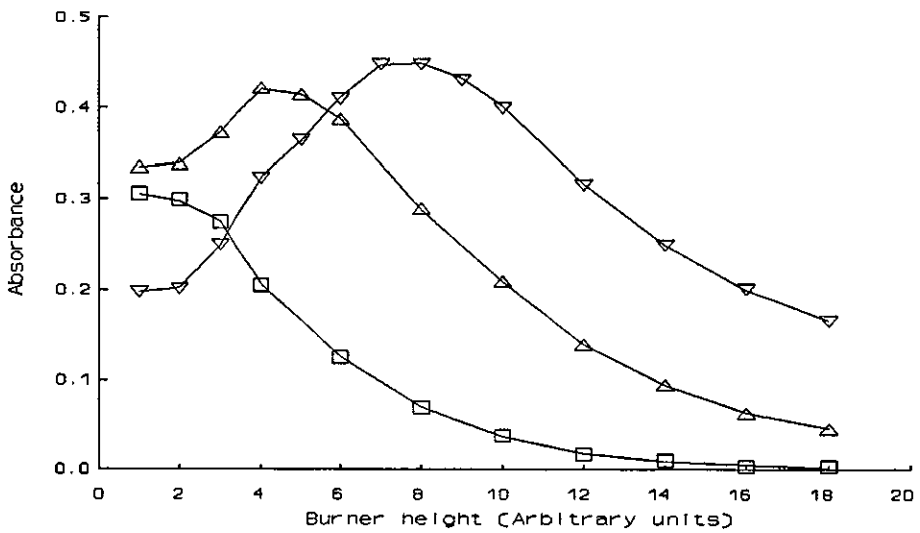

Fig. 3.3. Effect of burner height on the absorbance of 10 μg ml^{-1} of Ca, lamp current 7 mA, air flow setting (Arbitrary units) 27.5:(■), acetylene flow setting 18 (fuel-lean); (▲), acetylene flow setting 20 (stoichiometric); (▼), acetylene flow setting 23 (fuel-rich).

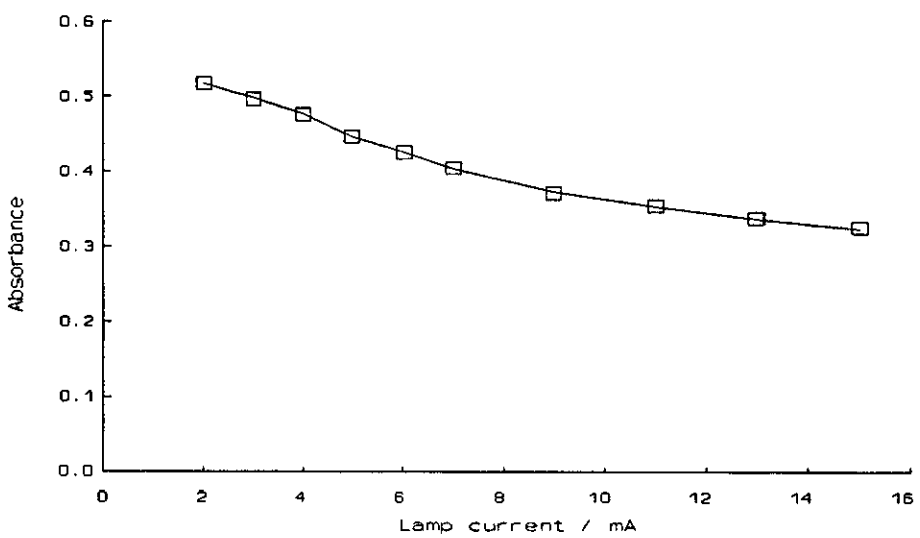

Fig. 3.4. Effect of lamp current on the absorbance of 10 μg ml^{-1} of Ca, air and acetylene flow settings 27.5 and 20.5, burner height 4 (Arbitrary units).

Table 3.1 Optimum SP9 Spectrometer variables for the determination of calcium.

Wavelength, nm	422.7
Slit width, nm	0.5
Lamp current, mA	2.0
Support gas/ flow setting, (Arbitrary units)	27.5/air
Fuel gas/flow setting, (Arbitrary units)	20.5/acetylene
Burner height, (Arbitrary units)	4
Background correction	OFF
Damping	OFF

A characteristic concentration (0.0044 A) of 0.05 $\mu g\ ml^{-1}$ for Ca was obtained which compared favourably with the manufacturer's value of 0.09 $\mu g\ ml^{-1}$ Ca [268]. The precision of the system based on a 0.2 $\mu g\ ml^{-1}$ Ca standard was 1.1% relative standard deviation (%RSD, n=9).

3.3.2 Calibration of Gilson Manipuls 3 peristaltic pump.

The peristaltic pump used to deliver the carrier stream was calibrated gravimetrically by the method of weighing by difference. The mass of water delivered for fixed times, at different pump speed settings (RPM) for two sizes of pump tubing (0.89, 2.79 mm i.d.) was noted. Pumping rate was calculated as the volume of water pumped in unit time in millilitres per minute. Water density was approximated to 1 $g\ cm^{-3}$ over the temperature range 20-25° C. The flow rate capabilities of the two pump tubings are shown in *Fig. 3.5.*

When applied to pumping carrier in manifolds connected to the spectrometer the flow rate was determined at regular intervals and for each change of pump variable, by the method of weighing by difference as described. This procedure was required to correct for the effect of nebulizer suction, changes in back pressure with manifold design and deterioration in the performance of pump tubing with age.

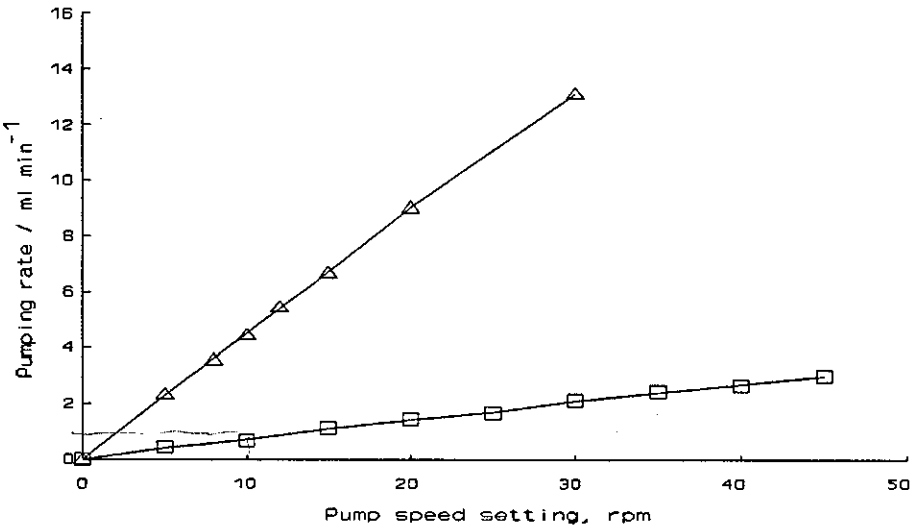

Fig. 3.5. Calibration graph for Gilson Manipuls-3 pump peristaltic pump: Pump tube dimensions; (▲), 2.79 mm i.d.; (■), 0.89 mm i.d.

3.3.3 Calibration of injection valve sample loop volume.

The volume of the sample loop used in the injection valve was calibrated gravimetrically by weighing a slug of liquid mercury delivered from it. The loop of the injection valve was filled with liquid mercury, manually from a plastic syringe, with the valve in the load configuration. After the valve was actuated into the inject position the mercury sample slug was driven out of the sample loop into a pre-weighed beaker with a stream of air, supplied by a second syringe. The volume of the sample injection loop was therefore calculated knowing the mass of mercury used to fill the sample loop and the density of liquid mercury (13.6 g cm^{-3}). For the injection valve used a sample loop volume of 29.3 ± 0.3 (n=5, ± 95% confidence interval) was calculated.

3.3.4 Effect of pumping flow rate on spectrometer response.

3.3.4.1 FI calcium signal response.

The spectrometer was operated at the optimum conditions (Table 3.1) connected to a manifold based on that shown in *Fig. 3.1.* A straight length of PTFE manifold tubing (300 mm, 0.5 mm i.d.) was used to connect the injection valve and the nebulizer.

The effect of pumping flow rate on the flow injection sample introduction of Ca in FAAS was studied. The sample loop, volume 29 µl, was filled with a 15 µg ml^{-1} Ca solution, injected into a water carrier stream and transported to the spectrometer. The peak-height was recorded on a Tekman TE200 chart recorder (10mV FSD, 100 mm min^{-1}). Triplicate sample injections were made for each carrier flow rate. The results of the study are shown in *Fig. 3.6.*

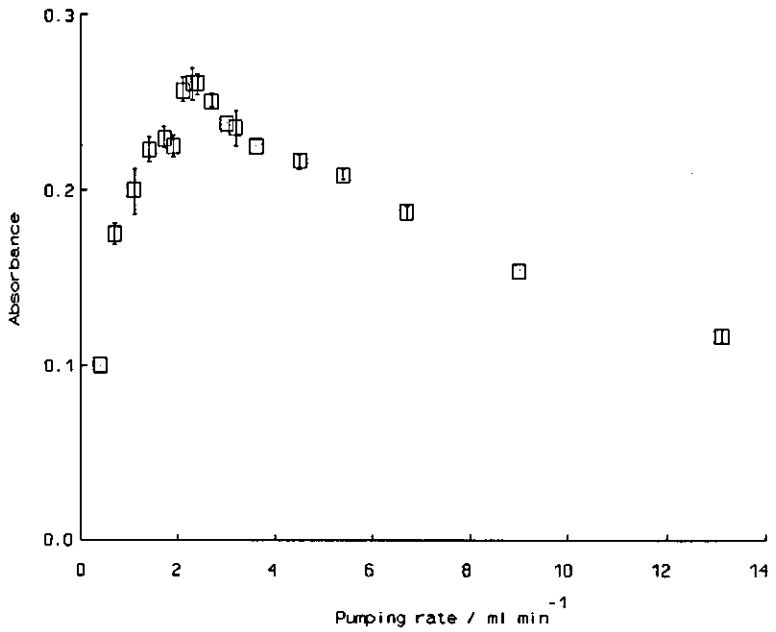

Fig. 3.6. Effect of pumping rate on the FI sample introduction of 15 µg ml^{-1} of Ca: 29 µl sample volume.

The results indicated that to achieve optimum signal response for the FI (29 µl) sample introduction of Ca the carrier flow rate should be maintained between 1.5 and 3.5 ml min^{-1}, (natural uptake rate of nebulizer 5.2 ml min^{-1}, nebulizer uptake tube 185 mm, 0.5 mm i.d.). Over this flow rate range the variation in signal response with flow rate was shown to be minimal. A carrier flow rate of 2.9 ml min^{-1} was chosen for later wide bore manifold investigation to optimize precision. The choice of carrier flow rate was made to limit the degree of imprecision encountered due to flow rate pulsations expected from a peristaltic pump and from the observations made in section 3.3.4.2 on the effect of sample introduction rate on the precision of spectrometer response.

3.3.4.2 Precision in the determination of lead with continuous and FI sample introduction.

The effect of sample introduction rate on the relative standard deviation (% RSD) of peak-height absorbance in the determination of Pb was investigated. The spectrometer was operated using the optimum variables, quoted by the manufacturer [268], shown in Table 3.2. A straight length of PTFE manifold tubing (300 mm, 0.5 mm i.d.) was used to connect the injection valve and the nebulizer. The natural uptake rate of the nebulizer was kept constant at 4.73 ml min^{-1} (nebulizer uptake tube 185 mm, 0.5 mm i.d.) throughout the study.

All quantification was made using the SP9 computer based on peak height absorbance data. For continuous sample introduction the RSD was calculated from nine two second integrations of the steady state absorbance signal. In the case of FI sample introduction, data was obtained from nine separate injections. The mean relative standard deviation (%RSD) in each case was calculated from two independent sets of nine determinations. Results obtained for the FI (200 µl) and continuous sample introduction of 10 µg ml^{-1} of Pb are shown in Table 3.3.

Table 3.2 Optimum SP9 spectrometer variables for the determination of lead [268].

Wavelength, nm	217.0
Slit width, nm	0.5
Lamp current, mA	5.0
Support gas/flow setting, (Arbitrary units)	28/air
Fuel gas/flow setting, (Arbitrary units)	21/acetylene
Burner height, (Arbitrary units)	3
Background correction	OFF
Damping	OFF

(I) Continuous sample introduction

Pumping rate ml min^{-1}	Absorbance	RSD (%)	Mean RSD (%)
0.4	(1) 0.056	1.7	
	(2) 0.056	2.1	1.9
1.1	(1) 0.148	1.2	
	(2) 0.149	0.7	1.0
2.4	(1) 0.392	0.6	
	(2) 0.391	1.4	1.0
3.5	(1) 0.408	1.2	
	(2) 0.410	0.6	0.9
5.0	(1) 0.466	0.9	
	(2) 0.470	1.2	1.1
6.2	(1) 0.482	0.9	
	(2) 0.489	1.2	1.1
7.2	(1) 0.524	1.2	
	(2) 0.518	1.6	2.4
8.1	(1) 0.540	2.0	
	(2) 0.541	1.4	1.7
9.4	(1) 0.544	1.4	
	(2) 0.541	1.2	1.3
10.3	(1) 0.535	0.5	
	(2) 0.536	1.5	1.0

(II) FI sample introduction (200 µl)

Pumping rate ml min^{-1}	Absorbance	RSD (%)	Mean RSD (%)
0.4	(1) 0.069	4.5	
	(2) 0.070	3.1	3.8
1.2	(1) 0.157	3.1	
	(2) 0.159	3.8	3.5
2.4	(1) 0.321	1.2	
	(2) 0.323	2.0	1.6
3.3	(1) 0.389	1.6	
	(2) 0.385	1.7	1.7
4.8	(1) 0.428	1.1	
	(2) 0.429	1.8	1.5
5.6	(1) 0.428	1.8	
	(2) 0.422	2.2	2.0
6.7	(1) 0.434	1.2	
	(2) 0.440	1.8	1.5
8.0	(1) 0.432	1.6	
	(2) 0.437	1.9	1.8
9.7	(1) 0.411	2.0	
	(2) 0.415	2.3	2.2
14.2	(1) 0.349	1.9	
	(2) 0.343	3.9	2.9

Table 3.3 Effect of sample pumping rate on the relative standard deviation (%RSD) of peak-height absorbance in the determination of lead.
(I) Continuous sample introduction.
(II) Flow injection sample introduction (200 µl).
(Manifold variables as in text, section 3.3.4.2).

From the results in Table 3.3 it was evident that the precision observed with continuous introduction was superior to that of FI over the whole range of pumping rates investigated. In both cases though optimum precision was achieved at or slightly below the natural uptake rate of the nebulizer. Much above the natural uptake rate of the nebulizer a deterioration in precision was observed which contradicts the work of Brown and Ruzicka [144].

3.3.5 Calculation of dispersion coefficient.

To quantify the performance of wide bore manifold tubing in obtaining on-line dilution the term dispersion coefficient (D) was used [120].

$$D = \frac{c_o}{c_m} \qquad (3.3.1)$$

Where c_o is the original analyte concentration and c_m is the analyte concentration at peak maximum after dispersion. Dispersion coefficient values were not calculated from the ratio of instrument responses because of the limited linear range of the spectrometer for calcium. For each manifold in turn a calcium calibration was produced for the steady state introduction of sample at 2.9 ml min^{-1}. Standard solutions of Ca were pumped directly in turn through the manifold (*Fig. 3.1*) in the place of the water carrier stream and their steady state signal responses recorded. Following the calibration a sample of known concentration (c_o) was injected (29 µl) directly into a water carrier stream (*Fig. 3.1*) pumped at the same flow rate (2.9 ml min^{-1}) and its transient signal response recorded. The peak-height (H_x) of the transient signal was then converted to a concentration term (c_x), (concentration of dispersed sample plug reaching the nebulizer) from the steady state calcium calibration, by interpolation as shown in *Fig. 3.7.* Having determined the concentration of the sample after the dispersion process (c_x) and knowing its original concentration (c_o) the dispersion coefficient was obtained from equation 3.3.1.

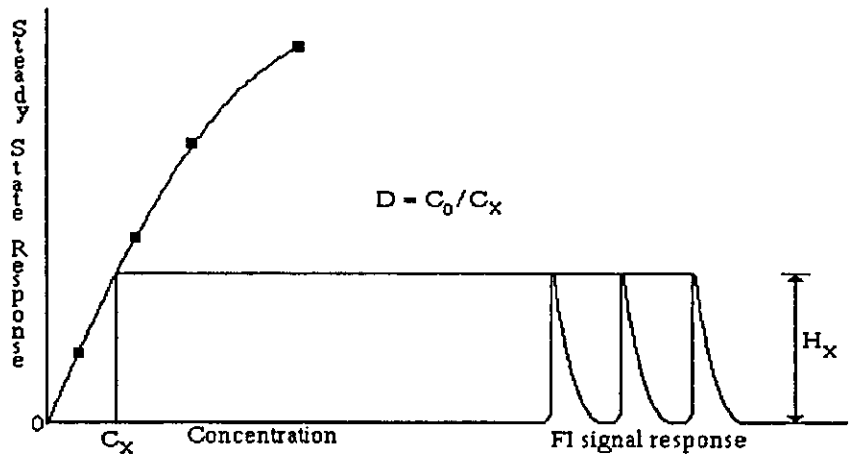

Fig. 3.7. Method applied to determine system dispersion coefficient: D, dispersion coefficient; c_o, concentration of injected standard; H_x, peak height of FI signal response produced by c_o; c_x, concentration of injected standard after dispersion.

3.3.6 Effect of manifold dimensions on dispersion coefficient.

The spectrometer was operated at the optimum conditions (Table 3.1) connected to the manifold as shown in *Fig. 3.1.* For each wide bore manifold investigated the section of wide bore tubing was connected to the injector and nebulizer by two lengths of manifold tubing, 90 mm (0.8 mm i.d.) and 140 mm (0.5 mm i.d.) respectively. A 15 μg ml^{-1} Ca standard was injected (29 μl) nine times into each manifold and the resulting FI signal responses were used to calculate the dispersion coefficients of each in turn as outlined previously (Section 3.3.5). The sample throughput reported for each was calculated on the basis of how many injections could be made in an hour. The time required to make a single determination was calculated from the chart recording based on the time interval between the sample injection and the return to the baseline of the transient FI signal response. The effect of wide bore manifold dimensions of length and internal diameter on both dispersion coefficient and throughput are shown in *Figs. 3.8 and 3.9* respectively.

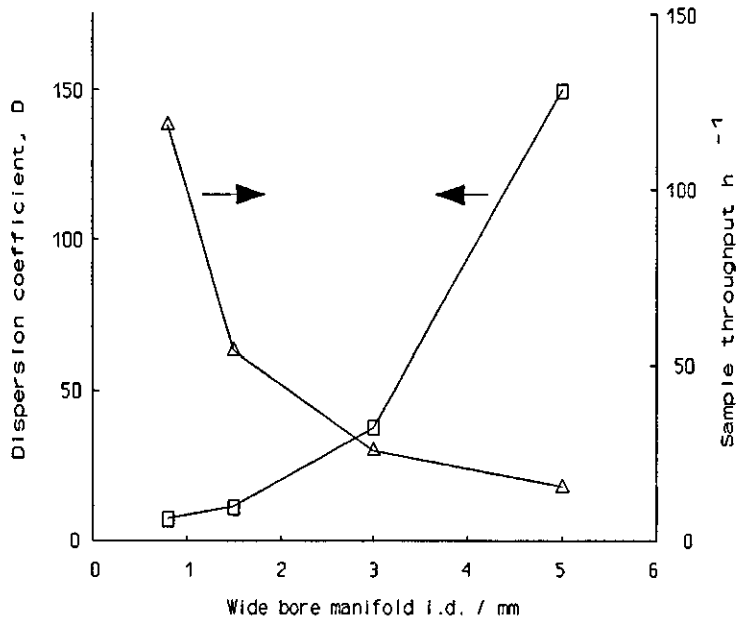

Fig. 3.8. Effect of wide bore manifold internal diameter on dispersion coefficient and sample throughput, manifold length 500 mm, pumping rate 2.9 ml min^{-1}, injection volume 29 µl (15 µg ml^{-1} Ca).

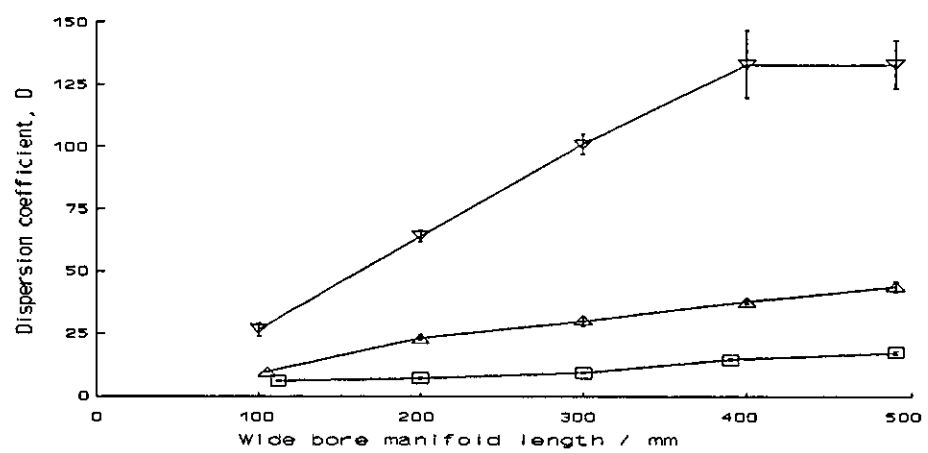

Fig. 3.9. Effect of wide bore manifold length on dispersion coefficient, pumping rate 2.9 ml min^{-1}, injection volume 29 µl (15 µg ml^{-1}). (■), 1.5 mm i.d.; (▲), 3.0 mm i.d.; (▼), 5.0 mm i.d.

Dispersion coefficients in excess of the target figure of 100 were obtained with 5.0 mm i.d. tubing. The RSD values were in the ranges 3.2-4.6, 1.6-6.0 and 4.6-13.0% (n=9) for the 1.5, 3.0 and 5.0 mm i.d. manifold tubes respectively. The 5.0 mm i.d. tubing limited sample throughput significantly. For manifold lengths of 100, 200, 300, 400 and 500 mm the throughput was 56, 36, 25, 22 and 19 h^{-1} respectively.

A practical limitation of the system was the retention and gradual build up of small air bubbles in the wide bore manifold tube. The carrier mean linear velocity was insufficient to wash the air bubbles out of the manifold. To prevent their contribution to the mixing characteristics they had to be therefore removed. This was achieved, with difficulty, by mechanically dislodging the air bubbles so allowing them to be passed directly through the manifold tube.

3.3.7 Effect of analyte concentration on dispersion coefficient.

The performance characteristics of the proposed manifold (*Fig. 3.1*) employing a single 100 mm (5.0 mm i.d.) wide bore reactor tube was investigated as outlined in section 3.3.6. For the use of calcium as a test analyte the spectrometer was operated at the optimum conditions shown in Table 3.1. For the use of zinc as the test analyte the spectrometer was operated at the optimum conditions shown in Table 3.4, based on the manufacturer's recommendations [268].

Table 3.4 Optimum SP9 Spectrometer variables for the determination of zinc.

Wavelength, nm	213.9
Slit width, nm	0.5
Lamp current, mA	8.0
Support gas/ flow setting, (Arbitrary units)	27.5/air
Fuel gas/flow setting, (Arbitrary units)	20.0/acetylene
Burner height, (Arbitrary units)	4
Background correction	OFF
Damping	OFF

The effect of analyte concentration on dispersion coefficient is shown in Table 3.5. The signal response peak shapes obtained are shown in *Fig. 3.10.*

Table 3.5 Variation in the dispersion coefficient with increasing analyte concentration; wide bore manifold 100mm (5.0 mm i.d.), injection volume 29 µl, pump flow rate 2.9 ml min^{-1}, (±95% confidence intervals).

Analyte concentration µg ml^{-1}	Dispersion coefficient, D	
	calcium	zinc
15	21.1±1.1 (n=4)	21.4±0.0 (n=3)
50	41.7±0.0 (n=2)	38.5±0.0 (n=3)
100	67.9±2.1 (n=4)	61.8±2.7 (n=3)
200	112.8±6.5 (n=4)	87.6±5.4 (n=3)
1000	182.7±10.8 (n=2)	187.5±4.9 (n=3)

The dispersion coefficient obtained was strongly dependent on concentration but independent of the analyte species. For both calcium and zinc the dispersion coefficient was found to increase with increasing analyte concentration (see Table 3.5). The variation in peak shapes with concentration (*Fig. 3.10*) showed that the effects must be due in some way to changes in the mixing characteristics of the manifold. Standards used in the investigation were prepared by serial dilution of stock 1000 µg ml^{-1} solutions (SpectrosoL, BDH), both prepared in 0.5 mol dm^{-3} nitric acid. Clearly therefore the prepared solutions used contained varying concentrations of nitric acid as well as the analyte species. The observed effects could therefore not be concluded to be solely analyte dependent. Investigation into the effect of nitric acid concentration on dispersion coefficient was therefore necessary.

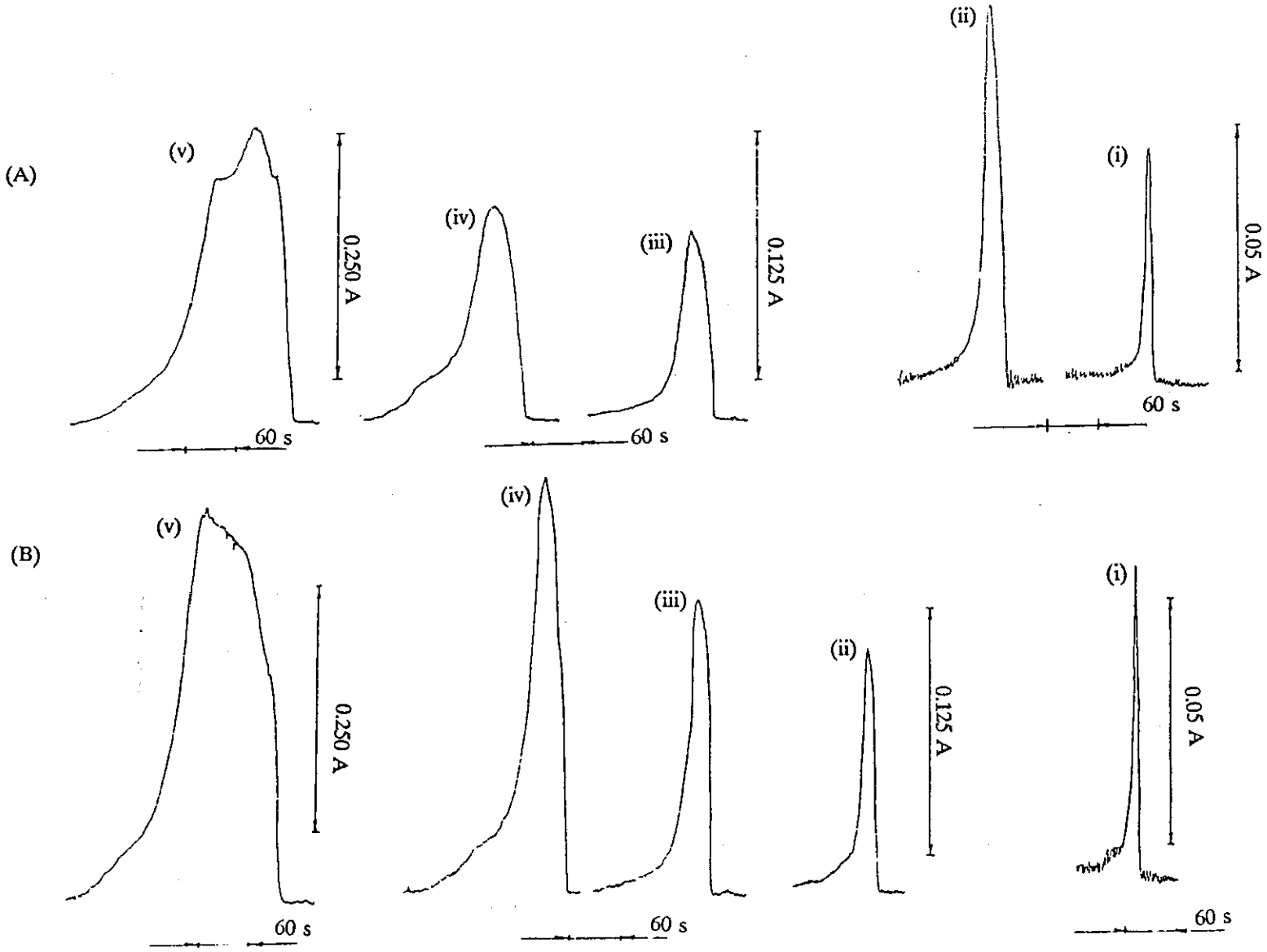

Fig. 3.10. Signal response peak shapes obtained with varying analyte concentration; (A), calcium, (B), zinc; (i), 15 μg ml^{-1}; (ii), 50 μg ml^{-1}; (iii), 100 μg ml^{-1}; (iv), 200 μg ml^{-1}; (v), 1000 μg ml^{-1}, (Manifold variables as Table 3.5).

3.3.8 Effect of nitric acid concentration on dispersion coefficient.

The spectrometer was operated at the optimum conditions (Table 3.1) connected to the manifold as shown in *Fig. 3.1.* A section of wide bore manifold tubing, 90 mm (5.0 mm i.d.) was connected to the injector and nebulizer by two lengths of manifold tubing, 80 mm (0.8 mm i.d.) and 50 mm (0.5 mm i.d.) respectively. A series of Ca standard solutions containing varying concentrations of nitric acid were prepared.

A study of the effect of nitric acid concentration of the dispersion coefficient obtained for a range of Ca standards (50-1000 $\mu g\ ml^{-1}$) was made. Standard solutions were injected in duplicate into an aqueous carrier stream (29 µl, 2.9 ml min^{-1}). The dispersion coefficient of each sample was calculated as outlined in section 3.3.5, based on the mean signal response of the two determinations. The effect of nitric acid concentration on the observed dispersion coefficient is shown in Table 3.6 and the resulting signal response peak shapes in *Fig. 3.11.*

Table 3.6 Effect of sample nitric acid concentration on dispersion coefficient; wide bore manifold tubing 90mm (5.0 mm i.d.), injection volume 29 µl, pump flow rate 2.9 ml min^{-1}, (Aqueous carrier).

Analyte Concentration $\mu g\ ml^{-1}$	Sample Preparation			
	Serial Dilution		Acid Matched	
	HNO_3 (mol dm^{-3})	D	HNO_3 (mol dm^{-3})	D
50	0.025	35.7	0.500	90.9
100	0.050	52.6	0.500	87.0
200	0.100	76.9	0.500	87.0
1000	0.500	85.5	0.500	85.5

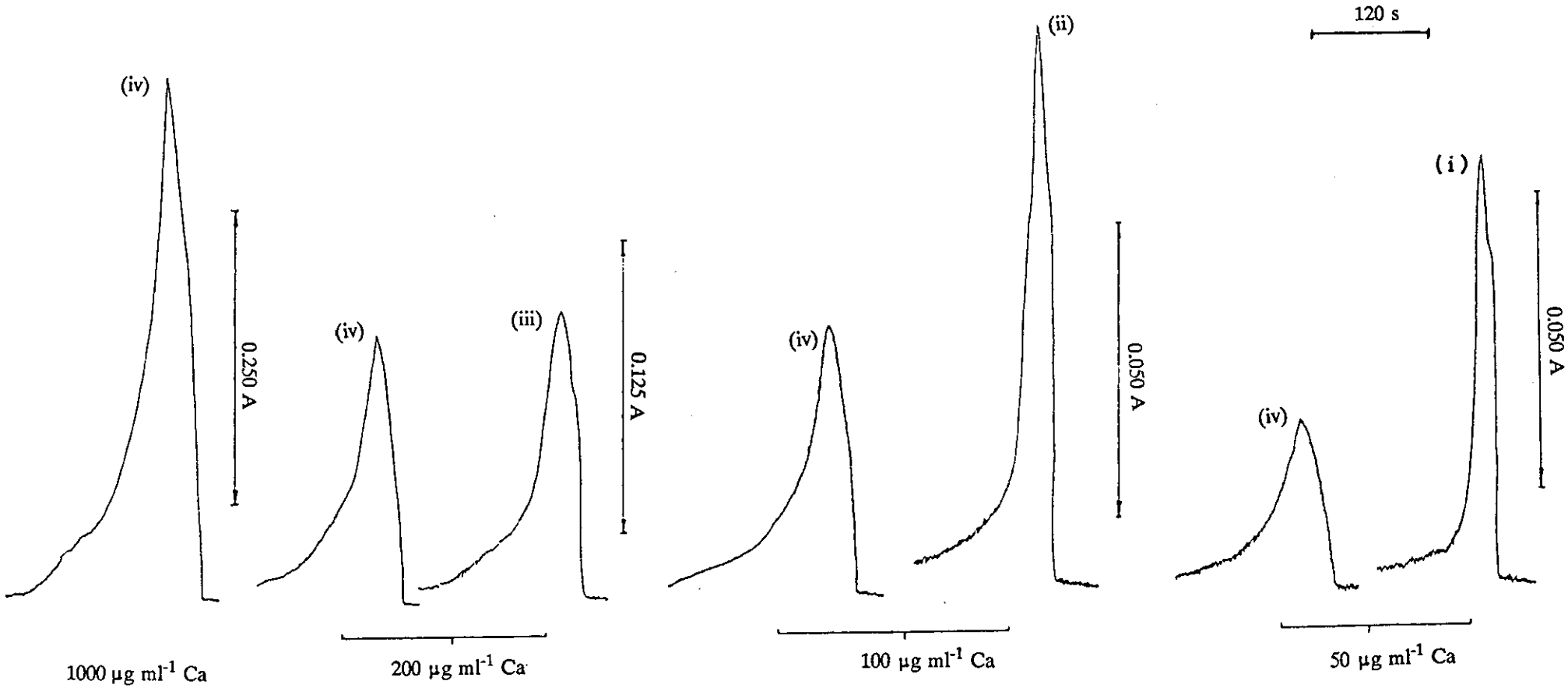

Fig. 3.11. Signal response peak shapes obtained with varying sample nitric acid concentration (mol dm^{-3}); (i), 0.025; (ii), 0.05; (iii), 0.100; (iv), 0.500: calcium concentrations 50, 100, 200 and 1000 µg ml^{-1}, (Manifold variables as Table 3.6).

A study of the effect of sample nitric acid concentration for a single Ca standard solution (50 μg ml^{-1}) was carried out. The injection volume of a new injection valve employed was calculated to be 21.1±4.1 μl (Section 3.3.3). Each standard solution was injected into the manifold into both aqueous and nitric acid (1.000 mol dm^{-3}) carrier streams (2.9 ml min^{1}). The effect of nitric acid concentration on dispersion coefficient and resulting signal response peak shapes for both carrier solutions are shown in *Figs. 3.12 and 3.13* respectively.

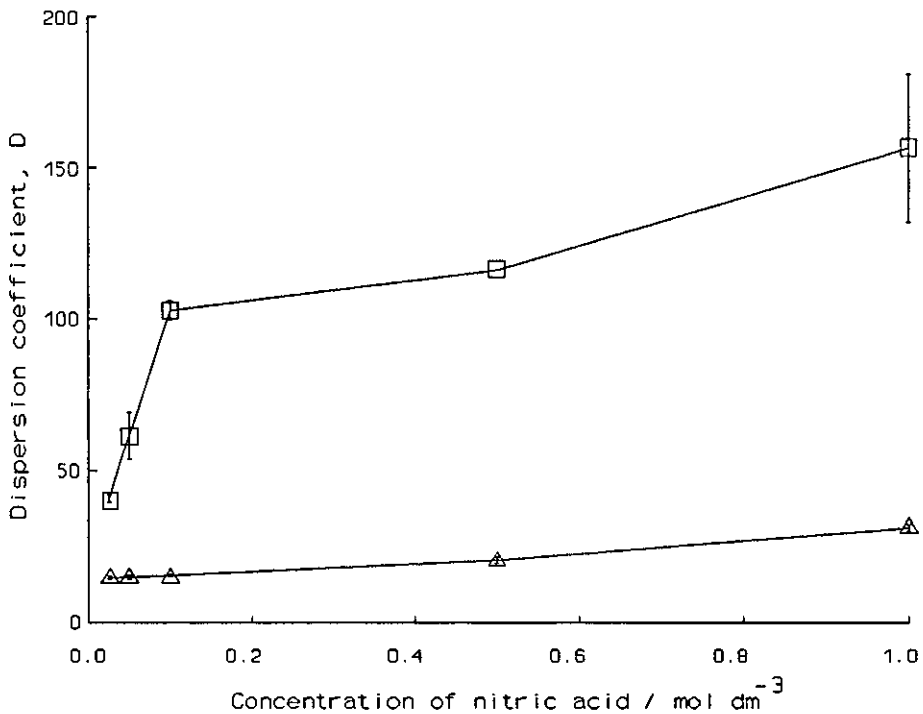

Fig. 3.12. Effect of nitric acid concentration on dispersion coefficient; wide bore manifold 90.0 mm (5.0 mm i.d.); injection volume 21 μl (50 μg ml^{-1} Ca); pump flow rate 2.9 ml min^{-1}. (■), Aqueous carrier; (▲), nitric acid carrier (1.000 mol dm^{-3}).

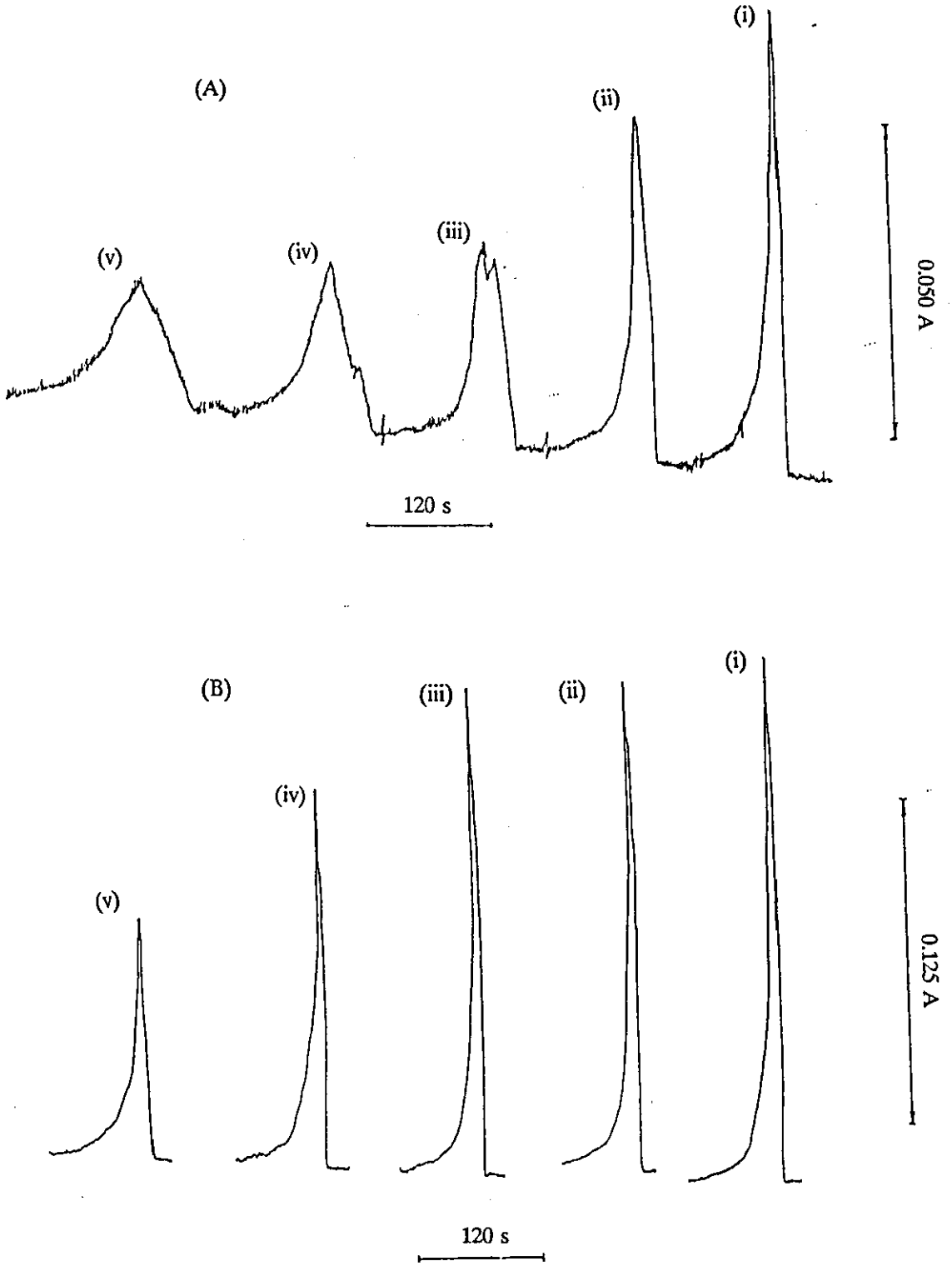

Fig. 3.13. Signal response peak shapes obtained with varying nitric acid concentration (mol dm^{-3}): (A), Aqueous carrier; (B), Nitric acid carrier (1.000 mol dm^{-3}); (i), 0.025; (ii), 0.050; (iii), 0.100; (iv), 0.500; (v), 1.000, (Manifold variables as *Fig. 3.12*).

The results obtained from the experimental work clearly indicated that the performance of the FI manifold was affected significantly by the acid concentration of the sample, as shown in Table 3.6 and *Fig. 3.12.* Increase in the sample acid concentration was shown to produce a corresponding increase in the observed dispersion coefficient. For an aqueous carrier stream a two fold increase in dispersion coefficient from 35.7 to 76.9 was obtained with a four fold increase in nitric acid concentration (0.025-0.100 mol dm^{-3}) . This increase in dispersion coefficient was accompanied by a noticeable change in the signal response peak shape as shown in *Figs. 3.11 and 3.12.* In general an increase in the acid concentration broadened the signal peak and introduced significant tailing. Peak shapes were very reproducible for each sample in turn.

From the results shown in Table 3.6 it was concluded that the dispersion coefficient was independent of the analyte concentration. At the 0.500 mol dm^{-3} nitric acid concentration only a 6% change in the observed dispersion coefficient was calculated for a 20 fold increase in concentration from 50 to 1000 μg ml^{-1} of Ca. It was concluded that the results shown in Table 3.5 and *Fig. 3.10* for Ca and Zn can be accounted for by the differences in nitric acid concentration of the sample solutions used. The most dramatic and unexpected results were obtained by simply changing the carrier solution from water to nitric acid (1.000 mol dm^{-3}), as shown in *Figs. 3.12 and 3.13.* With use of a 1.000 mol dm^{-3} nitric acid carrier the dispersion coefficients obtained were below 40, over the whole sample nitric acid concentration range investigated. For the aqueous carrier stream, values of dispersion coefficient as high as 150 were obtained through increasing the concentration of nitric acid in the sample to 1.000 mol dm^{-3}. Peak shapes obtained with the aqueous carrier were rather distorted and for the 50 μg ml^{-1} Ca standard solution, acidified to 0.100 mol dm^{-3}, a totally unexpected doublet peak was obtained (*Fig. 3.13 (iii)*). This observation was shown to be reproducible for repeated injections, and it was therefore, concluded that the effect arose from the mixing characteristics of the manifold. In contrast the peaks for the nitric acid carrier solution were single, narrow and sharp.

To investigate the unusual mixing characteristics visual observation of the mixing processes was proposed.

3.3.9 Visual investigation into the mixing characteristics of the wide bore manifold.

The manifold shown in *Fig. 3.1* was used, disconnected from the spectrometer. A section of PVC wide bore manifold tubing, 100 mm (5.0 mm i.d.) was mounted securely in the same orientation as that used with the spectrometer. Injections (21 μl) of a 0.25% m/v solution of methylene blue were made into the manifold and photographs were taken at predetermined intervals (s). A single photograph was taken for each injection in turn. The series of photographs obtained was used to follow the sample transport along the manifold and identify the mixing characteristics of the manifold for the variables used in earlier experimental studies. It was assumed that the mixing experienced by the methylene blue sample was identical to that of Ca standard solutions used for FAAS detection.

The effect of the sample acid concentration on the mixing characteristics was studied. Methylene blue sample solutions (0.25% m/v) were acidified to 0.025 and 0.500 mol dm^{-3} with nitric acid and injected separately into an aqueous carrier stream (2.9 ml min^{-1}). The sample transport is shown in *Figs. 3.14 and 3.15* respectively.

The effect of using a nitric acid carrier stream (1.000 mol dm^{-3}) on the mixing characteristics was studied. A single 0.25% m/v methylene blue sample (0.025 mol dm^{-3} HNO_3) was injected into the nitric acid carrier stream (2.9 ml min^{-1}). The sample transport is shown in *Fig. 3.16.*

Finally the effect of carrier flow rate on the mixing characteristics of the system was studied. A single 0.25% m/v methylene blue sample (0.025 mol dm^{-3} HNO_3) was injected into an aqueous carrier pumped at a flow rate of 18 ml min^{-1}. The sample transport is shown in *Fig. 3.17.*

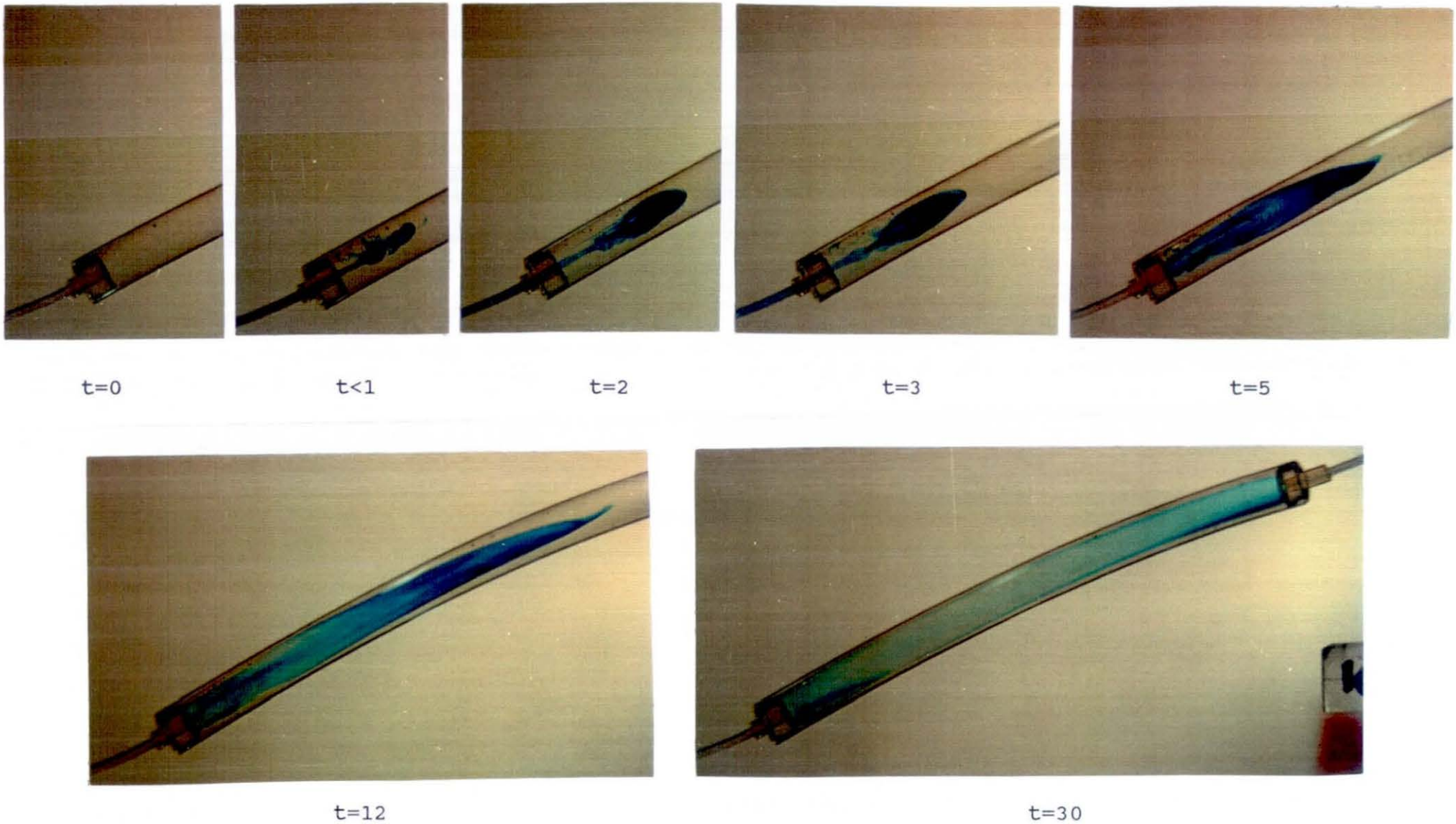

Fig. 3.14. Manifold mixing characteristics and sample transport: sample nitric acid concentration 0.025 mol dm^{-3} (0.25% m/v methylene blue); Aqueous carrier, 2.9 ml min^{-1}; t, time after sample injection (s).

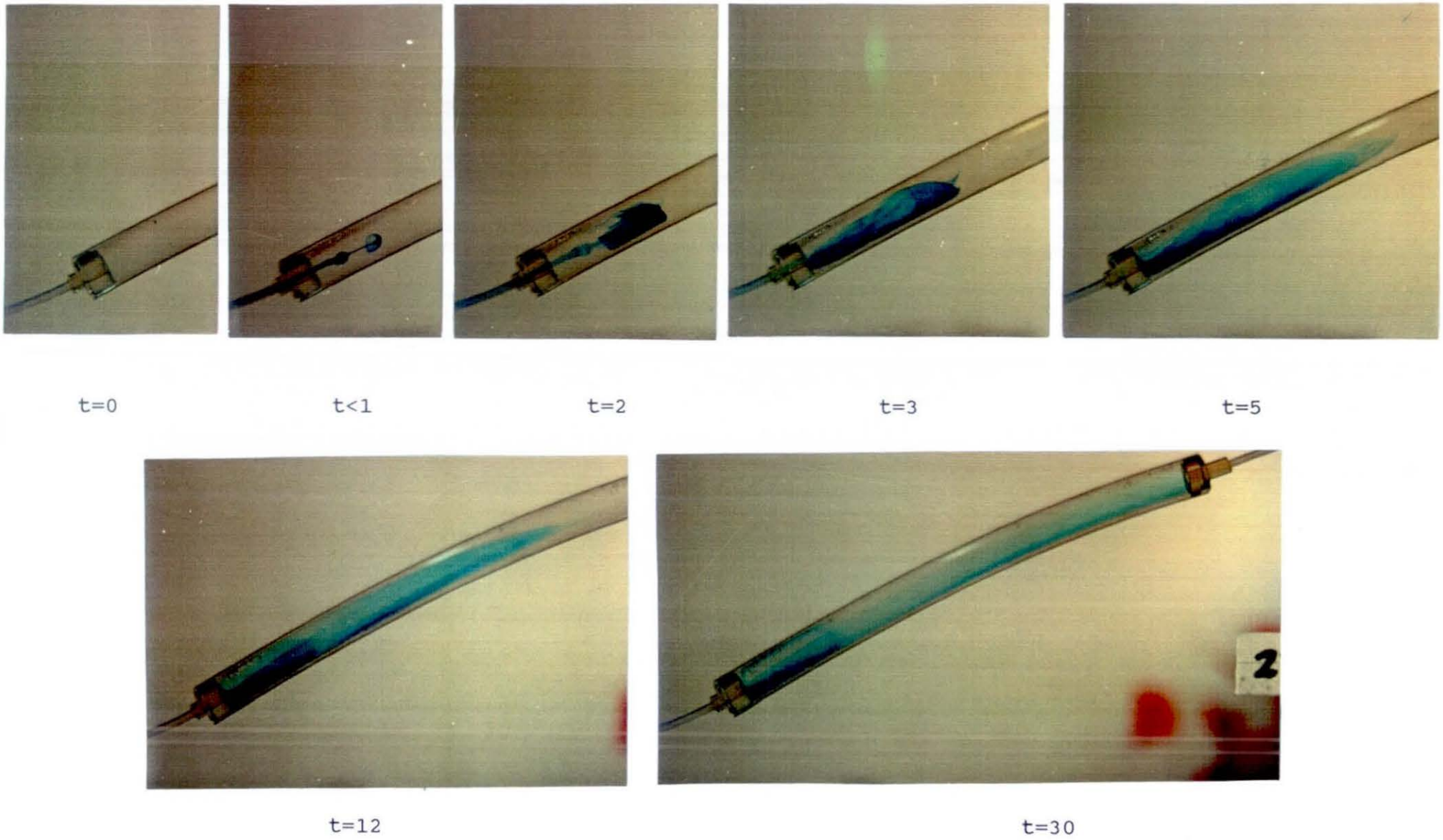

Fig. 3.15. Manifold mixing characteristics and sample transport: sample nitric acid concentration 0.50 mol dm^{-3} (0.25% m/v methylene blue); Aqueous carrier, 2.9 ml min^{-1}; t, time after sample injection (s).

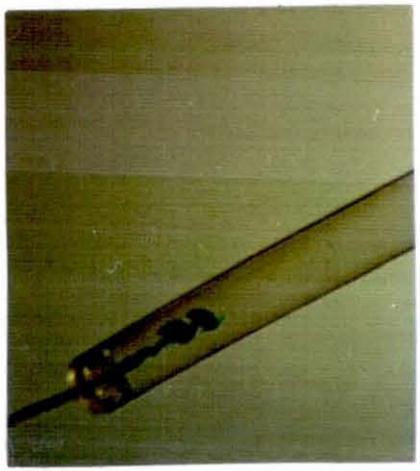

t<1

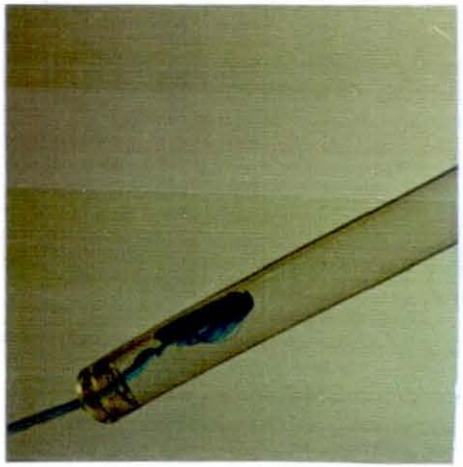

t=2

t=3

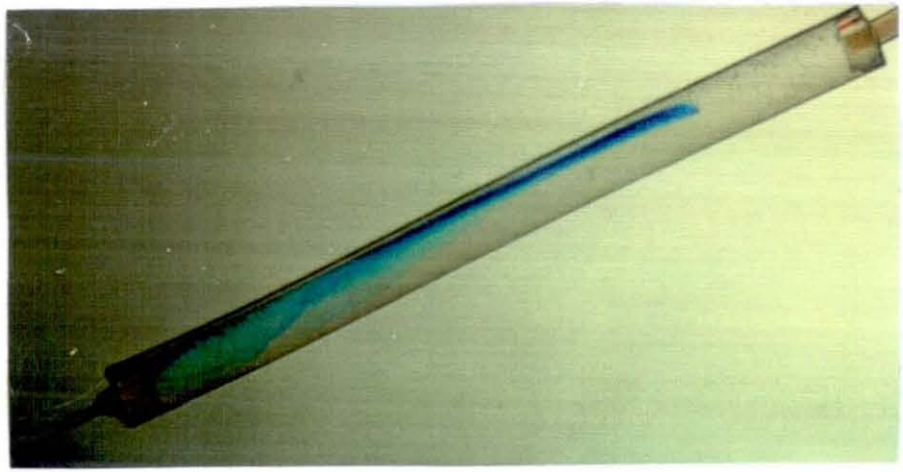

t=8

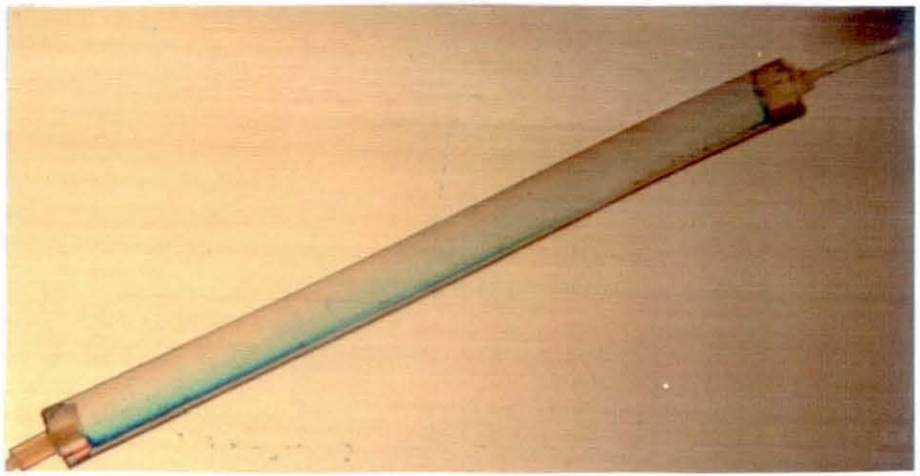

t=60

Fig. 3.16. Manifold mixing characteristics and sample transport: sample nitric acid concentration 0.025 mol dm^{-3} (0.25% m/v methylene blue); 1.000 mol dm^{-3} nitric acid carrier, 2.9 ml min^{-1}; t, time after sample injection (s).

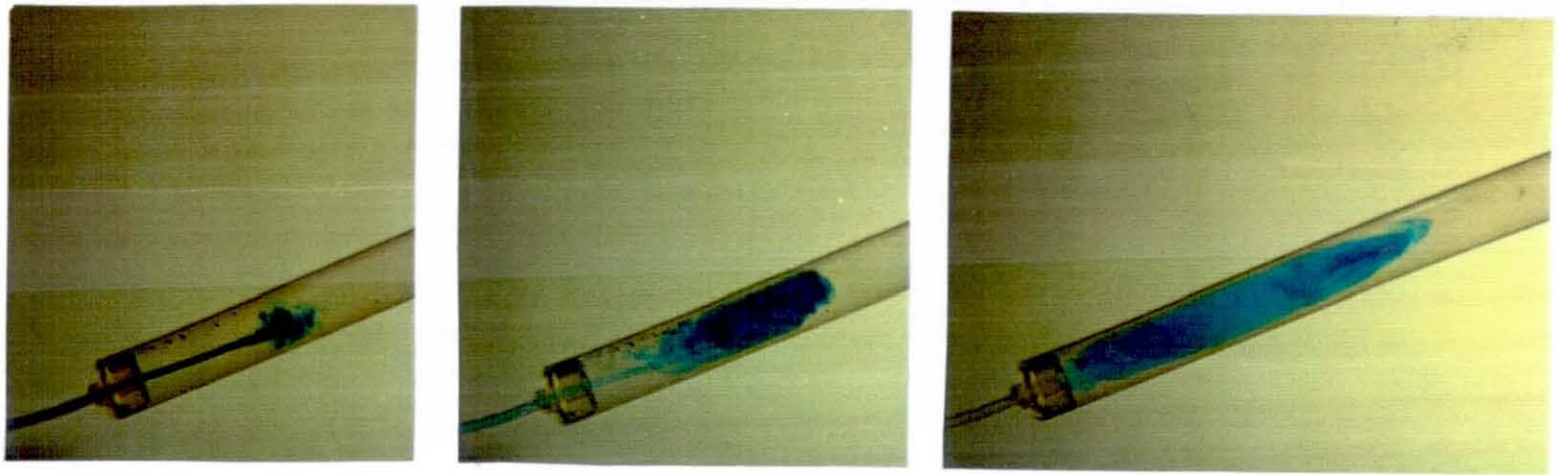

t<1 t<1 t<1

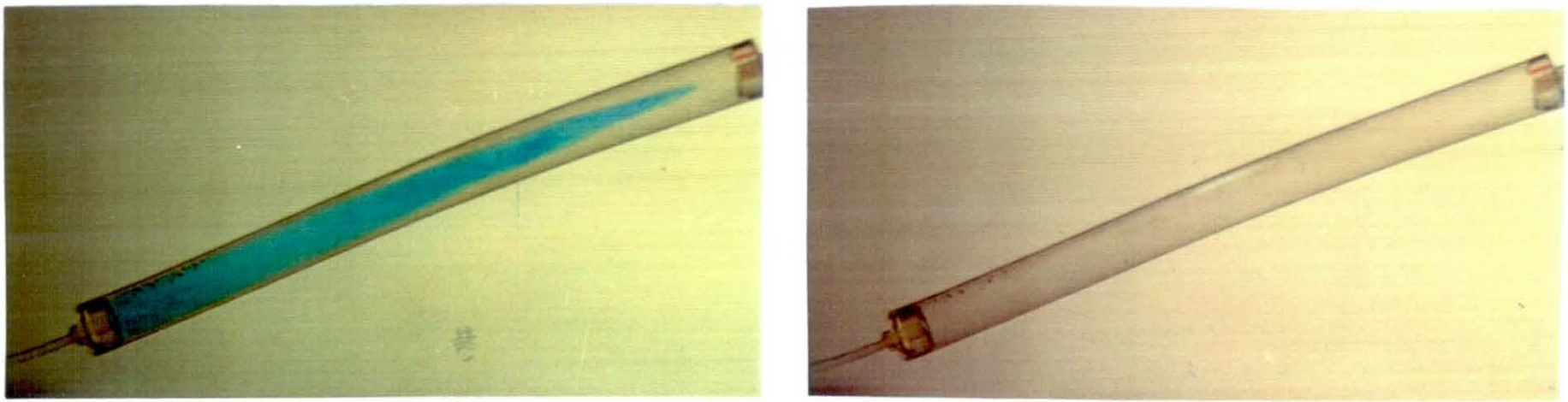

t=2 t=10

Fig. 3.17. Manifold mixing characteristics and sample transport: sample nitric acid concentration 0.025 mol dm^{-3} (0.25% m/v methylene blue); Aqueous carrier, 18.0 ml min^{-1}; t, time after sample injection (s).

3.3.9.1 Discussion.

The most notable observation was the effect of the instantaneous step change in mean carrier velocity moving from the narrow bore (0.8 mm i.d.) to the wide bore manifold tubing (5.0 mm i.d.). The mean carrier velocity was calculated to be 96.2 and 2.5 mm s^{-1} for the two tubes respectively. Fluid emerging from the smaller tubing was unable to follow the abrupt deviation of the tube boundary; consequently a turbulent jet developed [269]. Theory predicts that a turbulent jet is formed when a moving stream meets a stationary fluid. A sheet of vorticity is subsequently generated at the interface between the fluids, and this leads to the formation of a wedge shaped turbulent mixing layer, as shown in *Fig. 3.18.*

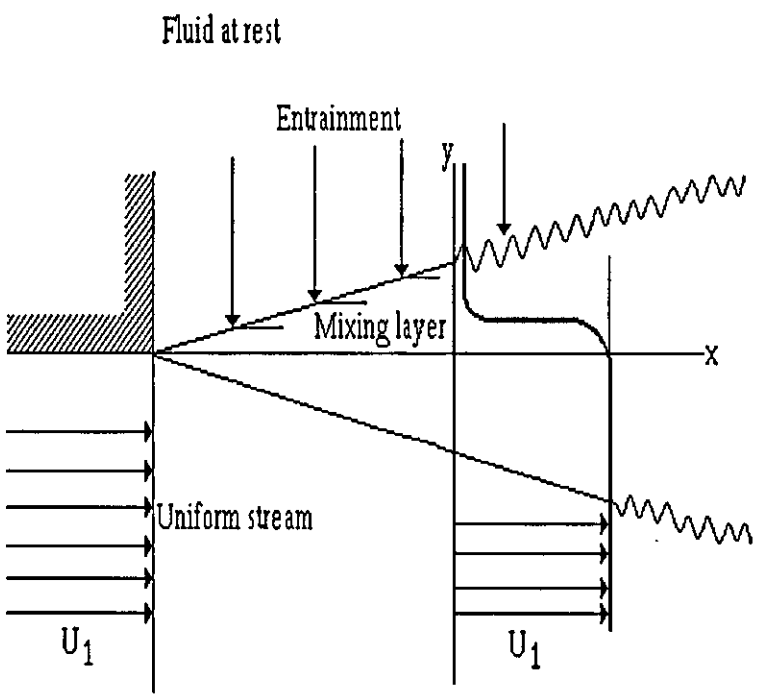

Fig. 3.18. Turbulent mixing layer.

It is suggested that similar mixing occurs in the system in question, taking into account the contribution made to mixing by the flow of carrier within the wide bore tubing itself. Mixing within the wide bore tubing at its inlet is suggested to be predominantly controlled by the characteristics of the turbulent jet. As the jet velocity attains equilibrium with that of the carrier velocity it is expected though that the mixing characteristics become more controlled by laminar flow, observed in the later portion of the wide tubing. A consequence of the turbulent jet is the

formation of turbulent eddies within the corners of the wide bore tubing inlet [270]. These such eddies were identified from observed recirculation of dye at the wide bore tubing inlet. Changes in the flow and mixing characteristics of the manifold were observed on increasing the acid concentration of the injected sample, (*Figs. 3.14 and 3.15*). After the initial flow of the acidified sample (0.50 mol dm^{-3} HNO_3) into the wide bore tubing the sample bolus was less well defined. The bolus was observed to be directed to the lowest part of the wall of the tube where the highest concentration of dye was visually identified and observed to move slowly along the tube. The observations made suggested that the changes in mixing characteristics were attributable to changes in the specific gravity of the sample with changing nitric acid concentration. Due to the low mean linear velocity of the carrier (2.5 mm s^{-1}) in the wide bore tube changes in sample density affected the rate and mode of sample transport through the manifold. The visual observations made gave good explanation for the variation in dispersion coefficient with nitric acid concentration (Section 3.3.8). High values of the dispersion coefficient obtained at high nitric acid concentrations were clearly achieved due to the slower transportation of the sample along the tubing wall, where the linear velocity approaches zero, producing as a result a prolonged period of sample dilution. Retention of sample beneath the manifold inlet port (*Fig. 3.15*, t=12) and the subsequent recirculation mixing is proposed as another mechanism for the increase in observed sample dilution.

Further evidence for the significant effect of specific gravity on the manifold performance was given by the visual observations made of the nitric acid carrier, (*Fig. 3.16*). The injected sample (0.025 mol dm^{-3} HNO_3) of a lower specific gravity than that of the 1.000 mol dm^{-3} nitric acid carrier, was observed to be transported along the upper wall of the tube. In comparison with the results of the previous investigations in which a water carrier was employed the sample was observed to undergo limited recirculation mixing. These observations accounted for the sharp narrow signal response peak shapes obtained in earlier experiments (*Fig. 3.13*).

With a higher carrier flow rate of 18.0 ml min^{-1} with a consequent higher mean linear velocity (15.3 mm s^{-1}) the sample was seen to be transported rapidly through the wide bore tube in less than ten seconds without any hold up "dead" volumes (*Fig. 3.17*). It was concluded that by increasing the carrier flow rate the specific gravity restrictions of the manifold could be reduced. Therefore, investigation into performance of the wide bore manifold at high carrier flow rate was made, (Section 3.3.10).

3.3.10 Effect of increased flow rate on system performance.

The spectrometer was operated at the optimum conditions (Table 3.1) connected to the manifold shown in *Fig. 3.1.* A section of PTFE wide bore manifold tubing, 90 mm (5.0 mm i.d.) was connected to the injector and nebulizer by two lengths of manifold tubing, 80 mm (0.8 mm i.d.) and 50 mm (0.5 mm i.d.) respectively.

A study of the effect of the concentration of nitric acid in the sample for a standard solution of 50 $\mu g\ ml^{-1}$ of Ca was carried out. Standard solutions were injected in turn into an aqueous carrier flowing at 18.0 ml min^{-1}. The dispersion coefficient was calculated for each determination (n=10) as outlined previously (Section 3.3.5). The effect of nitric acid concentration (0.025-1.000 mol dm^{-3}) on dispersion coefficient is shown in Table 3.7.

Table 3.7 Effect of sample nitric acid concentration on dispersion coefficient; Wide bore manifold, 90.0 mm (5.0 mm i.d.); pump flow rate 18 ml min^{-1}; injection volume 21 µl (50 $\mu g\ ml^{-1}$ Ca) (± 95% confidence interval).

Nitric acid concentration, mol dm^{-3}	Dispersion coefficient D	RSD (%), (n=10)
0.025	63.5±2.1	4.6
0.050	60.9±2.2	5.0
0.100	64.0±1.7	3.8
0.500	63.0±1.7	3.8
1.000	60.7±2.0	4.5

The effect of the manifold length (5.0 mm i.d.) on dispersion coefficient and signal response peak shapes for a single 50 $\mu g\ ml^{-1}$ Ca standard solution (1.000 mol dm^{-3} HNO_3) was studied. The standard solution was injected into an aqueous carrier flowing at 22 ml min^{-1}. The dispersion coefficient for each determination was calculated as outlined perviously (Section 3.3.5). The effect of manifold length (15-190 mm i.d.) on dispersion coefficient and signal response peak shapes is shown in *Figs. 3.19 and 3.20* respectively.

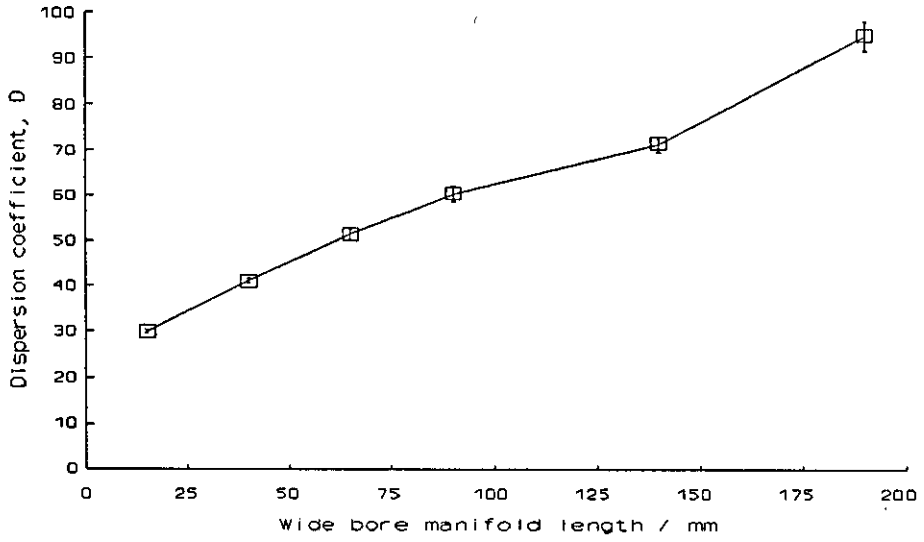

Fig. 3.19. Effect of manifold length on dispersion coefficient (5.0 mm i.d.); pumping rate 22 ml min^{-1}; injection volume 21 µl (50 µg ml^{-1} Ca).

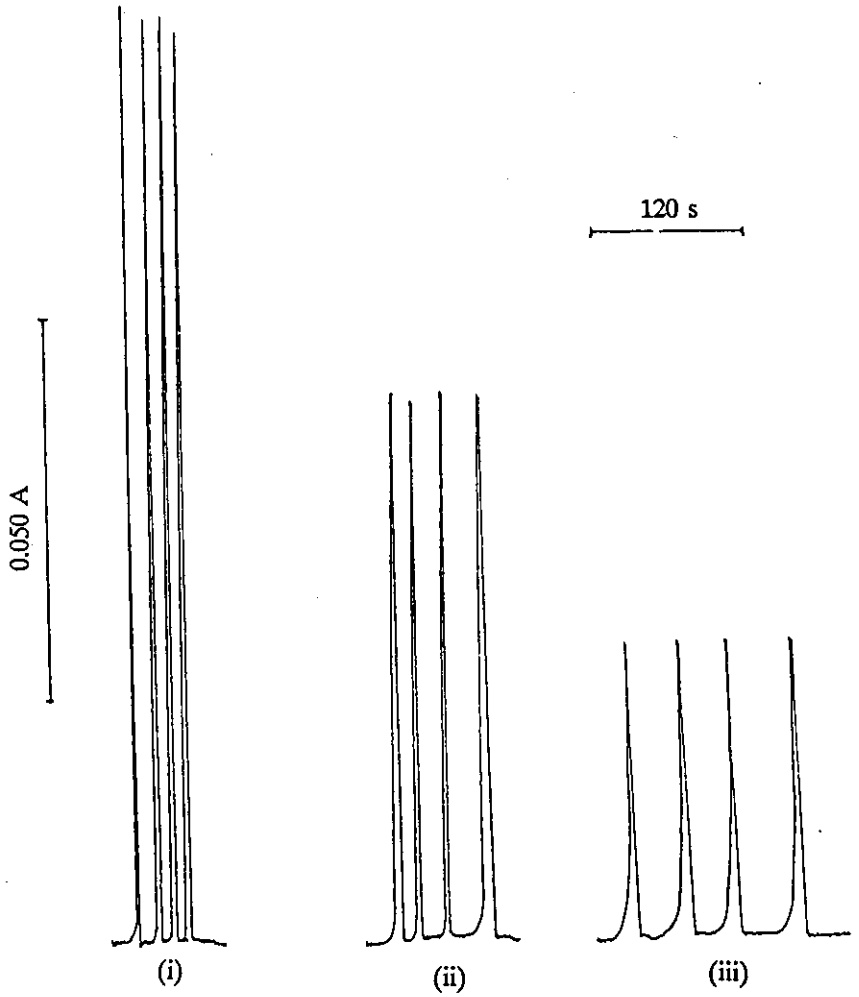

Fig. 3.20. Signal response peak shapes obtained at a high carrier flow rate with varying manifold length (5.0 mm i.d.). Aqueous carrier flow rate 22 ml min^{-1}; injection volume 21 µl (50 µg ml^{-1}). (i), 15 mm; (ii), 90 mm; (iii), 190 mm.

3.3.10.1 Discussion.

The use of a higher carrier flow rate (18.0 ml min^{-1}) was shown (Table 3.7) to eliminate the dispersion coefficient dependency on the specific gravity of the sample, over the nitric acid concentration range investigated (0.025-1.000 mol dm^{-3}). The precision though achieved at the high carrier flow rate was poor. Relative standard deviation (%RSD) values calculated for the dispersion coefficients obtained ranged between 3.8 and 5.0%. These relatively high figures may be explained by the imprecision of sample introduction using the manually operated rotary injection valve. The obtained signal response was observed to be affected by the rate at which the valve was actuated. To limit the imprecision the valve was actuated as smoothly and rapidly as possible for all work reported. Another reason for the poor precision may simply be the imprecision of the spectrometer response with the use of such a high sample introduction rate. From section 3.3.4.2 it had been shown, in the determination of Pb, that the precision for both steady state and FI sample introduction deteriorated at flow rates much above the natural uptake rate of the nebulizer.

Increments of dispersion coefficients between the values of 30 and 90 were achieved through varying the manifold tube length between 15 and 190 mm, (*Fig. 3.19*). No investigation was made at longer tube lengths due to the proposed gradual introduction of the previously observed specific gravity effects with increased sample residence within the tube. Improved sample throughput was obtained as an additional benefit of using a high carrier flow rate. From *Fig. 3.19* it was calculated that a dispersion coefficient of 90 would be possible with a corresponding throughput of 80 h^{-1}. As observed with the lower carrier flow rate (2.9 ml min^{-1}) the retention of air bubbles within the wide bore tubing was a major problem. Degassing the aqueous carrier solution however proved unsuccessful in preventing the formation of air pockets, following the nucleation of small air bubbles.

3.4 DISCUSSION.

The potential of FI with wide bore manifold tubing as a means of carrying out on-line dilution is limited. Although capable of values of dispersion coefficients up to and in excess of the target figure of 100, the dependence on the specific gravity of the sample limits the applicability in the handling of routine samples. Without accurate matrix matching of samples and standards, a significant error due to variations in the specific gravity of the samples with varying acid

concentrations, matrix components etc would be obtained. However, matrix matching, if possible at all, would increase the sample preparation time contradicting the objectives of the system.

Although the performance of the system is improved at a high carrier flow rate of 22 ml min^{-1} it still retains some inherent practical limitations. Retention and subsequent nucleation of tiny air bubbles in the manifold is a significant problem. Build up of these air bubbles clearly limits the reproducibility of mixing within the manifold. A suggested solution to this problem is the tapering of the wide bore tubing at its inlet and outlet. It is predicted though that this strategy would significantly alter the mixing characteristics of the whole system through the removal of the instantaneous step change in mean carrier velocity. This may limit the magnitude of dispersion coefficient achieved.

Precision of the system is clearly a limiting factor with relative standard deviations in the range of 3-5%. As previously discussed (Section 3.3.10.1) this may be attributed in part to the imprecision experienced in sample introduction using a manually operated rotary injection valve. It is possible that the precision could be improved through the use of an automatic injection valve. Results obtained in section 3.3.4.2 though suggest that the precision of the system is also restricted by the imprecision of the spectrometer response, since the sample is introduced at a flow rate significantly higher than the natural uptake of the nebulizer (5.2 ml min^{-1}). To overcome this problem it is suggested that the carrier flow could be split prior to the spectrometer, therefore permit the introduction of carrier to the nebulizer at or below its natural uptake rate [132].

The drawbacks of the system originate to some extent from the presence of several different types of hydrodynamic mixing regimes within the manifold. From visual observations made the specific gravity effects appear to occur with the onset of laminar flow, at a point when the sample solution flow velocity reaches equilibrium with that of the carrier solution in the wide bore tube. It is postulated therefore to optimize the system performance that mixing should be made totally turbulent by either limiting the manifold length at a high carrier flow rate, or possibly through the packing of the wide bore tube with glass beads (Packed bed reactor). This would produce a pseudo well stirred mixing chamber used previously by others with success [163-166].

CHAPTER FOUR

ELIMINATION OF COPPER INTERFERENCE BY CONTINUOUS FLOW MATRIX ISOLATION IN THE DETERMINATION OF Se^{IV} BY FI-HGAAS.

4.1 INTRODUCTION.

In recent years a variety of procedures for the automation of sample pretreatment in AAS have been developed with FI methodology. Systems capable of both preconcentration and matrix isolation employing liquid-liquid extraction [149, 183], ion exchange [188, 211] and precipitation [216, 221] have been developed, as reviewed in Chapter two (Section 2.3.4).

Few attempts have been made so far to use such systems for the removal of interference effects in hydride generation AAS. As a direct result, sample preparation in HGAAS remains a tedious time consuming operation limiting the overall performance, throughput and cost effectiveness of the technique. It is suggested, therefore, that the development of continuous flow systems in HGAAS, incorporating possible ion exchange [80] and precipitation [73-75] matrix isolation procedures would be of great benefit.

The first application of such a system was made by Ikeda [82] in 1985. A miniaturised suction-flow hydride generation system [235] (*Fig. 4.1 (I)*) was used for the determination of Se^{IV} in which a micro-column of chelating resin removed copper and nickel interferents. Although matrix isolation was carried out in-line the system relied on manual sample pipetting and had no facility for column regeneration.

Riby *et al.* [83] devised a system for the determination of As in a nickel based alloy (*Fig. 4.1 (II)*). An in-line micro-column of strong cation exchange material (SCX) was used for the removal of nickel. A timed sampling procedure was employed in which sample solution was aspirated continuously into the manifold at a known constant flow rate for a fixed time period. Although the analysis was successful some degree of compromise had to be made between the performance characteristics of the matrix isolation system and of the hydride generation manifold itself. Column regeneration was carried out after every four determinations by pumping a solution of 1 mol dm^{-3} HCl through the column to waste, after disconnecting the sample line. Intermittent replacement of the column was necessary due to compaction of the exchange material resulting in excessive back pressures within the system.

Recently Marshall and van Staden [71] described a similar system (*Fig. 4.1(III)*)for the removal of a variety of interferents (nickel, copper, cobalt, iron and chromium) in the determination of both As and Se. Samples were introduced directly into a carrier stream (0.05 mol dm^{-3} H_2SO_4 or 0.1 mol dm^{-3} HCl) via an air actuated injection valve and transported through the micro-column packed with cation exchange resin (AG50WX8). Column regeneration was achieved by pumping a 2 mol dm^{-3} solution of eluent HCl or H_2SO_4 (10 ml), directly through the column. It was found that inclusion of the micro-column in-line reduced the overall sensitivity as increased dispersion due to the presence of the column was produced giving rise to a smaller, broader signal response.

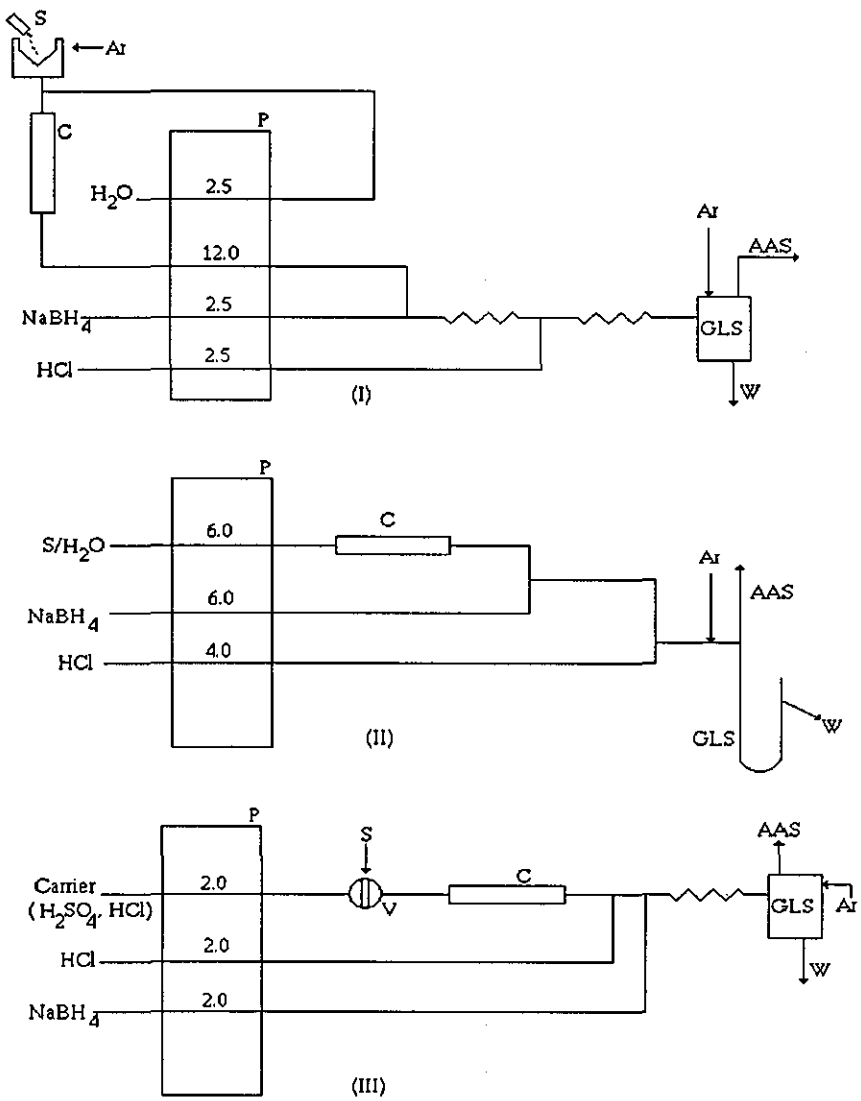

Fig. 4.1. Schematic diagrams of reported continuous flow matrix isolation HGAAS systems, (I) Ikeda [82]; (II) Riby *et al.* [83]; (III) Marshall and van Staden [71]. P, peristaltic pump; S, sample; C, micro-column; GLS, gas-liquid separator; V, injection valve; W, waste.

This chapter describes an investigation of a FI system for the determination of Se in copper by hydride generation AAS. The copper interference was eliminated with a continuous flow matrix isolation procedure based on a micro-column of strongly acidic cation exchange resin (Dowex 50W). The matrix isolation manifold and hydride generation were interfaced through the sample injection valve in a manner similar to that reported by Nord and Karlberg [183] for liquid-liquid extraction with FAAS. A direct comparison is made between the performance characteristics of this novel system design and those of previously reported systems [71, 82, 83]. Aspects of the work in this chapter have been published [271].

4.2 APPARATUS AND REAGENTS.

4.2.1 Apparatus.

A Philips scientific SP9 atomic absorption spectrometer equipped with a Philips data coded selenium hollow cathode lamp was used for all determinations. The signals were recorded on a Tekman TE 200 chart recorder (2-10 mV range), all measurements being expressed as peak height absorbance. A 50 mm Philips scientific universal burner was used to support the air-acetylene flame heated silica cell (120 mm x 8 mm i.d.). The spectrometer was operated under the conditions shown in Table 4.1 based on the manufacturer's recommendations [268]. The silica T-cell was aligned to maximise the intensity of lamp radiation, passing along its central axis reaching the monochromator.

Table 4.1 Philips SP9 spectrometer variables for the determination of selenium.

Wavelength, nm	196.0
Slit width, nm	1.0
Lamp current, mA	7.5
Support gas/ flow setting, (Arbitrary units)	28/air
Fuel gas/flow setting, (Arbitrary units)	15/acetylene
Background correction	OFF
Damping	OFF

In initial studies a Philips scientific PU9360 continuous flow vapour system was used [272]. The system was adapted for flow injection by the incorporation of a manual Rheodyne (Model 5020) fixed volume injection valve, as shown in *Fig. 4.2 (I)*.

The FI hydride generation manifold used for all matrix isolation work, shown in *Fig. 4.2 (II)*, was developed from the gas-liquid separator and hydride atomization systems of the Philips Scientific PU9360 continuous flow vapour system.

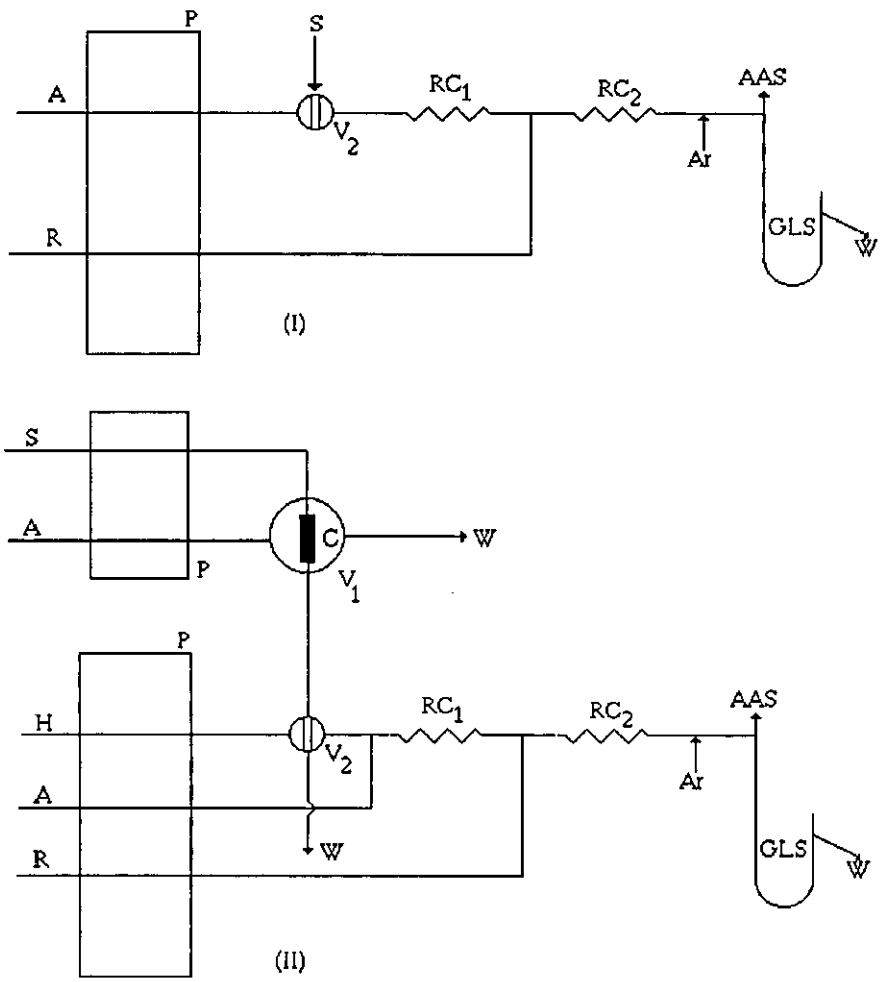

Fig. 4.2. Schematic diagrams of FI-HGAAS manifolds used.
(I) FI manifold based on PU9360 system; (II) FI manifold with continuous flow matrix isolation unit. P, peristaltic pump; S, sample; H, water; A, HCl; R, $NaBH_4$; W, waste; V_1, switching valve; V_2 sample injection valve; C, micro-column; GLS, gas-liquid separator; RC, Reactor coil.

Two peristaltic pumps were employed. A Gilson Minipuls 3 was used for the hydride generation manifold and a Gilson Minipuls 2 for the matrix isolation unit. Control of the flow rates was achieved through the application of different bore standard manifold pump tubing (Altec). Flow rates were determined for each channel as reported in section 3.3.2. Sample injection was achieved using a Rheodyne model 5020 fixed volume injection valve operated by an electronically activated valve switching unit (Anachem). Sample loops of various volumes were prepared using polytetrafluoroethylene (PTFE) tubing (0.5-1.5 mm i.d.) cut to appropriate lengths. The sample loops were calibrated using the procedure described in section 3.3.3. All manifold tubing consisted of 0.8 mm i.d. PTFE tubing (Anachem). Manifold channels were connected through three way connector T-pieces (Anachem). A length of polyvinylchloride (PVC) tubing (200 mm, 5.0 mm i.d.) was used to connect the gas-liquid separator and silica atomization T-cell.

A microbore glass column (50 x 3.0 mm i.d. (Anachem)) fitted with porous 25 μm PTFE frits, containing the cation exchange resin (Dowex 50W), was incorporated into the external sample loop of a rotary sample injection valve (Anachem).

4.2.2 Reagents.

Analytical-reagent grade water produced by a LiquiPure RG system (reverse osmosis followed by ion exchange), was used for all solutions and as a carrier stream. A sodium tetrahydroborate solution (1% m/v in a 0.1% m/v NaOH solution) was prepared using sodium tetrahydroborate pellets (SpectrosoL, BDH) and filtered through a Whatman 541 filter paper. With refrigeration, this solution was usable for up to 3 days. The hydrochloric acid reagent solutions were of SpectrosoL grade (BDH). All selenium (IV) standard solutions were prepared by dilution of a standard solution of selenous acid (SpectrosoL, BDH) containing 1000 μg ml^{-1} Se^{IV}. The atomization cell was conditioned with a 5% v/v solution of hydrofluoric acid (40% AnalaR, BDH). For the interference investigation, interferent standard solutions were prepared from copper (II) nitrate, cobalt (II) nitrate, iron (III) nitrate, nickel (II) nitrate (all SpectrosoL grade, BDH) and nickel (II) sulphate 7 hydrate (AnalaR, BDH).

For the matrix isolation investigation, copper standard solutions were prepared from copper (II) sulphate 5 hydrate (AnalaR, BDH). High purity argon was used as the purge

gas (99.998% Ar, BOC). A potassium hydrogen phthalate solution was prepared directly from the solid (LaB reagent, BDH). The digestion of copper metal reference materials was carried out using nitric acid (Aristar, BDH) and hydrochloric acid (Aristar, BDH). Two cation exchange resins were investigated, Dowex 50WX8 (Drymesh 100-200, 8% cross linkage) and Dowex 50WX12 (Drymesh 50-100, 12% cross linkage), both used in their hydrogen forms (Sigma Chemicals). Two copper metal reference materials, National Institute of Standards and Technology (NIST); Standard Reference Material (SRM) 454 unalloyed copper XI and Bundesanstalt fur material forschung und prufung (BAM) Certified Reference Material (CRM) 361 copper, were obtained from the Bureau of Analysed samples (Middlesbrough, U.K.).

4.3 ADAPTATION OF THE PHILIPS PU9360 CONTINUOUS FLOW VAPOUR SYSTEM FOR FI-HGAAS.

4.3.1 Optimization of system variables.

The spectrometer, operated according to the conditions shown in Table 4.1 was connected to the FI-HGAAS manifold (*Fig. 4.2 (I)*). The PU9360 continuous flow vapour system was operated under the conditions shown in Table 4.2, based on the manufacturer's recommendations [272]. Unless otherwise stated, a 100 ng ml^{-1} Se^{IV} standard acidified with 1.2 mol dm^{-3} HCl was used in the investigations of the effects of each parameter on the overall performance. No attempt was made to carry out an exhaustive optimization of the manifold variables since the basic aim of the study was to compare the performance of the PU9360 system for both continuous and FI sample introduction. A simple univariate optimization procedure was used for the reasons discussed in section 4.5.4.

Table 4.2 PU9360 Continuous flow vapour system operating parameters for the determination of Se^{IV} by HGAAS.

Reagent	Concentration	Flow Rate/ ml min^{-1}
HCl carrier	1.2 mol dm^{-3}	7.4
$NaBH_4$	1.0 % m/v	3.2
Ar	-	600

* Reactor coils RC_1 200 mm (0.8 mm i.d., straight), RC_2 270 mm (0.8 mm i.d., straight)

(I) Effect of flame stoichiometry.

The effect of flame stoichiometry on the steady state absorbance signal response was investigated. Sampling was achieved by pumping the standard solution continuously through the acid carrier channel (PU9360 under conventional operation). At a fixed air support gas flow setting of 28 (arbitrary units) an increase in signal absorbance from 0.406 to 0.575 was observed with a decrease in the acetylene flow rate setting from 20 to 15 (arbitrary units). An "optimum" acetylene flow setting of 15, producing a very fuel-lean flame, was chosen for all further work. At flow settings below 15 the flame was extinguished and so the system performance was restricted by the working limitations of the air-acetylene flame.

(II) Effect of argon carrier gas flow rate.

The effect of argon carrier gas flow rate on the FI (390 µl) and steady state (5000 µl) absorbance signal response is shown in *Fig. 4.3.*

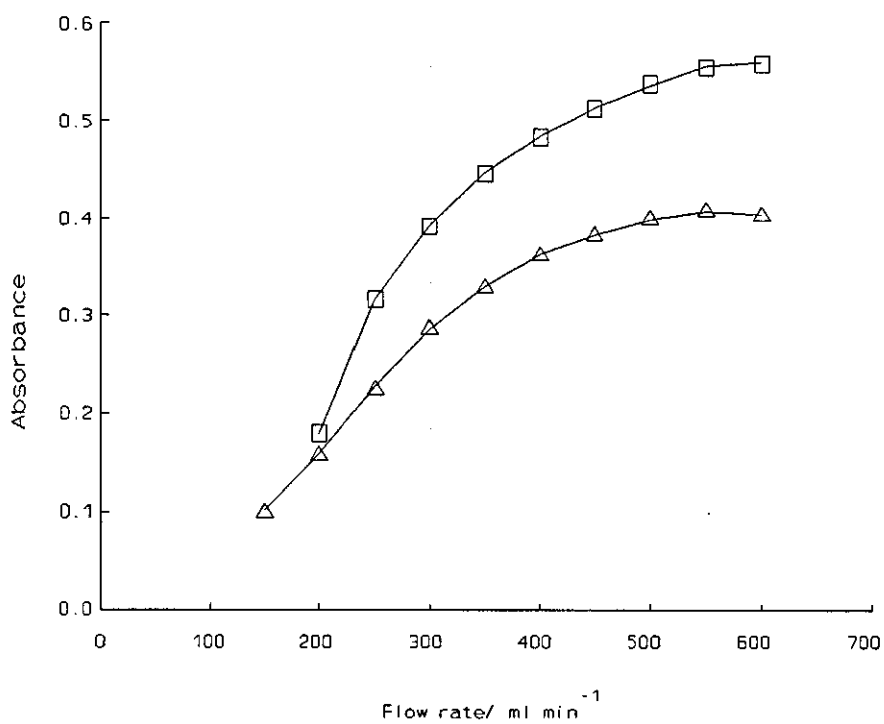

Fig. 4.3. Effect of the flow rate of Ar on the absorbance of 100 ng ml^{-1} of Se^{IV}. (■), Steady state (5000 µl); (▲), FI (390 µl). All other variables as in Table 4.2.

An optimum Ar flow rate of 600 ml min^{-1} was chosen based on sensitivity and an observed increased rate of transport of the hydride to the atomization cell producing

sharper FI signal peak responses. The reduced signal absorbance observed for the flow injection study was explained by the dominant effect of gas phase dilution within the large internal volume of the U-tube gas-liquid separator, designed for continuous flow operation. This effect was enhanced at higher Ar flow rates.

(III) Effect of manifold dimensions.

The effect of reactor coil length (RC_2, *Fig. 4.2 (I)*) on the sensitivity for Se^{IV} was negligible (<10%) over the range 270-2000 mm (FI, 390 µl). On the basis of throughput and postulated improved interference tolerance with reduced reaction time, (as reported by Astrom [13]) a rector length of 270 mm was chosen as optimum.

(IV) Effect of injection volume.

The effect of injection volume on the sensitivity of Se^{IV} is shown in *Fig. 4.4.* Increasing the injection volume gave rise to an increase in sensitivity until the steady state limit was reached at approximately 1000 µl. Employing a 390 µl injection volume 90% of the steady state sensitivity was achieved (characteristic concentration 0.83 ng ml^{-1} Se^{IV}).

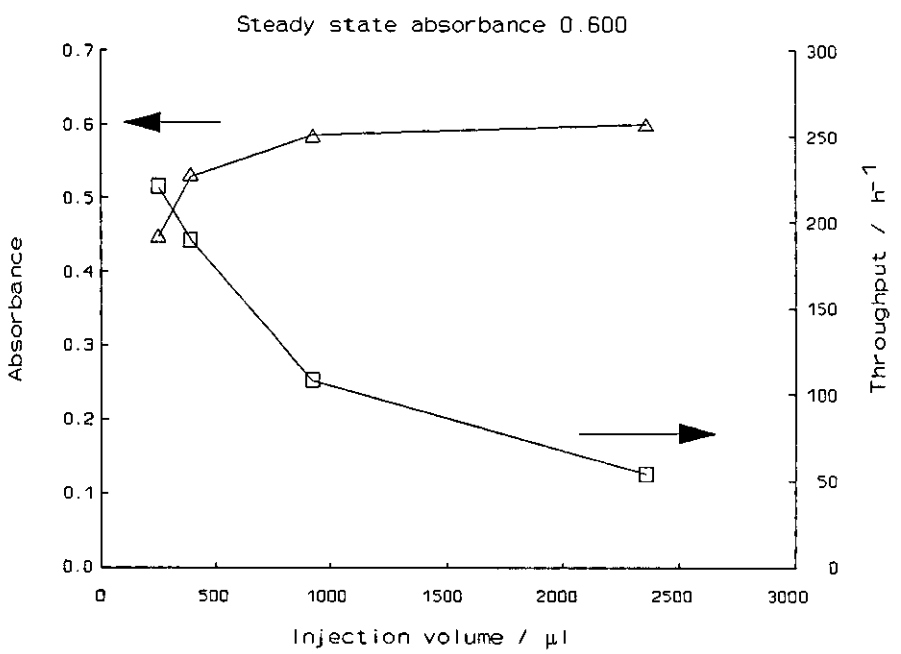

Fig. 4.4. Effect of injection volume on system performance for the determination of 100 ng ml^{-1} of Se^{IV}. All other variables as in Table 4.2.

Although large injection volumes favoured high sensitivity, reducing the injection volume reduced the sample volume requirement and improved the throughput capability (*Fig. 4.4*). For a 390 µl injection volume a throughput of 190 h^{-1} was achieved in comparison with 45 h^{-1} reported for steady state introduction [272]. The precision was less than 2% (RSD, n=9) for each injection volume investigated.

4.3.2 On-line sample acidification.

The FI-HGAAS manifold shown in *Fig. 4.2 (I)* was used with the values of parameters shown in Table 4.2. A procedure was investigated to permit on-line acidification of samples to eliminate the tedious and time consuming manual sample acidification step of the sample preparation. The method investigated was the on-line mixing of the hydrochloric acid carrier solution with the injected sample plug by the process of dispersion.

The effects of reactor coil lengths on the signal responses obtained in the determination of 50 ng ml^{-1} of Se^{IV} (390 µl) and 100 ng ml^{-1} of Se^{IV} (250 µl) are shown in Table 4.3.

Table 4.3 Effect of reactor coil length (RC_1) on the absorbance of a non-acidified Se^{IV} standard solution.

Reactor coil, mm (RC)	Peak height absorbance		
	Investigation (I)	Investigation (II)	Investigation (III)
200	0.147±0.020^{DP}	0.189±0.010^{DP}	0.302±0.005
600	0.158±0.006^{DP}	0.182±0.009^{DP}	0.320±0.008
750	0.176±0.009^{DP}	0.180±0.016^{DP}	0.349±0.007
1000	0.201±0.007	0.209±0.024	0.317±0.006
1500	0.212±0.007	0.217±0.004	-.-
2000	0.174±0.010	-.-	0.255±0.002

(I) RC_2 260 mm, injection volume 390 µl, (50 ng ml^{-1} Se^{IV})
(II) RC_2 2000 mm, injection volume 390 µl, (50 ng ml^{-1} Se^{IV})
(III) RC_2 260 mm, injection volume 250 µl, (100 ng ml^{-1} Se^{IV})
Other variables as Table 4.2 (± 95% confidence interval)
* DP Doublet peak (absorbance, largest of two peaks).

It was observed (Table 4.3) that for on-line acidification, no improvement in sensitivity could be obtained by increasing the sample injection volume. This was due to the increased dilution of the sample plug with prolonged dispersion, necessary to achieve acidification of the whole sample zone and produce a single response peak. For the optimum manifold dimensions 390 µl (RC_1 1500 mm, RC_2 2000 mm) and 250 µl (RC_1 750 mm, RC_2 260 mm) characteristic concentrations of 1.0 and 1.1 ng ml^{-1} Se^{IV} and throughputs of 90 and 140 h^{-1} respectively were obtained.

To optimize the performance of the system by applying on-line acidification through the dispersion process it is apparent that the injection volume should be kept to a minimum to reduce the manifold dimensions required to achieve mixing and therefore optimize throughput and reduce sample volume requirement.

4.3.3 Copper interference tolerance.

The interference of copper in the determination of Se^{IV} was investigated for the manifold shown in *Fig. 4.2(I)* operated under the values of the parameters shown in Table 4.2. ~~Table 4.3.~~ Samples containing 50 ng ml^{-1} Se^{IV} and varying concentrations of copper (copper(II)nitrate, SpectrosoL, BDH) were acidified to 1.2 mol dm^{-3} HCl and analysed directly without further sample preparation. The relatively sensitivity of each copper spiked sample was calculated with respect to a pure 50 ng ml^{-1} Se^{IV} standard solution, for which interference free determination was assessed as that producing a recovery of 100±10%.

For a sample injection volume of 254 µl, copper interference was observed at copper concentrations of above 0.50 µg ml^{-1}. At a copper concentration of 5.0 µg ml^{-1}, a relative sensitivity of 13.3% was gained and at 50 µg ml^{-1} of Cu no signal at all was observed. It was noted during the investigation that the overall sensitivity decreased with increased processing of interferent samples, and increased interferent concentration. This interference memory effect was to an extent, transient in nature since its magnitude decreased after interferent processing with repeated determination of interferent free standard solutions. The reactor coil (RC_2) was observed to have become discoloured with a fine grey precipitate. Although no attempt was made to identify this grey precipitate, it was proposed that it was in part responsible for the interference memory effect.

The acid concentration of both samples and carrier solution was increased to 6.0 mol dm^{-3} HCl, as a result of which the copper interference free determination of Se^{IV} was increased to 5.0 μg ml^{-1} of Cu. Neither interference memory effect or precipitated species were observed for FI sample introduction (254 μl) at this elevated acid concentration. This was not the case, though for steady state determinations. The interference free determination of Se^{IV} with an injection volume of 5000 μl was decreased to 0.5 μg ml^{-1} of Cu and an interference memory effect was very evident. Grey precipitate was observed in both rector coil and gas-liquid separator and, during sample processing, a reddish brown discoloration of the reaction mixture was clearly visible.

4.3.3.1 Discussion.

The interference memory effects observed throughout the investigation work are thought to be caused by a combination of two effects. The first of these effects is the retention of reduced copper and or copper species within the gas-liquid separator and reactor coil (RC_2)and their effect on the formation of the gaseous hydride and or the formed hydride itself. Pettersson *et al.* [241] reported similar memory effects in the determination of Se^{IV} in the presence of copper which they attributed to the contamination of manifold tubing. Evidence for this proposed mechanism was the actual identification of permanent precipitate within the reactor coil and the reduction in the magnitude of the memory effect with time, expected with the slow washout of interferent species from the gas-liquid separator. Increased interference tolerance and elimination of the memory effect at a high HCl concentration (6 mol dm^{-3}) is suggested to be explained by the increased solubility of the unidentified interfering species whether copper metal [14], copper boride species [47] or copper selenide [44, 46] and the formation of copper chloro complexes [46].

The second explanation for the interference memory effect is contamination of the silica atomization cell by copper species [46, 49]. It is suggested that species can be transported within a fine aerosol to the silica cell by the Ar carrier gas. Evidence for this effect was given in the later investigation into copper interference in the determination of As^{III} (Section 5.4.3). No interference memory effect was observed in the investigation in question when a PTFE membrane filter was fitted within the hydride transport tubing. In the same investigation it was shown that the interference free determination of As^{III} was possible with up to 1000 μg ml^{-1} of Cu despite the presence of a significant amount of permanent precipitate. It is

suggested, therefore, based on this observation that the major interference effect evident in the Se^{IV} study is due to the formation of copper selenide [44,46]. This does not dismiss though the possibility that the precipitation reaction plays some role in the interference mechanism or memory effects observed.

The improvement in interference tolerance with a reduction in sample volume is explained by the decrease in the absolute amount of interferent introduced into the HGAAS system [44,90]. With the introduction of a smaller amount of interferent (8% that used in the continuous flow system [272]) it is suggested that the solubility limit of the system is less likely to be exceeded, therefore the precipitation and accumulation of interferent species within the system is prevented [90].

4.3.4 Discussion.

The adaptation of the PU9360 continuous flow vapour system to FI-HGAAS was successful. From the results (Section 4.3.1) it is evident that in comparison with steady state analysis comparable sensitivity can be achieved with FI sample introduction but with the added advantages of superior throughput, reduced sample requirement and superior copper interference tolerance. A characteristic concentration of 0.83 ng ml^{-1} Se^{IV} (390 µl) compares favourably with 0.91 ng ml^{-1} Se^{IV} quoted by the manufacturer's for steady state analysis with the PU9360 system [272].

Incorporation of an on-line sample acidification step within the system by dispersion of the sample within an acid carrier stream has limitations. The procedure is restricted in many respects to low sample injection volumes (250 µl) for which performance characteristics comparable with pre-acidified samples are achieved. Use of high injection volumes (≥ 390 µl) requires excessively long reactor coil lengths to achieve adequate mixing and produces no improvement in sensitivity (Section 4.3.2).

The observed high copper interference in the determination of Se^{IV} is in agreement with the observations of others [14, 44-46]. Although some improvement in the system interference tolerance was achieved through the manipulation of system variables (Section 4.3.3) the maximum copper concentration tolerated in the system was restricted to 5.0 µg ml^{-1}.

From these observations there is clearly some need to improve the interference tolerance of the system further to extend its use to the analysis of real samples containing copper. The use of an on-line ion exchange matrix isolation procedure [71,82, 83] was therefore investigated.

4.4 DESIGN FEATURES OF A FI-HGAAS MANIFOLD INCORPORATING CONTINUOUS FLOW MATRIX ISOLATION.

A flow injection manifold was developed based on the design reported by Nord and Karlberg [183] for liquid-liquid extraction with FAAS, shown in *Fig. 4.2 (II)*. The matrix isolation and FI-HGAAS manifolds were made independent of each other and interfaced through the sample injection valve of the FI-HGAAS manifold. Sample pumped continuously through the column was sampled intermittently by the injection valve and introduced into the FI-HGAAS manifold. As the two flow systems were independent, the sample flow rate through the column could be kept low to keep the column efficiency high without having to compromise the sensitivity of the hydride generation manifold. The micro-column was incorporated within the sample loop of an injection valve to permit the intermittent regeneration of the column without the need to dismantle the manifold or replace the column as reported for previous systems [82, 83]. The regenerant solution flow was directed in the reverse direction to that of the sample to eliminate the possibility of column resin compaction.

4.4.1 System operation.

Calibration standard solutions, requiring no matrix isolation, were pumped continuously (2 ml min^{-1}) through the injection valve, bypassing the micro-column. The injection valve was actuated intermittently (load time, 20 s; and injection time, 10 s) thereby sampling the standard solution and introducing it into the hydride generation manifold.

Following the introduction of the standards, the micro-column was switched into the sample line and analytical-reagent grade water was continuously pumped through it to remove the hydrochloric acid. After washing the column, the sample was also introduced by continuous pumping. In order to fill the void volume of the column and pump tubing, the sample was pumped continuously for 60 s prior to sampling of the column eluent, as described for standard solutions. After triplicate injections, the micro-column was regenerated (using HCl) and the sample line washed with analytical-reagent grade water. [Hydrochloric acid (1.2 mol dm^{-3}) was pumped continuously through the micro-column

in the opposite direction to that of the sample flow (2 ml min^{-1}, 30 s)]. Following the short period of regeneration, the column was switched back in-line and the sampling procedure repeated. During the transfer of the uptake tube from sample to analytical-reagent grade water, the sample pump was stopped in order to prevent the introduction of air into the column. The hydride generation manifold was continuously run throughout the whole procedure, independently of the matrix-isolation unit. A summary of the sampling procedure including timing sequences is given in Table 4.4. At the start of each analysis, a standard solution of 1000 ng ml^{-1} Se^{IV} was injected two or three times. This procedure enhanced both the precision and sensitivity of the system for subsequent determinations (Chapter seven).

Table 4.4 Summary of the sampling procedure for matrix isolation including timing sequences.

Timing sequence (t)/ s	Operation
0	V_s*, H_2O pumped via column
20	V_s, sample pumped via column
80	V_I*, actuation, (load position)
100	V_I, actuation (inject position)
110	V_I, actuation (load position); injection procedure repeated to give triplicate injections
170	V_B#, HCl regenerent pumped via column, H_2O pumped via sample line
200	V_s, H_2O pumped via column, procedure repeated, t=0

*V_s, valve containing column in sampling configuration
✡V_I, sample injection valve
#V_B, valve containing column in bypass configuration

4.5 OPTIMIZATION OF THE FI-HGAAS MANIFOLD.

The flow injection manifold shown in *Fig. 4.2 (II)* was investigated with the independent matrix isolation unit removed. The system was optimized for the determination of Se^{IV} without any means of matrix isolation or other sample pretreatment (RC_1 100 mm, RC_2 100 mm (0.8 mm i.d.)).

4.5.1 Optimization of manifold variables for Se^{IV} determination.

The optimized variables for the FI-HGAAS manifold (Table 4.5) were obtained using a basic univariate approach, as used by Riby *et al.* [83]. In obtaining the optimum variables, sensitivity was a prime concern but consideration was also given to precision, interference tolerance and reliability of the system. Unless otherwise stated, the optimization of each manifold variable was carried out using an aqueous 100 ng ml^{-1} Se^{IV} standard, (Other variables as Table 4.5).

Table 4.5 Optimized variables for the determination of Se^{IV} by FI-HGAAS (409 µl).

Reagent	Concentration	Flow rate/ ml min^{-1}
H_2O carrier	-.-	6.0
HCl	6.0 mol dm^{-3}	4.2
$NaBH_4$	1.0% m/v	3.2
Ar	-.-	600

(I) Effect of Ar flow rate.

The effect of Ar carrier gas flow rate over the range 200-600 ml min^{-1} was studied. Increasing the argon flow rate caused a significant increase in peak-height absorbance and rate of transport of hydride to the atomization cell, as previously observed, (*Fig. 4.3*).

(II) Effect of aqueous carrier flow rate.

The relationship between the flow rate of aqueous carrier solution and resulting peak-height absorbance is shown in *Fig. 4.5*.It can be seen that to achieve maximum sensitivity, the carrier flow rate should be kept as high as possible. The optimum carrier flow rate was decided upon after consideration of precision (Table 4.6) and interference tolerance (Section 4.5.3 (I)). At a fixed acid reagent concentration the relative HCl concentration in the manifold is increased on reducing the aqueous carrier flow.

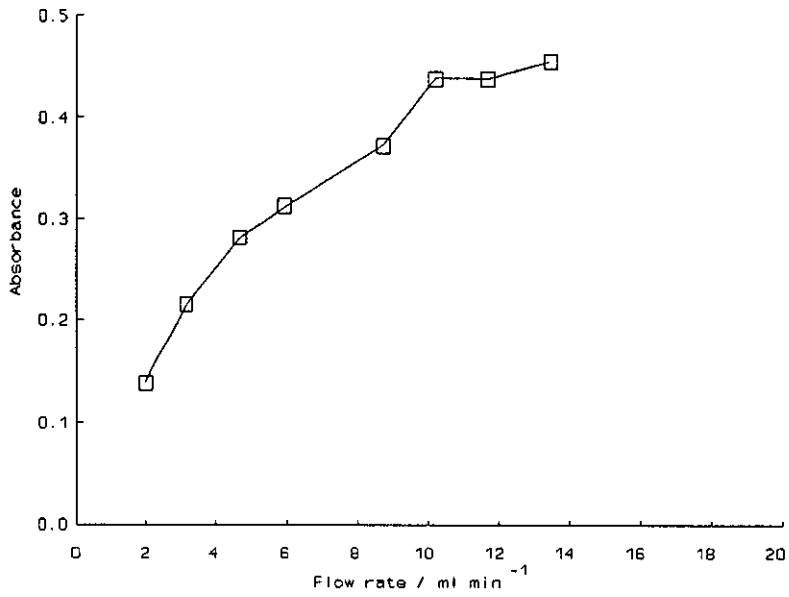

Fig. 4.5. Effect of flow rate of water carrier on the absorbance of 100 ng ml^{-1} of Se^{IV}. Concentration of HCl, 3.6 mol dm^{-3}. All other variables as in Table 4.5.

(III) Effect of HCl flow rate.

The effect of the hydrochloric acid flow rate on the sensitivity for Se^{IV} was observed to be negligible over the range 2-14 ml min^{-1}. This observation was unexpected and to some extent unexplained. The increase in hydrochloric acid flow rate which was predicted to reduce signal response by dilution appeared to be offset by an increased rate of transport through the gas-liquid separator, (Section 4.5.1 (VIII)).

(IV) Effect of HCl concentration.

The hydrochloric acid concentration was observed to have little or no effect on the Se^{IV} signal response over the range 1.2-7.2 mol dm^{-3}. The optimum hydrochloric acid concentration was decided upon after consideration of the copper interference tolerance of the system (Section 4.5.3).

(V) Effect of $NaBH_4$ flow rate.

The effect of sodium tetrahydroborate on the sensitivity for Se^{IV} was observed to be significant, as shown in *Fig. 4.6.*

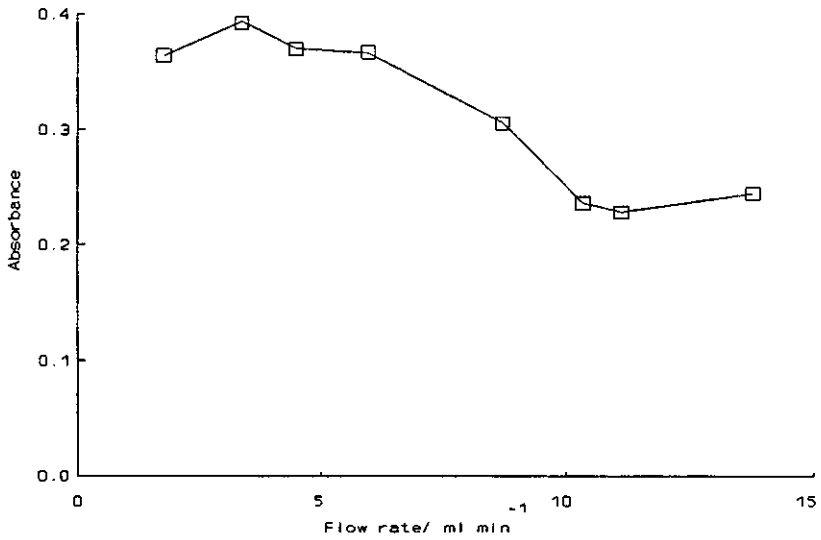

Fig. 4.6. Effects of flow rate of $NaBH_4$ solution on the absorbance of 100 ng ml^{-1} of Se^{IV}. Concentration of $NaBH_4$, 1.0% m/v, concentration of HCl, 3.6 mol dm^{-3}. All other variables as in Table 4.5.

(VI) Effect of $NaBH_4$ concentration.

The effect of sodium tetrahydroborate concentration on the sensitivity for Se^{IV} was observed to be significant, as shown in *Fig. 4.7.*

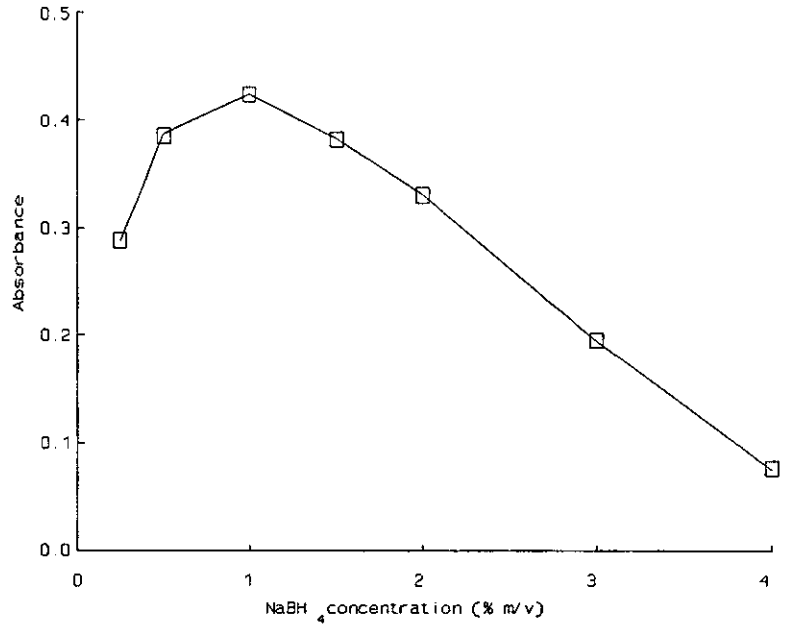

Fig. 4.7. Effect of the concentration of $NaBH_4$ solution on the absorbance of 100 ng ml^{-1} of Se^{IV}. Flow rate of $NaBH_4$, 3.2 ml min^{-1}; Concentration of HCl, 3.6 mol dm^{-3}. All other variables as in Table 4.5.

(VII) Effect of sample injection volume.

The effect of sample injection volume on the sensitivity for Se^{IV} was studied over the range (111-1501 µl). Increasing the injection volume produced an increase in peak-height absorbance as previously observed (*Fig. 4.4*). Although high injection volumes favoured high sensitivity, reducing the injection volume reduced sample volume requirement and improved throughput. An injection volume of 409 µl was chosen as the optimum producing 90% of the steady state signal response.

(VIII) Effect of total carrier transport rate.

The effect of total reagent carrier flow rate on the sensitivity for Se^{IV} was investigated keeping the ratio of the independent reagent flow rates constant, (H_2O:HCl:$NaBH_4$; 2.10:1.44:1.00). For both steady state and FI sample introduction increasing the total carrier transport rate was observed to improve Se^{IV} sensitivity as shown in *Fig. 4.8*. From this observation it was evident that the system performance was not solely dependent on the relative concentrations of reagents used and that to optimize the system the total reagent carrier transport rate should be kept at a maximum.

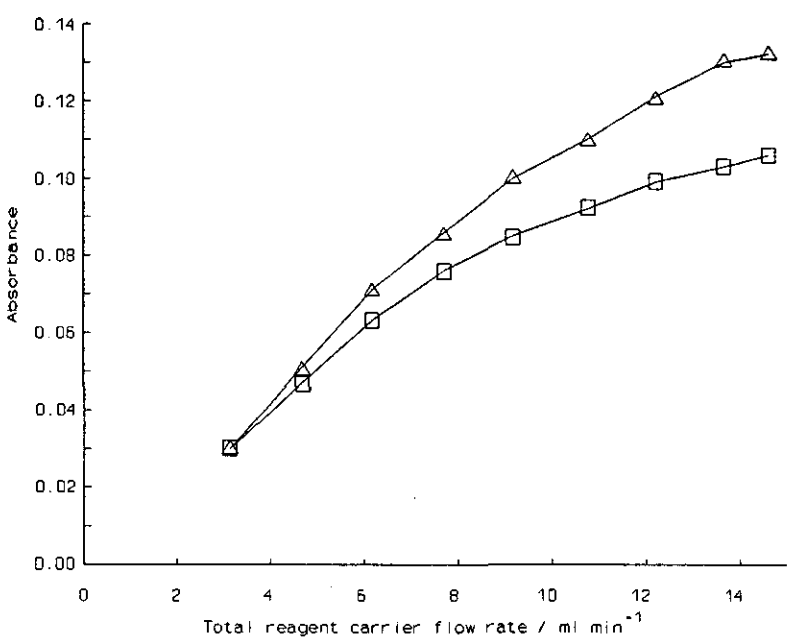

Fig. 4.8. Effect of total reagent carrier flow rate on the absorbance of 20ng ml^{-1} of Se^{IV}. Reagent carrier flow rates ratio H_2O:HCl:$NaBH_4$; 2.10:1.44:1.00. (▲), steady state; (■), FI (409 µl). All other variables as in Table 4.5.

4.5.2 Performance characteristics of FI-HGAAS manifold.

The performance characteristics of the FI-HGAAS manifold were investigated following its optimization. Performance data for combinations of aqueous carrier flow rate and injection volume are given in Table 4.6.

Table 4.6 FI-HGAAS manifold performance data for the determination of selenium.

H_2O carrier flow rate ml min^{-1}	Injection volume μl	Characteristic concentration	*RSD (%)	Throughput h^{-1}
6.2	409	0.96(0.39)✲	1.3	120
13.0	409	0.79(0.32)✲	1.5	180
13.0	922	0.50(0.46)✲	1.6	180

* Relative standard deviation (10 ng ml^{-1} Se^{IV}, n=9)
✲ Characteristic mass, ng

4.5.3 Optimization of manifold variables for interference tolerance.

The effects of manifold variables on the interference tolerance of the system in the determination of Se^{IV} were investigated for copper, nickel, cobalt and iron. Unless otherwise stated the manifold operating parameters used were as shown in Table 4.5. The relative sensitivity of each interferent sample was calculated against a pure 20 ng ml^{-1} Se^{IV} standard solution for which interference free determination was assessed as that producing a relative sensitivity of 100±10%.

(I) Effect of HCl concentration.

The effect of reagent hydrochloric acid concentration on copper interference is shown in *Fig. 4.9*. The interference tolerance of the system was significantly improved on increasing the hydrochloric acid concentration for the reasons discussed previously in section 4.3.3. An optimum hydrochloric acid concentration of 6 mol dm^{-3} was chosen for subsequent work after consideration of the interference tolerance, interference memory effect, hydrochloric acid consumption and the difficulty in pumping high concentration acids [82].

The effect of reagent acid concentration on the interference of cobalt, iron and nickel respectively in the determination of Se^{IV} is shown in Table 4.7.

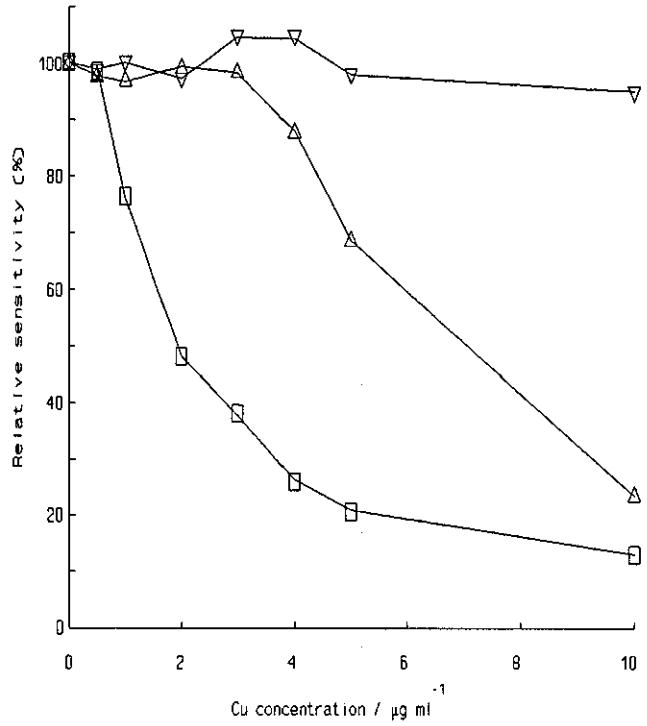

Fig. 4.9. Influence of the HCl concentration on the interference of copper in the determination of 20 ng ml^{-1} of Se^{IV}: (■), 2.4; (▲), 6.0 and (▼), 9.6 mol dm^{-3}. All other variables as in Table 4.5.

Table 4.7 Effect of reagent hydrochloric acid concentration on the interference of Ni(II), Co(II) and Fe(III) in the determination of 20 ng ml^{-1} of Se^{IV}; All other variables as in Table 4.5.

Interferent concentration µg ml^{-1}	Relative sensitivity (%)					
	Nickel		Cobalt		Iron	
	2.4*	6.0*	2.4*	6.0*	2.4*	6.0*
10	96.0	-.-	101.7	101.7	-.-	-.-
20	101.6	-.-	100.3	99.3	-.-	-.-
50	101.7	102.9	99.3	102.9	97.9	98.8
100	96.6	102.9	100.0	104.5	99.6	101.2
200	99.5	98.6	96.5	104.5	104.4	101.4
500	86.5	97.5	89.5	100.3	106.5	106.3
950	71.6	95.4	75.2	100.3	105.6	104.9

* HCl/mol dm^{-3}

It was found that the system has a significantly higher interference tolerance to nickel, cobalt and iron than for copper. The interference-free determination of 20 ng ml^{-1} of Se^{IV} was possible with the use of a 6.0 mol dm^{-3} HCl reagent stream in each case in the presence of up to 950 μg ml^{-1} of interferent. No precipitation or interference memory effect was observed throughout with the exception of the nickel study (2.4 mol dm^{-3} HCl) in which a slight interference memory effect was observed at high interferent concentrations (950 μg ml^{-1} Ni).

(II) Effect of sample injection volume.

The effect of sample injection volume on the interference of copper and nickel in the determination of 20 ng ml^{-1} of Se^{IV} is shown in *Fig. 4.10.*

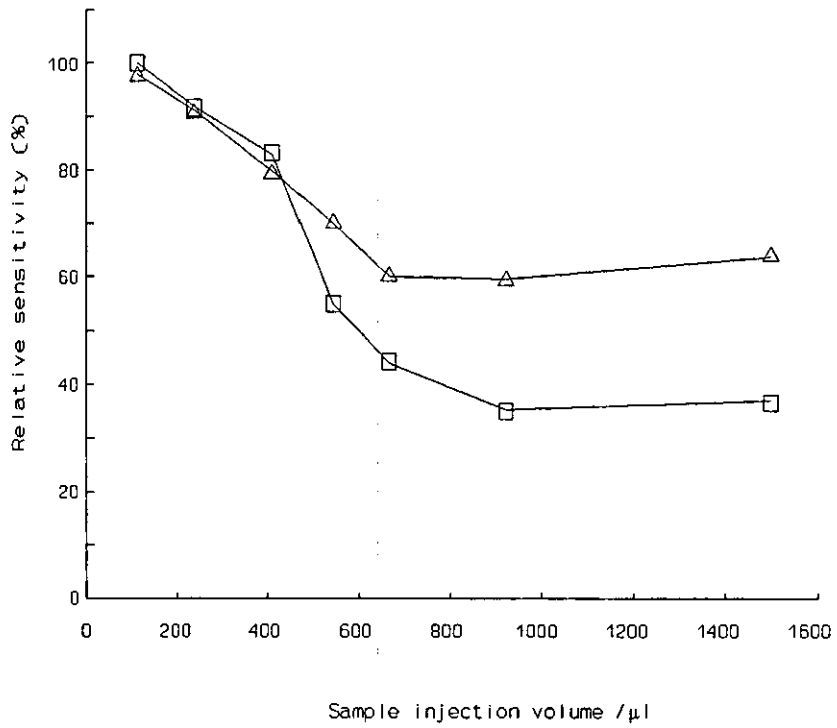

Fig. 4.10. Influence of sample injection volume on the interference of copper and nickel in the determination of 20 ng ml^{-1} of Se^{IV}. (▲), 3.0 μg ml^{-1} Cu; (■), 1000 μg ml^{-1} Ni. All other variables as in Table 4.5.

Improved interference tolerance obtained with reduced sample injection volume was in agreement with earlier work described in section 4.3.3 [44, 90]. This improvement was achieved, though, at the expense of sensitivity as covered in section 4.5.1(VII). In the case of copper on increasing the sample injection volume a, transient in nature, grey precipitate was observed as reported in section 4.3.3.

(III) Effect of total carrier transport rate.

The effect of total reagent carrier flow rate on the copper and nickel interference in the determination of Se^{IV} was investigated keeping the ratio of the independent reagent flow rates constant (H_2O:HCl:$NaBH_4$; 2.10:1.44:1.00). It was found (*Fig. 4.11*) that for both copper and nickel, the degree of interference decreased with increasing total reagent carrier flow rate. This observation was explained by a decrease in reaction time and therefore more rapid removal of hydride from the interferent matrix [13].

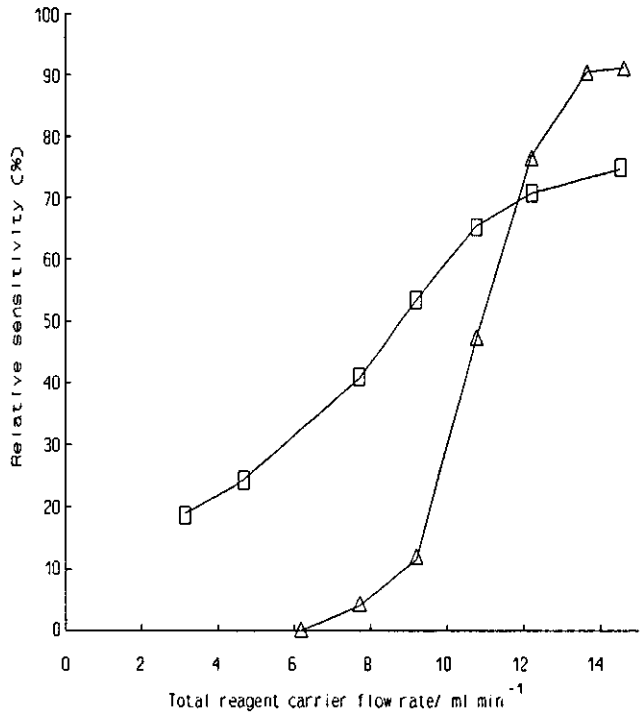

Fig. 4.11. Effect of the total reagent carrier flow rate on the copper and nickel interference in the determination of 20 ng ml^{-1} of Se^{IV}. (■), 4.0 μg ml^{-1} Cu; (▲), 1000 μg ml^{-1} Ni. All other variables as in Table 4.5.

4.5.4. Discussion.

For the optimization of the manifold operating parameters of the FI-HGAAS system it had been hoped that a simplex type optimization procedure [273] could have been used. This intention proved impractical though due to the observed day-to-day variations in system sensitivity (± 20 %) as described by Bax *et al.* [96].

Although a more rigorous approach to optimization could have been carried out, it was decided that it was not necessary as the intention of the work was to investigate the matrix isolation step, and improvements in system design to incorporate it.

From the summary of performance data shown in Table 4.8 it is clear that the performance of the optimized manifold compares favourably (Table 4.6) with other systems employing similar glass U-tube gas-liquid separators [12].

Table 4.8 Performance characteristics of FI-HGAAS systems reported for the determination of Se^{IV} using a glass U-tube gas-liquid separator.

Characteristic concentration ng ml^{-1}	RSD (%)	Injection volume µl	Throughput h^{-1}	Reference
0.34 (0.17)✡	0.8 (n=10)	500	120	88*
0.39 (0.23)✡	<1.0 (10 ng ml^{-1})	600	80	241
2.1 (0.7)✡	5.8 (20 ng ml^{-1}, n=6)	330	90	242

✡ characteristic mass, ng
* air-segmentation included.

For the U-tube gas-liquid separator it is evident that the system performance is not only affected by the relative concentrations of reagents used but also by the rate of transport of the hydride, as shown in *Fig. 4.8.* Optimum sensitivity was achieved by maximising the rate of transport of the hydride both in the aqueous and gas phases. McLaughlin *et al.* [242] made similar observations at a fixed HCl, $NaBH_4$ flow rates ratio of 1.4:1.0 with an increase in sensitivity as the flow rates of both reagents were increased. The performance limiting factor reported in their system though was the build up of back pressure and increase in the likelihood of rupturing tubing with increasing flow rates. In general, high total reagent carrier flow rates ($\geq$ 13 ml min^{-1}) have been reported for the use of U-tube gas-liquid separators [67, 88, 241].

The interference tolerance of the system to copper (*Fig. 4.9*) and cobalt, iron and nickel (Table 4.7) is in good agreement with that of the previous FI work [67, 82, 86, 88, 241]. Improved interference tolerance for copper and nickel with increased hydride transport, in the aqueous phase (*Fig. 4.11*) is explained by the shorter residence time of the hydride in the interfering matrix [13, 88, 90]. The improved interference tolerance for copper and nickel, observed at lower sample injection

volumes (*Fig. 4.10*), provides possible evidence as to why the interference tolerance reported for FI-HGAAS is so superior to that reported for both batch [84] and segmented continuous flow procedures [85]. Although both FI and continuous flow procedures employ the same basic operations, gas liquid separator design, flow rates etc., the sample sizes used are significantly different. The difference in sample size is even more significant in comparison with the batch [84] procedure. For the continuous flow [85] and batch [84] procedures the sample sizes used are, in general, between 10 and 25 times higher respectively than those used in flow injection.

The selection of sample injection volume for a particular determination is clearly important. Careful consideration must be made to the demands of the analysis, whether it be high sensitivity or interference tolerance due to the compromise that must be made of one or other.

4.6 OPTIMIZATION OF A CONTINUOUS FLOW MATRIX ISOLATION MANIFOLD FOR COPPER RETENTION.

The Dowex 50W cation exchange resin was chosen for use in this work because of its previously reported successful application to matrix isolation in hydride generation AAS [80]. The resin consists of sulphonic acid functional groups attached to a styrene divinylbenzene copolymer lattice. The total exchange capacity quoted for the dry resin (H^+ form) is 4.8 Meq/g [274].

4.6.1 Evaluation of cation exchange resin.

The effectiveness of two Dowex 50W cation exchange resins, Dowex 50WX12 50-100 and Dowex 50X8 100-200, to remove copper from solution was investigated. An aqueous slurry of each resin was packed into a micro-column (50 mm x 3.0 mm i.d.) under suction (~ 250 mg dry resin). The copper retention on the resin filled columns was then assessed by pumping a 1000 $\mu g\ ml^{-1}$ Cu standard solution (copper (II) sulphate 5 hydrate, pH 4.00) through the column and continuously monitoring the copper concentration of the column eluent by flame atomic absorption spectrometry (FAAS). The spectrometer was operated under the manufacturer's recommended optimum variables [268] and all quantification was made against aqueous copper standard solutions, pumped continuously into the nebulizer at the same flow rate as used in the column study. Breakthrough was judged to have occurred when the copper concentration of the column eluent exceeded 1.0 $\mu g\ ml^{-1}$. The figure of 1.0 $\mu g\ ml^{-1}$ Cu was chosen as

it is within the interference tolerance of the FI-HGAAS manifold as shown in section 4.5.3(I) when operated under the conditions listed in Table 4.5. The two resins were assessed against the criteria of copper retention efficiency and flow rate capability.

Although the 50-100 mesh resin permitted flow rates of up to 6.0 ml min^{-1} to be pumped through the column without major back pressure problems, its exchange efficiency was poor. The eluent concentrations determined for the initial introduction of copper to the column (leading edge of the sample) at 2.0 and 6.0 ml min^{-1} were 2.5 and 25 μg ml^{-1} Cu respectively. These figures increased drastically with continued pumping in each case. As expected for the smaller particle size resin (mesh 100-200) the exchange efficiency was found to be superior. Use of a smaller particle size, though, restricted the flow rate capability of the column to below 3.0 ml min^{-1}. The effect of both sample flow rate and sample pH on the copper retention of the 100-200 mesh resin is shown in *Figs. 4.12 and 4.13*, respectively. In the pH study pH adjustments were made with solutions of HCl and ammonia. The observed improvement in the efficiency of the resin with reduced sample flow rate (sample pH 4.0) was explained by an increased contact time between the copper ions and the active sites of the resin. In the pH study the retention of copper at pH values above 5.0 was not attempted because the addition of ammonia solution, in order to obtain such pH values, caused turbidity of the samples as a result of the formation of copper hydroxide. Such turbidity was assessed to be a source of analyte loss through co-precipitation [80].

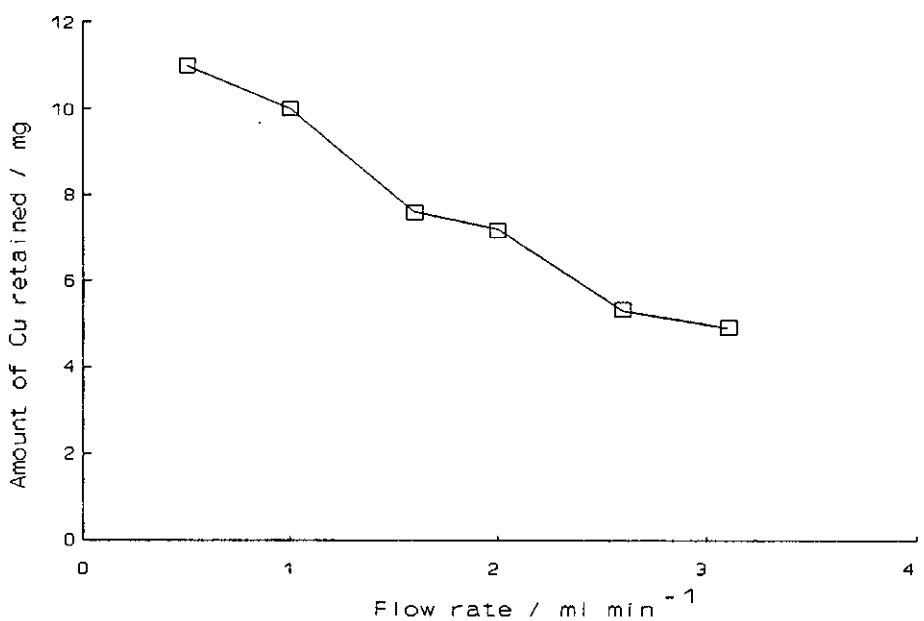

Fig. 4.12. Retention of copper as a function of sample flow rate through the 100-200 mesh resin, sample pH 4.00.

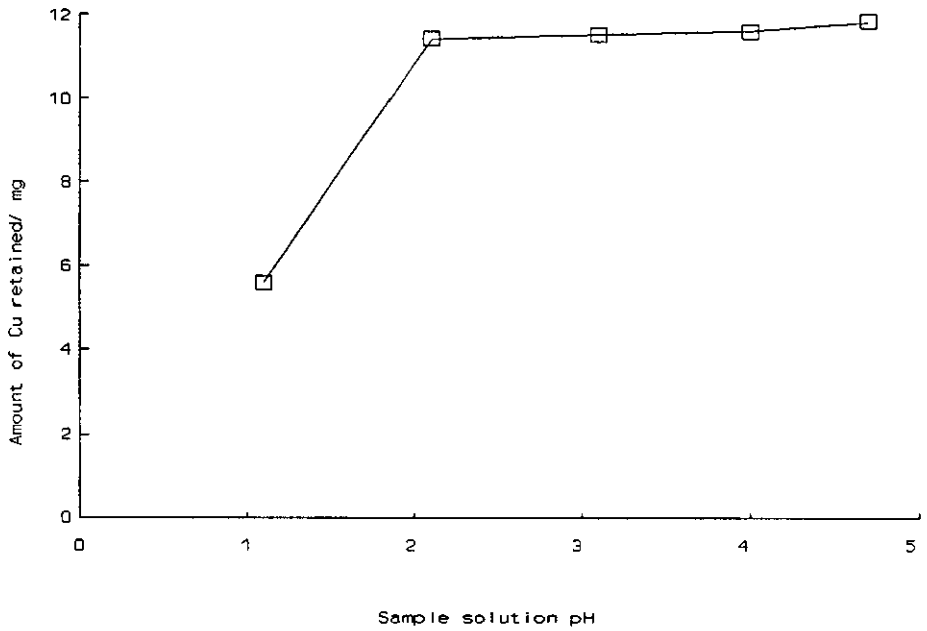

Fig. 4.13. Retention of copper as a function of sample pH on the 100-200 mesh resin; sample flow rate 2.0 ml min^{-1}.

The recovery of 100 ng ml^{-1} of Se^{IV} from the column (2 ml min^{-1}) was determined to be between 97.5 and 99.2% over the pH range of 1.00 to 4.80. The recoveries were calculated by comparing the signal response peak heights of the adjusted standards before and after passage through the column.

It was observed that on introducing the copper solution the resin became compacted at the column outlet leaving a void at the inlet. This was attributed to the drop in pH during ion exchange.

The 100-200 mesh resin was chosen for use in all subsequent work on the grounds of its superior exchange efficiency, over the 50-100 mesh resin. An optimum sample introduction flow rate through the column of 2.0 ml min^{-1} was chosen based on column efficiency and sampling rate. At a sampling flow rate of 2.0 ml min^{-1}, the 409 µl sample loop of the injection valve could be filled in 20 s.

4.6.2 Discussion.

From the observations made into the performance characteristics of the Dowex 50W X8 100-200 resin it was evident that the in-line incorporation of the column into the hydride generation manifold [71, 82, 83] would be detrimental to performance. The flow rate

restrictions required by the presence of the column (< 3 ml min^{-1}) would significantly limit sensitivity as shown in section 4.5.1(II). Restricting the carrier flow rate to 3.0 ml min^{-1} would result in a sensitivity 50% of that achieved at the optimum carrier flow rate (13 ml min^{-1}).

Due to the observed shrinkage of the cation exchange resin on continued introduction of copper it was anticipated that the precision achieved with the in-line incorporation of the column would be poor. Shrinkage of the resin would produce unreproducible mixing within the column and therefore unreproducible dilution of successive injected samples. Furthermore the presence of the column within the manifold would be detrimental to sensitivity due to its proposed significant contribution to the dispersion of the injected sample plug [71].

With the continuous flow matrix isolation system (Fig 4.2(II)) the drawbacks discussed for the in-line incorporation of the micro-column are clearly overcome. The sample flow rate through the micro-column can be kept low (2 ml min^{-1}), therefore optimizing the efficiency of the resin without having to make any change to the optimum carrier flow rate of the FI-HGAAS manifold. Shrinkage of the resin with the introduction of sample causes no detrimental effect on the performance of the system in terms of sensitivity and precision since the sample is introduced continuously and, therefore, undergoes no dilution within the column itself, prior to introduction into the optimized FI-HGAAS manifold.

4.7 DETERMINATION OF Se^{IV} IN A SYNTHETIC COPPER MATRIX.

The FI-HGAAS manifold (*Fig. 4.2(II)*) was operated under the optimum values of the operating variables shown in Table 4.5, according to the analysis sequence outlined in section 4.4.1. Two synthetic sample solutions containing 1000 μg ml^{-1} Cu were prepared, spiked with 20 and 100 ng ml^{-1} Se^{IV}. Both samples contained in the final sample solution, 0.25% m/v potassium hydrogen phthalate, added as a pH buffer, and pH adjusted to 4.00 with dilute ammonium solution. The recoveries of Se^{IV} from the two synthetic samples were determined in triplicate against aqueous standards of the same concentrations and found to be 119 and 108% respectively.

A similar investigation was subsequently carried out but the addition of potassium hydrogen phthalate was removed from the sample preparation step. Recoveries calculated for samples

spiked with 5.0, 10.0, 20.0, 30.0 and 50.0 ng ml^{-1} of Se^{IV} were 104.5, 102.4, 97.5 and 94.5% respectively.

4.7.1 Effect of potassium hydrogen phthalate on signal response.

The FI-HGAAS manifold (*Fig. 4.2 (II)*) was operated under the optimum values of the operating variables shown in Table 4.5, with the matrix isolation unit removed. The signal responses for a series of 20 ng ml^{-1} Se^{IV} standard solutions spiked with different potassium hydrogen phthalate concentrations were determined and compared with the response of an aqueous standard solution of the same concentration. The investigation was made to identify the possible sensitivity enhancing effect of potassium hydrogen phthalate on the determination of Se^{IV} by HGAAS, suggested by earlier results (Section 4.7).

The effect of potassium hydrogen phthalate concentration on the sensitivity for Se^{IV} is shown in Table 4.9. Over the optimum concentration range of 0.10 to 0.25% m/v a signal enhancement of the order of 10-15% was achieved. The decrease in signal response above 0.25% m/v was attributed to significant frothing observed in the gas-liquid separator resulting in reduced transport efficiency of the hydride.

Table 4.9 Effect of potassium hydrogen phthalate on the absorbance of 20 ng ml^{-1} of Se^{IV}. All other variables as Tables 4.5 (± 95% confidence interval).

Potassium hydrogen phthalate concentration (% m/v)	Peak-height absorbance		Relative sensitivity (%) x_{mean}
	Blank (n=3)	20 ng ml^{-1} Se^{IV}	
0	0.000	0.091±0.001	100
0.05	0.000	0.096±0.003	106
0.10	0.000	0.103±0.001	113
0.25	0.000	0.102±0.003	112
0.50	0.008±0.001	0.093±0.001	93
1.00	0.010±0.002	0.083±0.002	80

4.7.2 Discussion.

The interference free determination of Se^{IV} in a 1000 µg ml^{-1} copper matrix was successfully achieved without the need for addition of potassium hydrogen phthalate pH buffer. Although the potassium hydrogen phthalate gave a signal enhancement in the

determination of Se^{IV} it was concluded that its magnitude (<15%) does not warrant the expense and increase in sample preparation required in the matching of both standards and samples.

The role of potassium hydrogen phthalate cannot be conclusively explained other than by its catalytic action on the rate of hydride formation and increase in the efficiency of the hydride generation reaction. Agterdenbos and Bax [100] made similar observations of an increased rate of hydride formation on the addition of KI in a continuous flow system. Addition of 0.1 mol dm^{-3} potassium iodide to the $NaBH_4$ solution had the effect that only 0.001% m/v $NaBH_4$ solution was sufficient for the complete conversion of Se^{IV} from 2 mol dm^{-3} HCl in comparison with 0.16% m/v $NaBH_4$ in its absence. It is postulated, therefore, that potassium hydrogen phthalate and potassium iodide act on the formation of hydrogen selenide by the same or similar mechanism.

4.8 DETERMINATION OF Se^{IV} IN COPPER METAL STANDARD REFERENCE MATERIALS.

The analysis of two copper metal standard reference materials, NIST SRM 454 unalloyed copper and BAM 361 copper, was attempted.

4.8.1 Calibration and analysis procedures.

The FI-HGAAS manifold shown in *Fig. 4.2(II)* was operated under the optimum values of the operating variables shown in Table 4.5 according to the analysis sequence outlined in section 4.4.1. Aqueous Se^{IV} standard solutions (0-50 ng ml^{-1} Se^{IV}) were used for calibration which were sampled directly without undergoing matrix isolation. Replicate determinations of the Se^{IV} contents of both samples were made on single digest solutions. The column was regenerated after every third determination.

4.8.2 Sample digestion.

The method [82] used for the digestion of the two copper metal reference materials, NIST SRM 454 and BAM 361 was as follows.

A sample of copper metal (0.5 g) was accurately weighed into a clean Pyrex beaker (50-100 ml). To the beaker were added 10 ml of 8 mol dm^{-3} HNO_3 and the beaker was covered with a watch glass. The beaker was placed on a hot plate, heated to near dryness, then removed. Once cool, 10 ml of 6 mol dm^{-3} HCl were added and the beaker was placed in a steam bath. After approximately 15 min of heating, to dissolve the sample residue, the resultant solution was allowed to cool. The cool digest solution was transferred into a calibrated flask (100 ml) and diluted to volume with analytical-reagent grade water. Prior to analysis, the NIST SRM 454 and BAM 361 digests were further diluted to produce working samples containing 75 and 1000 $\mu g\ ml^{-1}$ of copper, respectively.

4.8.3 Sample pH adjustment.

Initially prior to analysis the metal digest solutions were pH adjusted to pH 4.00 with the addition of ammonia solution to optimize the performance of the matrix isolation step according to *Fig. 4.13*. This produced some degree of precipitation and significantly reduced the capacity of the column as shown in Table 4.10.

Table 4.10 Effect of ammonia solution added to achieve pH adjustment of copper digest (1000 $\mu g\ ml^{-1}$) on the copper retention of the micro-column (2.0 ml min^{-1}).

Digest pH	Copper retention/ mg
1.00*	7.14
1.20#	7.04
2.10#	5.78
3.20#	5.67
4.30#	3.37

* No pH adjustment of digest solution
\# pH adjustment with ammonia solution.

The reduction in capacity of the column was identified as owing to competition between copper and ammonium ions for the active sites on the resin. In order to overcome this problem the pH adjustment step was removed from the sample preparation. The pH values of the two analysed samples NIST SRM 454 and BAM 361 were 2.1 and 1.1 respectively. Therefore, even without pH adjustment the column capacity was still sufficient to permit triplicate injections of each sample solution before column

regeneration as the column capacity is greater than 5.0 mg copper. The removal of the pH adjustment step had the further advantage of reducing sample preparation time and the chance of sample contamination as well as avoiding precipitation and the consequent loss of analyte through co-precipitation [80].

4.8.4 Analysis results.

The results of the analysis of the reference materials are given in Table 4.11.

Table 4.11 Results of analysis of copper metal reference materials (±95% confidence limits).

Sample	Certified value for Se^{IV} / $\mu g\ g^{-1}$	Se^{IV} found/ $\mu g\ g^{-1}$
NIST SRM 454	479±8	476±7.2(n=6)
BAM 361	36±0.6	37.1±0.7(n=8)

4.8.5 System performance.

The performance characteristics of the FI-HGAAS system achieved for the analysis of copper metal standard reference materials are shown in Table 4.12. The detection limit of the system was calculated from the calibration graph and the error residuals based on the unweighted linear regression line [275].

Table 4.12 Performance characteristics of the FI-HGAAS system for the analysis of copper metal standard reference materials.

Calibration	0-50 ng ml^{-1} Se^{IV}
Slope	4.35 x 10^{-3} A ng^{-1} ml
Intercept	5.1 x 10^{-3} A
Correlation coefficient	0.9992
Characteristic concentration (0.0044 A)	1.0 ng ml^{-1}
Precision (RSD, 10 ng ml^{-1} Se^{IV}, n=12)	1.5%
Detection limit [275] ($3S_B$)	2.1 ng ml^{-1}
Throughput (triplicate determinations)	17 h^{-1}

4.9 DISCUSSION.

The results show (Table 4.11) that Se was successfully determined in the standard reference materials NIST SRM 454 and BAM 361. The sensitivity compares favourably with that of the conventional operation of the Philips PU9360 continuous flow system. For steady state analysis (sample volume 5.0 ml) a characteristic concentration of 0.91 ng ml^{-1} Se^{IV} was reported[268]. The copper interference tolerance of the two systems, 1000 and 0.5 μg ml^{-1} copper respectively, indicates the superior performance of the proposed FI-HGAAS system in the analysis of copper matrices.

One of the major advantages of this system design in comparison with others, is the high precision obtained. For the system of Riby *et al.* [83] and Ikeda [82] the RSDs quoted for the determinations of 10 ng ml^{-1} of As^{III} and 10 ng ml^{-1} of Se^{IV} were 3.0 and 3.8% respectively. These figures are clearly inferior to those quoted in this work (Table 4.6). A F-test[276] should be performed to statistically prove this but insufficient data is given in the two sets of work to permit the necessary calculation of standard deviation values.

It is suggested that the sample introduction procedures used in the two systems may be possible sources of imprecision. In the system of Ikeda [82] a 500 μl sample was introduced manually from a pipetman p-1000 pipette. Riby *et al.* [83] employed a timed injection procedure, pumping sample continuously into the system over a short period of time (10 s). The carrier pump tubing was transferred manually between the carrier and sample solutions. No indication was given though as to whether or not the pump was actually stopped during this transfer process. Although timing of the sampling step was performed with the use of a stopwatch it is evident that the precision of the sampling step is very susceptible to operator performance and slight fluctuations in flow rate. If infact the pump was not stopped during the transfer of pump tubing between solutions it is suggested the introduction of air into the system may be a further source of imprecision. Incorporation of the micro-columns in-line in both systems [82,83] is also postulated to limit precision due to the contribution to sample dilution made by the column, as discussed in section 4.6.2.

In the system of Riby *et al.* [83] the incorporation of the matrix isolation column in-line required a compromise in the performance characteristics for the matrix isolation and hydride generation procedures as discussed for the in-line incorporation of the column in the proposed system (Section 4.6.2). Although in the system of Riby *et al.* [83] high carrier flow rates of up to 9 ml min^{-1} were possible through the column, required to optimize sensitivity, the optimum matrix isolation characteristics were achieved at 2-4 ml min^{-1}. Even at a compromise of

6.0 ml min^{-1}, the system was susceptible to high back pressure and column compaction problems, requiring intermittent replacement of the column. No column compaction was reported by Marshall and van Staden [71] for in-line incorporation of a micro-column possibly due to the use of a 2 ml min^{-1} carrier flow rate. Use of such a low carrier flow rate may, as a result, account for the poor performance of the system, for which a limit of detection of 6 ng ml^{-1} Se^{IV} was quoted [240].

In the proposed system no problem with back pressure or column compaction was observed as the sample flow rate through the column was kept low (2 ml min^{-1}) and the HCl regenerent was directed through the column in the reverse direction to the sample flow. No column replacement was necessary over a period of 3 months continued use during which time no deterioration in column performance was noted. Keeping the sample flow low achieved the added advantage of an optimized matrix isolation step without any need to compromise the hydride generation performance.

Incorporating the matrix isolation column within the sample loop of an injection valve, the rapid intermittent regeneration of the column is possible without interrupting the operation of the hydride generation manifold, a facility absent in other systems. All retained interferent is eluted directly to waste, bypassing the FI-HGAAS manifold. Ikeda [82] reported no column regeneration facility in the system used. The column was simply replaced after every 25 determinations (column capacity, 50 mg of copper). By employing a relatively large column (2 ml resin), in order to increase the column capacity the sample throughput was restricted to 30 h^{-1}. Column regeneration was reported in the system of Riby *et al.* [83] but was undertaken manually, (prior to column regeneration, the water carrier line was disconnected from the rest of the hydride generation manifold and 1 mol dm^{-3} HCl was pumped through the column to waste). No indication of sample throughput capabilities were reported. In the work of Marshall and van Staden [71] column regeneration was achieved by pumping acid eluent (2 mol dm^{-3}) directly through the column, (total process time 15 mins). No indication though was given as to whether the column was disconnected from the FI-HGAAS manifold prior to this procedure. Without disconnection the elution of excessively high concentrations of interferent into the FI manifold would be detrimental on the grounds of possible interference memory effects, as observed in the course of this work (Section 4.3.3).

A major benefit of the proposed manifold design, with particular reference to the column regeneration step is the potential for automation. By using existing technology, full automation of the system is feasible [277]. Automation of previous systems [71, 82, 83] would be difficult without major modifications being made.

By employing the flow injection valve as an interface, the matrix isolation procedure could be applied directly to other flow injection hydride generation manifolds irrespective of their operating procedures, gas-liquid separator designs etc [13, 88-90, 239-242]. Based on the successful application of the Dowex 50W resin to matrix isolation in HGAAS [80] it is suggested that with only minor modifications the same system could be used for the determination of other hydride-forming elements in the presence of a variety of interfering species such as nickel, iron, cobalt and silver.

CHAPTER FIVE

ELIMINATION OF NICKEL INTERFERENCE BY CONTINUOUS FLOW MATRIX ISOLATION IN THE DETERMINATION OF As BY FI-HGAAS.

5.1 INTRODUCTION.

The successful determination of As in a nickel alloy (BCS 346) was reported by Riby *et al.* [83] in 1989. The system, which incorporated an in-line micro-column of strong cation exchange material (SCX), in a manner similar to other reported matrix isolation systems [71, 82], though had its limitations as discussed in Chapter four. These limitations were overcome in a new system design, outlined in Chapter four, which was used for the determination of Se^{IV} in copper matrices. The application of the same system to the determination of As in nickel alloy is considered feasible, with the possibility of achieving the same improvements in system performance, over that reported by Riby *et al.* [83], as was discussed in Chapter four.

A notable feature of the work of Riby *et al.* [83] was the use of a microwave sample digestion procedure which was reported to retain As in the +3 oxidation state [278]. Prevention of the oxidation of As to the +5 oxidation state, reported in conventional digestion procedures [279] was clearly beneficial. It is well documented that the sensitivity for As^{V} in HGAAS is inferior to that of As^{III}, particulary for FI-HGAAS [16,243], due to the slower hydride generation kinetics [280]. Elimination of this sensitivity difference has been achieved through optimization of system variables [235] and the application of pre-reduction reagents [16, 53, 243] of which potassium iodide has been used most commonly. In most cases the KI pre-reduction method has been applied manually for which reaction times of up to 1 hour are required to achieve quantitative reduction [16, 53, 243]. On-line KI pre-reduction of As^{V} has been implemented in FI-HGAAS but with rather limited performance data and some degree of compromise of the FI-HGAAS performance [58, 88] due to the need for increased reaction times. Both of these methods used a continuously flowing reagent stream of potassium iodide solution (50% m/v). The flow rates were 1.5 and 2.5 ml min^{-1}, which represents a consumption of 45 and 75 g h^{-1} KI respectively.

This chapter outlines the modification and use of the continuous flow matrix isolation system, previously described in Chapter four, for the determination of As in a nickel alloy (BCS 346) by FI-HGAAS. A novel stopped-flow KI pre-reduction procedure incorporated within the system, to obtain As in the +3 oxidation state, and therefore maximise sensitivity was used.

Stopped-flow methodology was employed to minimise reagent consumption and permit sufficiently long reaction times without the need for excessive reactor coil lengths. Direct comparisons are made with the system of Riby *et al.* [83]. Aspects of this chapter have been accepted for publication [282].

5.2 APPARATUS AND REAGENTS.

5.2.1 Apparatus.

Unless otherwise stated the apparatus used was identical to that described in Chapter four. A Philips Scientific SP9 atomic absorption spectrometer equipped with a Philips coded arsenic hollow cathode lamp was operated under the conditions shown in Table 5.1 based on the manufacturer's recommendations [268].

Table 5.1 Philips SP9 spectrometer variables for the determination of arsenic.

Wavelength, nm	193.7
Slit width, nm	1.0
Lamp current, mA	9.0
Support gas/ flow setting (Arbitrary units)	28/air
Fuel gas/ flow setting (Arbitrary units)	15/acetylene
Background correction	OFF
Damping, s	0.5

The FI hydride generation manifold used in Chapter four (*Fig. 4.2 (II)*) was modified as shown in *Fig. 5.1.* Additional pump channels were incorporated within the matrix isolation unit to permit addition of potassium iodide and HCl reagents in the stopped-flow KI pre-reduction step. A disposable gas-line filter (VROHO20 hydrophobic 0.2 μm PTFE membrane, PALL) was fitted in-line with the hydride transport tubing connecting the gas-liquid separator and the silica atomization cell.

All alloy digestions were carried out in a microwave-digestion unit (Oxford Laboratories, Model CEM MDS 81D). Polypropylene calibrated flasks were used to handle all digested sample solutions.

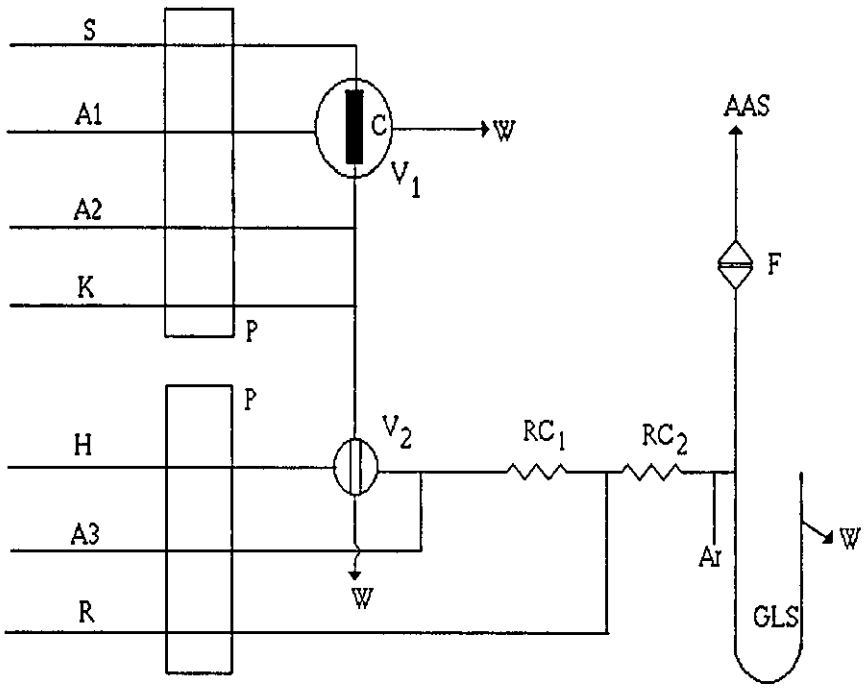

Fig. 5.1. Schematic diagram of the FI manifold with continuous flow matrix isolation and stopped-flow KI pre-reduction unit: P, Peristaltic pump; S, Sample; H, Water; A, HCl; R, $NaBH_4$; K, KI; W, Waste; V_1, switching valve; V_2 Sample injection valve; C, micro-column; F, PTFE membrane filter; and GLS, gas-liquid separator; and RC_1, Reactor coil.

5.2.2 Reagents.

Unless otherwise stated all reagents were identical to those used in the experiments described in Chapter four. All arsenic (III) standard solutions were prepared by dilution of a standard solution of arsenic trichloride (SpectrosoL, BDH) containing 1000 $\mu g\ ml^{-1}$ As. All arsenic (V) standard solutions were prepared from sodium arsenate, (AR, Fisons). For the optimization of the matrix isolation procedure, nickel (II) sulphate 7 hydrate (AnalaR, BDH) was used to prepare standard solutions. Interferent standard

solutions were prepared from antimony potassium tartrate (SpectrosoL, BDH), cobalt (II) chloride 6 hydrate (ACS reagent, Aldrich), copper sulphate 5 hydrate (AnalaR, BDH), nickel (II) sulphate 5 hydrate (AnalaR, BDH), selenous acid (SpectrosoL, BDH) and stannous chloride (AR, Fisons). Reagents used in the KI pre-reduction investigative work were hydrochloric acid (SpectrosoL, BDH), potassium iodide (AnalaR, BDH), sodium sulphite (SLR, Fisons) and sodium thiosulphate (GPR, BDH). The nickel based reference alloy was digested using nitric acid (Aristar, BDH) and hydrofluoric acid (40% Aristar, BDH). The nickel based certified reference alloy BCS 346 was obtained from the Bureau of Analysed Samples (Middlesbrough, U.K.).

5.3 DESIGN FEATURES OF NOVEL FI-HGAAS MANIFOLD INCORPORATING CONTINUOUS FLOW MATRIX ISOLATION AND STOPPED-FLOW KI PRE-REDUCTION.

The design features of the FI-HGAAS manifold with continuous flow matrix isolation were identical to those described in Chapter four (Section 4.4) but with the inclusion of a stopped-flow KI pre-reduction process *(Fig. 5.1)*. Inclusion of this step was found necessary to convert the As present in the digested nickel alloy sample to the +3 oxidation state and therefore improve sensitivity, as discussed in section 5.7.

The sample and KI pre-reduction reagents were pumped continuously through the sample loop of the injection valve interfacing the matrix isolation unit and the FI-HGAAS manifold. Stopping the pump of the matrix isolation unit therefore retained the reaction mixture within the sample loop. A stop time sufficient for the quantitative reduction of As^{V} to As^{III} under these static conditions was then implemented prior to sample introduction into the FI-HGAAS manifold through the activation of the injection valve.

Use of such a stopped-flow procedure permitted accurate and precise control of the KI pre-reduction reaction time without the need for excessive lengths of manifold tubing, any compromise of the FI-HGAAS performance characteristics and with minimal reagent consumption.

5.3.1 System operation.

System operation was identical to that reported in Chapter four (Section 4.4.1) but with the inclusion of control over the run and stop time of the matrix isolation unit pump, required in the KI stopped-flow pre-reduction procedure. The system, (*Fig. 5.1*) was operated under the optimized conditions shown in Table 5.2 according to the sampling procedure, including timing sequences, listed in Table 5.3.

Reagent	conc. /pH	flow rate	ml min^{-1}
(I) System Br_2 + LiOH			
H_2O carrier	— 0.9		
Br_2	— 1.05	0.15 M	
LiOH	— 1.05	0.24 M	
~~Reagent~~	—		
(II) System BrO_3^-/Br^- + ~~NaOH~~			
H_2O carrier	— (10) → 1 ml/min	1.5 M	
BrO_3^-/Br^-	— 200 ~~(added)~~ 0.5 ml/min	3.6×10^{-2} M	0.2 M
HCl	— 200 ~~(added)~~ 0.5 ml/min	2.5 M	
NaOH	— 10 ~~add~~ 0.5 ml/min	2.5 M	
III System ClO^-/Br^-		0.98 ml/min pH = 11	
ClO^-	— (200) red	10^{-1} M → pH	
Br^-	— (200) red	2.0 ml/min 10^{-1} M →	
H_2O carrier - 20	1 ml/min		

0.5 ml ~~soppers~~

When the Bromine solution was ~~Have through the system~~ prepared

Best sensitivity for $Br^-/BrO_3^- + OH^-$

Determination of the

A previous investigation of the pH of the sample solution showed it must be adjusted ~~by~~ ~~to~~ ~~30~~ ~~7.0~~ to pH 5.0 because it will be ~~sample pH~~ compared the aqueous ~~with~~ std solutions ~~which were prepared with~~ pH ~~is~~ 5.0.

Figure4 Effect of the

Table 5.2 Optimized variables for the FI-HGAAS manifold with continuous flow matrix isolation and stopped-flow KI pre-reduction. Injection volume 409 µl, reactor coil RC_2 600 mm (0.8 mm i.d.)

(I) Hydride generation AAS		
Reagent	Concentration	Flow rate/ ml min^{-1}
H_2O carrier	-.-	11.0
HCl (A3)	3.6 mol dm^{-3}	3.2
$NaBH_4$	1.0% m/v	3.2
Ar	-.-	400
(II) Continuous flow matrix isolation		
Reagent	Concentration	Flow rate/ ml min^{-1}
Sample	<1000 µg ml^{-1} Ni	2.2
HCl (column regenerant, A2)	1.2 mol dm^{-3}	2.2
(III) Stopped-flow KI pre-reduction		
Reagent	Concentration	Flow rate/ ml min^{-1}
HCl (A1)	12 mol dm^{-3}	2.2
KI	30% m/v	1.4

Table 5.3 Summary of the sampling procedure for matrix isolation and stopped-flow KI pre-reduction, including timing sequences.

Timing sequence (t)/s	Operation
0	V_S^*, H_2O pumped via column
10	V_S, sample pumped via column
70	$V_I^{\S}$, activation (load position)
80	Matrix isolation pump stopped
95	V_I, activation (inject position)
105	Matrix isolation unit pump started (procedure repeated from t=70 to give triplicate injections)
165	$V_B^{\#}$, HCl regenerant pumped via column, H_2O pumped via sample line
200	V_s^*, H_2O pumped via column (procedure repeated t=0)

V_S^* valve containing column in sample configuration; $V_I^{\S}$ sample injection valve; $V_B^{\#}$ valve containing column in bypass configuration.

5.4 OPTIMIZATION OF THE FI-HGAAS MANIFOLD.

The performance of the flow injection HGAAS manifold shown in *Fig. 5.1* was investigated with the independent matrix isolation/stopped flow KI pre-reduction unit removed. The system was optimized for the determination of As^{III} without any means of matrix isolation or other sample pretreatment.

5.4.1 Optimization of manifold variables for As^{III} determination.

The optimized conditions for the FI-HGAAS manifold (Table 5.2 (I)) with the membrane filter removed from the hydride transport tubing were obtained using a basic univariate approach, as used by Riby *et al.* [83] and implemented in Chapter four. In obtaining the optimum conditions sensitivity was a prime concern but consideration was also given to precision, interference tolerance, throughput and the reliability of the system. Unless otherwise stated the optimization of each parameter was carried out for an aqueous 20 ng ml^{-1} As^{III} standard (values of other variables are given in Table 5.2(I)).

(I) Effect of flame stoichiometry.

In initial studies the flame stoichiometry was found to have a significant effect on the sensitivity for As^{III}. The sensitivity was observed to increase with increased acetylene flow setting. This effect was found though to be non reversible, indicating a conditioning effect on the performance characteristics of the atomization T-cell through heating in a fuel-rich air-acetylene flame (air flow setting 28; acetylene flow setting 22), discussed in more detail in Chapter seven (Section 7.3). After this conditioning process the effect of flame stoichiometry on the sensitivity for As^{III} was negligible, producing less than a 15% variation in peak-height absorbance over the acetylene flow setting range of 14 to 21 (air flow setting 28). A fuel-lean air-acetylene flame (air flow setting 28, acetylene flow setting 15) was chosen for all subsequent work on the basis of superior precision.

(II) Effect of Ar carrier gas flow rate.

The relationship between the flow rate of the argon carrier gas and the resulting peak-height absorbance is shown in *Fig. 5.2.* An optimum Ar flow rate of 400 ml min^{-1} was chosen on the grounds of precision and throughput, whilst retaining

adequate sensitivity (85% of optimum, 150 ml min^{-1} Ar). Below 400 ml min^{-1}, precision deteriorated (RSD 2.0-4.4%, 20 ng ml^{-1} As^{III}, n=6) and significant peak broadening occurred, limiting throughput.

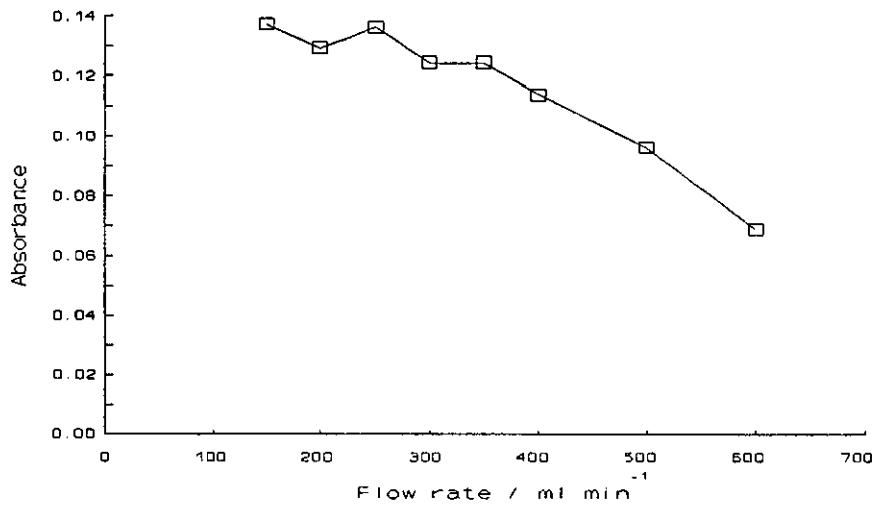

Fig. 5.2. Effect of the flow rate of Ar carrier gas on the absorbance of 20 ng ml^{-1} of As^{III}. Aqueous carrier flow rate, 9.2 ml min^{-1}; RC_2, 100 mm (0.8 mm i.d.). All other variables as in Table 5.2 (I).

(III) Effect of manifold variables.

The effect of reactor coil length (RC_2, *Fig. 5.1*) on the sensitivity for As^{III} is shown in *Fig. 5.3.* An optimum of 600 mm was chosen after consideration of throughput capability, back pressure build up and proposed interference tolerance [13].

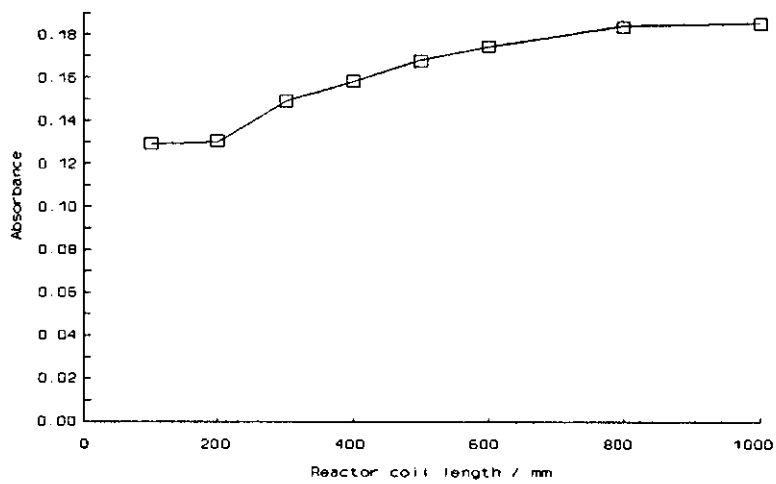

Fig. 5.3. Effect of the reactor coil length (RC_2, 0.8 mm i.d.) on the absorbance of 20 ng ml^{-1} of As^{III}. Aqueous carrier flow rate, 9.2 ml min^{-1}. All other variables as in Table 5.2(I).

(IV) Effect of aqueous carrier flow rate.

The relationship between the flow rate of the aqueous carrier solution and the resulting peak-height absorbance is shown in *Fig. 5.4.* An optimum flow rate of 11.0 ml min^{-1} was chosen to achieve optimum sensitivity and throughput.

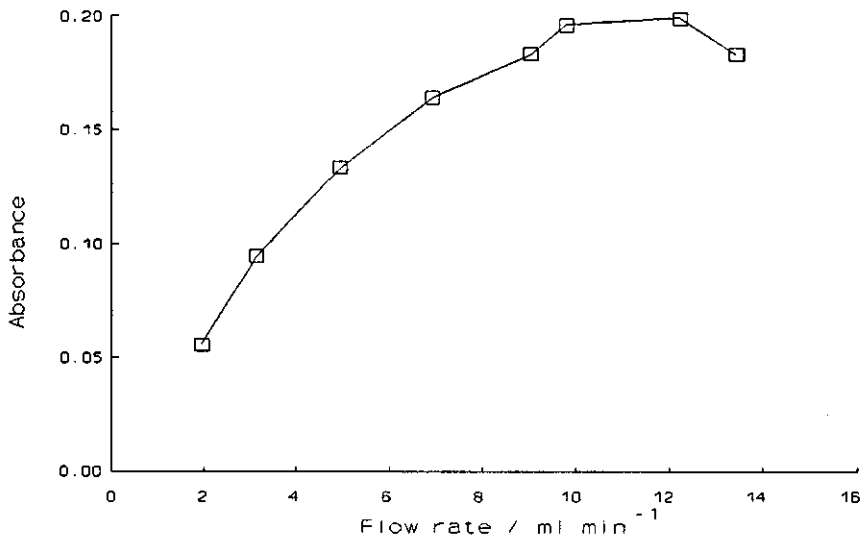

Fig. 5.4. Effect of the aqueous carrier flow rate on the absorbance of 20 ng ml^{-1} of As^{III}. All other variables as in Table 5.2(I).

(V) Effect of HCl flow rate.

The effect of hydrochloric acid flow rate on the sensitivity for As^{III} was observed to be negligible over the range 2-9 ml min^{-1}. Less than a 11% variation in sensitivity was observed over this range.

(VI) Effect of HCl concentration.

The relationship between the hydrochloric acid reagent concentration and the resulting peak-height absorbance is shown in *Fig. 5.5.* An optimum concentration of 3.6 mol dm^{-3} was chosen on the basis of sensitivity.

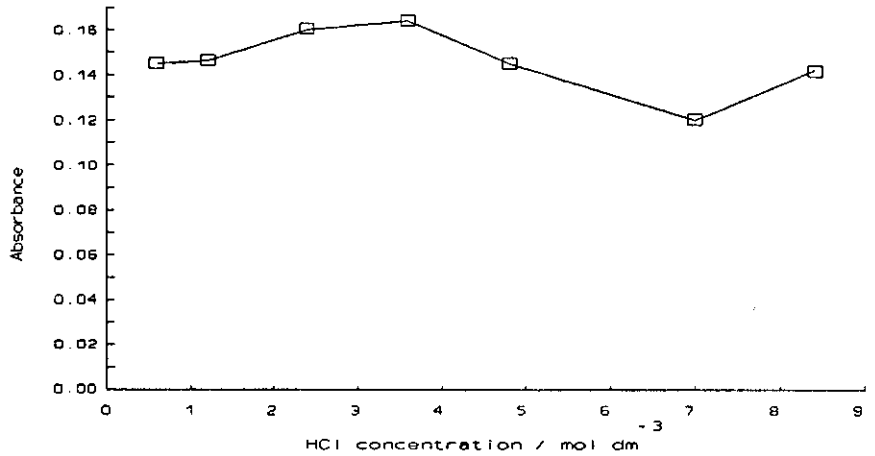

Fig. 5.5. Effect of concentration of HCl solution on the absorbance of 20 ng ml^{-1} of As^{III}. Flow rate of HCl, 3.2 ml min^{-1}. All other variables as in Table 5.2(I).

(VII) Effect of $NaBH_4$ flow rate.

The effect of sodium tetrahydroborate flow rate on the sensitivity for As^{III} was shown to be negligible over the range 3.2-8.7 ml min^{-1}. Less than a 5.0% variation in sensitivity was observed.

(VIII) Effect of $NaBH_4$ concentration.

The relationship between the concentration of sodium tetrahydroborate and the resulting peak-height absorbance is shown in *Fig. 5.6.* An optimum concentration of 1.0% m/v was chosen on the grounds of superior nickel interference tolerance at low sodium tetrahydroborate concentrations [46].

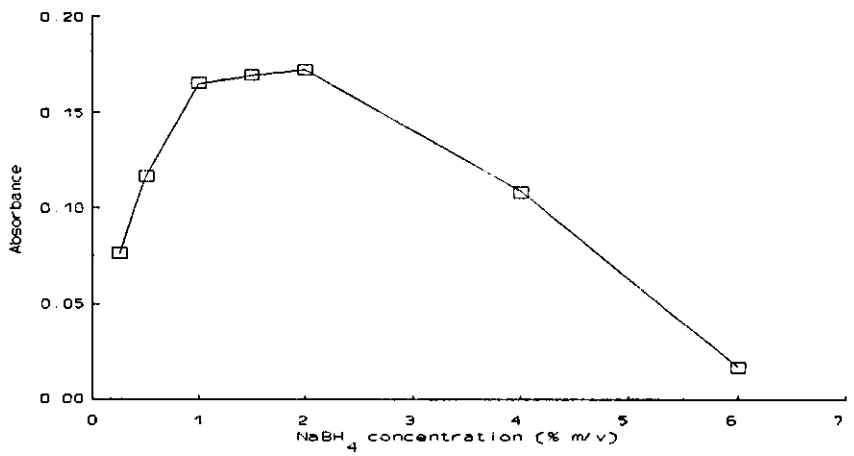

Fig. 5.6. Effect of the concentration of $NaBH_4$ solution on the absorbance of 20 ng ml^{-1} of As^{III}. Flow rate of $NaBH_4$, 3.2 ml min^{-1}. All other variables as in Table 5.2(I).

(IX) Effect of sample injection volume.

The effect of sample injection volume on the sensitivity for As^{III} is shown in *Fig. 5.7.* An injection volume of 409 µl was chosen for all subsequent work to optimize the throughput capability of the whole analysis system and achieve 75% of the optimum steady state sensitivity.

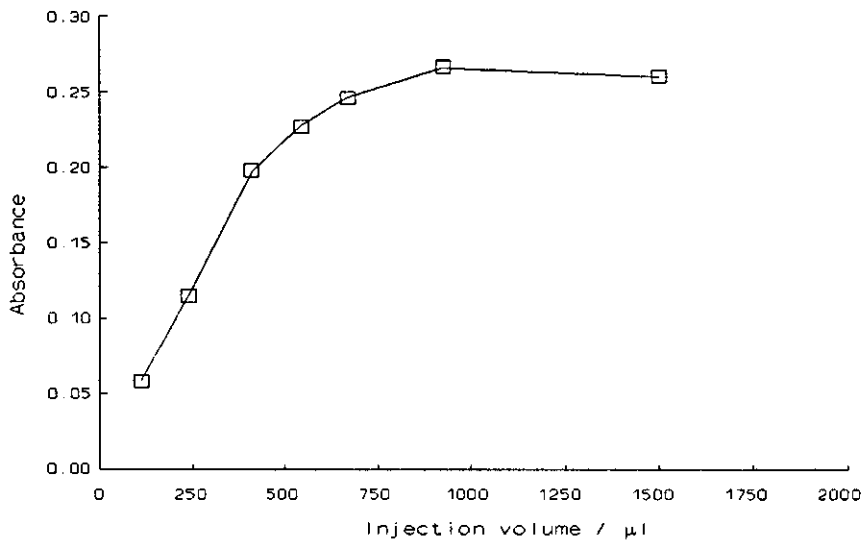

Fig. 5.7. Effect of injection volume on the absorbance of 20 ng ml^{-1} of As^{III}. All other variables as in Table 5.2(I).

5.4.2 Performance characteristics of FI-HGAAS manifold.

The performance characteristics of the FI-HGAAS manifold were measured for the values of the operating parameters shown in Table 5.2(I). A characteristic concentration (0.0044A) of 0.42 ng ml^{-1} of As^{III} and throughput capability of 110 h^{-1} were obtained. The relative standard deviations for 2 and 10 ng ml^{-1} As^{III} were 3.3 and 3.2%, respectively, (n=10).

5.4.3 Optimization of manifold variables for interference tolerance.

The interference tolerance of the FI-HGAAS manifold in the determination of As^{III} was investigated for copper, nickel, cobalt, antimony, tin and selenium. Unless otherwise stated the operating conditions used were those shown in Table 5.2(I). The relative sensitivity of each interferent sample was calculated against a pure 20 ng ml^{-1}

As^{III} standard solution. Interference free determination was assessed as that producing a relative sensitivity of 100±10%.

(I) Elimination of interference memory effects.

The interference free determination of 20 ng ml^{-1} of As^{III} was achieved with up to 100 μg ml^{-1} of Ni(II) and 50 μg ml^{-1} of Cu(II) respectively. In both investigations though the sensitivity of the As^{III} standard had to be determined before each interferent sample due to the presence of a significant interference memory effect. With increased interferent processing the overall sensitivity of the system was observed to deteriorate slowly in a manner similar tothat observed in the Se^{IV} interference tolerance studies (Section 4.3.3). For the nickel and copper interferents, the percentage reductions in sensitivity observed were 18.0 and 45.5% respectively. Sensitivity was regained in both cases by soaking the atomization T-cell in a 10% v/v solution of hydrofluoric acid (48% Aristar, BDH) for approximately 15 minutes, followed by rinsing in distilled water and drying. The restoration of optimum sensitivity following this washing process suggested that the interference memory effect was due to contamination of the silica T-cell by trace amounts of copper and nickel salts [46, 49], as discussed previously, (Section 4.3.3).

To eliminate the effect, prevention of the transport of such interferent species by the argon carrier gas to the atomization T-cell was required. A disposable gas-line membrane filter (PTFE, 0.2 μm) was fitted in-line with the hydride transport tubing as shown in *Fig. 5.1.* It was found that the filter caused a noticeable increase in back pressure which reduced the level of the aqueous reaction mixture in the gas-liquid separator. However, Ar flow rates of up to 500 ml min^{-1} were achieved without any loss of Ar or hydride through the separator drain. A direct comparison of the performance characteristics of the FI-HGAAS system with and without the membrane filter was made. The results are shown in Table 5.4.

Table 5.4 Performance data for the FI-HGAAS system for the determination of As^{III} with and without the membrane filter fitted. Manifold variables as in Table 5.2(I).

As^{III} concentration, ng ml^{-1}	NO FILTER		FILTER	
	Absorbance	RSD (%)	Absorbance	RSD (%)
2.0	0.019	3.3(n=10)	0.012	3.8(n=12)
10.0	0.110	3.2(n=10)	0.056	1.9(n=12)
20.0	0.195	2.4(n=6)	0.109	0.5(n=12)

(II) Interference tolerance for nickel.

The nickel interference tolerance of the FI-HGAAS system was investigated following the inclusion of the membrane filter within the gas-line. The effect of both HCl reagent concentration and reactor coil length (RC_2) on the nickel interference in the determination of As^{III} is shown in Table 5.5. No precipitation or colour change was observed in the gas-liquid separator or manifold tubing and no interference memory effect was experienced throughout the investigations. Operating parameters selected for subsequent work, shown in Table 5.2(I), were chosen on the basis of optimum sensitivity. The corresponding nickel interference tolerance of 100 μg ml^{-1} was considered more than sufficient for the proposed analysis of nickel alloy particulary with the implementation of matrix isolation prior to determination.

Table 5.5 Effect of hydrochloric acid concentration and reactor coil length (RC_2) on nickel interference in the determination of 20 ng ml^{-1} of As^{III}. All other variables as in Table 5.2(I).

Ni(II) concentration μg ml^{-1}	RELATIVE SENSITIVITY (%)		
	Investigation I	Investigation II	Investigation III
10	100.8	-.-	-.-
50	99.2	-.-	-.-
100	96.0	99.2	101.1
200	82.0	95.3	100.0
500	35.9	75.6	80.4
1000	13.9	35.2	40.2

Investigation I HCl 3.6 mol dm^{-3}, RC_2 600 mm (0.8 mm i.d.)
Investigation II HCl 7.2 mol dm^{-3}, RC_2 600 mm (0.8 mm i.d.)
Investigation III HCl 7.2 mol dm^{-3}, RC_2 100 mm (0.8 mm i.d.)

(III) Interference tolerance for copper.

The interference-free determination of As^{III} was achieved with up to 1000 μg ml^{-1} of Cu. During the analysis of high concentration copper samples a dirty brown precipitate was observed within the gas-liquid separator. The precipitate washed out of the gas-liquid separator within seconds of each injection. At concentrations above 500 μg ml^{-1} of Cu specks of a grey-black precipitate were also observed within the reactor coil (RC_2) at the merging point of the acidified sample solution with the sodium tetrahydroborate solution. These observations were very similar to those reported in the investigation of copper interference in the determination of Se^{IV}, (Section 4.3.3). Despite the presence of the precipitate, no interference memory effect was experienced.

(IV) Interference tolerance for cobalt.

The interference-free determination of As^{III} was achieved with upto 100 μg ml^{-1} of Co. No visible precipitation in or discolouration of the gas-liquid separator was observed on the analysis of the interferent samples and even at the 1000 μg ml^{-1} Co level no interference memory effect was experienced.

(V) Interference tolerance for antimony.

The interference-free determination of As^{III} was achieved with upto 0.02 μg ml^{-1} of Sb^{III} . No precipitation or discolouration within the gas-liquid separator was observed throughout the investigation. An interference memory effect was observed but was shown to be transient in nature. The interference memory effect was removed through the repeated determination of a 20 ng ml^{-1} As^{III} standard solution. The presence of Sb^{III} was observed to affect the signal response peak shape and introduce background absorption as shown in *Fig. 5.8.*

(VI) Interference tolerance of tin.

The interference-free determination of As^{III} was achieved with up to 0.1 μg ml^{-1} of Sn^{II}. No precipitation or discoloration within the gas-liquid separator was observed, yet a strong interference memory effect was experienced. Following the analysis 10 and 50 μg ml^{-1} Sn^{II} samples the As^{III} signal response was reduced to 83.0 and 36.0% of the original peak height signal response, respectively. This memory effect was removed by soaking the silica atomization T-cell in a 40% hydrofluoric acid solution for approximately 15 minutes.

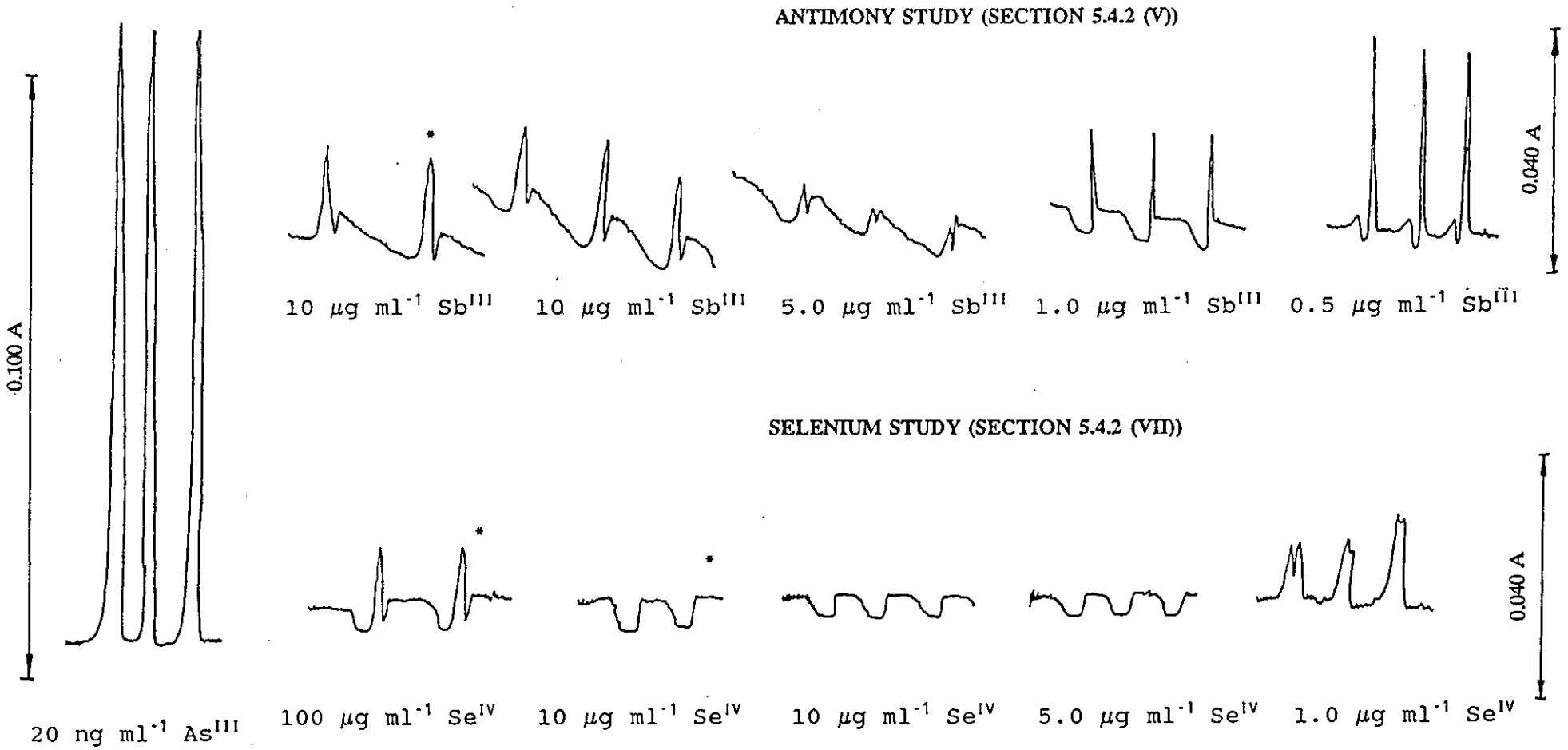

Fig. 5.8. Effect of antimony and selenium on the signal response obtained in the determination of 20 ng ml^{-1} of As^{III}. All other variables as in Table 5.2(I).
* No As^{III} Present.

(VII) Interference tolerance for selenium.

The interference-free determination of As^{III} was achieved with up to 0.01 $\mu g\ ml^{-1}$ of Se^{IV}. No significant memory effect was experienced but, as reported for Sb^{III} (Section 5.4.2 (V)), the presence of Se^{IV} affected the signal response as shown in *Fig. 5.8.* The investigation was repeated but each sample and standard was spiked at the 500 $\mu g\ ml^{-1}$ Cu level prior to determination. As a result of copper addition the interference free determination of As^{III} was possible with up to 10 $\mu g\ ml^{-1}$ Se^{IV}.

5.4.4 Discussion.

The sensitivity of the FI-HGAAS system following optimization (Section 5.4.2 characteristic concentration (0.0044A) 0.42 ng ml^{-1} As^{III}), compared favourably with the characteristic concentration figure of 0.32 ng ml^{-1} quoted for the PU9360 system when used for conventional steady state analysis [268]. In comparison with the optimization study made for Se^{IV} determination (Section 4.3.1) a significant difference was noted for the optimum argon carrier gas flow rate and reactor coil length (RC_2) in each case. Improved As^{III} sensitivity with reduced Ar carrier gas flow and increased reactor coil length may be explained in part by the slower rate of arsine formation relative to that of hydrogen selenide [27, 69]. The increased sensitivity with increased reactor coil length may well be attributed also to increased stripping of the hydride from solution prior to the gas-liquid separator[27], (Chapter six, Section 6.3).

Inclusion of the disposable membrane filter within the hydride transport line clearly eliminated the interference memory effect experienced in the analysis of copper and nickel samples (Section 5.4.3 (I)). From these observations it was concluded that the interference memory effect observed in the As^{III} study and also in earlier Se^{IV} studies (Section 4.3.3) was caused by the contamination of the silica atomization T-cell by trace amounts of copper and nickel salts, transported within a fine aerosol by the Ar carrier gas [46,49].

Inclusion of the membrane filter within the system, although detrimental to system sensitivity through increased dilution of the hydride in the gas phase was significantly beneficial to system precision (Table 5.4). This improved precision may be explained by the slight increase in back pressure within the system and the consequent dampening effect on pulsations in the Ar carrier gas flow rate. Prevention of the

transport of droplets of aqueous reaction mixture to the atomization T-cell may also have contributed to the improvement in precision.

The interference tolerance of the FI-HGAAS system was shown to be high for copper, cobalt and nickel. These observations are explained by the rapid separation of the hydride from the interfering matrix[13] and the limited absolute concentration of interferent introduced into the system [44,90] in each case, as discussed previously in section 4.5.3. The observed interference-free determination of As^{III} with up to 1000 $\mu g\ ml^{-1}$ of Cu in the presence of significant precipitate supports the suggestion that high copper interference observed in the determination of Se^{IV} (Section 4.5.3) is not due to the competition between precipitation and hydride evolution [14, 45]. The formation of copper selenide [44, 46, 49] is considered to be the more probable interference mechanism in this case.

The nickel interference tolerance of the system was significantly higher than the 5 $\mu g\ ml^{-1}$ Ni reported by Riby *et al.* [83]. A number of factors may be responsible for this. The 409 µl sample injection volume was less than 1000 µl used by Riby *et al.* [83] thus reducing the absolute amount of interferent introduced into the HGAAS system. Relative concentrations of sodium tetrahydroborate in each system calculated after correction for dilution from other reagent streams are also significantly different. In the proposed manifold a $NaBH_4$ concentration of 0.18% m/v was calculated in comparison with 0.38% m/v for the manifold of Riby *et al.* [83]. According to Welz and Schubert-Jacobs [46], a lower sodium tetrahydroborate concentration would be expected to give improved interference tolerance.

The addition of sodium tetrahydroborate prior to hydrochloric acid in the system of Riby *et al.* [83] may also be responsible for the inferior interference tolerance. This was demonstrated initially by Pierce and Brown [42] and further studied by Crock and Lichte [87]. Preferential reduction of nickel to the free metal or metal boride together with the lower solubility of such reduced interferent species could account for the observations made for this order of reagent addition.

Interference tolerances of the system to the hydride forming elements Sb^{III}, Sn^{II} and Se^{IV} were far inferior to that reported for Cu, Ni and Co. Interference in the gas phase [15] due to (i) radical population interference and (ii) analyte decay interference (possibly due to formation of diatomic molecules [40]) is proposed as the interference mechanism for the three interferents in question based on (a) a lack of

any precipitation, (b) the presence of memory and background effects and (c) the such low concentration (ng ml^{-1}) at which interference was observed.

In the study of antimony interference, the transient interference memory effect is attributed to the deposition of elemental antimony followed by its slow evaporation from the silica atomization T-cell surface, as reported by Narsito *et al.* [27]. The permanent interference memory effect observed with Sn^{II} may again be explained by deposition within the atomization cell [15, 101, 102]. It has been suggested that these deposits modify the silica surface of the T-cell, encourage hydrogen radical recombination and analyte decay [15].

Background absorption effects may be explained by the introduction of interferent hydride species to the atomization T-cell and the species produced as a result of their subsequent decomposition. These include dimer and other polymer species [93], and diatomic molecules such as AsSb [40].

The successful use of copper as a selenium interferent suppressant [69, 70] is explained by the marked difference in the interference tolerances of copper observed in Se^{IV} and As^{III} determinations (Sections 4.3.3 and 5.4.3 respectively). Although successful for the reduction in Se^{IV} interference the only problem with the procedure, on a practical level, was the formation of a significant quantity of precipitate within the system. With prolonged use the slow build up of precipitate would gradually block the flow line.

5.5 OPTIMIZATION OF THE CONTINUOUS FLOW MATRIX ISOLATION MANIFOLD FOR NICKEL RETENTION.

The efficiency of the Dowex 50WX8 100-200 cation exchange resin filled micro-column was investigated in the same manner as outlined in Chapter four (Section 4.6.1). The nickel capacity of the column was assessed by pumping a 1000 μg ml^{-1} Ni standard solution (nickel (II) sulphate 7 hydrate) through the column and continuously monitoring the column eluent by flame atomic absorption spectrometry. Spectrometer variables used were those recommended by the manufacturer [268]. A flow rate of 2.4 ml min^{-1} was used in all investigations on the basis of the results described in section 4.6.1 which indicated that improved exchange efficiency would be obtained at low flow rates. Breakthrough was judged to have occurred when the nickel concentration in the eluent exceeded 10 μg ml^{-1} of Ni, 10% of the hydride generation system's nickel interference tolerance. The effect of pH on the recovery of As^{III} from the column was

determined by comparing the signal response peak heights of pH adjusted standards before and after passage through the column. All pH adjustments were made by the addition of either HCl or ammonia solutions.

5.5.1 Effect of sample pH on nickel retention.

The effect of pH on the retention of nickel is shown in *Fig. 5.9.* Maximum retention was achieved at pH values above 2.0.

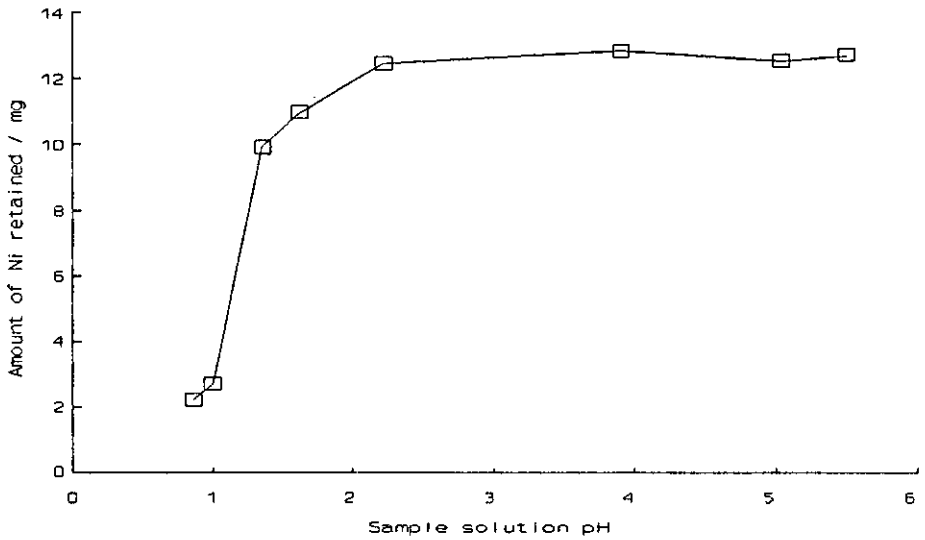

Fig. 5.9. Retention of Ni on the micro-column as a function of sample solution pH. Sample flow rate, 2.4 ml min^{-1}.

5.5.2 Effect of sample pH on As^{III} recovery.

The recovery of a 20 ng ml^{-1} As^{III} solution (sample flow rate 2.4 ml min^{-1}) over the pH range 1.00-5.94 was quantitative (96.9-103.2%).

5.5.3 Discussion.

From the results it was evident that to optimize the matrix isolation procedure the sample pH should be kept above a value of 2.00.

This design of matrix isolation system has a number of beneficial features, as previously discussed in detail in Chapter four (Section 4.6.2), which clearly makes it superior to in-line matrix isolation systems [71, 82, 83]. Mounting the column of the resin in the "injection" loop of a six port rotary valve allows intermittent regeneration

of the column while the determination is proceeding in the hydride generation manifold or standards are being introduced for calibration purposes. The direction of acid regenerent flow is opposite to that used to load the column and thus any tendency of the column contents to compact is minimised. As the resin is loaded in a continuous flow mode, the dimensions of the resin are not critical as the column makes no contribution to sample dispersion. In a flow injection manifold, such dimensional changes could eventually lead to measurable changes in dispersion coefficient.

5.6 DETERMINATION OF As^{III} IN A SYNTHETIC NICKEL MATRIX.

The FI-HGAAS manifold (*Fig. 5.1*) was operated with the stopped-flow KI pre-reduction reagent lines disconnected under the conditions shown in Table 5.2(I) and (II). Synthetic nickel sample solutions containing 1000 $\mu g\ ml^{-1}$ Ni (Ni(II) sulphate 7 hydrate) were prepared without any pH adjustment or addition of pH buffer, spiked with 10, 20, 50 and 100 $ng\ ml^{-1}$ of As^{III}. The recoveries of As^{III} from these synthetic samples (pH 5.50) were determined in triplicate against aqueous standards of the same determinand concentrations. The recoveries of 10, 20, 50 and 100 $ng\ ml^{-1}$ of As^{III} were 97.8; 97.8; 98.9; and 98.1% respectively.

5.7 DETERMINATION OF As IN A NICKEL BASED ALLOY REFERENCE MATERIAL.

The analysis of a single nickel based alloy BCS 346 was attempted.

5.7.1 Sample digestion.

The method [83] used for the digestion of nickel alloy reference material BCS 346 was as follows.

A sample of nickel alloy (1.00 g) was accurately weighed in duplicate into two PTFE microwave digestion bombs. To each bomb was added 20 ml 4% v/v HNO_3 and 2.5 ml 40% HF. The same acid digestion media was added to four other PTFE digestion bombs. The six bombs were capped, equally spaced within the microwave turntable and taken through the one hour digestion programme, (15 mins 30% power, 15 mins 50% power, 30 mins 40% power). Following the digestion programme the samples were left for one hour to cool. The bombs were uncapped, their contents transferred to 100 ml

polypropylene calibrated flasks and diluted to volume with analytical-reagent grade water. Prior to analysis the digests were further diluted to produce working samples containing 1000 μg ml^{-1} of Ni. Analysis of the working samples was carried out within 24 hours of digestion. After 24 hours the samples were observed to contain a significant amount of precipitated material.

5.7.2 Identification of As oxidation state.

Prior to the attempted analysis of nickel alloy reference material the effect of the microwave digestion procedure on the oxidation state of As was investigated. Aqueous standard solutions of As^{III} with and without nickel present were taken through the digestion procedure outlined in section 5.7.1. The As recoveries of these samples were subsequently determined against As^{III} standard solutions, as outlined in section 5.6. Results obtained from this investigation are shown in Table 5.6.

Table 5.6 Effect of microwave digestion procedure on the recovery of As^{III}. Manifold variables as in Table 5.2 (I,II).

Sample solution		Absorbance	Recovery (%)
STD 1	25ng ml^{-1} As^{III}	0.123(n=3)	-.-
*SMP 1	Blank	0.000(n=3)	-.-
*SMP 2	25ng ml^{-1} As^{III}	0.016(n=3)	13.0
*SMP 3	25ng ml^{-1} As^{III}	0.015(n=3)	12.2
*SMP 4	25ng ml^{-1} As^{III}, 500 μg ml^{-1} Ni	0.014(n=3)	11.4

*Samples taken through microwave digestion procedure.

In view of the results shown in Table 5.6, a pre-reduction step was applied to determine whether or not the low recoveries were caused by the oxidation of As^{III} to As^{V} during sample digestion. A batch procedure, reported by Welz and Melcher [53], employing potassium iodide as a reducing agent was used as follows. Digested sample solutions were prepared to contain potassium iodide and hydrochloric acid concentrations of 0.5% m/v and 4.8 mol dm^{-3} respectively. The samples were then allowed to stand for 30 minutes to allow quantitative reduction of As^{V} and then analysed in the same manner as outlined in section 5.6. The results obtained from this investigation are shown in Table 5.7. It was concluded that the low As recoveries were caused by the oxidation of As^{III} to As^{V} during the microwave digestion step, in direct contradiction of the observations of Riby *et al.* [83].

Table 5.7 Effect of microwave digestion procedure on the oxidation state of As. Manifold Variables as in Table 5.2 (I,II).

Sample solution		Absorbance	Recovery (%)
STD 1	25 ng ml^{-1} As^{III}	0.136(n=3)	-.-
STD 2	25 ng ml^{-1} As^{V}	0.025(n=3)	18.0
*SMP 1	25 ng ml^{-1} As^{III}	0.020(n=3)	14.7
*SMP 2	25 ng ml^{-1} As^{III}	0.020(n=3)	14.7
**SMP 3	Blank	0.007(n=3)	-.-
**SMP 4	25 ng ml^{-1} As^{III}	0.147(n=3)	102.9
**SMP 5	25 ng ml^{-1} As^{III}	0.145(n=3)	101.5

*Samples taken through microwave digestion procedure.
**Samples taken through microwave digestion procedure and KI pre-reduction procedure.

5.7.3 System performance for the determination of As^{V}.

The performance characteristics of the FI-HGAAS manifold (*Fig. 5.1*) for the determination of As^{V} was investigated to assess the possible use of an As^{V} calibration procedure in the analysis of nickel based alloy. A characteristic concentration of 5.5 ng ml^{-1} As^{V} was obtained for the manifold variables shown in Table 5.2. The interference free determination of 100 ng ml^{-1} of As^{V} was achieved with up to 100 µg ml^{-1} of Ni under the same conditions. The reduced sensitivity observed in the determination of As^{V} relative to that of As^{III} prevented analysis of the nickel alloy based on As^{V} quantification. It was concluded that an As^{V} pre-reduction step was needed in the analysis to permit determination and quantification as As^{III}.

5.7.4 On-line pre-reduction of As^{V}.

An on-line pre-reduction procedure for As^{V} employing the reduction chemistry reported by Sperling *et al.* [281] to produce the quantitative reduction of As^{V} to As^{III} in a reaction time of 4 s for FI-ETAAS, was investigated. The composition of the reducing reagent "cocktail" employed is given in Table 5.8.

Table 5.8 Reducing agent "cocktail" for the rapid on-line reduction of As^{V} to As^{III}.

100 ml	4.5 mol dm^{-3}	HCl
200 ml	1.5 mol dm^{-3}	Na_2SO_3
10 g	$Na_2S_2O_3$	
50 g	KI	

The manifold shown in *Fig. 5.10* was developed to permit the pre-reduction procedure to be applied after matrix isolation but prior to FI-HGAAS. Sample and reducing agent flow rates used were both 2.0 ml min^{-1} which permitted a reaction time in excess of 4.5 s for a 3 m long reactor coil (0.8 mm i.d.). The FI-HGAAS manifold shown in *Fig. 5.1* was operated under the optimum conditions shown in Table 5.2(I). Sample solution was sampled intermittently through the activation of the sample injection valve as outlined in Chapter four (Section 4.4.1).

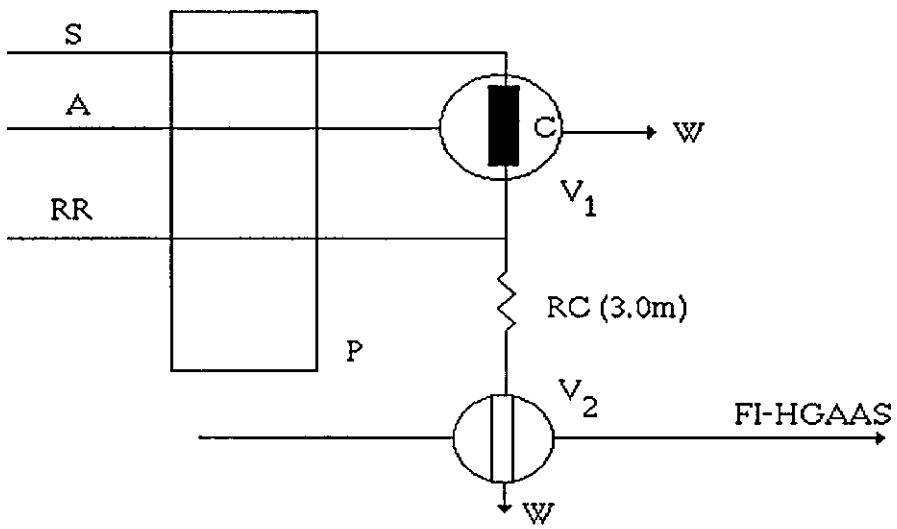

Fig. 5.10. Schematic diagram of continuous flow matrix isolation unit incorporating an on-line As^{V} pre-reduction step. P, peristaltic pump; S, sample; A, HCl; RR, reducing reagent; W, waste; V_1, switching valve; V_2, sample injection valve; C, micro-column.

In the proposed on-line pre-reduction system blank absorbance values were excessively high (> 1.00 A) making quantitative analysis impossible. The blank values were explained by the formation of hydrogen sulphide as a by-product of the hydride generation reaction, identified by its characteristic smell.

Because of the high background and the fact that hydrogen sulphide is toxic no further investigation of this pre-reduction chemistry was made.

5.7.5 Stopped-flow KI pre-reduction of As^V.

The use of a stopped-flow KI pre-reduction procedure was investigated to improve system sensitivity following the unsuccessful application of the on-line procedure described in section 5.7.4. The system used is shown in *Fig. 5.1* and discussed in section 5.3, operated under the optimum conditions shown in Table 5.2. The reducing agent used consisted of potassium iodide and hydrochloric acid. This reagent was used in a batch procedure by Welz and Melcher [53] and has been successfully applied to continuous flow systems by Pacey *et al.* [58] and Yamamoto *et al.* [88].

An investigation of the performance of the stopped-flow KI pre-reduction unit as a function of the stop-time, KI reagent concentration and HCl reagent concentration was made. The relative sensitivity of a 50 ng ml^{-1} As^V standard solution was compared directly with that of a 50 ng ml^{-1} As^{III} standard solution for three separate sets of operating conditions as shown in Table 5.9. The values of the operating parameters used in investigation C (Table 5.9) and a stop time of 15 s were chosen as optimum for the pre-reduction unit (Table 5.2(III)).

Table 5.9 Effect of manifold variables on the performance of the stopped-flow KI pre-reduction system for the reduction of 50 ng ml^{-1} of As^V. A, KI 1.4 ml min^{-1} (20% m/v), HCl 1.5 ml min^{-1} (12 mol dm^{-3}); B, KI 1.4 ml min^{-1} (30% m/v) HCl 1.5 ml min^{-1} (12 mol dm^{-3}); C, KI 1.4 ml min^{-1} (30% m/v), HCl 2.2 ml min^{-1} (12 mol dm^{-3}). All other variables as in Table 5.2(I,II).

Stop time/s	Relative sensitivity (%), (As^V wrt As^{III})		
	Investigation A	Investigation B	Investigation C
5	-.-	79.9	97.5
10	77.6	86.6	95.2
15	82.3	90.4	97.5
20	80.4	97.0	96.7
30	89.2	95.6	96.7
45	92.1	95.6	-.-
60	94.8	95.5	-.-

5.7.5.1 Discussion.

For the values of the operating parameters used in investigation C (Table 5.9) an average recovery of 96.74% (standard deviation 0.62% and 95% confidence interval ±0.77%) was obtained for stop times between 5 and 30 s. Clearly this is significantly different from 100% suggesting that not all the arsenic has been reduced. However, the conversion was considered sufficiently high enough to permit As^{III} quantification with the possible implementation of a correction factor. The benefits of the stopped-flow pre-reduction unit design, as reported for the matrix isolation unit, result from the independence of the procedure from the hydride generation chemistry. The conditions for efficient pre-reduction, therefore, may be optimized separately from those of the hydride generation reaction. Due to the use of relatively high carrier and reagent flow rates in the FI-HGAAS manifold, the implementation of an in-line KI pre-reduction procedure [58, 88] was dismissed. The reactor coil length required to permit sufficient time for the quantitative reduction of As^{V}, if possible in such a system, would be excessively long. It is proposed that this would compromise throughput capability, interference tolerance [13] and, due to the expected increase in back pressure, system reliability.

In the stopped-flow method, control of reaction time is achieved independently of any other parameter such as flow rate or tube length. To achieve a residence time of 15 s, without the implementation of the stopped-flow procedure, for the combined flow rate of 5.8 ml min^{-1} of sample and regents a reactor coil length of 2.9 m (0.8 mm i.d.) would be required in the matrix isolation/KI pre-reduction unit (*Fig. 5.10*). This strategy though would be far less economical with respect to sample and reagent composition. For the stopped-flow procedure the consumption of potassium iodide was 19.5 g h^{-1}. This figure could be reduced further by pumping reagents independently of the matrix isolation unit. In such a system the pumping of reduction reagents could be stopped during column regeneration. The calculated potassium iodide consumption was clearly superior to the figures of 45 and 75 g h^{-1} reported for in-line KI pre-reduction procedures [58, 88]. This was to a degree due to the fact that the potassium iodide reagent in the stopped-flow unit was not diluted by the reagents used in the FI-HGAAS manifold (H_2O carrier, HCl and $NaBH_4$). The stock concentration necessary (30% m/v) to achieve quantitative reductions of As^{V} was therefore reduced.

5.7.6 Calibration and analysis procedures.

The FI-HGAAS manifold shown in *Fig. 5.1* was operated under the optimum values of the operating variables shown in Table 5.2 according to the analysis sequence outlined in section 5.3.1. Aqueous As^{III} standard solutions (0-80 ng ml^{-1} As^{III}) were used for calibration. These were sampled directly without undergoing matrix isolation. Replicate determinations of the As content of the BCS 346 nickel based alloy, digested as outlined in section 5.7.1, were made on two separate digest solutions. The column was regenerated after every third determination. Calibration and analysis data is shown in Table 5.10.

Table 5.10 Calibration and analysis data for BCS 346.

Sample mass/g	Standard concentration / ng ml^{-1}	Absorbance			Mean absorbance	Corrected absorbance
	0.0	0.006	0.006	~~0.006~~ 0.007	0.0063	
	10.0	0.028	0.029	0.029	0.0287	
	20.0	0.051	0.051	0.052	0.0513	
	40.0	0.095	0.093	0.093	0.0937	
	60.0	0.132	0.133	0.132	0.1323	
	80.0	0.170	0.170	0.170	0.1700	
1.0399		0.103	0.101	0.101	0.1017	0.1051
1.0334		0.101	0.100	0.100	0.1003	0.1037

Regression equation $y=0.002046x + 0.008773$

$S_{y/x}$ 2.50586×10^{-3}

S_b 3.6359×10^{-5}

S_a 1.6327×10^{-3}

where y is absorbance, x concentration (ng ml^{-1}), $S_{y/x}$ is the standard deviation of the y residuals, S_b is the standard deviation of the slope and S_a is the standard deviation of the intercept [283]. The corrected absorbance values are those which would have been obtained had all the arsenic in the sample been reduced to As^{III}, (Relative signal response As^V wrt As^{III}, 96.74%).

5.7.7 Analysis results.

The results of the analysis of the reference material are given in Table 5.11, based on a unweighted least squares regression of the calibration data shown in Table 5.10. The standard deviations of the two results are 0.89 and 0.88 ng ml^{-1} for solution concentrations of 47.08 and 46.40 ng ml^{-1}, respectively [283]. The concentrations in the solid samples are therefore 45.27 and 44.90 $\mu g\ g^{-1}$ with confidence intervals ±2.37 and ±2.38 $\mu g\ g^{-1}$ respectively.

Table 5.11 Result of the analysis of BCS 346 nickel alloy reference material. (±95% confidence limits).

Sample	As found $\mu g\ g^{-1}$	Certified value for As $\mu g\ g^{-1}$
Sample 1	45.3±2.37	50.2±3.7
Sample 2	44.9±2.38	

5.7.8 Discussion.

On first inspection of the analysis results one may reach an instant conclusion that the analysis was unsuccessful. Applying the "t-test" [284] to the data shown in Table 5.11 the null hypothesis was in fact rejected for both samples (P=0.05), therefore, indicating a significant difference between the analytical results and certified value. However, this test requires a knowledge of the standard deviations of the two mean values to be compared and the number of replicates from which the two means were calculated. For the BCS 346 certified reference material the certificate gives four results from different analysts, namely 50.0, 51.8, 52.0 and 47.0 $\mu g\ g^{-1}$. Although the mean, standard deviation and 95% confidence interval from this data was calculated in the "t-test" the results were clearly an underestimation of the true uncertaintity since no consideration was paid to the uncertaintity of the results obtained from each analyst. As this data is not available on the certificate a truly accurate "t-test" cannot be undertaken, therefore, limiting the significance of the result achieved with the "t-test" applied.

For the data obtained in the analysis (Tables 5.10 and 5.11) standard deviations and 95% confidence intervals were calculated, taking into account the uncertaintity encountered when calculating a concentration from an unweighted linear regression [283]. Applying such a protocol even without a consideration of the uncertaintity due to the percentage reduction of As^{V} to As^{III}, the 95% confidence intervals of the measured value and the

certified value overlap. This, by definition, indicates partially that the values are not significantly different.

A proposed explanation for the rather low mean As recovery from the nickel alloy was interference in the determination of As from mutual hydride forming elements.From the certificate for the reference material although the concentrations of the individual hydride forming species (Se, Sb, Sn etc) were all within the interference tolerance limits of the system, as determined in section 5.4.3, no consideration was paid to their additive effect. A repeat analysis was attempted employing a lower sample concentration, therefore, lower absolute concentration of mutual hydride forming species but no results were obtained due to spectrometer failure.

5.7.9 System performance.

For the analysis of nickel based alloy (BCS 346) a characteristic concentration (0.0044A) of 2.1 ng ml^{-1} As was obtained. The detection limit of 3.9 ng ml^{-1} As was calculated from the resultant calibration graph [275]. A sample throughput of 18 h^{-1} was achieved with triplicate injections.

5.8 DISCUSSION.

As discussed in detail in Chapter four and earlier in this chapter (Section 5.5.3) the design features of the continuous flow matrix isolation system makes it superior to that of previous in-line systems [71, 82, 83]. Full automation of the system, including the stopped-flow pre-reduction procedure should be possible with existing apparatus [277]. It is also postulated that the same stopped-flow KI pre-reduction procedure could be applied to the determination of Sb with the same benefits as outlined in section 5.7.5.

For the direct application of the system to the determination of As in nickel alloy the detection limit was shown to be inferior to that of Riby *et al.* [83]. The values obtained for the two systems were 3.9 and 1.3 ng ml^{-1} of As, respectively. The detection limit of the stopped-flow FI-HGAAS system is restricted by the KI pre-reduction step, absent in the work of Riby *et al.* [83]. Prior to introduction into the FI-HGAAS system the sample was diluted by a factor of 2.7.

Some degree of controversy appears to exist as to the oxidation state of the As present in the nickel alloy following the microwave digestion procedure used (Section 5.7.1) [83, 278]. In the work of Riby *et al.* [278] the oxidation state of the As present following digestion was assumed to be +3 which was suggested to predominate at low pH. It appears though that no direct attempt was made to identify the species present. From the results described in section 5.7.2, the As is clearly present in the +5 oxidation state. In connection with this an interesting observation was made by Riby *et al.* [278] using a dual column system (SCX and SAX columns in series) permitting the simultaneous determination of As^{III} and As^{V}. In the determination of mixed aqueous As^{III} and As^{V} samples, separate signal responses were obtained for each species. In the presence of nickel though only a single As^{III} signal response was reported. This was thought to be a direct result of the nickel exchanging with the column and releasing hydrogen ions into the sample, hence lowering the pH. The introduction of hydrogen ions was considered to cause the conversion of As^{V} to As^{III}. These statements though are contradicted by the observations made in section 5.7.2. No conversion of As^{V} to As^{III} was observed for a digested synthetic sample containing nickel (500 $\mu g\ ml^{-1}$ Ni) following the cation exchange procedure with the hydrogen form cation exchange resin, used in this work.

Although the observations reported by Riby *et al.* [278] cannot be fully explained, it appears from their results that the cation exchange resin in the presence of Ni causes the rapid reduction of As^{V} to As^{III}. The proposed conversion of As^{V} to As^{III} simply due to a decrease of pH though is rejected since a similar effect would be expected in the present system and this was not observed. Some consideration was also given to the order of reagent addition in the system of Riby *et al.*[278]. Addition of sodium tetrahydroborate prior to hydrochloric acid it was suggested may have in fact caused the rapid pre-reduction of As^{V} to As^{III}. Results in Chapter six (Section 6.4.1) though show that adding sodium tetrahydroborate prior to HCl makes no significant difference of the hydride generation efficiency of As^{V} eliminating this possibility.

The observations made by Riby *et al.* [278] are clearly of considerable interest since it appears that the rapid quantitative reduction of As^{V} is possible by some mechanism yet to be fully elucidated. Further work is therefore clearly necessary to fully exploit its potential.

CHAPTER SIX

EVALUATION AND CHARACTERISATION OF THE PERKIN-ELMER FIAS-200 FI-HGAAS SYSTEM.

6.1 INTRODUCTION.

The successful application of flow injection to HGAAS [13], discussed in Chapter two, has eventually led to the development of a fully automated commercial FI-HGAAS system, the "FIAS-200", by the Perkin-Elmer corporation. Although basic performance data has been presented in sales documentation and in a single applications paper [243], to date very little information has been given on the characterisation of the instrument, its optimization or benefits of system design.

This chapter describes an investigation into the use of the FIAS-200 system for the determination of As by FI-HGAAS. The system performance was evaluated and compared directly with that of the in-house system design, detailed in Chapter five, in order to identify possible benefits of system design. System variables were optimized. These included the order of reagent addition [42,58,83,87,235], atomization temperature [87,88,235], rector and segmentor coil lengths [27,235]. Studies of these variables have been reported in the literature but with contradicting results as to the true optima. Following the optimization the direct application of the FIAS-200 system to the determination of As in nickel alloy without matrix isolation was assessed.

6.2 APPARATUS AND REAGENTS.

6.2.1 Apparatus.

A Perkin-Elmer PE3100 atomic absorption spectrometer equipped with a Perkin-Elmer arsenic hollow cathode lamp was operated under the conditions shown in Table 6.1, based on the manufacturer's recommendations. The FIAS-200 FI hydride generation system shown in *Fig. 6.1* and modifications of that manifold were used with the miniaturised gas-liquid separator shown in *Fig. 6.2(I)*. The only permanent modification made to the system was the inclusion of a miniature PTFE membrane filter (Millex-SR, 0.5µm, Millipore) in-line with the hydride transport tubing, connecting the gas-liquid separator and silica atomization cell. A silica atomization cell heated externally by a furnace, shown in *Fig. 6.3(I)* was used throughout the work.

Table 6.1 Perkin-Elmer PE3100 spectrometer variables for the determination of arsenic.

Wavelength, nm	193.7
Slit Width, nm	0.7 (low slit)
Lamp current, mA	18
Background correction	Off
Status	Computer control
Integration time, s (Default)	15
Signal quantification	Peak-height absorbance

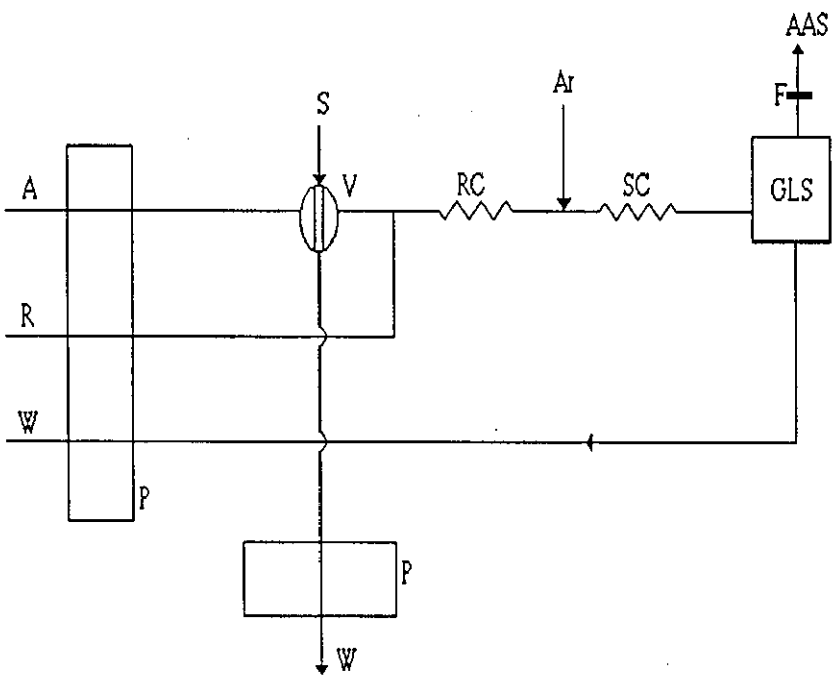

Fig. 6.1. Schematic diagram of the FIAS-200 FI-HGAAS system. P, peristaltic pump (stepper motor controlled); S, sample; A, HCl; R, $NaBH_4$; W, Waste; V, sample injection valve; F, PTFE membrane filter; GLS, gas-liquid separator.

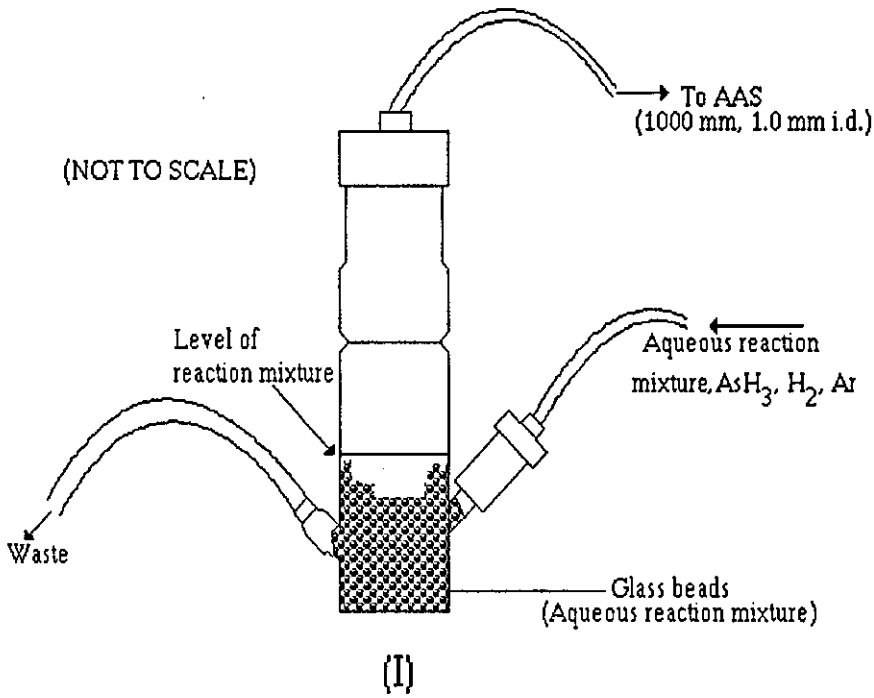

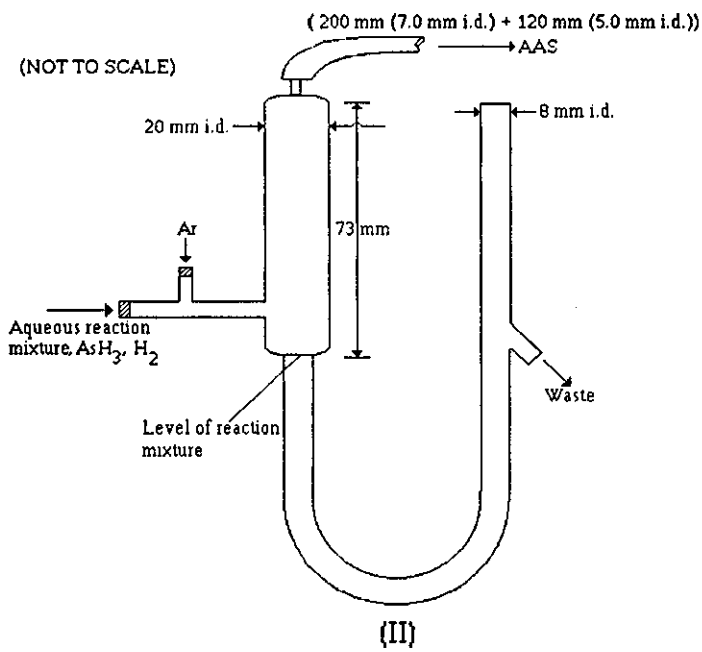

Fig. 6.2. Gas-liquid separator designs.
(I) FIAS-200 miniature gas-liquid separator, (Calculated internal volume 2.3 ml, excluding glass beads).
(II) PU9360 gas-liquid separator, (Calculated internal volume 23 ml).

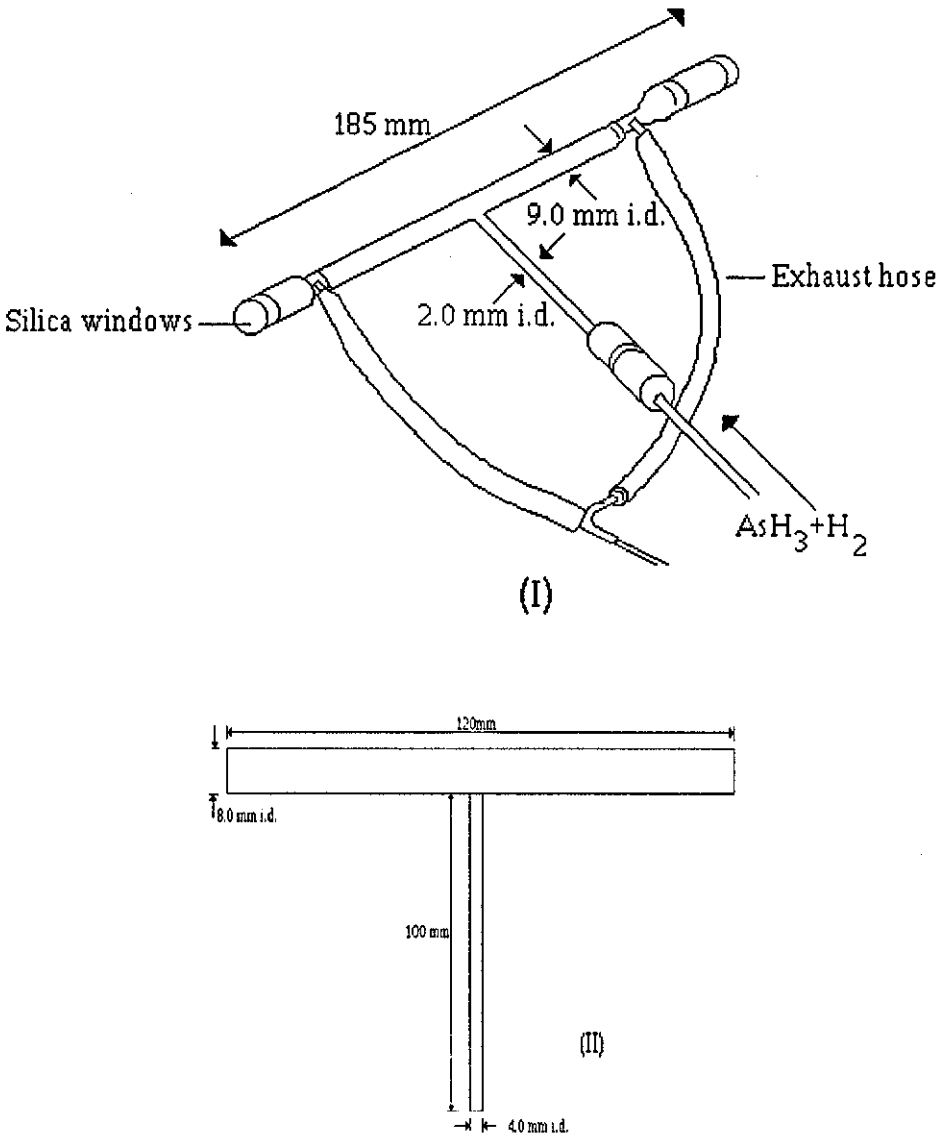

Fig. 6.3. Atomization cell designs.
(I) FIAS-200 Furnace heated silica T-cell.
(II) PU9360 Air-acetylene heated silica T-cell.

The peristaltic pumps, injection valve, furnace and spectrometer were all controlled with an IBM compatible computer, using the specifically designed FIAS-200 system software.

Where mentioned apparatus used for the in-house FI-HGAAS system reported in Chapter five was as detailed in that chapter (Section 5.2.1), based around the gas-liquid separator shown in *Fig. 6.2(II)* and externally flame heated silica atomization cell shown in *Fig. 6.3 (II)*.

6.2.2 Reagents.

An As^{V} stock standard solution (1000 μg ml^{-1}) was prepared by dissolving the appropriate mass of sodium arsenate (certified grade, Fisher) in analytical-reagent grade water. An As^{III} stock standard solution (1000 μg ml^{-1}) was prepared by dissolving the appropriate mass of arsenic trioxide (certified grade, Fisher) in sodium hydroxide solution (15 ml, 20% m/v) and then diluting to volume with reagent-grade water. Working standard solutions were prepared from these two stock solutions respectively by dilution with either HCl solution or reagent-grade water. Sodium terahydroborate solutions (in 0.1% m/v NaOH solution) were prepared using sodium tetrahydroborate solid (98%, Baker) and filtered through a Whatman 541 filter paper. With refrigeration, solutions were usable for up to 3 days. The hydrochloric acid reagent solutions were of A.C.S grade (Fisher). Conditioning and cleaning of the silica atomization cell was carried out using hydrofluoric acid (48% A.C.S grade, Fisher). For the nickel interference investigation work standard solutions were prepared from nickel (II) nitrate 6 hydrate (certified grade, Fisher). Reagents employed in the PU9360 system were as reported in Chapter five, section 5.2.2.

6.3 OPTIMIZATION OF FIAS-200 SYSTEM VARIABLES.

The spectrometer was operated under the conditions shown in Table 6.1, connected to the FI-HGAAS manifold (*Fig. 6.1*). The FIAS-200 system was operated using the values of the operating parameters shown in Table 6.2, based on the manufacturer's recommendations. Unless otherwise stated a 10 ng ml^{-1} As^{V} standard in 1.2 mol dm^{-3} HCl was used to investigate the effect of each operating parameter on the overall performance.

Table 6.2 FIAS-200 FI-HGAAS default variables for the determination of As^V (*Fig. 6.1*).

Reagent	Concentration	Flow rate/ ml min^{-1}
Sample	10 ng ml^{-1} As^V (1.2 mol dm^{-3} HCl)	9.8
HCl carrier	1.2 mol dm^{-3}	10.0
$NaBH_4$ reagent	0.5% m/v (0.1% m/v NaOH)	5.6
Ar	-.-	50
Injection volume	500 µl	
Atomization temperature	900°C	
Reactor coil	100 mm (1.0 mm i.d.)	
Segmentor coil	300 mm (1.0 mm i.d.)	

(I) Effect of argon gas flow rate.

The effect of the argon carrier gas flow rate on the absorbance signal response is shown in *Fig. 6.4.* An optimum Ar flow rate of 30 ml min^{-1} was chosen, after consideration was made to system precision, and applied in all subsequent work.

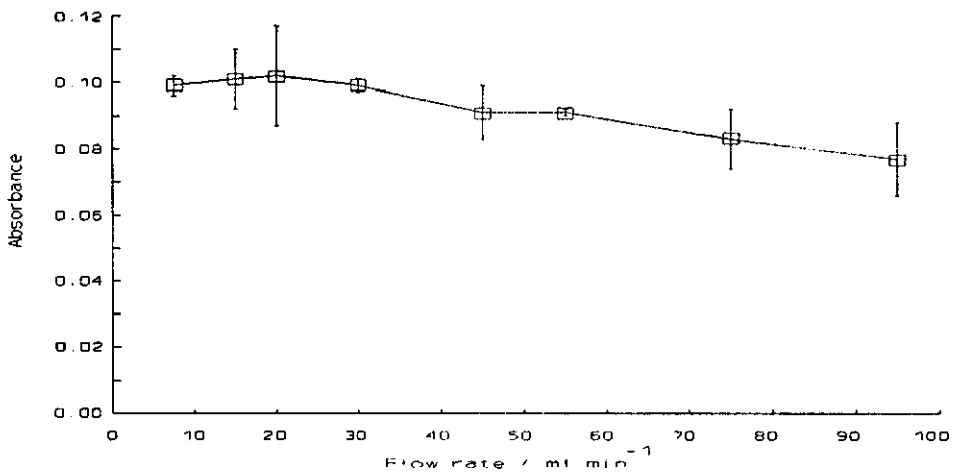

Fig. 6.4. Effect of the flow rate of Ar on the absorbance of 10 ng ml^{-1} of As^V. All other variables as in Table 6.2.

(II) Effect of atomization temperature.

The effect of atomization temperature on the sensitivity of As^V is shown in *Fig. 6.5.* To achieve optimum signal response it was shown that the atomization temperature should be

kept at 750 °C or above. An optimum atomization temperature of 800 °C was chosen for all subsequent work.

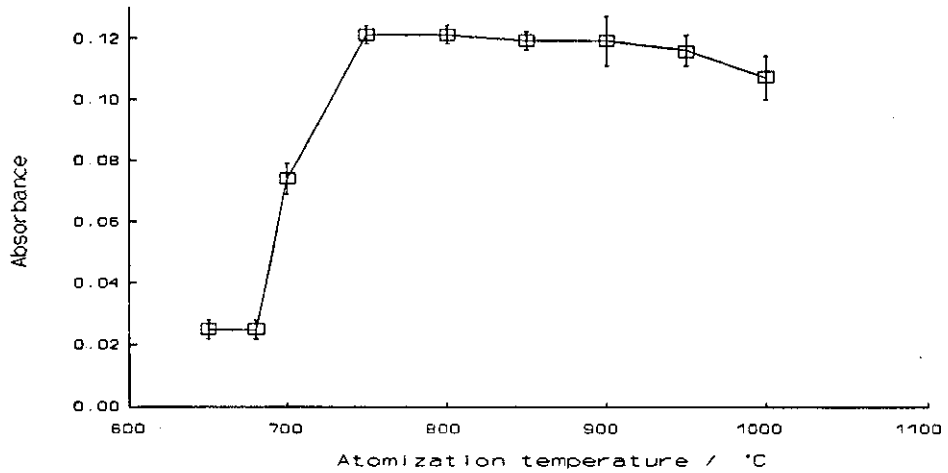

Fig. 6.5. Effect of the atomization temperature on the absorbance of 10 ng ml^{-1} of As^{V}. All other variables as in Table 6.2.

(III) Effect of reactor coil length.

The effect of reactor coil length (RC, *Fig. 6.1* (0.8 mm i.d.)) is shown in *Fig. 6.6.* Increasing the reactor coil length, although beneficial to As^{V} sensitivity was shown to be detrimental to both sample throughput and stability of Ar carrier flow. Deterioration in the stability of Ar carrier gas flow was explained by a significant increase in back pressure with increasing reactor coil length.

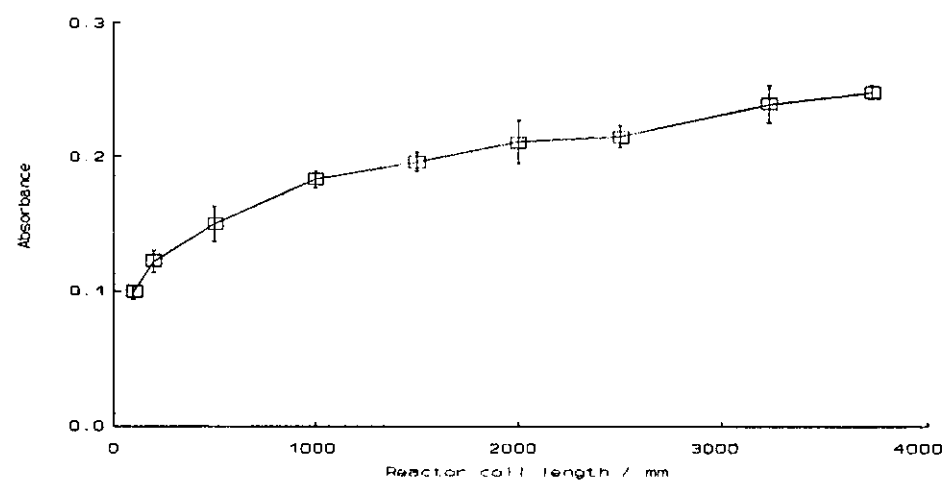

Fig. 6.6. Effect of the reactor coil length (0.8 mm i.d.) on the absorbance of 10 ng ml^{-1} of As^{V}. All other variables as in Table 6.2.

(IV) Effect of segmentor coil length.

The effect of segmentor coil length (SC, *Fig. 6.1* (0.8 mm i.d.)) on the As^V sensitivity is shown in *Fig. 6.7* for two reactor coil lengths (RC), 100 and 2000 mm (0.8 mm i.d.) respectively. For a reactor coil length of 2000 mm an increase in segmentor coil length was accompanied by a significant increase in back pressure and therefore Ar flow instability, as reported in section 6.3(III). Reduced As^V sensitivity with increased segmentor coil (RC, 2000 mm) could not be conclusively explained, other than possibly by a reduction in sample transport rate in the chemifold, with increasing back pressure. It was concluded that the optimum combination of reactor coil and segmentor coil lengths was 2000 and 300 mm (0.8 mm i.d.) respectively. This produced an As^V sensitivity and precision slightly less than maximum without any back pressure problems. Under these optimum conditions, a characteristic concentration of 0.15 ng ml^{-1} for As^V and a precision of 1.1% (RSD, 10 ng ml^{-1} As^V, n=4) were achieved.

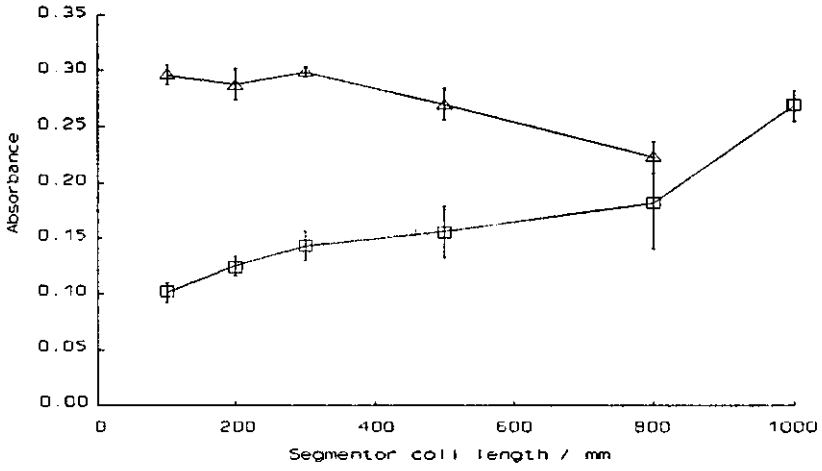

Fig. 6.7. Effect of the segmentor coil length (0.8 mm i.d.) on the absorbance of 10 ng ml^{-1} of As^V. (■), RC 100 mm (0.8 mm i.d.); (▲), RC 2000 mm (0.8 mm i.d.). All other variables as in Table 6.2.

6.3.1 Discussion.

An optimum atomization temperature of 800 °C was in close agreement with those reported previously of 850 °C [87], 950 °C [88] and 1000 °C [235]. In agreement with the findings of Ikeda [235] no improvement in sensitivity could be achieved at an atomization temperature above 900 °C.

The improved sensitivity observed with increased reactor and segmentor coil lengths was to an extent expected from the results obtained in the earlier As^{III} study (Chapter five, Section 5.4.1 (III)) in which As^{III} sensitivity was shown to increase with rector coil length, and the observations of others [27, 69, 235]. Increased reaction time achieved with increased reactor coil lengths was given as an explanation for the increased As^{V} sensitivity particulary when considering the slow rate of formation of arsine from As^{V} [27, 69]. Aggett and Aspell [280] postulated that arsine generation from As^{V} is a two step reaction, the As^{V} being reduced to As^{III} before arsine formation. Reduction of As^{V} to As^{III} was considered to be the rate determining step. An increase in the efficiency of hydride stripping from the aqueous reaction mixture with a combined increase in reactor and segmentor coil length may also account for the observed increase in As^{V} sensitivity [27].

On the basis of the optimization investigation the characteristic concentration achieved for As^{V} of 0.15 ng ml^{-1} was clearly significantly superior to the figure of 5.5 ng ml^{-1} achieved with the PU9360 system (Chapter five, Section 5.7.3) but without prior optimization of manifold variables. Even allowing for the that fact the PU9360 was not optimized for the determination of As^{V}, the significant difference in sensitivities of the two systems clearly gives some indication of the superior performance characteristics of the FIAS-200 system.

6.4 DIRECT COMPARISON BETWEEN THE PERFORMANCE CHARACTERISTICS OF THE FIAS-200 AND PU9360 FI-HGAAS SYSTEMS.

An experiment was undertaken to make a direct comparison between the characteristics of the FIAS-200 and those of the in-house PU9360 FI-HGAAS systems. The FI-HGAAS manifold optimized for the determination of As^{III} on the PU9360 system (Chapter five, *Fig. 5.1*) was applied as directly as possible to the FIAS-200 system. An extra pump channel was included to permit the inclusion of an aqueous carrier stream into which the sample was injected prior to in-line acidification and $NaBH_4$ addition, achieved through confluence mixing with pumped reagent streams. The manifold variables employed in the modified FIAS-200 system are shown in Table 6.3, transferred as directly as possible from Table 5.2(I), (Chapter five).

Table 6.3 FIAS-200 FI-HGAAS variables based on the manifold variables optimized for the PU9360 system for the determination of As^{III}, (Chapter five, Table 5.2 (I)).

Reagent	Concentration	Flow rate/ ml min^{-1}
Sample	Non acidified	9.8
H_2O carrier	-.-	11.3
HCl reagent	3.6 mol dm^{-3}	3.5
$NaBH_4$ reagent	1.0% m/v (0.1% m/v NaOH)	3.5
Ar	-.-	30
Injection volume	500 µl	
Atomization temperature	800°C	
Reactor coil length, RC_2	600 mm (0.8 mm i.d.)	
Segmentor coil, SC	300 mm (0.8 mm i.d.)	

The notable differences between the two systems that could not be physically overcome in the investigation were

(I) absence of a segmentor coil in the PU9360 system

(II) significantly lower Ar flow in FIAS-200 system

(III) mismatch of sample injection volumes (FIAS-200, 500 µl; PU9360, 409 µl).

Irrespective of these differences it was assumed that any significant differences in performance characteristics could be attributed to the design features of the FIAS-200 gas-liquid separator and atomization cell respectively.

The results of the investigation are given in Table 6.4. Data for the PU9360 system was obtained directly from Chapter five, sections 5.4.3 and 5.7.3 respectively.

Table 6.4 Comparison of performance characteristics of the FI-HGAAS systems for the determination of As (variables as Table 6.2).

	PU9360		FIAS-200	
	As^{III}	As^{V}	As^{III}	As^{V}
Characteristic concentration, ng ml^{-1}*	0.80	5.50	0.08	0.30
Characteristic mass, ng	0.33	2.25	0.04	0.15
RSD (%) (10 ng ml^{-1} As)	1.9(n=12)	3.1(n=4)	1.8(n=4)	4.4(n=6)

* (0.0044A)

6.4.1 Effect of the order of reagent addition.

The effect of the order of reagent addition on the determination of As^V was investigated to identify whether there is any significant benefit in adding sodium tetrahydroborate to the sample, before acidification [83, 235]. The FI-HGAAS manifold detailed in Chapter five, *Fig. 5.1*, was applied directly to the FIAS-200 system and operated according to the variables shown in Table 6.2. Performance data for both orders of reagent addition for the determination of 10 ng ml^{-1} of As^V are given in Table 6.5.

Table 6.5 Effect of the order of reagent addition on the sensitivity of As^V. All other variables as in Table 6.2, (± 95% confidence limits).

Reactor coil length/ mm (0.8 mm i.d.)	Absorbance		
	Investigation I	Investigation II	Investigation III
100	-.-	0.174±0.005	0.201±0.007
200	0.112±0.003	0.154±0.002	0.208±0.006
500	-.-	0.141±0.005	0.238±0.008
600	0.154±0.006	-.-	-.-
1000	0.187±0.007	0.133±0.004	0.246±0.011
2000	0.208±0.005	0.122±0.002	0.283±0.010

Investigation I
HCl addition prior to $NaBH_4$
10 ng ml^{-1} As^V aqueous standard
RC_1, 100 mm (0.8 mm i.d.)
RC_2, varied
SC, 300 mm (0.8 mm i.d.)

Investigation II
$NaBH_4$ addition prior to HCl
10 ng ml^{-1} As^V aqueous standard
RC_1, varied
RC_2, 600 mm (0.8 mm i.d.)
SC, 300 mm (0.8 mm i.d.)

Investigation III
$NaBH_4$ addition prior to HCl
10 ng ml^{-1} As^V (1.2 mol dm^{-3} HCl)
RC_1, varied
RC_2, 600 mm (0.8 mm i.d.)
SC, 300 mm (0.8 mm i.d.)

6.4.2 Discussion.

The sensitivity of the FIAS-200 system in the determination of As^{III} was in good agreement with the Perkin-Elmer literature (Characteristic concentration 0.1 ng ml^{-1} As^{III}, 500 µl). Explanation for its superior performance in comparison with the PU9360 system is postulated to be due to one or more of the following features, listed in order of importance.

(I) Reduced gas-liquid separator volume.

As detailed in *Fig. 6.2* the internal volume of the miniature gas-liquid separator used in the FIAS-200 system (excluding the volume taken up by the glass beads) was calculated to be only 10% that of the PU9360 gas-liquid separator. Reduced dilution of arsine (in the gas phase) could account for the increased sensitivity as observed by others when miniature gas-liquid separators were used [13, 67, 70, 89]. The difference in internal volume of the two gas-liquid separators was of the same magnitude as the difference in sensitivity observed.

(II) Reduced hydride transport tubing volume.

The internal volume of the hydride transport tubing used in the FIAS-200 system was calculated to be 0.79 ml which was significantly lower than the corresponding volume of 10.1 ml calculated for the PU9360 system. Reduced dilution in the gas-phase could therefore account for the difference in sensitivity as discussed in section 6.4.2(I).

(III) Reduced Ar flow rate.

Dilution in the gas-phase with a 400 ml min^{-1} Ar flow rate, used in the PU9360 system, was expected to be significantly higher than in the FIAS-200 system, which employed a flow rate of only 30 ml min^{-1}. The increase in As^{III} sensitivity with reduced Ar flow for the PU9360 system, shown in section 5.4.1(II) (Chapter five), is possible evidence for this suggestion [96].

(IV) Superior atomization cell design.

In the FIAS-200 system the optimum atomization temperature was achieved reproducibly through control of the furnace unit. In the PU9360 system, in comparison, the optimum atomization conditions were restricted by the limitations of the air-acetylene flame, as discussed in section 5.4.1(I) (Chapter five). Differences in the dimensions of the atomization T-cells (*Fig. 6.3*) may also account for the differences in sensitivity of the two systems. Atomization cell dimensions have been shown to play a critical role in system performance [13, 15, 235].

(V) Incorporation of a segmentor coil.

The incorporation of a segmentor coil in the FIAS-200 system could aid the hydride stripping process from the aqueous reaction mixture [27] based on the observations made in section 6.3(IV).

Although the results indicated that the miniaturisation of the whole system was beneficial to system sensitivity a drawback was the resultant increase in back pressure. This makes manifold fracture and leakage more likely, particularly with prolonged use on a routine basis. A great deal of care was required to achieve the fine balance between the relative flow rates of reaction mixture entering and exiting the gas-liquid separator. Contamination of the atomization T-cell from aqueous reaction products was frequently experienced prior to the inclusion of the in-line membrane filter.

Based on the results shown in Table 6.5 the addition of sodium tetrahydroborate prior to HCl in the FI-HGAAS system was not considered beneficial. An increase in sensitivity was observed for the addition of sodium tetrahydroborate prior to hydrochloric acid, only when determining a pre-acidified standard. This is due to an increase in the total reaction time and, therefore, increased hydride generation prior to gas-liquid separation. On the basis that little or no improvement in sensitivity was observed after taking into account total reaction time, and the suggested reduction in interference tolerance adding $NaBH_4$ prior to HCl (Chapter five, Section 5.4.4) [42, 87], the optimum order of reagent addition is concluded to be HCl followed by $NaBH_4$.

6.5 ELIMINATION OF THE DIFFERENCES IN SIGNAL RESPONSE FOR As^{III} AND As^{V} THROUGH MANIFOLD OPTIMIZATION.

The FIAS-200 system was set up with the FI manifold used on the PU9360 system (Chapter five, *Fig. 5.1*). The manifold variables employed in the FI-HGAAS system are shown in Table 6.3. Two studies of the effect of manifold dimensions and operation on the relative responses of As^{V} and As^{III} were made. The objective was to eliminate the difference in the relative signal responses and therefore any possibility of oxidation state interference effects in real sample analysis.

6.5.1 Effect of manifold dimensions.

The relative signal responses of 10 ng ml^{-1} of As^{V} and As^{III} were investigated with increasing reactor coil length (RC_2, 0.8 mm i.d.). It was hoped from the observations made in section 6.3(III) that by increasing the reactor coil length, and therefore reaction time, quantitative hydride generation from As^{V}[280] could be achieved. The results of the study are shown in Table 6.6. Although an increase in the signal response ratio (As^{V}/As^{III}) was observed with increasing reactor coil length at reactor coil lengths in excess of 3000 mm, high back pressures made the system unreliable, so further investigation was not attempted.

Table 6.6 Effect of reactor coil length(RC_2) on the relative signal responses of 10 ng ml^{-1} As^{V} and As^{III}. Manifold variables as in Table 6.3, (±95% confidence interval).

Reactor coil mm (0.8 mm i.d.)	Absorbance		Absorbance ratio As^{V}/As^{III}
	As^{V}	As^{III}	
100	0.092±0.003	0.487±0.017	0.19
200	0.096±0.008	0.502±0.015	0.19
500	0.121±0.006	0.495±0.012	0.24
1000	0.151±0.006	0.509±0.014	0.30
1500	0.162±0.010	0.509±0.011	0.32
2000	0.162±0.013	0.505±0.016	0.32
3000	0.181±0.008	0.463±0.012	0.39

6.5.2 Implementation of a stopped-flow procedure.

A stopped-flow procedure was investigated in an attempt to increase reaction time without the back pressure limitations encountered in section 6.5.1. After making a sample injection and allowing the sample plug to mix with both HCl and $NaBH_4$, the pumps driving the manifold were stopped for a preprogrammed time interval, trapping the sample mixture within the reactor coil, (3000 mm, 0.8 mm i.d.). It was thought that by trapping the sample and reagent zones the hydride generation reaction would continue to completion under static conditions. In practice, however, this stopped-flow system proved impractical due to the formation of hydride and hydrogen. This gas formation within the manifold tubing generated sufficient pressure to force the reaction mixture out of the reaction coil and, therefore, caused the slow loss of hydride.

6.5.3 Discussion.

The results in section 6.5 showed that the difference in relative signal response between As^{V} and As^{III} could not be eliminated simply by increasing the reaction coil length. An interesting observation made was the negligible effect of reactor coil length on the As^{III} signal response. This was in direct contradiction to the observations with the PU9360 system using the same manifold variables (Chapter five, Section 5.4). This observation indicated that possibly the hydride generation reaction was in fact complete before reaching the segmentor coil for all reactor coil lengths studied (100-3000 mm). The increased As^{III} signal response with increased reactor coil length, obtained with the PU9360 system, may therefore, be assumed to be due to increased hydride stripping from solution [27] achieved in the FIAS-200 system, in the segmentor coil.

Decreasing the carrier flow rates was considered as a further means of increasing the reaction time without producing the problems of the build up of back pressure, but was not implemented as it was considered that the overall system performance would be adversely affected. Extension of the reaction time either by increasing the reactor coil length or by reducing the carrier flow rate is clearly expected to compromise the beneficial characteristics of FI-HGAAS of sensitivity, interference tolerance and throughput (Chapter five, Section 5.4). Ikeda [235] reported the successful optimization of FI-HGAAS manifold variables to eliminate the difference in relative signal responses of As^{V} and As^{III}. To achieve this, though, sodium tetrahydroborate addition was made prior to hydrochloric acid, and a reactor coil of 1000 mm (3.0 mm i.d.) with a carrier flow rate of only 2.5 ml min^{-1} were used. The observations made in Chapter five,

(Section 5.4) and Chapter six, (Section 6.4) would suggest that under such conditions the overall sensitivity and interference tolerance would be adversely affected. In fact the interference free determination of 10 ng ml^{-1} As was achieved in the presence of 5, 10, and 3 μg ml^{-1} of Co^{2+}, Cu^{2+}, and Ni^{2+} respectively [235]. These figures are significantly lower than the values reported in Chapter five, (Section 5.4).

6.6 OPTIMIZATION FOR NICKEL INTERFERENCE TOLERANCE IN THE DETERMINATION OF As^V.

A study was made into the nickel interference tolerance of the FIAS-200 system in the determination of As^V. The FIAS-200 system was set up with the FI manifold used in the PU9360 system (Chapter five, *Fig. 5.1*). The values of the operating parameters used are shown in Table 6.3. The sensitivity for each test solution relative to that of a pure As^V standard solution was calculated. An interference free determination was taken as one which produced a relative sensitivity of 100±10%.

(I) Effect of reactor coil length.

The effect of reactor coil length on the nickel interference in the determination of 10 ng ml^{-1} of As^V is shown in *Fig. 6.8.* During the investigation no precipitation or interference memory effects were observed. An optimum reactor coil length of 100 mm (0.8 mm i.d.) was chosen for subsequent work.

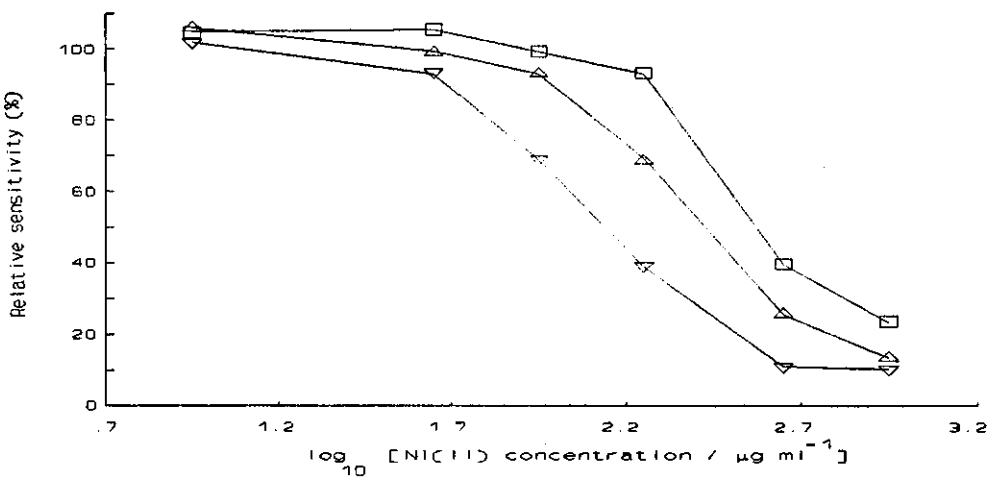

Fig. 6.8. Influence of reactor coil length (RC_2, 0.8 mm i.d.) on the interference of nickel in the determination of 10 ng ml^{-1} of As^V. (■), 100 mm; (▲), 600 mm; (▼), 2000 mm. All other variables as in Table 6.3.

(II) Effect of hydrochloric acid reagent concentration.

The effect of hydrochloric acid concentration on the nickel interference in the determination of 20 ng ml^{-1} of As^V is shown in *Fig. 6.9*. No precipitation or interference memory effects were observed throughout the investigation.

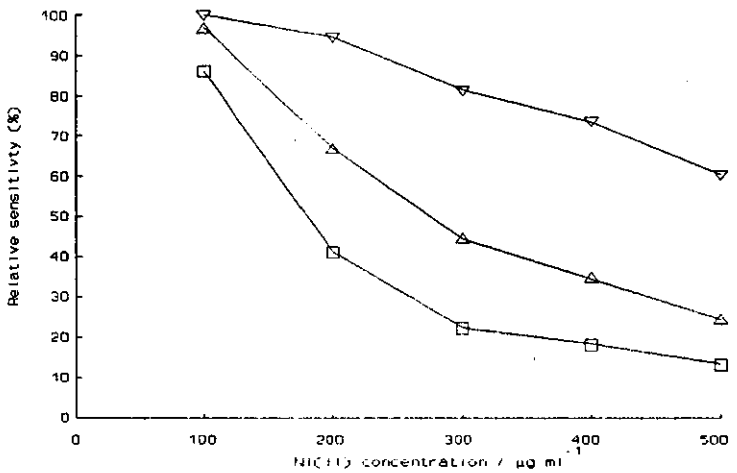

Fig. 6.9. Influence of HCl concentration on the interference of nickel in the determination of 20 ng ml^{-1} of As^V. (▾), 9.6 mol dm^{-3}; (▴), 7.2 mol dm^{-3}; (■), 3.6 mol dm^{-3}. RC_2, 100 mm (0.8 mm i.d.). All other variables as in Table 6.3.

6.6.1 Discussion.

Improved nickel interference tolerance with reduced reactor coil length [13] and increased hydrochloric acid concentration [43, 45, 46] was in agreement with the observation made with the PU9360 system in Chapter five, (Section 5.4.3(II)). An unexpected observation made though during the study, that could not be conclusively explained, was that the system interference tolerance was lower for the determination of 20 ng ml^{-1} of As^V than 10 ng ml^{-1} of As^V, for the same manifold variables. This finding did not agree with those of Meyer *et al.*[44] who concluded that the interference was independent of analyte to interferent ratio.

6.7 DISCUSSION.

The inferior performance characteristics obtained for the PU9360 system (Chapter five) relative to those of the FIAS-200 system are attributed to the use of a larger gas-liquid separator developed for continuous flow methodology and its incompatibility with FI-HGAAS, as discussed in section 6.4. It is thought that the superior sensitivity achieved with the FIAS-200 system and the high nickel interference tolerance (Section 6.6) would permit the direct analysis

of the nickel based alloy BCS 346 (50 $\mu g\ g^{-1}$ As) for arsenic. Use of the continuous flow matrix isolation unit, reported in Chapter five in conjunction with the FIAS-200 system would further extend the performance of the system and, therefore, permit the determination of even lower concentrations of As in similar nickel matrices.

CHAPTER SEVEN

INVESTIGATION OF THE ATOMIZATION PROCESS IN HYDRIDE GENERATION ATOMIC ABSORPTION SPECTROMETRY.

7.1 INTRODUCTION.

It is apparent from the relevant literature (reviewed in Chapter one) that some controversy still remains concerning the atomization process in HGAAS. Irrespective of the atomization mechanism involved, it is evident that the atomization step contributes significantly to the overall performance characteristics of the HGAAS procedure. The development of a full understanding of the atomization procedures has lagged behind that of the hydride generation procedure itself and in many respects, remains the 'Achilles heel' of the technique. Limitations reported for the externally heated silica atomization cell include poor day-to-day performance and stability [93,96], limited linear working range [93,95], gas-phase interferences [40,41,69], interference memory effects [101,102] and the necessity for frequent T-cell conditioning [91,93]. The use of a graphite furnace appears to provide a solution to these restrictions [40,41] and therefore makes it a feasible alternative to the externally heated silica atomization T-cell. However, investigation into the atomization mechanism in the externally heated silica atomization cell and procedures to improve its overall performance are still of great importance in further improving the performance of the HGAAS technique in its present format. Although the graphite furnace has shown promise as a suitable successor to the silica atomization cell present limitations may, unless overcome, restrict its use on a routine basis in the future. The required use of complex lengthy furnace heating programmes, enhanced background absorption effects and restricted furnace lifetimes have all been documented in the use of such graphite furnaces [40,41].

7.2 APPARATUS AND REAGENTS.

7.2.1 Apparatus.

All apparatus used was identical to that reported in Chapters four, five and six, based on the in-house PU9360 and commercial FIAS-200 FI-HGAAS systems. The externally heated flame and furnace atomization cells investigated were those shown in *Fig. 6.3* (I and II), (Chapter six).

7.2.2. Reagents.

All reagents used in the PU9360 in-house FI-HGAAS system were identical to those described in Chapters four and five. Reagents used with the FIAS-200 system were identical to those described in Chapter six.

7.3 CONDITIONING PROCEDURES FOR THE SILICA ATOMIZATION T-CELL.

The PU9360 in-house FI-HGAAS systems shown in *Figs. 4.2(II) and 5.1* were used for the determination of Se^{IV} and As^{III} respectively. Manifold variables used were those shown in Tables 4.5 and 5.2(I) respectively.

A study was made into the effect of T-cell surface condition on system performance and the use of conditioning procedures to achieve the optimum surface condition. Unless otherwise stated 20 ng ml^{-1} As^{III} and Se^{IV} aqueous standards were used to investigate the effect of each conditioning procedure on the overall performance.

(I) Effect of T-cell surface.

In the determination of Se^{IV} new, unused atomization T-cells were shown to produce less than 25% the sensitivity achieved with the previously conditioned cells, in constant use. A similar observation was made for the determination of As^{III}. Three separate T-cells of different ages and analytical histories, used previously in the determination of Se^{IV}, were shown to differ significantly in performance. Mean absorbance values obtained for the three T-cells in the determination of 20 ng ml^{-1} of As^{III}, prior to any conditioning, were 0.062±0.005, 0.088±0.006 and 0.108±0.004 (±95% confidence interval) for identical FI-HGAAS variables. An interesting observation made was that the T-cell that gave the best performance in the determination of Se^{IV} gave the poorest performance in the determination of As^{III}. The critical requirement for a specific surface condition was evident from the observations made in Chapter four (Section 4.3.3) and Chapter five (Section 5.4.3). Poisoning of the silica atomization T-cell surface by trace amounts of the interferent species Ni and Cu and hydride forming elements Sb and Sn [15,102] resulted in a drastic reduction in sensitivity.

(II) Effect of HF soaking.

The effect of a hydrofluoric acid conditioning procedure, based on that used by Welz and Melcher [91], was investigated. T-cells were soaked in solutions of HF for a period of 30 minutes (concentrations as quoted, *Figs. 7.1 and 7.2*), rinsed in analytical-reagent grade water and then thoroughly dried prior to use. Results for the conditioning procedure for both As^{III} and Se^{IV} determinations are shown in *Figs. 7.1 and 7.2* respectively.

(III) Effect of processing high determinand concentrations.

The effect of processing high determinand concentrations on sensitivity in the determination of both As^{III} and Se^{IV}, with and without HF conditioning, was investigated. High determinand concentrations (1000, 10,000 ng ml^{-1}) were injected (409 µl) into the system prior to determining lower analyte concentrations. Results are shown in *Figs. 7.1 and 7.2* respectively.

(IV) Effect of flame stoichiometry.

Based on the observations described in Chapter five (Section 5.4.1(I)) a study was made of the effect on sensitivity of conditioning, by heating the silica atomization T-cell within a fuel-rich air-acetylene flame. Three silica T-cells were heated separately in a fuel-rich air-acetylene flame (acetylene flow setting 22, air 27) for a period of five minutes, with the FI-HGAAS system connected and operational. The effect of this conditioning procedure on the sensitivity of As^{III} is shown in Table 7.1.

Table 7.1 Effect of heating the silica atomization T-cell in a fuel-rich air-acetylene flame on system performance in the determination of 20 ng ml^{-1} of As^{III}. All other variables according to Table 5.2(I), (±95% confidence interval).

T-CELL	Absorbance	
	Pre-conditioning	Post-conditioning
No. 1	0.062±0.005	0.109±0.003
No. 2	0.108±0.004	0.124±0.006
No. 3	0.088±0.006	0.137±0.019

The same conditioning procedure was applied to a silica T-cell following a hydrofluoric acid (40%) soak as described in section 7.3(II). A percentage increase in sensitivity observed in the determination of 20 ng ml^{-1} of As^{III} was 274%, an increase in mean absorbance (n=3) from 0.043 to 0.161. In further investigations it was observed that the conditioning effect could still be achieved with the FI-HGAAS system disconnected from the T-cell. The conditioning effect was found to be rather transient in nature. Each day prior to analysis conditioning was required to obtain maximum sensitivity.

In the determination of Se^{IV}, the increase in sensitivity obtained following the conditioning procedure was less impressive. Percentage increases in signal response in the measurement of 20 ng ml^{-1} of Se^{IV} for two silica T-cells were 11.0 and 15%, with increases in mean absorbance (n=3) of 0.144 to 0.160 and 0.149 to 0.171, respectively. The reduced percentage increase relative to that for As^{III} was explained by the good performance characteristics of the two T-cells prior to implementing the flame conditioning procedure.

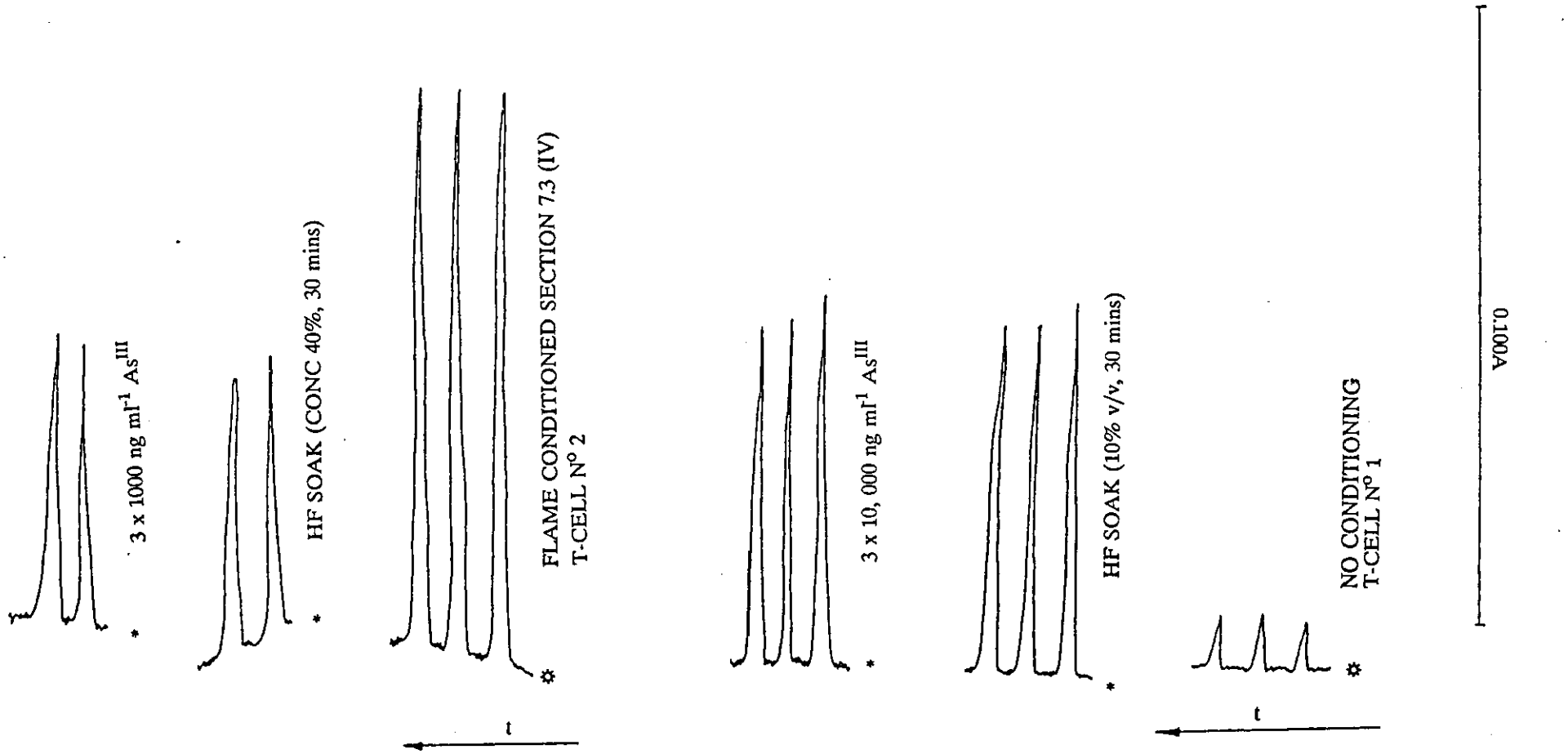

Fig. 7.1. Effect of silica atomization T-cell conditioning procedures on the sensitivty for As^{III}. (II), HF soaking; (III), High determinand concentrations: 20 ng ml^{-1} of As^{III}, 409 µl. All other variables as in Table 5.2(I).

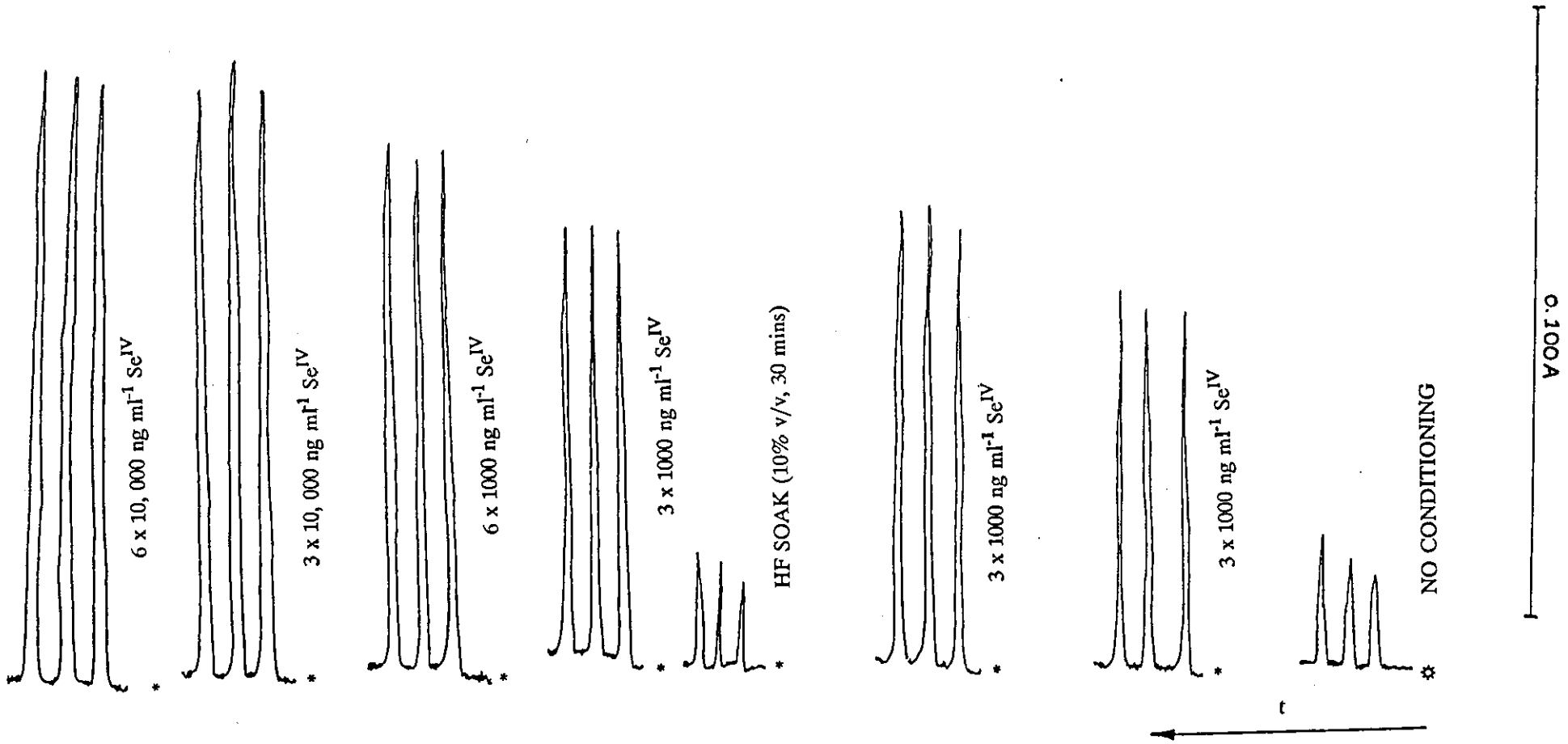

Fig. 7.2. Effect of silica atomization T-cell conditioning procedures on the sensitivty for Se^{IV}. (II), HF soaking; (III), High determinand concentrations: 20 ng ml^{-1} of Se^{IV}, 409 µl. All other variables as in Table 4.5.

7.3.1 Discussion.

Comparing the relative benefits of each of the conditioning procedures for the determination of As^{III} and Se^{IV} was made difficult since the standardisation of each T-cell was difficult, and the condition of each was changeable throughout the study. Therefore, comparison of observations made were more on a qualitative basis, from which the following conclusions were reached.

Conditioning of the T-cell with HF in the determination of As^{III} was observed to be beneficial in agreement with the findings of others [91, 96]. Agterdenbos and Bax [100] proposed that the process removes the active sites on the silica surface which promote the recombination of radicals (e.g., $H + H \rightarrow H_2$ or $H + OH \rightarrow H_2O$) and possibly dimerization reactions such as $2Se \rightarrow Se_2$. In direct contradiction though no obvious benefit was observed in the determination of Se^{IV} and in fact the process was observed to be detrimental to a partly conditioned T-cell. An explanation for this was that the HF has an etching and therefore cleaning action on the silica T-cell surface. Vast improvements in sensitivity would therefore be expected only for badly contaminated [49,91] or new T-cells [91].

In the case of Se^{IV} significant conditioning of the T-cell surface appears to be possible through the processing of high concentrations of hydride alone [49,93,101]. This effect may not though be totally attributed to conditioning of the T-cell since the study was carried out on a recently cleaned down system. In agreement with the findings of Reamer *et al.* [104] it is suggested that processing high concentrations of hydrogen selenide eliminates available adsorption sites on the walls of the gas-liquid separator and transport tubing, therefore, deactivates the surface to further SeH_2 adsorption. Processing high concentrations of arsine produced negligible changes in sensitivity. This was again in agreement with the literature since no direct improvement in As^{III} sensitivity appears to have been obtained through the processing of high concentrations of arsine. Only an improvement in reproducibility was reported [103]. Processing high concentrations of hydride may, as postulated by Evans *et al.* [101], form some form of catalytic film on the T-cell surface which contributes to the atomization mechanism. Removal of this film with HF soaking would therefore account for the deterioration in sensitivity observed in the Se^{IV} study. In agreement with the suggestion of Evans *et al.* [101] it was concluded that a separate pre-conditioned silica T-cell should be kept specifically for each element on the basis of these observations.

The beneficial conditioning effect of heating the T-cell in a fuel-rich air-acetylene flame in the determination of both As^{III} and Se^{IV} could not be conclusively explained. On the basis of the atomization mechanism proposed by Welz and Melcher [91] though the high partial pressure of hydrogen expected in the reducing environment of the fuel-rich flame may play a significant role through increased hydrogen radical formation. Increased radical formation at the T-cell surface would also be expected to increase atomization efficiency according to the mechanism proposed by Bax *et al.* [96] through the catalytic action of such radical species.

7.4 DETERMINATION OF HIGH CONCENTRATIONS OF As^{III} AND Se^{IV}.

The effects of various atomization parameters on the signal responses obtained in the determination of high concentrations of As^{III} and Se^{IV} (100, 1000 and 10,000 ng ml^{-1}) were studied. Such high concentrations had previously been observed to produce rather unusual doublet signal response peak shapes (Section 7.3). The study was undertaken, therefore in an attempt to identify the cause of this effect and, therefore, gain more insight into the processes occurring within the silica atomization T-cell.

The PU9360 in-house FI-HGAAS systems shown in *Figs. 4.2(II) and 5.1*, used for the determination of Se^{IV} and As^{III}, were operated under the conditions shown in Table 4.5 and 5.2(I) respectively. The FIAS-200 system shown in *Fig. 6.1* was operated under the conditions shown in Table 6.2.

(I) Default.

The signal response peak shapes obtained for 1000 and 10,000 ng ml^{-1} of Se^{IV} and As^{III} using the PU9360 system with the manifold variables shown in Table 4.5 and 5.2(I) respectively are shown in *Fig. 7.3.*

(II) Increased sodium tetrahydroborate concentration.

The signal response peak shapes for 1000 and 10,000 ng ml^{-1} of Se^{IV} and As^{III} were measured as in section 7.4(I) for an increased sodium tetrahydroborate reagent

concentration of 5.0% m/v. The reagent concentration was increased in order to increase the quantity of hydrogen produced in the reaction and transported to the atomization T-cell. Results are shown in *Fig. 7.3.*

(III) Fuel-rich air-acetylene flame.

The effect of using a fuel-rich air-acetylene flame (air flow setting 27, acetylene 22) on the signal response peak shapes for 1000 and 10,000 ng ml^{-1} of Se^{IV} and As^{III}, using the PU9360 system, are shown in *Fig. 7.3.*

(IV) Atomization temperature.

The effect of atomization temperature on the signal response peak shapes for 100 and 1000 ng ml^{-1} of As^{V}, using the FIAS-200 system, is shown in Table 7.2 and *Fig. 7.4.*

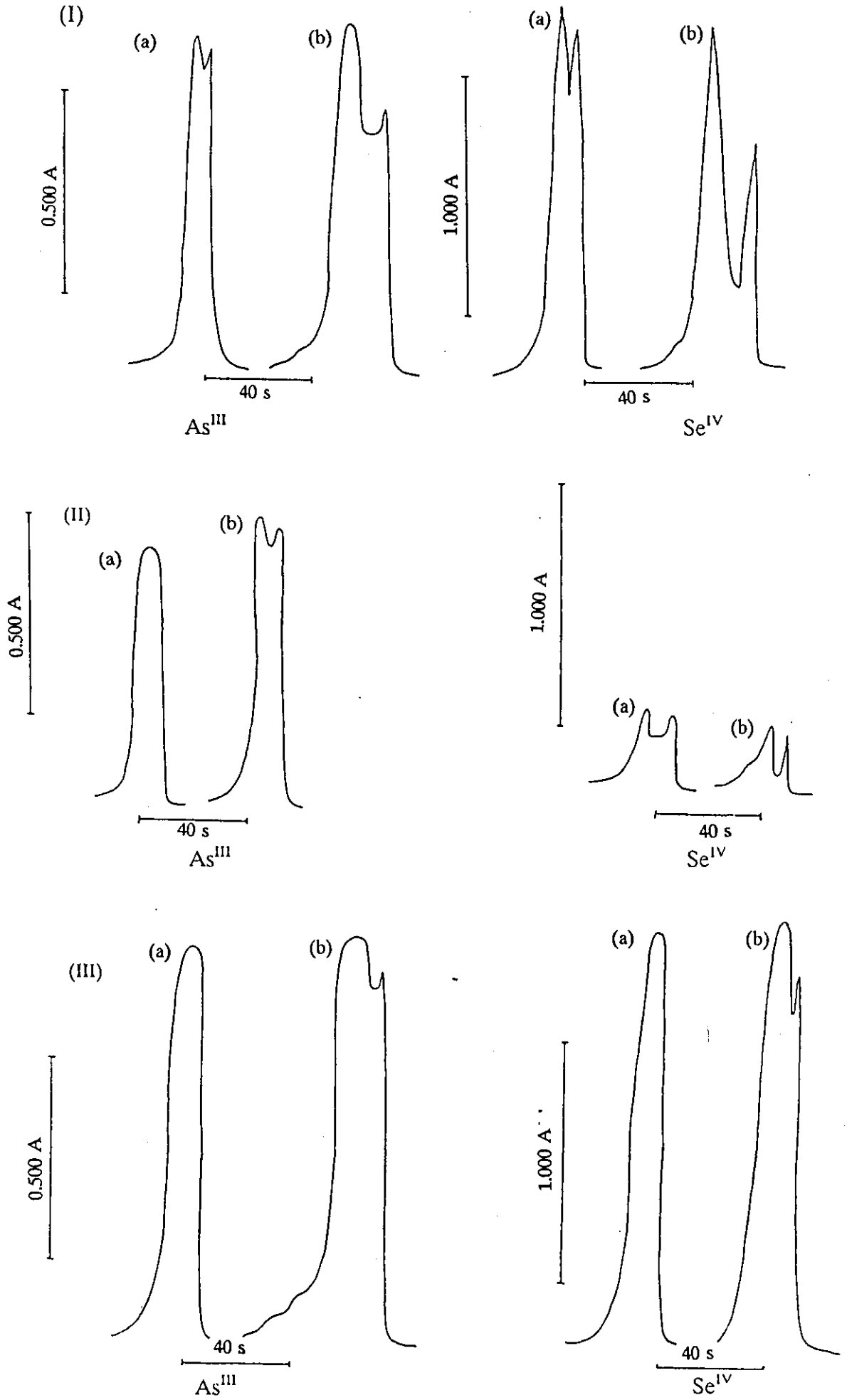

Fig. 7.3. Signal response peak shapes obtained in the determination of high As^{III} and Se^{IV} concentrations. (a),1000 ng ml^{-1};(b),10,000 ng ml^{-1}. (I), Default variables (1% m/v $NaBH_4$); (II), 5.0% m/v $NaBH_4$; (III), Fuel-rich air-acetylene flame. All other variables as in Table 4.5 and 5.2(I).

Table 7.2 Effect of atomization temperature on peak-height absorbance and peak shape in the determination of 100 and 1000 ng ml^{-1} As^{V}, (±95% confidence interval). All other variables as in Table 6.2.

Atomization temperature/ °C	100 ng ml^{-1} As^{V}		1000 ng ml^{-1} As^{V}	
	Absorbance	Peak shape	Absorbance	Peak shape
650	0.026±0.004	-.-	0.027±0.003	-.-
680	0.045±0.008	Doublet	0.028±0.002	-.-
700	0.256±0.022	Doublet	0.189±0.022	Doublet
750	0.577±0.009	Singlet	0.554±0.020	Doublet
800	0.579±0.006	Singlet	0.701±0.016	Doublet
850	0.563±0.010	Singlet	0.725±0.007	Doublet
900	0.540±0.008	Singlet	0.707±0.010	Singlet
950	0.488±0.012	Singlet	0.656±0.010	Singlet
1000	0.432±0.007	Singlet	0.624±0.006	Singlet

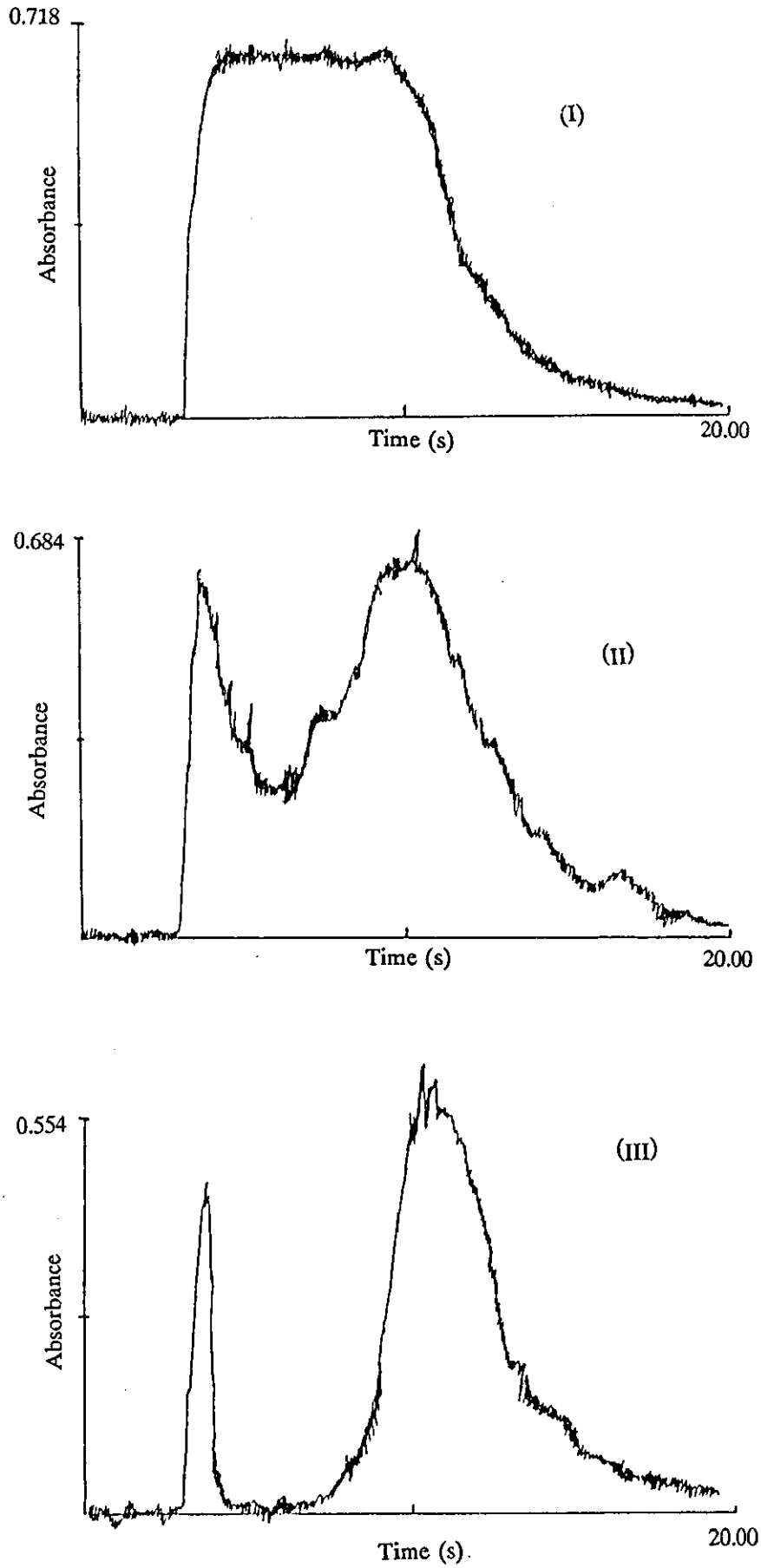

Fig. 7.4. Effect of atomization temperature on the signal response peak shape in the determination of 1000 ng ml^{-1} of As^{V}. (I), 900°C; (II), 800 °C; (III), 750°C. All other variables as in Table 6.2.

7.4.1 Discussion.

The doublet signal response peak profiles observed at elevated concentrations of Se and As were similar to those reported by Agterdenbos *et al.* [93] and Guo *et al.* [243] respectively. Agterdenbos *et al.* [93] showed that at a concentration of 4.75 $\mu g\ ml^{-1}$ of Se^{IV} (T = 800 °C) a doublet shaped absorbance signal was obtained for the steady state generation of the hydride. Zero absorbance at the centre of the signal response was attributed to total dimerization of Se atoms. Absorbance peaks at the start and finish of sample introduction were explained by the lower relative partial pressures of Se atoms in the atomization cell, therefore the occurrence of little or no dimerization.

The negligible effect on doublet peak character with increased $NaBH_4$ concentration in the determination of Se^{IV} and the reduction in overall absorbance was in agreement with the observations of Bax *et al.* [94]. Increased hydrogen concentration within the atomization cell appears to be detrimental to selenium atomization. Decreased doublet peak character, observed in he determination of As^{III} with increased $NaBH_4$ concentration, was attributed to one of two possible effects. Based on the proposal of Bax *et al.* [96] the observations may simply be attributed to a reduction in the partial pressure and residence time of As atoms within the atomization cell, therefore reduced dimerization. On the basis of the atomization mechanism proposed by Welz and Melcher [91] though reduced doublet peak character could be attributed to increased hydrogen partial pressure within the atomization cell, therefore, increased hydrogen radical formation. Reduced overall sensitivity observed in the determination of As^{III} appears to favour the postulation of Bax *et al.* [96].

An interesting but rather contradicting observation was the effect of atomization temperature and flame stoichiometry on the atomization profile. Atomization of high concentrations of As clearly required high atomization temperatures, using the furnace heated T-cell, as reported by Guo *et al.* [243], possibly due to increased hydrogen radical formation [91]. Reduced doublet peak character at the same time was observed using a relatively cool fuel-rich air-acetylene flame. This observation gives possible evidence to there being two different atomization mechanisms for the two T-cell heating methods. It is difficult to be certain of this fact though since the actual atomization temperature within the fuel-rich air-acetylene flame heated silica T-cell could not be determined. In the case of the electrically heated T-cell any active

species must be formed within the T-cell as a result of direct heating. For the flame heated T-cell, active radical species may also be formed (within the flame), which may be capable of passing into the T-cell through its open ends.

7.5 EFFECT OF AIR ADDITION ON THE ATOMIZATION OF ARSENIC.

The FIAS-200 system shown in *Fig. 6.1* (Chapter six) was used throughout and operated, unless otherwise stated, using the operating parameters shown in Table 6.2.

A study was made of the effect of air-addition on system performance in the determination of As^V. Throughout the HGAAS literature numerous contradicting observations have been made as to the benefits and drawbacks of air or oxygen addition [82,88,91,95,96,98,227]. An investigation was made, therefore, to identify whether or not in the case of As^V the addition of air was beneficial to the atomization process.

(I) Air-segmentation of carrier stream.

The FI-HGAAS manifold shown in *Fig. 6.1* was modified to include an extra pump channel and therefore permit air introduction into the HCl carrier stream. Air was pumped directly from the laboratory (10 ml min^{-1}) into the HCl carrier (10 ml min^{-1}) thereby producing an air-segmented carrier stream into which the sample was injected. Modification of the manifold resulted in an improvement in sensitivity of 15% in the determination of 10 ng ml^{-1} of As^V, (Mean peak-height absorbance (n=6) increased from 0.247 to 0.284).

(II) Air addition to Ar carrier stream.

The FIAS-200 system shown in *Fig. 6.1* (RC, 2000 mm; SC, 300 mm (0.8 mm i.d.)) was used with the modification that air was introduced via the Ar carrier delivery unit. A peristaltic pump was used to introduce air (10 ml min^{-1}) directly from the laboratory into the Ar supply (30 ml min^{-1}) prior to entering the FI-HGAAS system.

The effect of air-addition on the signal response of 10 ng ml^{-1} of As^V over the atomization temperature range of 600 to 1000°C is shown in *Fig. 7.5.*

The effect of air-addition on the signal response of 1000 ng ml^{-1} of As^V over the atomization temperature range of 600 to 1000°C is shown in Table 7.3 and *Fig. 7.6.*

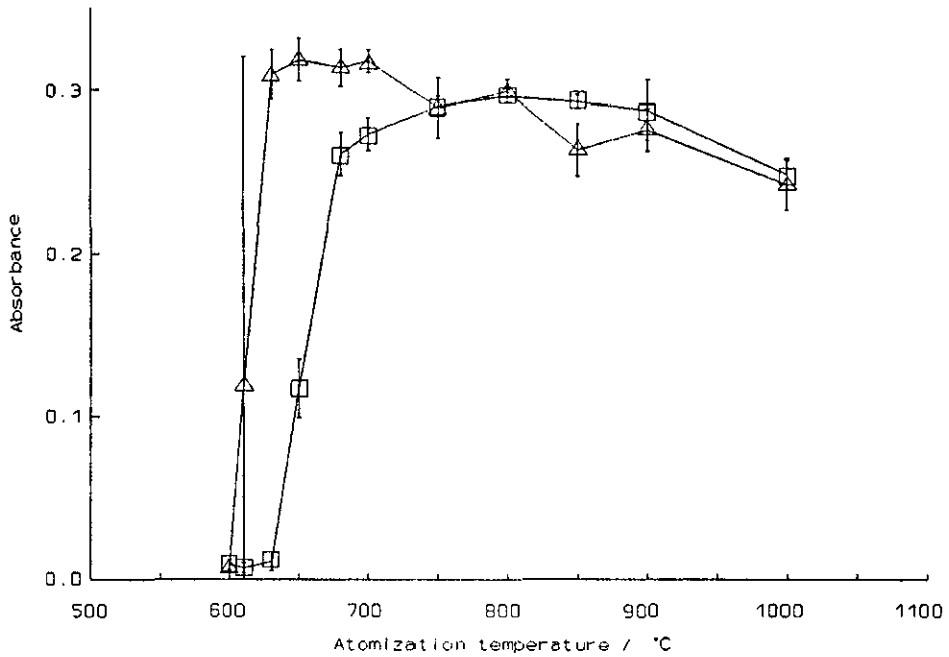

Fig. 7.5. Effect of atomization temperature on the absorbance of 10 ng ml^{-1} of As^{V}. Ar, 30 ml min^{-1}; (▲), 10 ml min^{-1} air; (■), no air. All other variables as in Table 6.2.

Table 7.3 Effect of atomization temperature on the peak-height absorbance and peak shape in the determination of 1000 ng ml^{-1} of As^{V} with air-addition. (±95% confidence interval). Ar, 30 ml min^{-1}; Air 10 ml min^{-1}. All other variables as in Table 6.2.

Atomization temperature/°C	Absorbance	Peak shape
600	0.024±0.003	-.-
650	0.819±0.016	Multiple peaks
700	0.836±0.011	Multiple peaks
750	0.831±0.010	Steady state
800	0.824±0.003	Steady state
900	0.819±0.024	Steady state
1000	0.819±0.019	Steady state

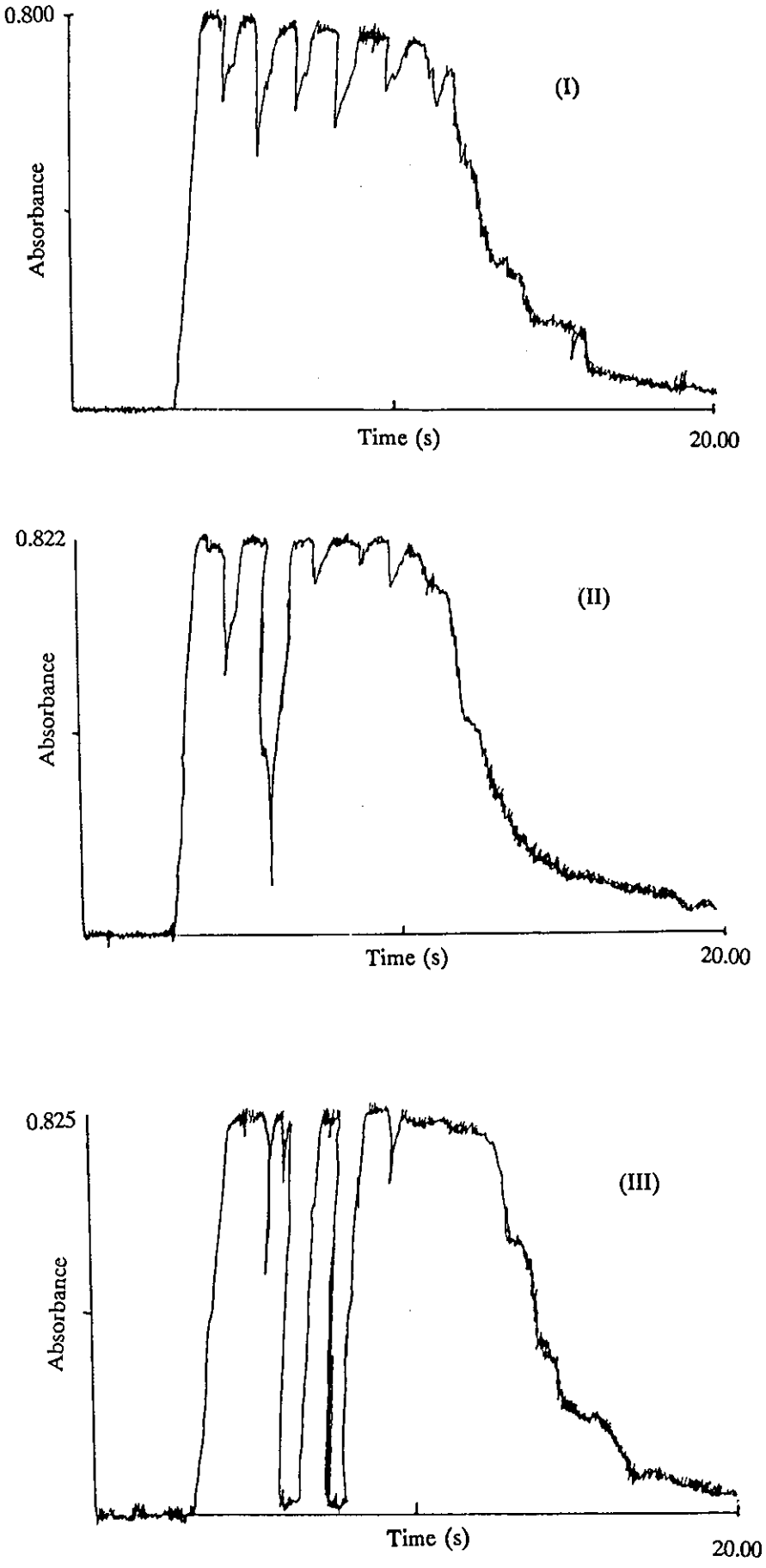

Fig. 7.6. Effect of atomization temperature on the signal response peak shape in the determination of 1000 ng ml^{-1} of As^{V} with air addition. Ar, 30 ml min^{-1}; Air, 10 ml min^{-1}. (I), 900° C; (II), 800 °C; (III), 750° C. All other variables as in Table 6.2.

(III) Pure air carrier stream.

The FIAS-200 system shown in *Fig. 6.1* (RC, 2000 mm; SC, 300 mm (0.8 mm i.d.)) was used but the Ar carrier supply was replaced by an air carrier (30 ml min^{-1}) obtained from a compressed air supply. The signal response of 10 ng ml^{-1} of As^{III} was investigated and compared with that obtained with a pure Ar carrier.

With the use of a pure air carrier stream sensitivity was identical to that for an Ar carrier but rather distorted and spiked response peak shapes were obtained as shown in *Fig. 7.7.* With prolonged use the sensitivity slowly deteriorated. The mean peak-height absorbance (n=6) decreased from 0.315 to 0.241 over a period of about one hour.

7.5.1 Discussion.

Air addition was clearly beneficial in the atomization of As as shown in *Figs. 7.5 and 7.6,* but only at atomization temperatures below ~ 800 °C. These findings were in agreement with those of others in the determination of As[91,96], Se[95] and Sn[227]. At the same time in direct contradiction with the work of Parisis and Heyndrickx [98] who observed a positive effect of oxygen on the atomization of hydride forming elements (As^{III}, Sb^{III}, Se^{IV}, Bi^{III}, Sn^{IV}) at temperatures above 800°C.

On the basis of these findings the increase in sensitivity observed as a results of air-segmenting the HCl carrier stream (Section 7.5(I)) was explained simply by reduced dispersion in the aqueous phase, as reported by Yamamoto *et al.* [88].

The results appear to favour the atomization mechanism proposed by Welz and Melcher [91]. According to this mechanism, at low atomization temperatures (600-800 °C) hydrogen radical formation is expected to be significantly increased by the presence of extra oxygen, but to a lower extent at higher temperatures (≥ 800 °C), where the quartz T-cell is postulated to have a catalytic effect on hydrogen radical formation. The temperature dependency on the beneficial effect of oxygen addition (*Fig. 7.5*) does not appear to be explained by the proposed atomization mechanism of Bax *et al.* [96], according to equation 1.4.9 (Chapter one), unless by the increased formation of OH to H radicals which it was suggested catalysed the reaction [96].

In the use of a pure air carrier stream the rather distorted atomization profiles could not be conclusively explained. The reduction in sensitivity with time though was attributed to the slow poisoning of the silica T-cell surface by trace impurities within the unpolished air supply.

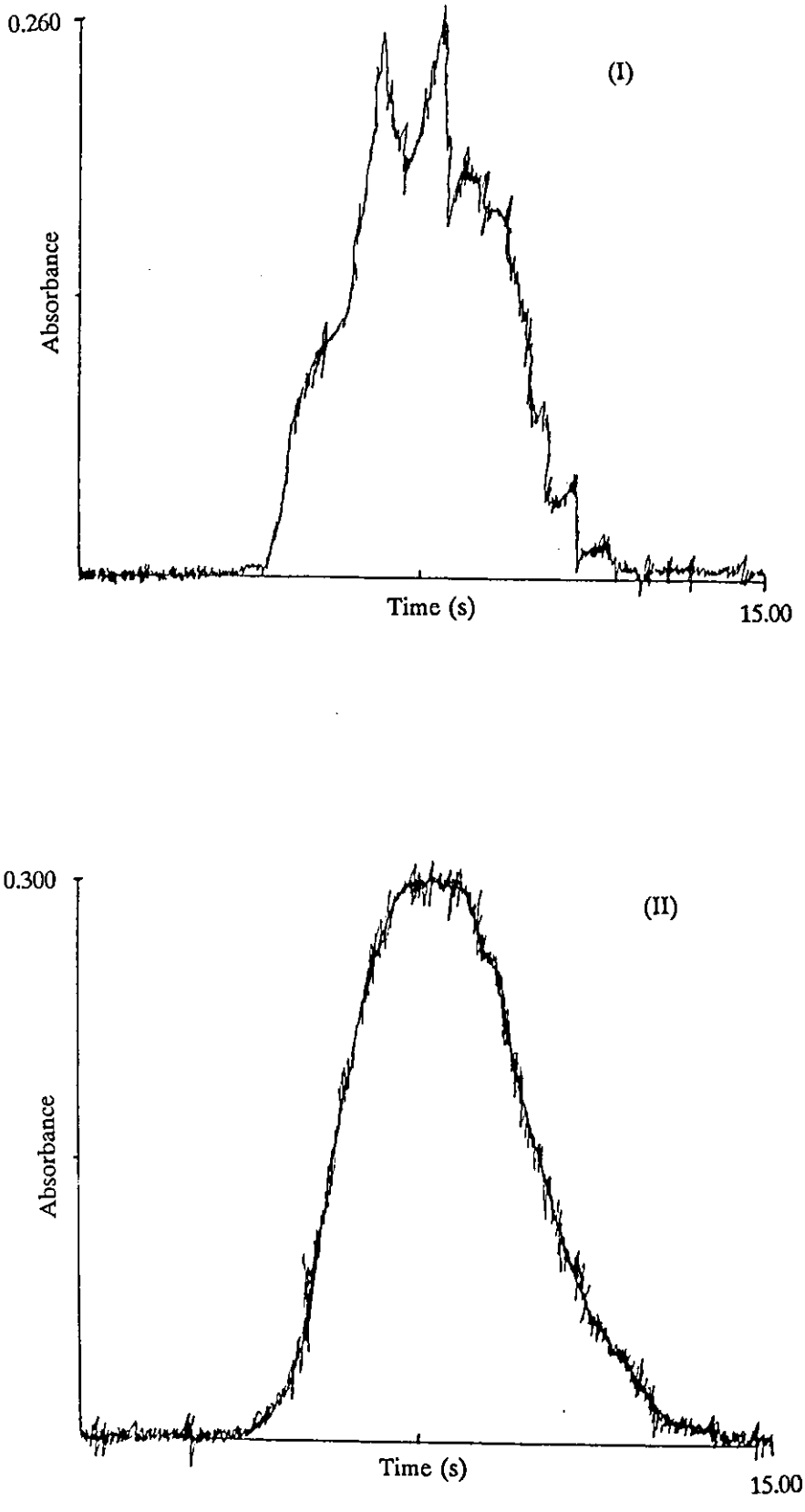

Fig. 7.7. Effect of carrier on the signal response peak shape in the determination of 10 ng ml^{-1} of As^{V}. Atomization temperature 800 °C. (I), Air, 30 ml min^{-1}; (II), Ar, 30 ml min^{-1}. All other variables as in Table 6.2.

7.6 DISCUSSION.

On the basis of the observations made no clear atomization mechanism could be proposed. Further work is therefore clearly needed (Chapter eight). Explanation for the observations made was particularly hampered by what appears to be so much contradicting data in previously reported work. This is most likely due to the significant variations in system design, atomization procedure, operational variables, determinand and reagent concentrations etc., employed in these previous studies. Direct comparison of the performance data of one study with that of another is difficult because there appears to be little standardisation of operational variables.

Although no conclusive evidence for a particular atomization mechanism was obtained, the critical involvement of the silica T-cell in the atomization process and its rather delicate nature was clearly evident. Optimum performance of the silica cell is dependent on numerous variables such as surface condition, temperature, hydride and gaseous reaction species. As discussed earlier (Section 7.1) for these reasons it is considered that a new method of atomization is required (such as electrothermal) to allow the technique of HGAAS to achieve its full potential, particulary in interference free routine analysis.

CHAPTER EIGHT
CONCLUSIONS AND SUGGESTIONS FOR FURTHER WORK

8.1 CONCLUSIONS.

In Chapter one, the development and application of hydride generation in AAS was reviewed. Particular attention was paid to the various interference effects associated with the technique including both the mechanisms of interference and methods of overcoming them. The literature shows that there is a significant interest in the study of interference effects, but as is evident from the review, the experimental evidence has not yet resulted in unambiguous explanations for both the aqueous and gas phase interferences studied. This can be attributed to the variety of systems and operating parameters used in the various studies. The interference tolerance of the technique has been shown to be critically dependent on both the nature of the apparatus and reagent concentrations used. The review reveals that, in some cases, the mechanism involved is both analyte and interferent specific which may also account for the numerous apparently contradicting observations made and conclusions drawn.

Many attempts have been made to overcome the interference effects in HGAAS but procedures proposed can be tedious. In many cases the procedures are manual, analyte and interferent specific and are only successful to a limited degree.

One of the most significant advances made in HGAAS in terms of reducing the extent of interferences has been the successful implementation of flow injection (FI) procedures (Reviewed in Chapter two). Optimization and control of the hydride generation process through the use of FI has been shown by several research groups to reduce the magnitude of interferences observed. The added advantages of reduced sample requirement, reduced reagent consumption, enclosed system design and the potential for full automated operation makes the coupling of FI with HGAAS all the more appealing.

The successful application of FI to the wider subject area of atomic absorption spectrometry (AAS) was evident in the review of the subject made in Chapter two. The more recent work indicates that the technique of FI is no longer looked on as being simply a method of achieving fast sample presentation to the spectrometer but is emerging as a versatile method for on-line sample pretreatment.

It is clear that a present trend in the nature of commercial chemical instrumentation is for the use of computers for the control of system components and for data handling. This though is increasing the cost and complexity of the procedures undertaken, particulary in the area of

on-line dilution and calibration. As an alternative approach, a simple cheap procedure for achieving variable on-line dilution using wide bore manifold tubing was investigated as documented in Chapter three.

Although it might be argued that major breakthroughs have been achieved in both FAAS and ETAAS through the use of on-line sample matrix isolation procedures for both preconcentration and interference removal, little attempt has been made to adapt similar procedures to HGAAS. Considering the interference limitations of HGAAS the further investigation of FI-HGAAS and, more importantly, of matrix isolation procedures was deemed to be of significant interest and benefit. Developments in this area are described in Chapters four and five.

The use of wide bore manifold tubing (up to 5.0 mm i.d.) to achieve controlled on-line dilution for FAAS was unsuccessful. Dispersion coefficient values up to and in excess of 100 were obtained, through the optimization of manifold dimensions, but the procedure was limited by variations in dispersion coefficients arising from differences in specific gravities between the sample and carrier fluids. Visual investigation of the mixing characteristics of the system showed that the effect of specific gravity on the dispersion characteristics was caused at least in part by the low linear velocity of the carrier solution in the wide bore manifold tubing. The step change in carrier velocity which was evident at the junction between the narrow bore connecting tubing and the wide bore tubing was shown to create complicated mixing characteristics which varied over the length of the manifold tube. The specific gravity effect could be partially eliminated by the use of an elevated carrier flow rate. However, the precision of the system was shown to be poor (RSD, 3-5%). Retention and nucleation of air bubbles remained a problem and increased back pressure became of concern.

The use of a continuous flow matrix isolation procedure coupled with flow injection hydride generation atomic absorption spectrometry permitted the successful determination of Se in copper metal. In the system, a micro-column manifold (for the selective retention of the copper interferent) was interfaced with the hydride generation manifold through a sample injection valve. The two manifolds, being independent of each other, could each be fully optimized. In previous designs of in-line matrix isolation systems this had not been possible. This design also permitted the inclusion of a rapid column regeneration step which made full automation of the system feasible.

Optimization of the FI-HGAAS manifold achieved a sensitivity comparable with that of continuous flow hydride generation atomic absorption spectrometry but with the added

advantages of reduced sample requirement, superior throughput and vastly improved interference tolerance. The high interference tolerance of the FI-HGAAS system to such species as cobalt, copper, iron and nickel was shown to be due to a combination of the low sample volume used and the rapid transport and release of the hydride from the aqueous phase. The interference tolerance of the FI-HGAAS system itself was shown to be critically dependent on the sample injection volume and the total transport rate of the carrier and reagent streams.

In the analysis of the two copper metal standard reference materials NIST 454 and BAM 361 the system was shown to have a characteristic concentration of 1.0 ng ml^{-1} of Se^{IV}, limit of detection of 2.1 ng ml^{-1}, relative standard deviation of 1.5% (10 ng ml^{-1} Se^{IV}, n = 12) and sample throughput of 51 h^{-1}.

The system was subsequently applied to the determination of As in nickel alloy. Contrary to earlier reports, the microwave digestion procedure did not retain the As in the digested matrix in the +3 oxidation state. As the sensitivity for As^{V} was, too low, modification of the system was necessary to permit the on-line pre-reduction of As^{V} to As^{III}. A stopped-flow pre-reduction procedure was implemented after the matrix isolation step. The sample and reducing agent were retained in the sample loop of the injection valve for a predetermined time interval prior to introduction into the hydride generation manifold. Again being independent of the hydride generation process, the procedure could be optimized fully without any compromise of the FI-HGAAS performance characteristics. Direct comparison with previous in-line pre-reduction procedures showed that the system had the added advantages of considerably reduced reagent consumption, superior control of the reaction time and the removal of any need for long rector coils and the problems of back pressure they produce.

Further evidence for the high interference tolerance of FI-HGAAS was obtained from a study of the interferences of cobalt, copper and nickel in the determination of As. Incorporation of a PTFE membrane filter in the hydride transport line was found to be beneficial in eliminating interference memory effects and their deterioration of sensitivity. The interference tolerance of the system to other hydride forming elements was shown to be far less impressive. This was considered to be due to the limitations of the externally heated silica T-cell atomizer.

A characteristic concentration of 2.0 ng ml^{-1} of As and limit of detection of 3.9 ng ml^{-1} of As were obtained with the pre-reduction procedure for a set of operating parameters optimized with respect to interference tolerance, throughput and sensitivity. Results were presented for the analysis of a nickel standard reference material, BCS 346.

The performance characteristics of the commercial FIAS-200 FI-HGAAS system were investigated for the determination of As. The sensitivity achieved with the system (0.08 ng ml^{-1} As^{III}) was found to be an order of magnitude better than that observed with the system based on the PU9360 unit. The increased sensitivity was attributed to the reduced volumes of the gas-liquid separator and hydride transport tubing, the reduced argon carrier flow and the atomization cell design of the FIAS-200 system.

Some interesting observations were made regarding the order of reagent addition. No improvement in sensitivity was found in the determination of As^{V} when adding the sodium tetrahydroborate prior to hydrochloric acid. For the same determination, increasing the reactor coil length increased the sensitivity (this was not the case in the determination of As^{III}). Although the difference in relative sensitivity of As^{III} and As^{V} was shown to be minimised through the control of reactor coil length, it could not be eliminated through the optimization of manifold parameters alone.

On the basis of the high sensitivity achieved using the FIAS-200 system for the determination of As^{V} (characteristic concentration 0.44 ng ml^{-1}) and its observed high interference tolerance to nickel, results obtained indicated that the system would permit the direct analysis of the nickel based alloy BCS 346 (50 $\mu g\ g^{-1}$ As). Following the optimization of both the reactor coil length and hydrochloric acid reagent concentration, the interference free determination of 20 ng ml^{-1} of As^{V} in the presence of upto 200 $\mu g\ ml^{-1}$ Ni was shown to be possible. It is suggested though that the incorporation of the continuous-flow matrix isolation unit, documented in Chapter five, would further extend the performance of the system and therefore permit the determination of even lower concentrations of As in similar nickel matrices.

From the investigation of the hydride atomization process no clear cut conclusions could be reached regarding the mechanism of the atomization process. However, some interesting observations were made, particulary of the critical involvement of the silica atomization T-cell in the process in question. The performances of both flame and furnace heated silica atomization cells were observed to be dependent on a number of parameters. The age and quality of the silica surface was shown to be critical. The addition of air to the atomization cell proved beneficial but only at low temperatures (<800°C). At the optimum atomization temperature (≥800°C) the addition of air produced no improvement in sensitivity. A number of conditioning procedures were shown to be beneficial including HF soaking, processing high determinand concentrations and flame treatment. The rather delicate nature of the atomization cell though clearly was shown to be a limiting factor regarding the range of analyses that could be undertaken with the system. The investigation of alternative atomization methods is suggested to be of considerable importance.

8.2 SUGGESTIONS FOR FURTHER WORK

8.2.1 Further investigation into on-line dilution in FAAS through the application of FI and wide bore manifold tubing.

Despite of the specific gravity limitations encountered with the use of wide bore tubing it is considered that the procedure still has potential. With a number of minor modifications, and further investigation it is predicted that the system could meet the initial performance specifications namely to achieve dilution factors up to 100 with a precision of 1% relative standard deviation or better. Optimization of the wide bore manifold tubing geometry should overcome the major practical problem of air retention and nucleation. The exit port of the wide bore tubing could be made conical in shape, as shown in *Fig. 8.1*, which would remove the dead volumes and subsequent retention of air bubbles experienced with the earlier design (*Fig. 3.2*).

Fig. 8.1. Schematic diagram of modified wide bore manifold tube shape.

The inlet to the wide bore tube should though be kept as used in earlier work to retain the "turbulent jet" mixing characteristics, caused by the abrupt step change in carrier velocity and resulting high sample dispersion. To aid the washout of air bubbles further the carrier flow rate should be kept at the high value of ~20 ml min^{-1}. Keeping the carrier flow rate high would further benefit throughput and the elimination of the specific gravity effects. To minimise these latter effects, it is suggested that the manifold tube length be restricted to less than 200 mm. The loss of dispersion expected with this limitation could be counteracted by the use of a smaller sample injection volume. Although difficult to construct from narrow bore manifold tubing, injection loop volumes of the order of 10 µl are possible. Use of either a pneumatically or electrically activated injection valve would improve reproducibility in sample introduction particulary when employing such a high carrier flow rate. The poor precision expected at the high carrier velocity used could be overcome by directing a portion of carrier to waste prior to the nebulizer when operated normally [132]. Peak area quantification would also improve the

method due to its less critical dependence on mixing efficiency [167], therefore, higher tolerance to specific gravity effects.

In addition to these discussed modifications a network manifold [159] of a design similar to that shown in *Fig. 8.2* would be constricted and evaluated. This design would be simple, cheap and robust using few component parts. The system could be used with a single manifold tube therefore a fixed dispersion coefficient which is possible if the analyst is dealing with a high number of similar samples. Alternatively the system could be used with a variety of manifold tube dimensions selecting appropriate wide bore tubing with either manually or automatically operated switching valves. Each channel would be calibrated independently.

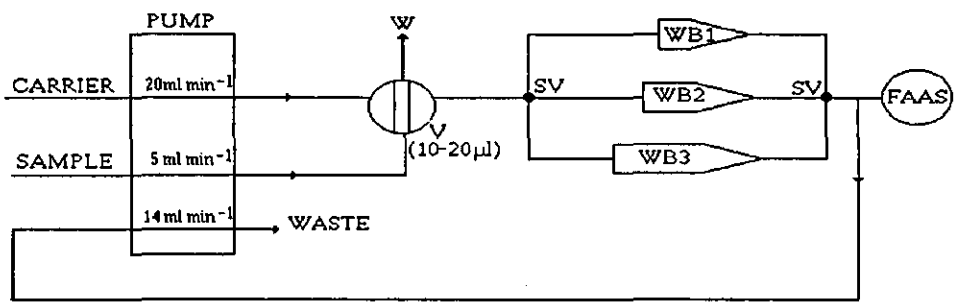

Fig. 8.2. Schematic diagram of a network variable dispersion manifold system using wide bore manifold tubing. SV, switching valves; V, electrically or pneumatically activated injection valve; WB, wide bore tubing; W, waste.

8.2.2 Extension of on-line matrix isolation procedures in HGAAS.

Following the success of the developed continuous flow matrix isolation system for the removal of copper interference in the determination of Se^{IV} by HGAAS, it is suggested that the some system could be applied to the analysis of a variety of other copper matrices. Based on the findings of Hershey and Keliher [80], regarding the use of Dowex 50W cation exchange resin for interference reduction in HGAAS, it is possible that the system could also be used for the determination of a variety of other analytes in similar sample matrices. Results obtained in the investigation [80] suggest that there is scope for

the analysis of high interference matrices such as cobalt, copper, lead, nickel and silver for such determinands as As, Bi, Sb and Se. Considering the use of other ion exchange resins, of which there are numerous, each with its own specific working characteristics, the system could in theory be tailored to each analytical problem faced.

Of possibly even greater interest and benefit, through the careful choice of ion exchange resin and control of the ion exchange chemistry the same methodology could be applied to the matrix isolation of mutual hydride forming elements. Results presented in Chapter five demonstrated the poor interference tolerance of hydride forming elements to each other in the determination of As and the critical interferences observed in the presence of Sb, Se and Sn at ng ml^{-1} concentrations.

Hershey and Keliher [80] documented that Chelex 100 resin had a high affinity for Bi, Te and, to a lesser extent, Sb (pH 2.00). The AG50WX16 resin (purified Dowex 50WX16 resin) was shown to have an affinity for Te. Use of these resins and others in the developed system should, therefore, permit the rapid matrix isolation and subsequent interference free determination of selective hydride forming elements in mixed matrices. Using combinations of such resins may also permit multielement determinations presently unachievable using HGAAS.

To date on-line matrix isolation in HGAAS has been restricted to the use of solid phase extraction [71, 82, 83]. Despite the fact that over the years a number of manual precipitation procedures have been used for matrix isolation in HGAAS [72-75], it appears that no attempt has been made to implement them in either continuous flow or FI systems. The review presented in Chapter two clearly showed that interest in on-line precipitation procedures in FAAS has grown significantly recently due its capability to perform both preconcentration and interference removal [150, 220-224].

There would be no reason in principle why similar systems could not be developed for use in HGAAS. Debrah *et al.* [220] recently described a system for the precipitation and subsequent preconcentration of copper hydroxide on a nylon filter. It is suggested that this system could be used to remove copper interference in the determination of Se^{IV} and other hydride forming elements. Using the same principle the matrix isolation of nickel would also be possible as demonstrated manually by Welz and Melcher [74] and Wickstrom *et al.* [75]. One possible problem with such a system would be the capacity of the procedure. In previous preconcentration work, the masses of retained metals were in the low µg range whereas for use in the proposed system the filter device would have

to cope with possible mg quantities. Precipitation and retention on a filter of such concentrations may subsequently introduce flow and back pressure restrictions. For this reason an investigation of a variety of filter media may well be required. To limit the effect of such restrictions the precipitation manifold could be interfaced with a FI-HGAAS system through the sample injection valve as demonstrated in Chapters four and five respectively. The ion exchange column fitted in the sample loop of the second injection valve would be replaced directly by a filter device (possibly a membrane filter). A schematic diagram of the proposed system in shown in *Fig. 8.3.*

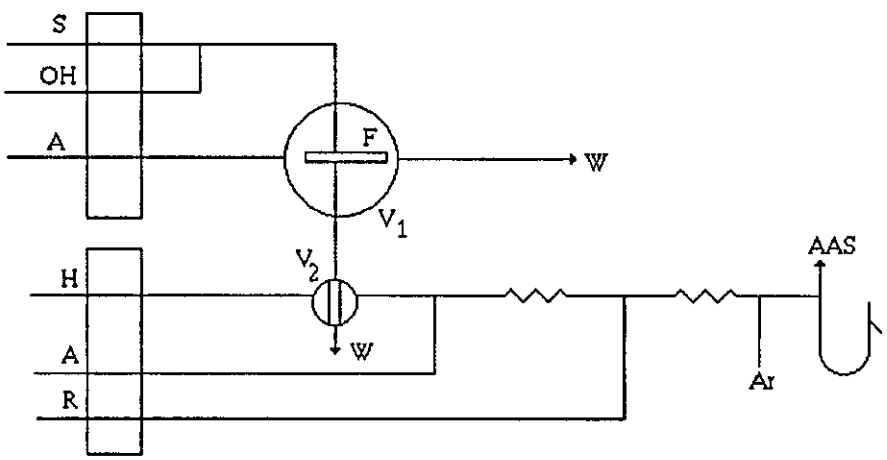

Fig. 8.3. Schematic diagram of a FI-HGAAS manifold incorporating continuous flow matrix isolation using precipitation. P, peristaltic pump; S, sample; H, water; A, HCl; R, $NaBH_4$; OH, Sodium hydroxide; V_1, switching valve; V_2, sample injection valve; F, nylon filter; G, gas-liquid separator; W, waste.

Further modification of the proposed system may also permit the use of analyte co-precipitation procedures for matrix isolation [72,73]. This strategy would clearly be more complicated since following the precipitation and retention of the analyte species on the filter an elution step would be needed to introduce the sample into the HGAAS system. Such a procedure though would permit preconcentration of the sample. The use of on-line precipitation in HGAAS on first inspection appears promising but in depth investigation is clearly required particulary into the kinetics of the precipitation reactions to permit their successful implementation in a flowing system. Use of stopped-flow methodology, as demonstrated in Chapter five, may be required to overcome possible kinetic restrictions.

8.2.3 Sensitivity enhancement studies.

From the findings described in Chapter six it was evident that the maximum sensitivity obtained with the FI-HGAAS system, developed in-house, was limited by the gas-liquid separator design. Comparison studies made with the purpose built FIAS-200 FI-HGAAS system indicated the benefits of miniaturisation of the gas-liquid separator. Investigation into improvements in gas-liquid separator design possibly through miniaturisation [67,70,234] or use of membrane separators [58,89,239] would prove invaluable, particulary for the in-house system, extending the range of analyses to which it could be applied with increased sensitivity. With improved sensitivty it is suggested that the analysis of samples such as blood, urine, fish and other biological tissues would be feasible.

The matrix isolation interface used for interference removal purposes, could with modification be equally as successfully be used for preconcentration. Using such ion exchange resins as D-201 (strongly basic microporous anion exchanger, Shenyang Organic Chemicals) and CPG-8-hydroxyquinoline (chelating ion exchanger, Pierce Chemical Co., USA) the preconcentration of both Se and Bi should be possible [180,203] and the use of other resins could extend the preconcentration capability further. The preconcentration unit shown in *Fig. 8.4* would be interfaced to the FI-HGAAS system through the sample injection valve permitting independent optimization of the two units.

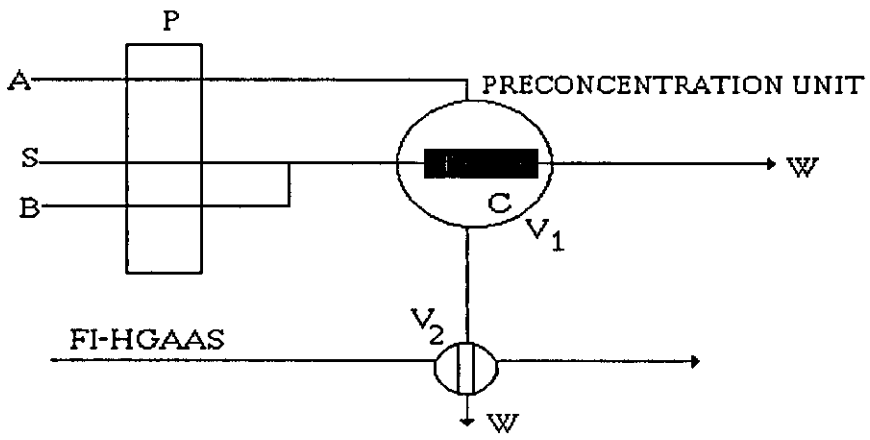

Fig. 8.4. Schematic diagram of proposed preconcentration unit interface with the FI-HGASS system. P, peristaltic pump; S, sample; A, HCl; B, Buffer solution; V_1 switching valve; V_2 sample injection valve; C, column; W, waste.

In the proposed system sample plus buffer would be pumped at a low flow rate through the column to maximise retention efficiency. After the specified preconcentration interval the column would be activated into the elution position. In the elution cycle the preconcentrated analyte would be stripped from the column by a continuously flowing stream of acid (possibly HCl) and transported to the sample loop of the injection valve. With controlled timing and the use of a low eluent flow rate it would be possible to trap a high percentage of the eluted sample plug, if not all, within the sample loop prior to introduction into the HGAAS system. Such a procedure has been achieved in recent FI-ETAAS methods [213,215]. If the acid eluent concentration was sufficiently high the need for further on-line acidification of the sample plug would be removed. It is suggested that the use of such a procedure would prove useful for the analysis of simple matrices such as tap and mineral waters. At present such analyses are impossible by conventional HGAAS procedures due to insufficient detection limits.

8.2.4 Further investigation and evaluation of the stopped-flow As^V pre-reduction unit.

The stopped-flow As^V pre-reduction unit described in Chapter five showed significant promise in preliminary results. Further optimization of the unit including the use of heating is suggested to improve its performance. Based on the success of the system in the case of As, it can be assumed that it could equally as successfully be applied to the on-line pre-reduction of Sb^V to Sb^{III} using the same chemistry [16].

Results obtained for the determination of As in an nickel based alloy (Chapter five) were to an extent inconclusive and in contradiction with the findings of Riby *et al.* [83]. As discussed in Chapter five these findings tend to indicate that in the system of Riby *et al.* [83] arsenic present as As^V after digestion was infact pre-reduced quantitatively to As^{III} on-line. If this is the case the authors of the work have developed a very rapid and effective method for the conversion of As^V to its more sensitive As^{III} oxidation state. Explanation for the observations made remains to be reached, therefore, further investigation would be of significant interest and value. A number of factors need close inspection including the properties of the SCX column particulary in the presence of nickel ions. It is very possible that the presence of nickel under certain conditions could in fact catalyse the pre-reduction mechanism in some way. The addition of sodium tetrahydroborate prior to hydrochloric acid in the FI-HGAAS system may also play some role in the pre-reduction chemistry.

8.2.5 Atomization Studies.

Further investigation into the atomization mechanism of the externally heated silica atomization cell is required following the rather inconclusive findings described in Chapter six.

To restrict observations made to the atomization process alone and eliminate contributions made by the hydride generation reaction it is proposed that arsine and hydrogen selenide should be supplied from commercially available gas-cylinders (Messer-Griesheim), as used by Welz and Melcher [91] in their early work. Using such a procedure various trends could be identified along with the active participitation of such species as hydrogen and oxygen. This approach would still though only permit calculated estimates of the atomization mechanism, as has been the case for nearly all published work to date. To conclusively identify the mechanism investigation on the molecular level and the identification of active reaction species and products would be needed. Clearly, to achieve this techniques such as mass spectrometry would be necessary, as used by Welz *et al.* [99] in recent work.

The use of graphite furnace atomizers [40, 41], would appear from early reports to be the way forward for HGAAS. Using furnace temperatures of the order of 2000-3000° C atomization is achieved solely by thermal dissociation. The need for careful control of reaction and interferent species entering the atomization cell and the condition of the atomization cell, required with the externally heated silica cell, is therefore removed. Employing a graphite furnace atomizer previously unachievable multielement determinations using HGAAS should be possible. The performance of the system would, therefore, compare favourably with that reported for the coupling of hydride generation to inductively coupled plasma atomic emission spectrometry ICP-AES [285]. Investigation into the use of a graphite furnace atomizer in a FI-HGAAS system it is suggested would produce a robust high performance HGAAS system. High interference tolerance in the aqueous phase would be achieved by using FI and through the use of a graphite furnace improved gas-phase interference tolerance would. Present drawbacks evident with the use of graphite furnaces of increased background absorption, limited graphite cuvette life times, complicated timing sequences and reduced throughput capability would all need to be investigated. A further benefit of the system would be the capability to carry out in-situ preconcentration in the graphite furnace itself [30,31]. Replicate injections of sample in the FI system would permit preconcentration without any deterioration of interference tolerance, expected in the aqueous phase with continuous sample introduction.

REFERENCES

1. Walsh, A., *Spectrochim. Acta*, 1955, **7**, 108.
2. Ebdon, L., *"Introduction to Atomic Absorption Spectroscopy,"* Heyden, London, 1982.
3. Cantle, J. E., *"Atomic Absorption Spectrometry,"* Elsevier, Amsterdam, 1982.
4. L'vov, B. V., and Slavin, W., *J. Anal. At. Spectrom.*, 1991, **6**, 191.
5. Holcombe, J. A., and Hassel, D. C., *Anal. Chem.*, 1990, **62**, 169R.
6. Hill, S. J., Dawson, J. B., Price, W. J., Shuttler, I. L., and Tyson, J. F., *J. Anal. At. Spectrom.*, 1991, **6**, 187R.
7. L'vov, B., *Spectrochim. Acta.*, 1961, **17**, 761.
8. Kahn, H. L., and Schallis, J. E., *At. Absorpt. Newsl.*, 1968, **7**, 5.
9. Bailar, J. C., Emeleus, H. J., Nyholm, Sir R., and Trotman-Dickenson, A. F., *"Comprehensive Inorganic Chemistry,"* **Vol. 2**, Pergaman, London, 1973.
10. Holak, W., *Anal. Chem.*, 1969, **41**, 1712.
11. Thompson, K. C., and Thomerson, D. R., *Analyst*, 1974, **99**, 595.
12. Vijan, P. N., and Wood, G. R., *At. Absorpt. Newsl.*, 1974, **13**, 33.
13. Astrom, O., *Anal. Chem.*, 1982, **54**, 190.
14. Smith, A. E., *Analyst*, 1975, **100**, 300.
15. Dedina, J., *Anal. Chem.*, 1982, **54**, 2097.
16. Sinemus, H. W., Melcher, M., and Welz, B., *At. Spectrosc.*, 1981, **2**, 81.
17. Sneddon, J., ed., *"Sample Introduction in Atomic Spectroscopy,"* Elsevier, Amsterdam, 1990.
18. Hershey, J. W., and Keliher, P. N., *Appl. Spectrosc. Rev.*, 1989-90, **25**, 213.
19. Godden, R. G., and Thomerson, D. R., *Analyst*, 1980, 105, 1137.
20. Brooks, R. R., Ryan, D. E., and Zhang, H., *Anal. Chim. Acta*, 1981, **131**, 1.
21. Nakahara, T., *Prog. Anal. At. Spectrosc.*, 1983, **6**, 163.
22. Dedina, J., *Prog. Anal. At. Spectrosc.*, 1988, **11**, 251.
23. Goulden, P. D., and Brooksbank, P., *Anal. Chem.*, 1974, **46**, 1431.
24. Pollock, E. N., and West, S. J., *At. Absorpt. Newsl.*, 1972, **11**, 104.
25. Dedina, J., *Fresenius Z. Anal. Chem.*, 1986, **323**, 771.
26. Agterdenbos, J., and Bax, D., *Anal. Chim. Acta*, 1986, **188**, 127.

27. Narsito, Agterdenbos, J., and Santosa, S. J., *Anal. Chim. Acta*, 1990, **237**, 189.

28. Yamamoto, M., Yamamoto, Y. and Yamashige, T., *Analyst*, 1984, **109**, 1461.

29. Apte, S. C., and Howard, A. G., *J. Anal. At. Spectrom.*, 1986, **1**, 379.

30. Sturgeon, R. E., Willie, S. N., Sproule, G. I., and Berman, S. S., *J. Anal. At. Spectrom.*, 1987, **2**, 719.

31. Doidge, P. S., Sturman, B. T., and Rettberg, T. M., *J. Anal. At. Spectrom.*, 1989, **4**, 251.

32. Griffin, H. R., Hocking, M. B., and Lowery, D. G., *Anal. Chem.*, 1975, **47**, 229.

33. Dalton, E. F., and Malanoski, A. J., *At. Absorpt. Newsl.*, 1971, **10**, 92.

34. Lansford, M., McPherson, E. M., and Fishman, M. J., *At. Absorpt. Newsl.*, 1974, **13**, 103.

35. Siemer, D. D., and Hagemann, L., *Anal. Lett.*, 1975, **8**, 323.

36. Dedina, J., and Rubeska, I., *Spectrochim. Acta,* 1980, **35B**, 119.

37. Andreae, M. O., *Anal. Chem.*, 1977, **49**, 820.

38. Schmidt, F. J., and Royer, J. L., *Anal. Lett.*, 1973, **6**, 17.

39. Chu, R. C., Barron, G. P., and Baumgarner, P. A. W., *Anal. Chem.*, 1972, **44**, 1476.

40. Dittrich, K., Mandry, R., Udelnow, C., and Udelnow, A., *Fresenius Z. Anal. Chem.*, 1986, **323**, 793.

41. Krivan, V., and Petrick, K., *Fresenius Z. Anal. Chem.*, 1990, **336**, 480.

42. Pierce, F. D., and Brown, H. R., *Anal. Chem.*, 1976, **48**, 693.

43. Kirkbright, G. F., and Taddia, M., *Anal. Chim. Acta*, 1978, **100**, 145.

44. Meyer, A., Hofer, Ch., Tölg, G., Raptis, S., and Knapp, G., *Fresenius Z. Anal. Chem.*, 1979, **296**, 337.

45. Welz, B., and Melcher, M., *Analyst*, 1984, **109**, 569.

46. Welz, B., and Schubert-Jacobs, M., *J. Anal. At. Spectrom.*, 1986, **1**,23.

47. Bye, R., *Talanta*, 1986, **33**, 705.

48. Wade, R. C., Holah, D. G., Hughes, A. N., and Hui, B. C., *Catal. Rev. Sci. Eng.*, 1976, **14**, 211.

49. Bax, D., Agterdenbos, J., Worrell, E., and Kolmer, J. B., *Spectrochim. Acta*, 1988, **43B**, 1349.

50. Aggett, J., and Boyes, G., *Analyst*, 1989, **114**, 1159.

51. Narsito, Agterdenbos, J., and Bax, D., *Anal. Chim. Acta*, 1991, **244**, 129.

52. Aggett, J., and Hayashi, Y., *Analyst*, 1987, **112**, 277.

53. Welz, B., and Melcher, M., *Analyst*, 1984, **109**, 573.

54. Castillo, J. R., Martinez, M. C., and Mir, J. M., *At. Spectrosc.*, 1988, **9**, 179.

55. Belcher, R., Bogdanski, S. L., Henden, E., and Townshend, A., *Analyst*, 1975, **100**, 522.

56. Peacock, C. J., and Singh, S. C., *Analyst*, 1981, **106**, 931.

57. Bye, R., Engvik, L., and Lund, W., *Analyst*, 1983, **55**, 2457.

58. Pacey, G. E., Straka, M. R. and Gord, J. R., *Anal. Chem.*, 1986, **58**, 504.

59. Yamamoto, M., Shohji, T., Kumamaru, T., and Yamamoto, Y., *Fresenius Z. Anal. Chem.*, 1981, **305**, 11.

60. Lajunen, L. H., Merkkiniemi, T. and Häyrynen, H., *Talanta*, 1984, **31**, 709.

61. Chan, C. C. Y., *Anal. Chem.*, 1985, **57**, 1482.

62. De Doncker, K., Dumarey, R., Dams, R., and Hoste, J., *Anal. Chim. Acta*, 1985, **169**, 339.

63. Bye, R., *Analyst*, 1985, **110**, 85.

64. Boampong, C., Brindle, I. D., Le, X., Pidwerbesky, L., and Ceccarelli Ponzoni, C. M., *Anal. Chem.*, 1988, **60**, 1185.

65. Welz, B., and Melcher, M., *Analyst*, 1984, **109**, 577.

66. Bye, R., *Analyst*, 1986, **111**, 111.

67. Wang, X., and Fang, Z., *Kexue Tongbao*, 1986, **31**, 791.

68. Wickrom, T., and Lund, W., *Anal. Chim. Acta*, 1988, **208**, 347.

69. Welz, B., and Melcher, M., *Anal. Chim. Acta*, 1981, **131**, 17.

70. Wang, X., and Fang, Z., *Fenxi Huaxue*, 1988, **16**, 912.

71. Marshall, G. D., and van Staden, J. F., *J. Anal. At. Spectrom.*, 1990, **5**, 681.

72. Bédard, M., and Kerbyson, J. D., *Anal. Chem.*, 1975, **47**, 1441.

73. Bédard, M., and Kerbyson, J. D., *Can. J. Spectrosc.*, 1976, **21**, 64.

74. Welz, B., and Melcher, M., *Anal. Chim. Acta*, 1983, **153**, 297.

75. Wickstrom, T., Lund, W., and Bye, R., *J. Anal. At. Spectrom.*, 1991, **6**, 389.

76. Bye, R., *Anal. Chem.*, 1985, **57**, 1481.

77. Jones, J. W., Capar, S. G., and O'Haver, T. C., *Analyst*, 1982, **107**, 353.

78. Narasaki, H., and Ikeda, M., *Anal. Chem.*, 1984, **56**, 2059.

79. Narasaki, H., *Anal. Sci.*, 1986, **2**, 141.

80. Hershey, J. W., and Keliher, P.N., *Spectrochim. Acta*, 1989, **44B**, 329.

81. Hershey, J. W., and Keliher, P.N., *Spectrochim. Acta*, 1986, **41B**, 713.

82. Ikeda, M., *Anal. Chim. Acta*, 1985, **170**, 217.

83. Riby, P. G., Haswell, S. J., and Grzeskowiak, R., *J. Anal. At. Spectrom.*, 1989, **4**, 181.

84. Pierce, F. D., and Brown, H. R., *Anal. Chem.*, 1977, **49**, 1417.

85. Subramanian, K. S., *Fresenius Z. Anal. Chem.*, 1981, **305**, 382.

86. Fang, Z., Xu, S., Wang, X., and Zhang, S., *Anal. Chim. Acta*, 1986, **179**, 325.

87. Crock, J. G., and Lichte, F. E., *Anal. Chim Acta*, 1982, **144**, 223.

88. Yamamoto, M., Yasuda, M., and Yamamoto, Y., *Anal. Chem.*, 1985, **57**, 1382.

89. Yamamoto, M., Takada, K., Kumamaru, T., Yasada, M., Yokoyama, S., and Yamamoto, Y., *Anal. Chem.*, 1987, **59**, 2446.

90. Burguera, J. L., ed. *"Flow Injection Atomic Spectroscopy,"* Marcel Dekker, New York, 1989.

91. Welz, B., and Melcher, M., *Analyst*, 1983, **108**, 213.

92. Welz, B., and Schubert-Jacobs, M., *Fresenius Z. Anal. Chem.*, 1986, **324**, 832.

93. Agterdenbos, J., van Noort, J. P. M., Peters, F. F., Bax, D., and Ter Heege, J. P., *Spectrochim. Acta*, 1985, **40B**, 501.

94. Bax, D., Peters, F. F., van Noort, J. P. M., and Agterdenbos, J., *Spectrochim. Acta*, 1986, **41B**, 275.

95. Agterdenbos, J., van Noort, J. P. M., Peters, F. F., and Bax, D., *Spectrochim. Acta*, 1986, **41B**, 283.

96. Bax, D., Van Elteren, J. T. and Agterdenbos, J., *Spectrochim. Acta*, 1986, **41B**, 1007.

97. Narsito, and Agterdenbos, J., *Anal. Chim. Acta*, 1987, **197**, 315.

98. Parisis, N. E., and Heyndrickx, A., *Analyst*, 1986, **111**, 281.

99. Welz, B., Schubert-Jacobs, M., Sperling, M., Styris, D. L., and Redfield, D. A., *Spectrochim. Acta*, 1990, **45B**, 1235.

100. Agterdenbos, J. and Bax, D., *Fresenius Z. Anal. Chem.*, 1986, **323**,783.

101. Evans, W. H., Jackson, F. J. and Dellar, D., *Analyst*, 1979, **104**, 16.

102. Petrick, K., and Krivan, V., *Fresenius Z. Anal. Chem.*, 1987, **327**, 338.

103. Van Cleuvenbergen, R. J. A., Van Mol, W. E., and Adams, F. C., *J. Anal. At. Spectrom.*, 1988, **3**, 169.

104. Reamer, D. C., Veillon, C., and Tokousbalides, P. T., *Anal. Chem.*, 1981, **53**, 245.

105. Akman, S., Gene, O., and Balkis, T., *Spectrochim. Acta*, 1982, **37B**, 903.

106. Foreman, J. K., and Stockwell, P. B., *"Automatic Chemical Analysis"*, Ellis Horwood, Chichester, 1975.

107. Varcarcel. M., and Luque de Castro, M. D., *"Auotmatic Methods of Analysis,"* Elsevier, Amsterdam, 1988.

108. Skeggs, L. T., *Ann. J. Pathol.*, 1957, **28**, 311.

109. Ruzicka, J., and Hansen, E. H., *Anal. Chim. Acta,* 1975, **78**, 145.

110. Betteridge, D., *Anal. Chem.*, 1978, **50**, 832A.

111. Ruzicka, J., and Hansen, E. H., *Chem. Tech.*, 1979, 756.

112. Ragner, C. B., *Anal. Chem.*, 1981, **53**, 20A.

113. Ruzicka, J., *Phil. Trans. R. Soc. Lond.,* 1982, **305A**, 645.

114. Stewart, K. K., *Anal. Chem.*, 1983, **55**, 931A.

115. Karlberg, B. I., *Inter. Lab.*, 1983, **13**, 82.

116. Ruzicka, J., *Anal. Chem.*, 1983, **55**, 1040A.

117. Ruzicka, J., and Hansen, E. H., *Anal. Chim. Acta*, 1986, **179**, 1.

118. Clark, G. D., Whitman, D. A., Christian, G. D., and Ruzicka, J., *Crit. Rev. Anal. Chem.*, 1990, **21**, 357.

119. Ruzicka, J., and Hansen, E. H., *"Flow Injection Analysis,"* 1st Ed. Wiley, New York, 1981.

120. Ruzicka, J., and Hansen, E. H., *"Flow Injection Analysis,"* 2nd Ed. Wiley, New York, 1988.

121. Valcarcel, M., and Luque de Castro, M. D., *"Flow Injection Analysis, Principles and Applications,"* Ellis Horwood, Chichester, 1987.

122. Karlberg, B., and Pacey, G. E., *"Flow Injection Analysis: A Practical Guide,"* Elsevier, Amsterdam, 1989.

123. Department of Applied Analytical Chemistry, Faculty of Engineering, Kyushu University, Hakozaki, Higashiku, Fukuoka 812, Japan.

124. International Conference on Flow Injection Analysis I, Amsterdam, September 1979, *Anal. Chim. Acta*, 1980, **114**, 1; II, Lund, June 1981, *Anal Chim. Acta*, 1983, **145**, 1; III, Birmingham, GB, September, 1985, *Anal. Chim. Acta*, 1986, **179**, 1; IV, Las Vegas, April 1988, *Anal. Chim. Acta*, 1988, **214**, 1; V, Kumamoto, August 1991.

125. Gisin, M., Thommen, C., and Mansfield, K. F., *Anal. Chim. Acta*, 1986, **179**, 149.

126. Lown, J. A., Koile, R., and Johnson, D. C., *Anal. Chim. Acta*, 1980, **116**, 33.

127. Ruzicka, J., Hansen, E. H., and Ramsing, A. U., *Anal. Chim. Acta*, 1982, **134**, 55.

128. Sherwood, R. A., Rocks, B. F., and Riley, C., *Analyst*, 1985, **110**, 493.

129. Erickson, B. C., Ruzicka, J., and Kowalski, B. R., *Anal. Chem.*, 1987, **59**, 1246.

130. Bergamin F, H., Krug, F. J., and Zagatto, E. A. G, *Anal. Chim. Acta*, 1978, **97**, 427.

131. Ruzicka, J., and Hansen, E. H., *Anal. Chim. Acta*, 1983, **145**, 1.

132. Zagatto, E. A. G., Krug, F. J., Bergamin F, H., Jorgensen, S. S., and Reis, B. F., *Anal. Chim. Acta*, 1979, **104**, 279.

133. Wolf, W. R., and Stewart, K. K., *Anal. Chem.*, 1979, **51**, 1201.

134. Tyson, J. F., *TrAc. trends Anal. Chem.*, 1985, **4**, 124.

135. Tyson, J. F., *Analyst*, 1985, **110**, 419.

136. Gallego, M., Luque de Castro, M. D., and Valcarcel, M., *At. Spectrosc.*, 1985, **6**, 16.

137. Ruzicka, J., *Fresenius Z. Anal. Chem.*, 1986, **324**, 745.

138. Tyson, J. F., *Anal. Chim. Acta*, 1988, **214**, 57.

139. Tyson, J. F., *Anal. Chim. Acta*, 1990, **234**, 3.

140. Tyson, J. F., *Spectrochim. Acta. Rev.*, 1991, **14**, 169.

141. Cresser, M. S., *Anal. Chim. Acta*, 1975, **80**, 170.

142. Rocks, B., Sherwood, R. A., Bayford, L. M., and Riley, C., *Ann. Clin. Biochem.*, 1982, **19**, 338.

143. Attiyat, A. S., and Christian, G. D., *Talanta*, 1984, **31**, 463.

144. Brown, M. W., and Ruzicka, J., *Analyst*, 1984, **109**, 1091.

145. Harnly, J. M., and Beecher, G. R., *J. Anal. At. Spectrom.*, 1986, **1**, 75.

146. Tyson, J. F., Adeeyinwo, C. E., and Bysouth, S. R., *J. Anal. At. Spectrom.*, 1989, **4**, 191.

147. Yoza, N., Aoyagi, Y., Ohashi, S., and Tateda, A., *Anal. Chim. Acta*, 1979, **111**, 163.

148. Garcia, I. L., Cordoba, M. H., and Sanchez-Pedreno, C., *Analyst*, 1987, **112**, 271.

149. Sweileh, J. A., and Cantwell, F. F., *Anal. Chem.*, 1985, **57**, 420.

150. Adeeyinwo, C. E., and Tyson, J. F., *Anal. Chim. Acta*, 1988, **214**, 339.

151. Fang, Z., and Welz, B., *J. Anal. At. Spectrom.*, 1989, **4**, 83.

152. Fang, Z., Welz, B., and Sperling, M., *J. Anal. At. Spectrom.*, 1991, **6**, 179.

153. Tyson, J. F., *Fresenius Z. Anal. Chem.*, 1988, **329**, 663.

154. Tyson, J. F., Adeeyinwo, C. E., Appleton, J. M. H., Bysouth, S. R., Idris, A. B., and Sarkissian, L. L., *Analyst*, 1985, **110**, 487.

155. McGowan, K. A., and Pacey, G. E., *Anal. Chim. Acta*, 1988, **214**, 391.

156. Rocks, B. F., Sherwood, R. A., and Riley, C., *Clin. Chem.*, 1982, **28**, 440.

157. Rocks, B. F., Sherwood, R. A., and Riley, C., *Ann. Clin. Biochem.*, 1984, **21**, 51.

158. Reis, B. F., Jacintho, A. O., Mortatti, J., Krug, F. J., Zagatto, E. A. G., Bergamin F, H., and Pessenda, L. C. R., *Anal. Chim. Acta*, 1981, **123**, 221.

159. Tyson, J. F., Mariara, J. R., and Appleton, J. M. H., *J. Anal. At. Spectrom.*, 1986, **1**, 273.

160. Tyson, J. F., and Bysouth, S. R., *J. Anal. At. Spectrom.*, 1988, **3**, 211.

161. Fernandez, A., Gomez-Nieto, M. A., Luque de Castro, M. D., and Valcarcel, M., *Anal. Chim. Acta*, 1984, **165**, 217.

162. Tyson, J. F., Appleton, J. M. H., and Idris, A. B., *Analyst*, 1983, **108**, 153.

163. Tyson, J. F., Appleton, J. M. H., and Idris, A.B., *Anal. Chim. Acta*, 1983, **145**, 159.

164. Tyson, J. F., and Appleton, J. M. H., *Talanta*, 1984, **31**, 9.

165. Stewart, K. K., and Rosenfeld, A. G., *Anal. Chem.*, 1982, **54**, 2368.

166. De la Guardia, M., Carbonell, V., Morales, A., and Salvador, A., *Fresinius Z. Anal. Chem.*, 1989, **335**, 975.

167. Beinrohr, E., Csemi, P., and Tyson, J. F., *J. Anal. At. Spectrom.*, 1991, **6**, 307.

168. Bysouth, S. R., and Tyson, J. F., *J. Anal. At. Spectrom.*, 1987, **2**, 217.

169. Burguera, J. L., Burguera, M., Rivas, C., De la Guardia, M., and Salvador, A., *Anal. Chim. Acta*, 1990, **234**, 253.

170. Tyson, J. F., *Analyst*, 1984, **109**, 319.

171. Bysouth, S. R., and Tyson, J. F., *Anal. Chim. Acta*, 1986, **179**, 481.

172. Sperling, M., Fang, Z., and Welz, B., *Anal. Chem.*, 1991, **63**, 151.

173. Olsen, S., Ruzicka, J., and Hansen, E. H., *Anal. Chim. Acta*, 1982, **136**, 101.

174. Tyson, J. F., *Anal. Proc.*, 1981, **18**, 542.

175. Tyson, J. F., and Idris, A. B., *Analyst*, 1984, **109**, 23.

176. Tyson, J. F., and Idris, A. B., *Analyst*, 1981, **106**, 1125.

177. Araujo, M. C. U., Pasaquini, C., Bruns, R. E., and Zagatto, E. A. G., *Anal. Chim. Acta*, 1985, **171**, 337.

178. Fang, Z., Harris, J. M., Ruzikca, J., and Hansen, E. H., *Anal. Chem.*, 1985, **57**, 1457.

179. Valcarcel, M., and Luque de Castro, M. D., *J. Chromatogr.*, 1987, **393**, 3.

180. Fang, Z., Zhu, Z., Zhang, S., Xu, S., Guo, L., and Sun, L., *Anal. Chim. Acta*, 1988, **214**, 41.

181. Karlberg, B., *Anal. Chim. Acta*, 1988, **214**, 29.

182. Karlberg, B., *Fresenius Z. Anal. Chem.*, 1988, **329**, 660.

183. Nord, L., and Karlberg, B., *Anal. Chim. Acta*, 1981, **125**, 199.

184. Nord, L., and Karlberg, B., *Anal. Chim. Acta*, 1983, **145**, 151.

185. Kuban, V., Komarek, J., and Cajkova, D., *Collect. Czech. Chem. Commun.*, 1989, **54**, 2683.

186. Gallego, M., and Valcarcel, M., *Anal. Chim. Acta*, 1985, **169**, 161.

187. Jimenez, de Bias, O., Pereda de Paz, J. L., and Mendez, J. H., *J. Anal. At. Spectrom.*, 1990, **5**, 693.

188. Olsen, S., Pessenda, L. C. R., Ruzicka, J. and Hansen, E. H., *Analyst*, 1983, **108**, 905.

189. Lui, Y., and Ingle, J. D., *Anal. Chem.*, 1989, **61**, 520.

190. Fang, Z., Ruzicka, J., and Hansen, E. H., *Anal. Chim. Acta*, 1984, **164**, 23.

191. Fang, Z., Xu, S., and Zhang, S., *Anal. Chim. Acta*, 1987, **200**, 35.

192. Fang, Z., Xu, S., and Zhang, S., *Anal. Chim. Acta*, 1984, **164**, 41.

193. Fang, Z., and Welz, B., *J. Anal. At. Spectrom.*, 1989, **4**, 543.

194. Ruzicka, J., and Arndal, A., *Anal. Chim. Acta*, 1989, 216, 243.

195. Fang,Z., Guo, T., and Welz, B., *Talanta*, 1991, **38**, 613.

196. Bengtsson, M., Malamas, F., Torstensson, A., Regnell, O., and Johansson, G., *Mickrochim. Acta*, 1985, III, 209.

197. Malamas, F., Bengtsson, M., and Johansson, G., *Anal. Chim. Acta*, 1984, **160**, 1.

198. Marshall, M. A., Mottola, H. A., *Anal. Chem.*, 1985, **57**, 729.

199. Bysouth, S. R., Tyson, J. F., and Stockwell, P. B., *Anal. Chim. Acta*, 1988, **214**, 329.

200. Bysouth, S. R., Tyson, J. F., and Stockwell, P. B., *Analyst*, 1990, **115**, 571.

201. Kuban, V., Komarek, J., and Zdrahal, Z., *Collect. Czech. Chem. Commun.*, 1989, **54**, 1785.

202. Devi, S., Habib, K. A. J., and Townshend, A., *Quim. Anal.*, 1989, **8**, 159.

203. Zhang, S., Xu, S.,and Fang, Z., *Quim. Anal.*, 1989, **8**, 191.

204. Zhang, Y., Riby, P., Cox., A. G., McLeod, C. W., Date, A. R., and Cheung. Y. Y., *Analyst*, 1988, **113**, 125.

205. Coetzee, P. P., Taljaard, I., and de Beer, H., *Fresenius J. Anal. Chem.*, 1990, **336**, 201.

206. Shah, A., and Devi, S., *Anal. Chim. Acta*, 1990, **236**, 469.

207. Pacey, G. E., and Bubnis, B. P., *Int. Lab.*, 1984, 26.

208. Milosavljevic, E. B., Ruzicka, J., and Hansen, E. H., *Anal. Chim. Acta*, 1985, **169**, 321.

209. Milosavljevic, E. B., Solujic, L., Nelson, J. H., and Hendrix, J. L., *Mickrochim. Acta*, 1985, III, 353.

210. Patel, B., Haswell, S. J., and Grzeskowiak, R., *J. Anal. At. Spectrom.*, 1989, **4**, 195.

211. Kamson, O. F., and Townshend, A., *Anal. Chim. Acta*, 1983, **155**, 253.

212. Beinrohr, E., Cakrt, M., Rapta, M., and Tarapci, P., *Fresenius Z. Anal. Chem.*, 1989, **335**, 1005.

213. Fang, Z., Sperling, M., and Welz, B., *J. Anal. At. Spectrom.*, 1990, **5**, 639.

214. Porta, V., Abollino, O., Mentasti, E., and Sarzanini, C., *J. Anal. At. Spectrom.*, 1991, **6**, 119.

215. Sperling, M., Yin, X., Welz, B., *J. Anal. At. Spectrom.*, 1991, **6**, 295.

216. Martinez-Jimenez, P., Gallego, M., and Valcarcel, M., *Analyst*, 1987, **112**, 1233.

217. Martinez-Jimenez, P., Gallego, M., and Valcarcel, M., *J. Anal. At. Spectrom.*, 1987, **2**, 211.

218. Martinez-Jimenez, P., Gallego, M., and Valcarcel, M., *Anal. Chim. Acta*, 1987, **193**, 127.

219. Martinez-Jimenez, P., Gallego, M., and Valcarcel, M., *Anal. Chem.*, 1987, **59**, 69.

220. Debrah, E., Adeeyinwo, C. E., Bysouth, S. R., and Tyson, J. F., *Analyst*, 1990, **115**, 1543.

221. Adeeyinwo, C. E., and Tyson, J. F., *Anal. Proc.*, 1989, **26**, 58.

222. Adeeyinwo, C. E., and Tyson, J. F., *Anal. Proc.*, 1989, **26**, 375.

223. Esmadi, F., Kharoaf, M., and Attiyat, A. S., *Microchem, J.*, 1989, **40**, 277.

224. Fang, Z., Sperling, M., and Welz, B., *J. Anal., At. Spectrom.*, 1991, **6**, 301.

225. Schulze, G., Koschany, M., and Elsholz, O., *Anal. Chim. Acta*, 1987, **196**, 153.

226. Koropchak, J. A., and Allen, L., *Anal. Chem.*, 1989, **61**, 1410.

227. Vijan, P. N., and Chan, C. Y., *Anal. Chem.*, 1976, **48**, 1788.

228. Vijan, P. N., and Wood, G. R., *Analyst*, 1976, **101**, 966.

229. Arab-Zavar, M. H., and Howard, A. G., *Analyst*, 1980, **105**, 744.

230. El-Awady, A. A., Miller, R. B., and Carter, M. J., *Anal. Chem.*, 1976, **48**, 110.

231. Howard, A. G., and Arab-Zavar, M. H., *Analyst*, 1981, **106**, 213.

232. Comber, S. D. W., and Howard, A. G., *Anal. Proc.*, 1989, **26**, 20.

233. Campbell, A. T., and Howard, A. G., *Anal. Proc.*, 1989, **26**, 32.

234. Wang, X., and Fang, Z., *Fenxi Huaxue*, 1986, **14**, 738.

235. Ikeda, M., *Anal. Chim. Acta*, 1985, **167**, 289.

236. De Andrade, J. C., Pasquini, C., Baccan, N., and Van Loon, J. C., *Spectrochim. Acta*, 1983, **38B**, 1329.

237. Birnie, S. E., *J. Autom. Chem.*, 1988, **10**, 140.

238. Pasquini, C., Jardim, W. F., De Faria, L. C., *J. Autom. Chem.*, 1988, **10**, 188.

239. Chan, W. F., and Hon, P. K., *Analyst*, 1990, **115**, 567.

240. Marshall, G. D., and van Staden, J. F., *J. Anal. At. Spectrom.*, 1990, **5**, 675.

241. Pettersson, J., Hansson, L., and Olin, A., *Talanta*, 1986, **33**, 249.

242. McLaughlin, K., Dadgar, D., Smyth, M. R., and McMaster, D., *Analyst*, 1990, **115**, 275.

243. Guo, T., Erler, W., Schulze, H., and McIntosh, S., *At. Spectrosc.*, 1990, **11**, 24.

244. Chan, C. C. Y., Baig, M. W. A., and Lichti, P. A., *Anal. Lett.*, 1990, **23**, 2259.

245. Mindel, B. D., and Karlberg, B., *Lab. Pract.*, 1981, **30**, 719.

246. Fang, Z., Welz, B., and Schlemmer, G., *J. Anal. At. Spectrom.*, 1989, **4**, 91.

247. De Andrade, J. C., Strong III, F. C., and Martin, N. J., *Talanta*, 1990, **37**, 711.

248. Garcia, I. L., Sobejano, F. O., and Cordoba, M. H., *Analyst*, 1991, **116**, 517.

249. Borja, R. M., Salvador, A., De La Guardia, M., Burguera, J. L., and Burguera, M., *Quim. Anal.*, 1989, **8**, 241.

250. Zagatto, E. A. G., Jacintho, A. O., Pessenda, L. C. R., Krug, F. J., Reis, B. F., and Bergamin F, H., *Anal. Chim. Acta*, 1981, **125**, 37.

251. Rocks, B. F., Sherwood, R. A., Turner, Z. J., and Riley, C., *Ann. Clin. Biochem.*, 1983, **20**, 72.

252. Burguera, M., Burguera, J. L., and Alarcon, O. M., *Anal. Chim. Acta*, 1986, **179**, 351.

253. Burguera, M., Burguera, J. L., and Alarcon, O. M., *Anal. Chim. Acta*, 1988, **214**, 421.

254. Carbonell, V., De La Guardia, M., Salvador, A., Burguera, J. L., and Burguera, M. , *Anal. Chim. Acta*, 1990, **238**, 417.

255. Yuan, D., Wang, X., Yang, P., and Huang, B., *Anal. Chim. Acta*, 1991, **243**, 65.

256. Nygren, O., Nilsson, C., and Gustavsson, A., *Analyst*, 1988, **113**, 591.

257. Burguera, M., Burguera, J. L., Rivas, P. C., and Alarcon, O. M., *At. Spectrosc.*, 1986, **7**, 79.

258. Burguera, J. L., Burguera, M., and Alarcon, O. M., *J. Anal. At. Spectros.*, 1986, **1**, 79.

259. Burguera, J. L., Burguera, M., La Cruz O, L., and Naranjo, O. R., *Anal. Chim. Acta*, 1986, **186**, 273.

260. Burguera, J. L, Burguera, M., Randon, C. E., Rivas, C., Burguera, J. A., and Alarcon, O. M., *J. Trace Elem. Electrolytes Health DIS.*, 1987, **1**, 21.

261. Becerra, G., Burguera, J. L., and Burguera, M., *Quim. Anal.*, 1987, **6**, 52.

262. Burguera, M., Burguera, J. L., Garaboto F, A. M., and Alarcon, O. M., *Quim. Anal.*, 1987, **6**, 227.

263. Van Staden, J. F., and Van Rensburg, A., *Analyst*, 1990, **115**, 605.

264. Santelli, R. E, Gallego, M., and Valcarcel, M., *J. Anal. At. Spectrom.*, 1989, **4**, 547.

265. Taylor, C. G., and Trevaskis, J. M., *Anal. Chim. Acta*, 1986, **179**, 491.

266. Zagatto, E. A.G, Bahia, F., Gine, M. F., and Bergamin F, H., *Anal. Chim. Acta*, 1986, **181**, 265.

267. Thorburn Burns, D., Chimpalee, N., and Harriott, M., *Fresenius Z. Anal. Chem.*, 1989, **335**, 566.

268. Philips Analytical, "*Atomic Absorption Data Book*," 5th Ed., Philips Scientific , Cambridge, 1988.

269. Kay, J. M., and Nedderman, R. M., "*Fluid mechanics and transfer processes*," Cambridge University Press, Cambridge, 1988, pp 209-216.

270. Massey, B.S., "*Mechanics of fluids*," 6th Ed., Van Nostrand Reinhold (International), 1989, pp 199-215.

271. Offley, S. G., Seare, N. J., Tyson, J. F., and Kibble, H. A. B., *J. Anal. At. Spectrom.*, 1991, **6**, 133.

272. Philips Analytical, "*PU9360 Continuous flow vapour system user manual*," Philips Scientific Cambridge, 1988.

273. Miller, J. C., and Miller, J. N., "*Statistics for Analytical Chemistry*," Ellis Horwood, Chichester, 1984, pp 162-165.

274. Dow Chemical Company, "*A Laboratory Manual on Ion Exchange*," Dow Chemicals, U.S.A., 1982, p 26.

275. Miller, J. C., and Miller, J. N., "*Statistics for Analytical Chemistry*," Ellis Horwood, Chichester, 1984, pp 96-100.

276. Miller, J. C., and Miller, J. N., "*Statistics for Analytical Chemistry*," Ellis Horwood, Chichester, 1984, pp 57-59.

277. Bysouth, S. R., Tyson, J. F., and Stockwell, P. B., *J. Autom. Chem.*, 1989, **11**, 36.

278. Riby, P. G., Ph. D. Thesis, "The determination of hydride generating elements in nickel based alloy," Thames Polytechnic, U.K., 1989.

279. Kuldvere, A., *Analyst*, 1989, **114**, 125.

280. Aggett, J., and Aspell, A. C., *Analyst*, 1976, **101**, 341.

281. Sperling, M., Yin, X., and Welz, B., CSI meeting, Bergen, Norway, June 1991.

282. Tyson, J. F., Offley, S. G., Seare, N. J., Kibble, H. A., and Fellows, C., *J. Anal. At. Spectrom.*, 1992, (Accepted for publication).

283. Miller, J. C., and Miller, J. N., "Statistics for Analytical Chemistry," Ellis Horwood, Chichester, 1984, pp.90-96.

284. Miller, J. C., and Miller, J. N., "Statistics for Analytical Chemistry," Ellis Horwood, Chichester, 1984, pp.53-56.

285. Thompson, M., Pahlavanpour, B., Walton, S. J., and Kirkbright, G. F., *Analyst*, 1978, **103**, 705.